



HAL
open science

High-frequency nonlinear dynamics of a laser diode with phase-conjugate feedback

Emeric Mercier

► **To cite this version:**

Emeric Mercier. High-frequency nonlinear dynamics of a laser diode with phase-conjugate feedback. Autre. CentraleSupélec, 2016. Français. NNT : 2016CSUP0010 . tel-01692760

HAL Id: tel-01692760

<https://theses.hal.science/tel-01692760>

Submitted on 25 Jan 2018

HAL is a multi-disciplinary open access archive for the deposit and dissemination of scientific research documents, whether they are published or not. The documents may come from teaching and research institutions in France or abroad, or from public or private research centers.

L'archive ouverte pluridisciplinaire **HAL**, est destinée au dépôt et à la diffusion de documents scientifiques de niveau recherche, publiés ou non, émanant des établissements d'enseignement et de recherche français ou étrangers, des laboratoires publics ou privés.



CentraleSupélec



N°d'ordre : 2016-34-TH

CentraleSupélec

École doctorale EMMA

« Énergie, Mécanique et Matériaux »

LMOPS, « Laboratoire Matériaux Optiques, Photonique et Systèmes »

Thèse de doctorat

Domaine : SPI

Spécialité : Photonique

Soutenance prévue le 19 Octobre 2016 par

Émeric Mercier

à CentraleSupélec, Metz, France.

**HIGH-FREQUENCY NONLINEAR DYNAMICS OF A
LASER DIODE WITH PHASE-CONJUGATE FEEDBACK**

Composition du jury :

Directeur de thèse :	Pr. Marc Sciamanna	CentraleSupélec
Co-directrice de thèse :	Pr. Delphine Wolfersberger	CentraleSupélec
Président du jury :	Pr. Thomas Erneux	Université Libre de Bruxelles
Rapporteurs :	Dr. Habil. Stefan Breuer	Technische Universität Darmstadt
	Pr. Alexis Fischer	Université Paris 13
Examineur :	Dr. Miguel Cornelles Soriano	Universitat de les Illes Balears

To my lovely Elodie.

ABSTRACT

In this thesis, I present my research work on phase-conjugate feedback in a semiconductor laser, especially how high-frequency solutions appear in this system.

First, I study a simple theoretical model adapted from the well-known Lang-Kobayashi rate equations modeling a laser with conventional feedback. Using mostly numerical simulation of the rate equations, I present how the fundamental solutions of the laser with phase-conjugate feedback known as external-cavity modes (ECMs) appear. I describe their stability properties with respect to the two most important parameters of the system, namely feedback rate and external-cavity length – directly proportional to the induced time-delay. I show that by driving the system with a large feedback rate, we can obtain self-pulsating solutions at harmonics of the external-cavity frequency reaching frequencies beyond several gigahertz regardless of the external-cavity length.

Secondly, I use numerical simulations to show how these high-frequency fundamental solutions are destabilized into different chaotic regimes with distinct characteristics. In the regime of low-frequency fluctuations, I show that itinerancy among ruins of (ECMs) underlies power-dropouts. I describe how this itinerancy among ECMs can be observed in the experiment since each ECM brings its own radiofrequency spectral signature. In the regime of coherence collapse, I reproduce the emergence of extreme events observed experimentally in previous works. Some subtle properties are well-reproduced. With these first two results, I conclude that the model used is accurate enough to qualitatively reproduce dynamics observed experimentally.

Finally, I study the system experimentally. With a first experiment, I am able to actually observe the itinerancy among ruins of ECMs thanks to an oscilloscope with a large sampling-rate and a technique called *short-time Fourier transform*. With this same setup, I also report on optical chaos with a bandwidth up to 27 % larger than the bandwidth of optical chaos from the same laser with conventional feedback. With a second experiment, I am able to observe experimentally the succession of bifurcations that leads the laser from a steady-state, through oscillations and chaos, to the regime V. Among the most successful achievements, I report on observation of high-frequency ECMs of frequency equal to the thirteenth harmonic (8 GHz) of the external-cavity frequency (616 MHz).

RÉSUMÉ

Dans cette thèse, je présente mon travail de recherche sur la rétroaction optique à conjugaison de phase dans un laser à semi-conducteurs et je décris en particulier l'apparition de solutions à hautes fréquences.

Tout d'abord, j'étudie un modèle théorique simple adapté des équations de taux de Lang-Kobayashi modélisant un laser avec rétroaction optique conventionnelle. J'utilise principalement des outils numériques (simulation) pour montrer comment apparaissent les solutions fondamentales d'un laser à conjugaison de phase connues sous le nom de modes de cavité externe (MCE). Je décris leur comportement face à des variations du taux de rétroaction et de la longueur de la cavité externe, proportionnelle au délai. Je montre qu'en imposant un fort taux de rétroaction, il est possible d'obtenir des solutions oscillantes à des harmoniques de la fréquence de cavité externe atteignant plusieurs gigahertz quelle que soit la longueur de cavité externe.

Ensuite, j'utilise la simulation numérique pour montrer comment ces solutions fondamentales à haute fréquence sont déstabilisées vers différents régimes chaotiques. Dans un régime de fluctuations à basses fréquences, je montre que la trajectoire du système avant une chute de puissance est itinérante sur les ruines des MCE, phénomène observable sur une trace temporelle puisque chaque MCE a une signature radio-fréquence spectrale différente. Dans un cas de chaos complètement développé, je montre comment le modèle reproduit l'apparition d'événements extrêmes avec une précision suffisante pour observer certaines subtilités montrées dans une étude expérimentale précédente. Ces deux premiers résultats me permettent de conclure quant à la validité du modèle pour obtenir des résultats qualitatifs.

Enfin, j'étudie expérimentalement le système. Une première expérience permet d'observer l'itinérance sur les ruines de MCE grâce à un grand taux d'échantillonnage et une *transformée de Fourier sur courte durée*. Cette expérience me permet aussi de montrer qu'utiliser une rétroaction optique à conjugaison de phase plutôt que conventionnelle permet d'obtenir un chaos optique avec une bande passante jusqu'à 27 % plus grande. Une seconde expérience permet d'observer la succession de bifurcations menant le laser depuis son état stationnaire, jusqu'au régime V en passant par des régimes oscillants et chaotiques. Entre autres importants résultats, j'observe des MCE avec des fréquences correspondant à la treizième harmonique (8 GHz) de la fréquence de cavité externe (616 MHz).

PUBLICATIONS

LIST OF PUBLICATIONS IN PEER-REVIEWED JOURNALS

- M. Virte, M. Sciamanna, É. Mercier and K. Panajotov, “Bistability of time-periodic polarization dynamics in a free-running VCSEL”, *Optics Express*, 22 (2014), p. 6772, DOI: <http://dx.doi.org/10.1364/OE.22.006772>.
- M. Virte, É. Mercier, H. Thienpont, K. Panajotov and M. Sciamanna, “Physical random bit generation from chaotic solitary laser diode”, *Optics express*, 22 (2014), p. 17271, DOI: <http://dx.doi.org/10.1364/OE.22.017271>.
- É. Mercier, D. Wolfersberger and M. Sciamanna, “Bifurcation to chaotic low-frequency fluctuations in a laser diode with phase-conjugate feedback”, *Optics Letters*, 39.13 (2014), p. 4021, DOI: <http://dx.doi.org/10.1364/OL.39.004021>.
- É. Mercier, A. Even, E. Mirisola, D. Wolfersberger and M. Sciamanna, “Numerical study of extreme events in a laser diode with phase-conjugate optical feedback”, *Physical Review E*, 91.4 (2015), p. 042914, DOI: <http://dx.doi.org/10.1103/PhysRevE.91.042914>.
- É. Mercier, D. Wolfersberger and M. Sciamanna, “High-frequency chaotic dynamics enabled by optical phase-conjugation”, *Scientific Reports*, 6 (2016), p. 18988, DOI: <http://dx.doi.org/10.1038/srep18988>.

LIST OF SUBMITTED PUBLICATIONS IN PEER-REVIEWED JOURNALS

- É. Mercier, C. Uy, L. Weicker, M. Virte, D. Wolfersberger and M. Sciamanna, “Self-determining high-frequency oscillation from an external-cavity laser diode”.
- D. Rontani, É. Mercier, D. Wolfersberger and M. Sciamanna, “Enhanced complexity of optical chaos in a laser diode with phase-conjugate feedback”.

PARTICIPATIONS IN INTERNATIONAL CONFERENCES

- É. Mercier, M. Virte, K. Panajotov and M. Sciamanna, “Bistability of limit-cycles in a free-running VCSEL”, *IS-PALD* (2013).
- É. Mercier, A. Karsaklian Dal Bosco, D. Wolfersberger and M. Sciamanna, “Bifurcation to chaos and extreme events in a laser diode with phase-conjugate feedback”, *Semiconductor Lasers and Laser Dynamics VI*, 91340J (2014), DOI: <http://dx.doi.org/10.1117/12.2052087>.
- D. Wolfersberger, A. Karsaklian dal Bosco, É. Mercier and M. Sciamanna, “Harmonic fundamental self-pulsations from a laser diode using phase-conjugate optical feedback”, *Semiconductor Lasers and Laser Dynamics VI*, 91340K (2014), DOI: <http://dx.doi.org/10.1117/12.2052302>.
- M. Sciamanna, D. Wolfersberger, A. Karsaklian Dal Bosco and É. Mercier, “New insight into laser diode dynamics from phase-conjugate optical feedback”, *Workshop on Nonlinear Dynamics of Semiconductor Lasers*, Berlin WIAS Institute, **Invited** (2014).
- M. Sciamanna, A. Karsaklian Dal Bosco, V. Caullet, É. Mercier, N. Marsal and D. Wolfersberger, “Extreme events driven by feedback in a nonlinear optical cavity”, *Workshop on Rogue waves, dissipative solitons, plasmonics, supercontinuum and special fibres*, ICFO (Barcelona), **Invited** (2014).
- É. Mercier, D. Wolfersberger and M. Sciamanna, “Numerical study of extreme events and chaos in a laser diode with phase-conjugate feedback”, *Advanced Photonics*, JM5A.46 (2014), DOI: <http://dx.doi.org/10.1364/BGPP.2014.JM5A.46>.
- M. Sciamanna, É. Mercier, A. Karsaklian Dal Bosco, M. Virte, L. Weicker and D. Wolfersberger, “Advanced bifurcation study of a laser diode with phase-conjugate feedback”, *OWTNM* (2015).
- D. Wolfersberger, É. Mercier, A. Karsaklian Dal Bosco and M. Sciamanna, “Deterministic optical rogue waves in a laser diode with time-delayed feedback”, *European Semiconductor Laser Workshop* (2015).
- M. Sciamanna, É. Mercier, C. Uy, L. Weicker and D. Wolfersberger, “High-frequency pulsating dynamics in a laser diode with phase-conjugate feedback”, *European Semiconductor Laser Workshop* (2015).

- É. Mercier, D. Wolfersberger and M. Sciamanna, “Phase-conjugate feedback in a semiconductor laser enables large chaotic bandwidth”, *IS-PALD* (2015).
- É. Mercier, C. Uy, D. Wolfersberger and M. Sciamanna, “Mapping self-pulsing frequencies in a semiconductor laser with phase-conjugate feedback”, *IS-PALD* (2015).
- É. Mercier, D. Wolfersberger and M. Sciamanna, “Improving the chaos bandwidth of a semiconductor laser with phase-conjugate feedback”, *Semiconductor Lasers and Laser Dynamics VII*, 98920G (2016), DOI: <http://dx.doi.org/10.1117/12.2227826>.
- M. Sciamanna, D. Wolfersberger, Chi-Hak Uy and É. Mercier, “Characteristics of optical chaos from a laser diode with phase-conjugate feedback”, *Workshop on Nonlinear Dynamics of Semiconductor Lasers*, Berlin WIAS Institute, **Invited** (2016).
- É. Mercier, D. Rontani, D. Wolfersberger and M. Sciamanna, “Properties of optical chaos from a laser diode with phase-conjugate feedback”, *ICONO* (Minsk), **Invited** (2016).

ACKNOWLEDGMENTS

Doing a PhD was like embarking on a three-year long adventure. There were ups and downs along this journey, and there were always people to carry me through them. This adventure is reaching its end and I am grateful for all the people that I have met thanks to it, for all the relationships that it helped strengthen, and for all the people that led me to embark on it.

I would like to acknowledge first the support of my two PhD supervisors, Marc Sciamanna and Delphine Wolfersberger, who encouraged me all along to bring out the best in me. They would always find time and answers for me when I had doubts over my work or when I was struggling to make progress. I know I can sometimes be a bit stubborn, but they have always pushed me in the right direction and their support has helped me turn our collective work into fruitful results I think we can all be satisfied with.

Around my supervisors were other colleagues, Nicolas Marsal, Damien Ron-tani, Lionel Weicker, Chi-Hak Uy with whom I enjoyed many moments. They provided opportunities for friendly discussions, and I have had the chance to collaborate with most of them on different aspects of my work. They made me feel as part of a team that works together with common goals.

I want to thank more specifically the two persons with whom I shared my office. Mathieu Lauffer who obtained his PhD last year and would often be the source of happiness and positive feelings in our office. Noémi Wiersma who always felt like a partner in this adventure since we started it and will be finishing it both at the same time. We could always understand each other and I am happy to count her as a friend.

I would like to thank other people in CentraleSupélec that have helped me with different problems and formalities. Gilles Berlin was always there to provide me with IT-related assistance (often with a smile and jokes). Mario Fernandes who happily helped me design and build mechanical pieces required for my experiments, his expertise was always welcomed. Fabienne Munier, our energetic secretary who makes sure that all our trips to conferences and other scientific events go well. Yann Liber from the library who has helped me find several publications and books that I did not have access to and that I needed for my research.

I would like to thank my family, who has always supported me and trusted me to make my own choices throughout my education. I am happy with the

path I have chosen. They would probably like to see me more often nowadays but they understand when I have too much work and I cannot come.

I would like to thank my friends, who offered support or distraction when needed. Especially, I would like to thank Pauline. I have known you for a very long time now and I still enjoy our discussions. I know we can count on each other and I would like to see you more often.

I have special thanks to address to all the wonderful professors of physics and mathematics who communicated their passion and knowledge with enthusiasm to the curious child, teenager, and student that I was (and still am). Your dedication has helped me choose the right path for myself through high school, college and beyond. I would certainly not be there without you.

Finally, I want to thank Elodie the most. You are my life companion and meeting you was the best thing that happened to me. I am thankful for your love and unconditional support during this three years. You filled me with motivation during the downs, you were there to congratulate me and to celebrate with me during the ups, and you helped me realize when I needed to take breaks. This adventure would not have been as successful as it was without you at my side.

Thank you to everyone! I wish the best of luck and success to Chi-Hak and the other PhD students that will come after me.

CONTENTS

Abstract	v
Résumé	vi
Publications	vii
Acknowledgments	xi
Contents	xiii
Acronyms	xvii
PREFACE	1
1 LASER DYNAMICS AND PHASE-CONJUGATION	5
1.1 Lasers	6
1.1.1 Principle	6
1.1.2 Semiconductor laser	8
1.1.3 Properties of a laser diode	10
1.2 Unlocking non-linear dynamics	14
1.2.1 History and fundamentals of chaos theory	14
1.2.2 Stability of lasers	16
1.2.3 Experimental schemes for observing chaos with a semiconductor laser	18
1.2.4 Properties of optical chaos from feedback	20
1.2.5 Applications of optical chaos	21
1.3 Phase-conjugate feedback	24
1.3.1 Phase-conjugate mirror	24
1.3.2 Experimental schemes	25
1.4 Semiconductor laser with phase-conjugate feedback	30
1.5 Conclusion	35
1.5.1 Motivations	35
1.5.2 Objectives	35
1.5.3 Outline	36

I	THEORY AND SIMULATION	37
2	MODEL AND SIMULATION OF A LASER DIODE WITH PHASE-CONJUGATE FEEDBACK	39
2.1	Rate equation model of a semiconductor laser with feedback	40
2.2	Normalized rate equations for a laser diode with PCF	43
2.2.1	Normalization	43
2.2.2	Steady-state solutions	44
2.3	Numerical simulation and analysis toolbox	48
2.3.1	Runge-Kutta algorithm	48
2.3.2	Bifurcation diagrams	49
2.3.3	Signal analysis	51
2.3.4	Summary	54
2.4	Conclusion	57
3	SELF-DETERMINING HIGH-FREQUENCY SELF-PULSATIONS	59
3.1	Evolution of the frequency of an external-cavity mode	60
3.2	Birth of an external-cavity mode	64
3.3	Difference with conventional optical feedback	67
3.4	Conclusion	69
4	LOW-FREQUENCY FLUCTUATIONS AND ITINERANCY ON EXTERNAL-CAVITY MODES	71
4.1	A common type of dynamics in laser diodes with optical feedback	72
4.2	Properties of LFF in a laser diode with PCF	76
4.3	Itinerancy	78
4.4	Deterministic coherence resonance	82
4.5	Conclusion	85
5	EXTREME EVENTS IN THE CHAOTIC DYNAMICS OF A LASER WITH PHASE-CONJUGATE FEEDBACK	87
5.1	History and definition of a criterion	88
5.2	Statistical characterization of extreme events	93
5.2.1	Counting and characterizing extreme events	93
5.2.2	Time between extreme events	97
5.2.3	Bifurcation to extreme events	98
5.3	Conclusion	102
	CONCLUSIONS OF OUR THEORETICAL WORK	103

II	EXPERIMENT	105
6	ITINERANCY AMONG EXTERNAL-CAVITY MODES AND CHAOS BANDWIDTH OF A LASER DIODE WITH PHASE-CONJUGATE FEEDBACK	107
6.1	Laser diode	108
6.2	Phase-conjugate mirror	110
6.2.1	SPS crystal	110
6.2.2	Self-pumped ring cavity setup	111
6.3	Operation and measurements	114
6.3.1	Complete experimental setup	114
6.3.2	Measurements in the time domain	116
6.3.3	Measurements in the radio-frequency domain	117
6.3.4	Measurements of the optical spectrum	117
6.3.5	Clarification about the mirror dynamics	118
6.4	Low-frequency fluctuations	120
6.4.1	Radio-frequency content of the signal	120
6.4.2	Spectrogram – observing the itinerancy experimentally	121
6.5	Chaos bandwidth and properties	124
6.6	Theoretical investigation of chaos properties	129
6.7	Conclusion	133
7	BIFURCATIONS TO HIGH-ORDER EXTERNAL-CAVITY MODES	135
7.1	Experimental setup	136
7.1.1	Laser diode	136
7.1.2	CAT configuration	137
7.1.3	Barium titanate crystal	138
7.1.4	Experimental setup and phase-conjugation performance	139
7.2	Bifurcations from steady-state operation to regime V	143
7.2.1	Evolution of dynamics with mirror reflectivity	144
7.2.2	High-order external-cavity modes	148
7.2.3	Regime V	149
7.2.4	Instability of the mirror	150
7.3	Conclusion	152
III	CONCLUSION	153
8	CONTRIBUTIONS AND PERSPECTIVES	155
8.1	Summary of the results	155
8.2	Perspectives	158
8.2.1	Chaos properties	158

CONTENTS

- 8.2.2 Understanding the physics 158
- 8.2.3 Other perspectives 159

IV APPENDICES 161

- A NORMALIZATION OF THE MODEL 163
- B NUMERICAL INTEGRATION OF THE MODEL 165
- C FRENCH SUMMARY – RÉSUMÉ EN FRANÇAIS 171
 - C.1 Introduction 172
 - C.1.1 Diode laser 172
 - C.1.2 Dynamique non-linéaire – Chaos 173
 - C.1.3 Chaos dans une diode laser 174
 - C.2 Résultats théoriques 177
 - C.2.1 Modes de cavité externe 177
 - C.2.2 Fluctuations à basses fréquences 178
 - C.2.3 Événements extrêmes 179
 - C.3 Résultats expérimentaux 183
 - C.3.1 Itinérance 183
 - C.3.2 Bifurcations 187
 - C.4 Conclusion 189

BIBLIOGRAPHY 191

ACRONYMS

ADC	Analog to Digital Converter
CCD	Charge-Coupled Device
COF	Conventional Optical Feedback
DFB	Distributed Feedback
EC	External Cavity
ECM	External-Cavity Mode
FFT	Fast Fourier Transform
FSR	Free Spectral Range
LASER	Light Amplification by Stimulated Emission of Radiation
LFF	Low-Frequency Fluctuations
MASER	Microwave Amplification by Stimulated Emission of Radiation
PCF	Phase-Conjugate Feedback
PCM	Phase-Conjugate Mirror
RF	Radio-Frequency
RK	Runge-Kutta
SLM	Spatial Light Modulator
SS	Steady-State
STFT	Short-Time Fourier Transform
VCSEL	Vertical-Cavity Surface-Emitting Laser

PREFACE

Words can be funny. For example, *laser* is actually the name of a plant also known as *silphium*. It comes from the latin *laserpicium* which tends to designate the resin that used to be extracted from different parts of the plant, shortened to *laser* when talking about the plant as a whole – *silphium* is the greek word for the plant. It was widely used during antiquity all around the Mediterranean basin and it was renowned for its culinary and medicinal properties which included birth control. It was the pride and wealth of the city of Cyrene – located in the North of the current Lybia – but it is now thought to be extinct and the word saw less and less use through the ages.

The modern use of the word *laser* does not really have an etymology as we generally expect. It is actually an acronym meaning Light Amplification by Stimulated Emission of Radiation (LASER), which is simply a description of how the device it designates works: it is a device that uses the physical process of stimulated emission of radiation to amplify light. LASER itself comes from another acronym: Microwave Amplification by Stimulated Emission of Radiation (MASER) and the first name suggested for a laser was *optical maser*.

As time passed, the LASER device grew to be more and more popular and the acronym became a common word, *laser*, with a plural *lasers*. It also gave birth to two verbs: 1/ *to lase* which is used to tell when a laser device enters its operational regime of amplification by stimulated emission, and 2/ *to laser* which means to apply a laser to something, as in surgical use for example, or to do something very precisely, in reference to the high directionality and low divergence of a laser beam.

The success of the laser device in popular culture, especially in science fiction but also in action films such as *Goldfinger* in 1964 a few years only after it had been invented, contributed to spreading the use of the acronym as a common word, to the point that probably most people do not know its original meaning¹. But lasers in the real world are generally far from what we see in fiction, either in terms of power, or in terms of size, even if significant development has been done in the recent years to make laser-based weaponry for purposes ranging from anti-ballistic measures to non-lethal riot control.

¹ To cite a similar example, I did not know until recently that the word *scuba* originated from an acronym too, meaning Self-Contained Underwater Breathing Apparatus (SCUBA).

The first application of lasers that comes to mind is maybe the laser pointer, making use of the high intensity and low divergence of a laser beam. Lasers can be used for leisure purposes, with light shows making good use of them. They can be used for leveling, distance-measuring, drilling, sawing, detection, aiming. Other applications that people have most probably heard about include medical and cosmetic uses: laser eye surgery, to replace scalpels, tumor removal, hair removal, tattoo removal.

But one of the most important applications that has driven investment and research over several decades is the use of laser diodes based on semiconductor materials for telecommunications, in conjunction with optical fiber for guiding light. It is mostly hidden from the eyes of users, but it is almost everywhere. The combination of low losses in the fiber compared to copper cables, its insensitivity to perturbations and crosstalk, and the possibility to modulate laser diodes quite fast have been really advantageous. Over the last decades, all long-distance communication lines have been replaced by optical fiber, with more and more cables at the bottom of the oceans all around the world. Continental and regional networks soon followed. And now metropolitan networks are transitioning too to allow optical fiber access to all residents with so-called *Fiber To The Home (FTTH)*.

This impulse has led to development of laser diodes for numerous wavelengths. The initial goal was to reach the 1550 nm wavelength where optical fibers present the minimum losses due to absorption. Other motivations such as storage on optical disks pushed to find materials suitable for emission at low wavelengths, where diffraction occurs for smaller apertures, which is what allows to store more data on Blu-Rays than on DVDs or CDs. As such, laser diodes with wavelengths ranging from 375 to 3500 nm are commercially available, although there are some wavelengths in between that are not accessible.

With new technologies such as VCSELs, we now have access to laser diodes with even lower power consumption and in the future, the development of lasers on silicon could have a big impact for integration with existing integrated circuits.

All of this did not happen without any difficulties of course. Coupling a laser diode into an optical fiber or putting it in front of the reflective surface of an optical disk can reflect some of the light back into the laser, a phenomenon we call optical feedback. It can lead the laser diode to dynamical regimes where it is completely unstable, with periodic oscillations or chaotic solutions depending on the intensity of the feedback. This problem can be solved by using an optical isolator, adequate coating, or angle-polished connections.

But if this phenomenon can be seen as a problem for engineers trying to design a stable system of telecommunications, it has also been seen as an oppor-

tunity for studying interesting dynamics by some scientists. After discovering that optical feedback had an impact on laser diode stability, scientists began to purposefully add reflection in front of a laser diode to understand the behavior of the laser. This has led to the discovery that a laser diode with feedback is capable of producing deterministic chaos.

Chaos appears random at first sight, but it can be shown that it is the output of a deterministic system. The first thoughts about chaos date back from the beginning of the twentieth century by Poincaré, but the chaos theory really emerged after a discovery by Lorenz in 1962. He found that some systems are sensitive to initial conditions, in the sense that a small modification of the initial state of a system can lead to great differences in its behavior after some time, also known as the butterfly effect. This is in part why we cannot reliably predict weather, which is a chaotic system, for more than a few days.

Studies of optical chaos showed that it is made of fast-evolving dynamics reaching bandwidths of several gigahertz. This makes a chaotic laser a good substitute to study experimentally chaos and its properties: it is really compact and capable of generating large amounts of data in only a few seconds. Beside understanding the physics of generating optical chaos, recent years have seen the emergence of chaos-based applications in random number generation and encryption of communications.

The work of this thesis lies in the continuation of these two motivations: understanding the physics of complex systems and chaotic dynamics, as well as thinking about potential applications of our findings. Here, we study a special kind of optical feedback, namely Phase-Conjugate Feedback (PCF) which involves effects from non-linear optics. As such, we will also discuss a bit about this additional complexity, but it will not be the center of the study since PCF is used as a means to an end. Indeed, through the work presented here, we want to show that using this special kind of feedback can lead to faster, more complex dynamics, interesting physics and potentially better results in applications.

In Chapter 1 we will introduce all the basic concepts of laser physics, chaos, and non-linear dynamics that are necessary for the overall understanding of the thesis. In Part I (Chapters 2 to 5), we present everything related to the model and the results of our simulations. Chapter 2 will present how we derive the model for our system and the numerical techniques we use, as well as tools from signal analysis. These tools and techniques will be put to use in Chapter 3 to study the behavior of fundamental self-pulsating solutions of the laser with PCF, in Chapter 4 to explain the mechanism that leads to the observation of Low-Frequency Fluctuations (LFF), and in Chapter 5 to reproduce chaotic dynamics with abnormally intense events. Part II (Chapters 6 and 7) presents the results of

our experimental investigations. In Chapter 6, we go back to the experiment after having gained much insight from our theoretical findings and we also test if our system exhibits optical chaos with characteristics potentially suitable for applications. In Chapter 7 we propose a second experimental configuration aimed at observing harmonic solutions of frequencies up to almost ten gigahertz. Finally we conclude on the contributions of this thesis to the field of non-linear dynamics and chaos in laser diodes in Chapter 8, as well as suggesting perspectives for future work.

LASER DYNAMICS AND PHASE-CONJUGATION

This first chapter is an introduction to the three concepts on which is built the work presented in this thesis. Some basic scientific knowledge is needed to grasp the physics involved but I hope it can provide the unfamiliar readers with a good idea of the premises and main results.

Section 1.1 is an introduction to the physics governing the operation of lasers and more specifically semiconductor lasers which are studied in this thesis. In Section 1.2 are presented the concepts of chaos theory and how complex systems can generate non-linear dynamics. It also provides several experimental configurations in which a semiconductor laser can be used to exhibit chaotic behavior, one of them being optical feedback to which our work is dedicated. To be precise, we use a special kind of mirror: a Phase-Conjugate Mirror (PCM). The operating principle of such a mirror and the nonlinear optics required to build it are presented in Section 1.3. A state of the art of Phase-Conjugate Feedback (PCF) in lasers is presented in Section 1.4. Finally, Section 1.5 contextualizes the work of this thesis and provides the outline of the document.

1.1 LASERS

1.1.1 *Principle*

The word 'laser' is actually an acronym which stands for Light Amplification by Stimulated Emission of Radiation (LASER), because it makes use of the stimulated emission of photons in an active medium. This mechanism was proposed by Albert Einstein [1, 2] in 1916 as a part of the old quantum theory. The existence of the phenomena was confirmed in 1928 by Rudolf W. Ladenburg.

To explain briefly the different kinds of interaction that can occur between light and matter, let us consider a single atom with two atomic levels: the ground level (of energy E_1) and the excited level (of energy E_2) – quantum mechanics dictates that an electron must have a discrete level of energy. Then there are three possible ways the system can evolve, depending on the initial conditions (see corresponding diagrams in Fig. 1.1).

1. Absorption: the electron is originally in the ground level, a photon with a frequency ν such that its energy $h\nu = \Delta E = E_2 - E_1$ hits the atom. Then the photon is absorbed and the electron jumps to the excited level.
2. Spontaneous emission: the electron is originally in the excited level. Without any interaction, it can spontaneously relax to the ground level by emitting a photon of energy ΔE in the process. The emitted photon has a random phase and direction of propagation. This phenomenon is analogous to the decay of radioactive materials.
3. Stimulated emission: the electron is originally in the excited level. Then, a photon of energy ΔE hits the atom, making the electron relax to the ground level, and emitting a second photon of energy ΔE , with the same phase and direction of propagation. This can be seen as a form of amplification.

We see now that the process of stimulated emission can be used to emit light at a specific wavelength, with a narrow linewidth where photons are in phase, a property we call coherence which is useful for making light interfere with itself. However, stimulated emission by itself is not enough to make a laser.

Indeed, a medium at room temperature is not likely to have most of its electrons in an excited state, which means that there cannot be enough stimulated emission to maintain amplification or a continuous field of emission. For amplification by stimulated emission to be the dominant process, we need to find a way to excite a lot of electrons, at least half the population to reach a state called

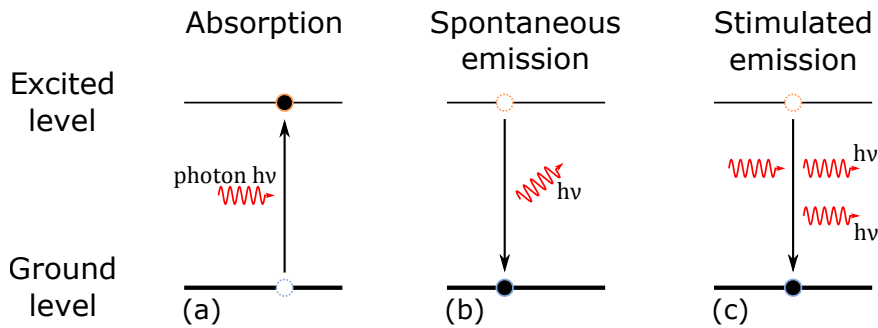


Figure 1.1: Three different mechanisms for light-matter interaction are presented here with a simple two-atomic-level atom which has an electron that can be on the ground level or on the excited level. (a) Absorption happens when the atom absorbs energy from a photon of energy $h\nu$ and transfers it to the electron which goes from the ground level to the excited level. (b) Spontaneous emission is the opposite, when an electron spontaneously and randomly relaxes to the ground level, its energy is converted into a photon of random phase and direction. (c) Stimulated emission needs an incoming photon to force the relaxation of an electron and to create a perfect copy – in phase, energy, and direction – of the first photon in the process.

population inversion. We do this by pumping, either optically from an auxiliary source of light or electrically via a bias current.

But even with pumping, it is not enough to create a laser. One needs to put the active medium inside a resonator, which is a cavity composed of two mirrors, with at least one of them being semi-transparent. The resonator helps confine photons inside the gain medium and along a direction of propagation to enhance the gain from stimulated emission. Hence, most photons are inside the cavity and only a small fraction of them exits the laser.

When the gain inside the cavity exceeds the losses – due to absorption in the medium, and the loss of photons exiting the cavity – the laser reaches its threshold and starts to emit a coherent beam of light. A typical intensity-versus-pump characteristic of a laser in Fig. 1.2 shows that emission starts after the pump parameter reaches a threshold at which the gain equals the losses.

The three requirements for building a laser can therefore be summarized as: 1/ a medium capable of spontaneous emission at the desired wavelength, 2/ pumping to achieve population inversion, and 3/ a cavity which acts as a resonator [3]. Of course, real-life examples of lasers are more complicated than the simple image presented here, e.g. it has been shown that a laser with only two states of energy cannot emit a continuous wave [4].

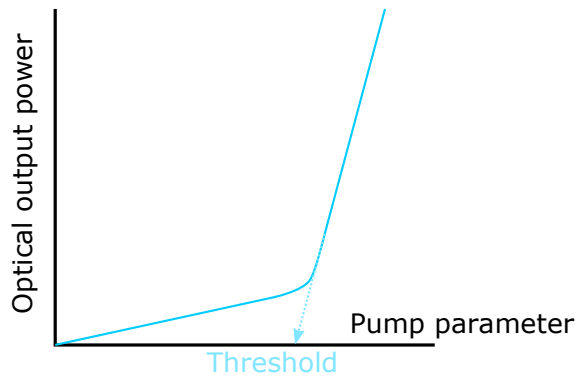


Figure 1.2: Schematic illustration of the intensity-versus-pump characteristic of a laser. Before threshold, emitted light is mostly due to spontaneous emission, and the system is not in the lasing state. Around threshold, the gain overcomes the losses and most of the photons are produced thanks to stimulated emission, hence creating a highly coherent and directional laser beam, with potentially high power.

1.1.2 Semiconductor laser

Making a laser with semiconductor material as the gain medium is a little more complicated. In semiconductor materials the energy levels are distributed in a conduction band and a valence band. A given range of energy between the highest energy of the valence band and the lowest energy of the conductive band – called bandgap – is forbidden for the electrons. Energy levels within conduction and valence bands can act similarly to the two atomic levels described previously.

Most lasers use a double-heterostructure where a thin active layer of positively doped (p-type) semiconductor material with low bandgap, is clad between strongly-doped n-type and p-type layers, represented in Fig. 1.3. The cladding layers have a larger bandgap, thus creating an energy well for holes and electrons inside the active region. This structure can be electrically pumped to add electrons to the conduction band or holes in the valence band. At the junction, where electrons and holes are confined in the active region, they can recombine to emit a photon (through spontaneous or stimulated emission) with an energy corresponding to the energy of the bandgap. As was the case with our first example of a laser, increasing the pumping leads to the population inversion, where lasing is possible. We should note here that for a laser diode, we talk about carrier density – proportional to the injection current – rather than population.

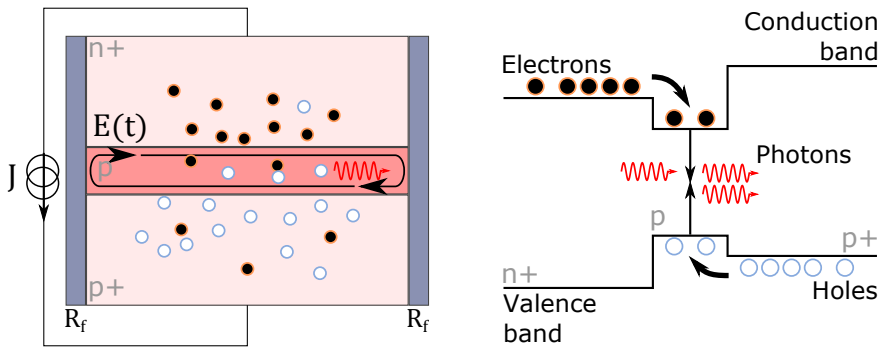


Figure 1.3: Schematic representation of a double heterostructure, commonly used in edge-emitting laser diodes. On the left, we see a cross-section of a laser, where light would be emitted towards the left and the right. The thin positively-doped active layer is clad between two strongly-doped (denoted by the + sign) n- and p-type materials. The structure is forward-biased with an electric current, bringing electrons in the n-type region and holes in the p-type region. On the right is the bandgap representation of the structure along the vertical axis, where we see the electrons and holes being trapped in the energy well formed by the three layers to enhance electron-hole recombination via stimulated emission.

Since its invention [5], a lot of so-called *bandgap engineering* has been done – and it is still going on – to find suitable materials and arrangements for the design of laser diodes emitting at any desired wavelength.

Laser diodes present an additional advantage. The n-doped and p-doped layers have a smaller refractive index than the active layer, a structure which acts as a guide for the light generated in the laser. This effect contributes to the reduction of losses in the cavity, and thus to a reduction of the lasing threshold. It allows to make lasers requiring low pumping energy, which has been essential for the development of telecommunications via optical fibers.

Now that we understand roughly what is going on inside a laser, we can try to find a phenomenological model that would help us understand and simulate how a laser behaves. For this, we will use the two variables I the intensity of the laser beam and N the population or carrier density. As we have seen, we need to model several phenomenons:

1. pumping, which contributes to the increase of carriers, modeled by its constant rate R .

2. stimulated emission, which is proportional to the intensity of the laser beam and to the carrier density, with a gain parameter g . It contributes to an increase of I and it consumes carriers, which makes N decrease, by the quantity $gI(t)N(t)$.
3. spontaneous emission, which consumes carriers by a quantity $\frac{N(t)}{\tau_s}$, but since photons emitted that way are random in phase and direction, they do not really contribute to the laser intensity. Thus, we neglect the influence of spontaneous emission on I . τ_s is called the population/carrier lifetime.
4. cavity losses, which lead to a decrease of the laser intensity by a quantity $\frac{I(t)}{\tau_p}$. τ_p is called the photon lifetime.

The behavior of a laser can thus be simply modeled as follows:

$$\frac{dI(t)}{dt} = gI(t)N(t) - \frac{I(t)}{\tau_p}, \quad (1.1)$$

$$\frac{dN(t)}{dt} = R - gI(t)N(t) - \frac{N(t)}{\tau_s}. \quad (1.2)$$

With these equations laid down, it is now simple to see that the pumping needs to be large enough to compensate for the consumption of carriers by stimulated and spontaneous emission. We also see that a laser is fundamentally a nonlinear system, because the modeling of stimulated emission implies the presence of a multiplication between the carrier density and the intensity of the laser field.

1.1.3 *Properties of a laser diode*

Relaxation-oscillation frequency

We can now try to figure out what is going to happen when the laser is turned on. After the onset of an injection current step, the carrier density will increase mostly linearly. Once there is a large number of carriers, and a few photons are present in the cavity, stimulated emission can begin, and the laser intensity increases rapidly. Associated with the increase of output power the carrier density decreases because carriers are consumed by stimulated recombination. The decrease in carriers leads to a decrease of laser power down to situation where the carrier density can build up again, and the cycle goes on with less and less

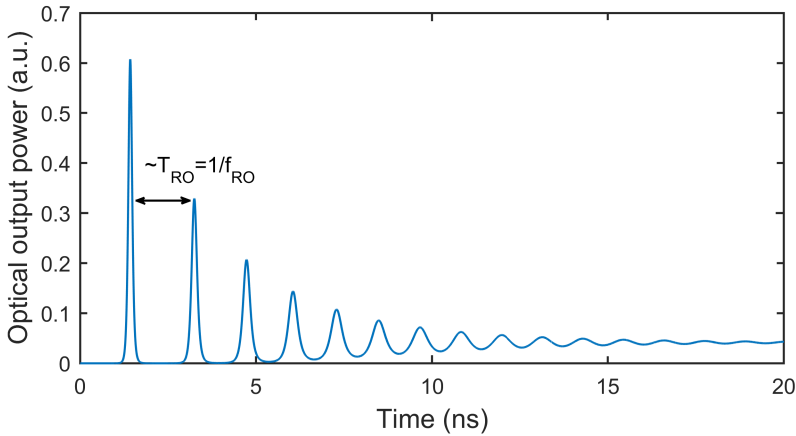


Figure 1.4: At $t = 0$, the injection current is turned on. The carrier density builds up until stimulated emission consumes all the carriers and the process repeats until the system reaches an equilibrium and continuous wave emission. The pulses occur at a frequency we call relaxation oscillation frequency and they are exponentially damped as time goes by.

oscillation amplitude until the laser settles on a steady-state of continuous wave operation, as illustrated in Fig. 1.4.

This dampened oscillating motion observed at the turn-on of the laser is called the relaxation oscillation, which happens at a specific frequency f_{RO} . It is one of the most important characteristics of a laser diode. Often, it represents the frequency range of the dynamics that a specific laser diode can exhibit. The value of f_{RO} can be derived from Eqs. (1.1), (1.2) (detailed by Uchida in Ref. [6]):

$$f_{RO} = \frac{1}{2\pi} \sqrt{\frac{p-1}{\tau_p \tau_s}}, \quad (1.3)$$

where $p = \frac{R}{R_{th}}$ is the pump parameter with R being the pump strength and R_{th} its value at the lasing threshold. For semiconductor lasers, the frequency of relaxation oscillations is typically of the order of a few gigahertz.

Even during normal operation of a laser diode at its steady-state, it is common to observe irregular oscillations at a frequency close to f_{RO} due to thermal and quantum noises in the gain medium, or due to perturbations in the pump. As such, it is easy to imagine that any additional perturbation that we are going to add to the system is prone to excite – regularly or irregularly – this *natural* frequency of the laser. This can lead to observation of sustained oscillations at the

relaxation frequency, also called undamped relaxation oscillations, or to chaotic dynamics¹.

Henry factor

However, a semiconductor laser is more complex than that and it is possible to obtain a set of equations that describes more accurately our system by considering a traveling-wave model. Indeed, inside the laser cavity we can consider that there are two waves traveling, one forward and another backward with the same optical frequency, schematically represented in Fig. 1.3. Using boundary conditions at the laser facets and properties of the semiconductor material, it is possible to derive another set of equations [6]:

$$\frac{d\hat{\mathbf{E}}(t)}{dt} = \left[\frac{1 + \imath\alpha}{2} \left\{ G_N(N(t) - N_0) - \frac{1}{\tau_p} \right\} + \imath\omega \right] \hat{\mathbf{E}}(t), \quad (1.4)$$

$$\frac{dN(t)}{dt} = \frac{I}{q} - \frac{N(t)}{\tau_e} - G_N(N(t) - N_0)|\hat{\mathbf{E}}(t)|^2, \quad (1.5)$$

where $\hat{\mathbf{E}}(t)$ is the complex electric field and $N(t)$ the real carrier density. N_0 is the carrier density at which the medium becomes transparent, G_N is the gain for stimulated emission, τ_p and τ_e are the decay rate of photons and carriers in the laser. And here, we introduce the parameter α [7] known under several names: the Henry factor, the linewidth enhancement factor or simply the alpha factor. It represents the ratio of the real and imaginary parts of the complex electric susceptibility and it is quite large for semiconductor lasers, with values typically ranging between 2 and 7.

The Henry factor is primarily responsible of enhancing the linewidth of the emitted beam by factor $1 + \alpha^2$, which is quite significant with the typical values mentioned, hence its name of *linewidth enhancement factor*. A large value of α also makes the laser more sensitive to perturbations. Thus, it is easier to observe chaotic dynamics in a laser with a large alpha factor.

This approach to modeling a semiconductor laser is useful because we could not have guessed the existence of the Henry factor from the phenomenological approach we used to establish Eqs. (1.1) and (1.2). Indeed α is a parameter that couples the phase and amplitude of the electric field, hence it cannot be

¹ Nonlinear and complex dynamics, highly sensitive to initial conditions, that can appear in systems with three or more degrees of freedom. See Sec. 1.2 for an introduction on chaos and nonlinear dynamics.

accounted for in intensity rate equations. However, by considering $\alpha = 0$, it is easy to show that Eqs. (1.4) and (1.5) are equivalent to our previous model.

When including the modeling of the effects of optical feedback in Part I, we will use Eqs. (1.4) and (1.5) as our starting point, as it has historically been done by Lang and Kobayashi in Ref. [8].

1.2 UNLOCKING NON-LINEAR DYNAMICS

1.2.1 *History and fundamentals of chaos theory*

The history of chaos and nonlinear dynamics can be traced back to the end of the nineteenth century with the theorem of Poincaré-Bendixon (1881-1901) stating that for a given continuous two-dimensional system modeled by

$$\frac{dx}{dt} = f(x), \quad (1.6)$$

where f is a function from the plane to the plane, the asymptotic solutions can only be a fixed point or a limit cycle. A limit-cycle would be an ellipsis in phase-space², meaning that the variables follow a periodic evolution. However, that theorem cannot be extended to dimensions $n > 2$. It is therefore possible to observe more complex solutions in systems of higher order.

When studying the three-body problem after King Oscar II of Sweden put up a prize that would be awarded to anyone finding a solution, Poincaré and his peers – Mittag-Leffler, Weierstraß, Sundman – formulate the first ideas about bifurcations of complex systems, quasiperiodicity, and mention that, in the case of planet orbits around the sun, small variations in the initial conditions can have a great influence on the predicted motion of planets [9].

Throughout the twentieth century, other hints at chaotic behavior and turbulent motion were found in radio engineering, fluid physics, but the lack of a proper theory impeded further development and a full understanding.

The advent of electronic computing and some experiments like the logistic map helped mathematicians formulate what we now call the *chaos theory* in the second half of the twentieth century. Pioneering work was done by Lorenz starting in 1963 when he was studying a weather model based on Navier-Stokes equations:

$$\frac{dx}{dt} = \sigma(x - y), \quad (1.7)$$

$$\frac{dy}{dt} = \rho x - xz - y, \quad (1.8)$$

$$\frac{dz}{dt} = xy - \beta z, \quad (1.9)$$

² A space composed of variables representing the system e.g. angular position and velocity of a pendulum, in which a periodic evolution would be represented as an ellipsis. See Sec. 2.3.3 for more details.

where x , y , and z are the three variables of the system and σ , ρ , and β are the parameters. Simulating these equations on a computer, Lorenz obtained non-regular oscillations and discovered accidentally that the system was very sensible to initial conditions. When printing the values of a point in the middle of one simulation, he only had access to approximations of the real values stored in the computer's memory. By injecting this mid-simulation approximate state as the starting point of another simulation, he found that the computer would predict different trajectories for the three variables [10] as illustrated in Fig. 1.5. This discovery led to the modern chaos theory, with links to the fractal theory that was developed around the same time by Mandelbrot.

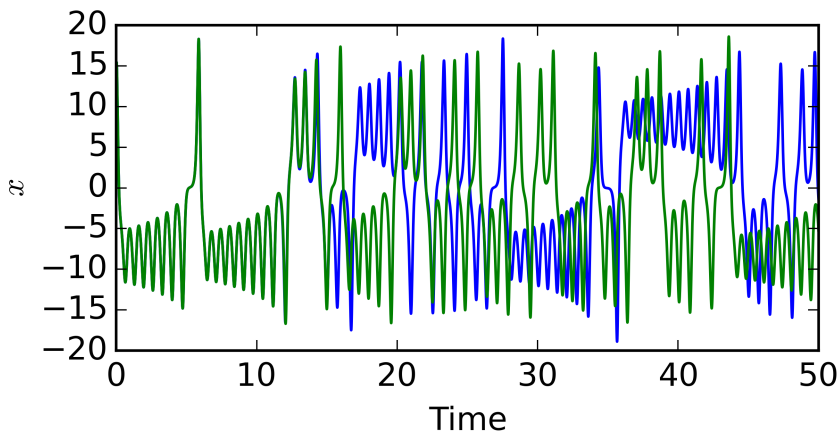


Figure 1.5: Simulation of Eqs. (1.7)-(1.9) with a Runge-Kutta (RK) algorithm for two initial states that differ only slightly. For a little duration, the two trajectories (blue and green) follow the same evolution, but after a long enough time, they are completely different.

Although there is no single and universal mathematical definition of chaos, we can keep in mind these three properties of a chaotic system:

1. Determinism: all the dynamics exhibited are not due to any kind of perturbation, be it internal noise or external forcing.
2. Sensitivity to initial conditions: two trajectories with slightly different initial states will become more and more different as time goes by (see Fig. 1.5). The divergence rate can be measured by so-called Lyapunov exponents of the system on which we give more details in Section 1.2.4.
3. The possible trajectories of the system will form a strange attractor in an adequate phase-space (see illustration in Fig. 1.6). It was later shown that

there were links between this kind of attractors and fractals which are objects of non-integer dimension [11].

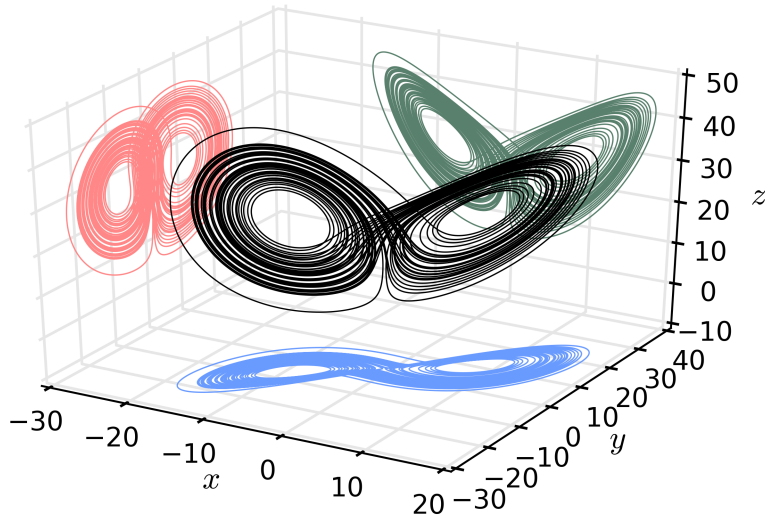


Figure 1.6: Approximation with a single trajectory of the strange attractor characterizing the Lorenz set of equations. It is dubbed the butterfly.

Since then, chaos has been explored in many different fields of physics. In particular, we can now wonder about the stability of lasers: is it possible to obtain chaotic dynamics from a solitary laser without forcing or perturbation?

1.2.2 *Stability of lasers*

To answer the question about the stability of lasers, people have traditionally used a model derived from the Maxwell-Bloch equations, introducing the polarization via Schrödinger equations. This gives the following set of equations for a single-mode laser [12]:

$$\frac{d\mathbf{E}(t)}{dt} = -\frac{\kappa_c}{\gamma_{\parallel}} [\mathbf{E}(t) + A\mathbf{P}(t)], \quad (1.10)$$

$$\frac{d\mathbf{P}(t)}{dt} = -\mathbf{P}(t) - \mathbf{E}(t)D(t), \quad (1.11)$$

$$\frac{dD(t)}{dt} = \frac{\gamma_{\parallel}}{\gamma_{\perp}} \left[1 - D(t) + \frac{1}{2}(\mathbf{E}^*(t)\mathbf{P}(t) + \mathbf{E}(t)\mathbf{P}^*(t)) \right], \quad (1.12)$$

where $\mathbf{E}(t)$ is the complex slowly varying envelope of the electric field, $\mathbf{P}(t)$ is the complex atomic polarization and $D(t)$ is the real population inversion. κ_c , γ_{\parallel} , and γ_{\perp} are the decay rates of, respectively, the electric field, the population inversion, and the atomic polarization.

These equations and parameters are used to separate the different kind of lasers into three classes [13]. In class C lasers the three decay rates are of the same order of magnitude and the three equations are needed to fully model the behavior of the laser, e. g. He-Ne lasers operating at the 3.39 μm line. With three state variables ($\mathbf{E}(t)$, $\mathbf{P}(t)$, and $D(t)$) governed by three equations, class C lasers are thus candidates for exhibiting chaos. In fact, it has been shown that Eqs. (1.10)-(1.12) are directly equivalent to the Lorenz Eqs. (1.7)-(1.9) [14]. As such, this makes a laser an interesting system for studying chaotic behavior, with time scales much faster than the time scales of weather dynamics.

Class A lasers are characterized by their polarization and population inversion decay rates being very large compared to the electric field decay rate, which means that variables \mathbf{P} and D are considered to be dependent of \mathbf{E} , thus only one equation is needed to describe the system, e. g. He-Ne lasers operating at the 632.8 nm line. These lasers are considered to be strongly stable and cannot exhibit chaotic dynamics in free-running operation.

Finally, between those two classes lie class B lasers, a category that includes semiconductor lasers for which only the polarization decay rate can be considered very large when compared to the other decay rates. Polarization can therefore be adiabatically eliminated [12]. Thus we consider $\frac{d\mathbf{P}(t)}{dt} = 0$ in previous equations, which gives $\mathbf{P}(t) = -\mathbf{E}(t)D(t)$ and the system can be modeled as follows [6]:

$$\frac{d\mathbf{E}(t)}{dt} = \frac{\kappa_c}{\gamma_{\parallel}} (-1 + AD(t))\mathbf{E}(t), \quad (1.13)$$

$$\frac{dD(t)}{dt} = \frac{\gamma_{\parallel}}{\gamma_{\perp}} (1 - D(t) - |\mathbf{E}(t)|^2 D(t)). \quad (1.14)$$

This approach using Maxwell-Bloch equations confirms what we already gathered from Eqs. (1.4) and (1.5) that we derived with a traveling-wave model: semiconductor lasers can be modeled with three equations (\mathbf{E} is complex) but the phase equation is decoupled from the two other equations. Thus they only have two degrees of freedom and according to the Poincaré-Bendixon theorem they cannot exhibit chaotic dynamics on their own³. However, by adding a source of perturbation, modulation, we add degrees of freedom to the system which can lead to unstable operation of the laser. Several schemes have been proposed and thoroughly analyzed throughout the years and we briefly present them in the next section.

1.2.3 Experimental schemes for observing chaos with a semiconductor laser

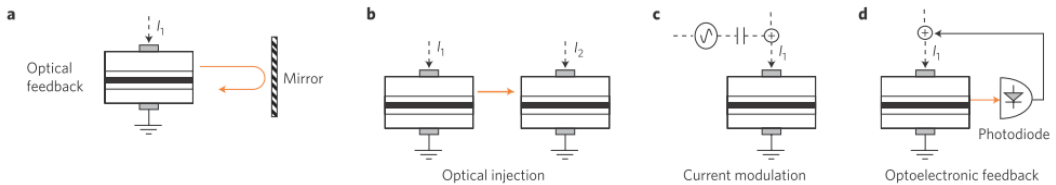


Figure 1.7: (a) Optical feedback from a conventional mirror. (b) Unidirectional optical injection from a master laser on the left into a slave laser on the right. (c) Modulation of the injection current of the laser diode. (d) Hybrid optoelectronic feedback where the output of a photodetector drives the injection current of the laser. Figure from [16].

Three main techniques – and a lot of variations around those – have been proposed and are used to drive a laser diode to chaotic dynamics (see illustrations in Fig. 1.7):

1. **Optical injection.** It consists of unidirectionally injecting the light from a so-called *master* laser into a *slave* laser. By adjusting the frequency detuning between the two lasers, and the relative intensity injected in the slave laser, a wide range of dynamics can be unlocked [17–19]. Some experiments focus on the injection of a chaotic master laser in a slave laser [20].
-
- 3 It has been shown that some laser diodes can emit chaotic output power without any additional perturbation, e.g. a quantum-dot Vertical-Cavity Surface-Emitting Laser (VCSEL) in Ref. [15] but this is a more complicated kind of laser with two competing polarization modes. This intrinsic complexity means that a third equation needs to be added to faithfully model the polarization dynamics, adding a degree of freedom to the system, which makes this example consistent with the arguments presented here.

2. External current modulation. Through modulation of the injection current of the laser diode, one can also obtain non-linear dynamics. It seems simple at first glance but it is in fact hard to obtain good experimental results because it requires strong and fast modulation to enter nonlinear regimes and the route to chaos is typically blurred by laser noise [21, 22].
3. Feedback. Simply adding a mirror in front of the laser to feed part of the emitted beam back into the laser cavity is enough to destabilize the laser into non-linear dynamics [16, 19]. The laser interacts with a time-delayed version of the power it emitted, thus introducing an important parameter: the length of the External Cavity (EC).

The first two solutions simply add an equation to the system, thus making it three-dimensional, which is enough to produce chaos as we have seen previously. The third technique is a little bit more complicated: by introducing a time-delay τ into the system, we create in fact an infinite-dimensional system. Indeed, the initial state of the system is not simply a set of values at $t = 0$ anymore, but it requires the complete knowledge of the evolution of the system on the interval $[-\tau, 0]$.

By introducing a delay τ in the system, we also introduce the associated frequency $f_{EC} = \frac{1}{\tau}$ in the dynamics of the system. Dynamics can then be classified in two main categories:

1. $f_{EC} \gg f_{RO}$. For short cavities, the observed dynamics typically include pulsating behavior at the external-cavity frequency [23, 24] and quasiperiodicity in the form of regular pulse packages [25, 26].
2. $f_{EC} \ll f_{RO}$. For long cavities, the dynamics are generally more complex, with fully-developed chaos in the form of Low-Frequency Fluctuations (LFF) [27–29], coherence collapse [30]. The chaotic attractors are typically high-dimensional [31] and the Radio-Frequency (RF) spectra are the most broadband [32, 33].

Additional work has been done through the last decades by considering different types of feedback: pure Conventional Optical Feedback (COF) as we have just described, optoelectronic feedback where the intensity of the laser is measured by a photodetector which modulates the injection current of the laser (see Fig. 1.7-(d)), filtered feedback where only one longitudinal mode is fed back, incoherent feedback [34], polarization-rotated feedback especially in VCSELs which can emit light in one of two orthogonal polarization states resulting in switching

dynamics between different polarization modes. VCSELs are particularly interesting for their low threshold current resulting in low energy consumption, their circular output beam, and their geometry where emission by the top surface instead of the edge allows for easier design of arrays.

In the work presented here, we study the specific case of PCF where the phase-conjugate of the electric field of the laser output is fed back into the cavity after a delay τ . COF is also briefly studied for the sake of comparison when necessary.

1.2.4 Properties of optical chaos from feedback

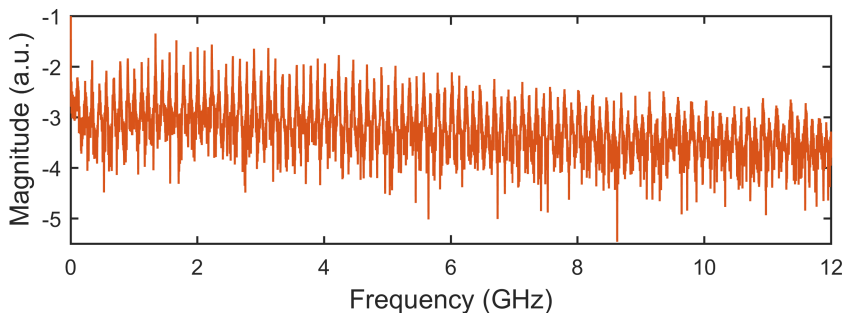


Figure 1.8: Example of an RF spectrum of the laser output intensity exhibiting chaotic dynamics in the long-cavity regime.

Adding a new frequency in the system in the form of f_{EC} can make for complex dynamics to study. RF spectra of a laser diode with feedback in a chaotic regime usually show excitation of the EC frequency and a lot of its harmonics, especially for long cavities as illustrated in Fig. 1.8. This is usually explained by some itinerancy among so-called External-Cavity Modes (ECMs) [28, 35] where the hopping between the different modes generates the numerous frequency components.

It is not uncommon to observe the frequency of relaxation oscillations being excited too, as suggested previously. In the example of Fig. 1.8, it can be seen around 2 GHz where the baseline of the spectrum is slightly higher.

We can use different measurements to characterize chaotic dynamics:

- These broadband RF spectra can be characterized by their bandwidth, a measure useful when considering applications of optical chaos. Of course, the usual definition of the bandwidth being the cutoff frequency at -3 dB cannot be considered here because of the resonances of harmonics of f_{EC} .

A commonly adopted definition [36, 37] defines the bandwidth of a chaotic system as the frequency which includes 80 % of the total power, which is quite simple to compute. Other definitions have been proposed that could lead to a better identification of the real bandwidth available but they have yet to be tested on different configurations [38].

- A dynamical system can be characterized by its Lyapunov exponents which form a spectrum. These exponents measure how quick two similar time traces converge or diverge. Having an infinite number of degrees, a laser with feedback theoretically has an infinite number of Lyapunov exponents. They can be derived from the equations themselves or can be estimated on time traces [39] but they are generally very hard to obtain.

Thankfully, since only the positive exponents are useful to characterize chaotic behavior – because they are the ones estimating the divergence, whereas the negative ones would make similar trajectories converge – the actual dimension of such a system is considered to be equal to the number of positive Lyapunov exponents. In some cases, the knowledge of the largest one only is enough to characterize the system [31, 40–42].

- The complexity of a chaotic system can also be characterized by its unpredictability, which has historically been measured by the Kolmogorov-Sinai entropy. It can be derived from the positive Lyapunov exponents of the system or it can be estimated through other means. But it is generally another quantifier that is hard to compute.

Recently, another quantifier, permutation entropy, has been shown to be easier to compute on time traces and it gives results similar to the ones that would give Kolmogorov-Sinai entropy [42, 43]. Thus, it is a possible alternative for characterizing a chaotic system. It is based on the probabilities of apparition of different ordinal patterns in time traces and gives good results if the traces are very long.

1.2.5 *Applications of optical chaos*

Systems that exhibit the appropriate properties as just described, i. e. large complexity and large bandwidth, can be considered for several applications [16].

First, they can be used for chaos communication, which requires the synchronization of two laser diodes through optical injection (see Fig. 1.7), where the master laser is the emitter and the slave is the receiver. By choosing similar internal parameters for the two lasers, we can make sure that the chaos produced

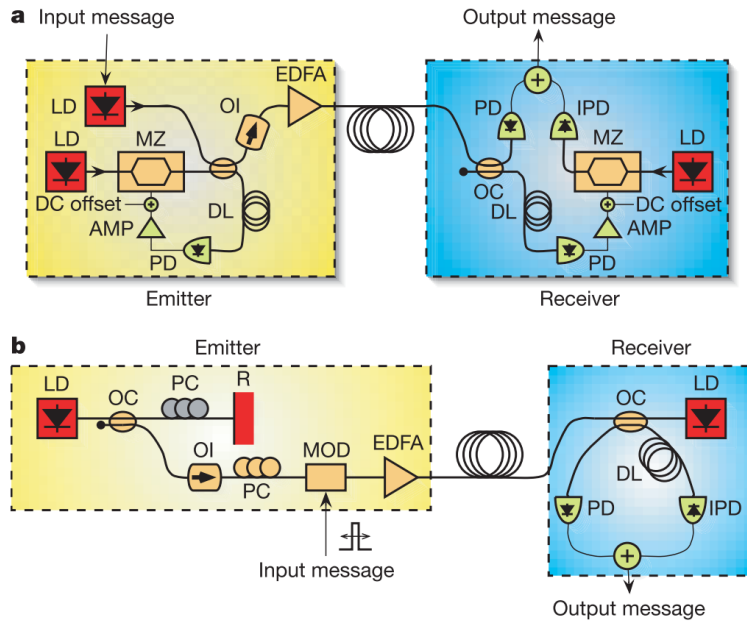


Figure 1.9: Two schematic setups operating at $1.55 \mu\text{m}$ and tested for chaos-encrypted communications. (a) The optoelectronic scheme in which the output of the laser diode is strongly and nonlinearly modulated. (b) The all-optical scheme in which optical feedback is used to destabilize the emitting laser and the message is modulated on the output signal of the laser diode. In both cases the message is recovered by subtraction of the carrier from the signal received. Figure from Ref. [44].

by the master is reproduced by the slave [45, 46]. A signal can then be added to the chaotic carrier – provided that the signal is weak enough when compared to the carrier, and strong enough not to be drowned in noise – and the slave laser will synchronize on the chaos only, thus allowing to recover the signal with a simple subtraction [47]. An eavesdropper can only recover the signal if they possess a similar laser device. The complexity of the chaos is also important for the eavesdropper not to be able to reconstruct the carrier. The chaotic bandwidth is important to guarantee a high-speed operation of the encrypted line of communication [44]. Figure 1.9 presents two examples of schemes used for chaos-encrypted communications and tested on the metropolitan area network of the city of Athens, Greece.

Second, they can be used for generation of random numbers, even though randomness and chaos are two distinct concepts [15, 48]. Since a chaotic system is sensitive to initial conditions, even a tiny amount of noise can be amplified by

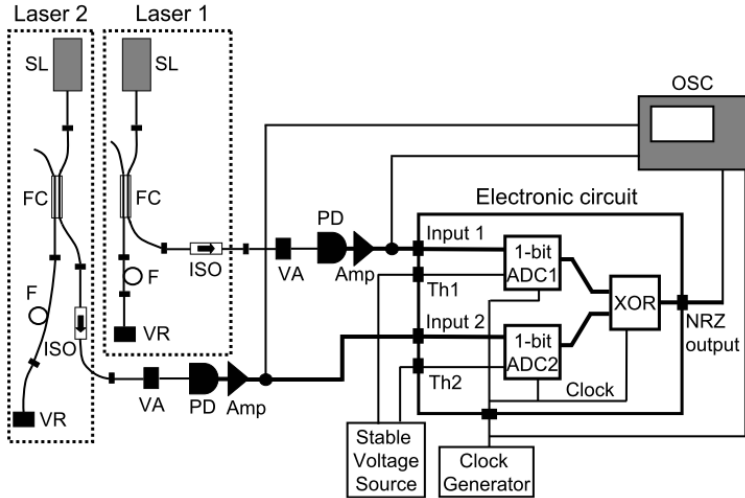


Figure 1.10: The chaotic outputs of two laser diodes with optical feedback are measured by two 1-bit Analog to Digital Converters (ADCs). A simple logic gate, here a XOR is used to combine the two bits. The stream of bits at the output of the logic gate has proven to be random. Figure from Ref. [48].

the chaotic system, provided it has at least one large Lyapunov exponent. Random number generators based on optical chaos are thus often characterized by their entropy and they are capable of producing random bits at bit rates up to hundreds of $\text{Gb}\cdot\text{s}^{-1}$. They are far quicker than traditional generators based on, e. g. thermal noise sources. Figure 1.10 illustrates the first experimental configuration used to generate random numbers from optical chaos [48].

Finally, they can be used for a range of other applications, including optical sensing at long distances with so-called chaotic radars or replication of transistor-like behavior [16].

1.3 PHASE-CONJUGATE FEEDBACK

PCF is a special kind of optical feedback where the electric field of the output beam of a laser diode is phase-conjugated before being fed back into the laser cavity. However, unlike conventional mirrors which are standard pieces of optical equipment, PCMs are not readily available in a single component. They have to be built by using additional optical techniques.

1.3.1 Phase-conjugate mirror

Mathematically speaking, two optical waves are considered to be phase-conjugated to each other if their complex amplitude functions are conjugated with respect to their phase factors. This means that, considering a planar complex wave traveling through space along z -axis [49]

$$\vec{\mathbf{E}}(z, x, y, t) = \vec{\mathbf{E}}(z, x, y) \exp(-i\omega t) = \vec{\mathbf{A}}(z, x, y) \exp [i(kz + \phi(z, x, y)) - i\omega t], \quad (1.15)$$

then the backward frequency-degenerate phase-conjugated wave is defined as

$$\vec{\mathbf{E}}'(z, x, y, t) = \vec{\mathbf{E}}'(z, x, y) \exp(-i\omega t) = \vec{\mathbf{A}}'(z, x, y) \exp [-i(kz + \phi(z, x, y)) - i\omega t]. \quad (1.16)$$

This is only a simple example. Of course, in real-life applications, the waves are not necessarily monochromatic and the phase-conjugated wave can be non-degenerate, in which case the detuning between the two waves can have a more or less important impact. But this is enough to understand how a PCM works.

To illustrate how it works (see Fig. 1.11) let us consider a plane wave interacting with a disturbing medium before being reflected and see how a conventional mirror and a PCM differ. The disturbing medium distorts the wave front and by reflecting on a conventional mirror, the backwards wave is distorted again by the medium (see Fig. 1.11-(a)). However, since the backwards wave keeps the same wavefront after reflection on a PCM, passing through the disturbing medium the second time cancels the anomaly and the plane wave is restored (see Fig. 1.11-(b)).

It is interesting to note that the tilt of the PCM has no importance since the mirror will always generate the backwards phase-conjugated wave. This is a really useful property for optical feedback since we do not have to worry about

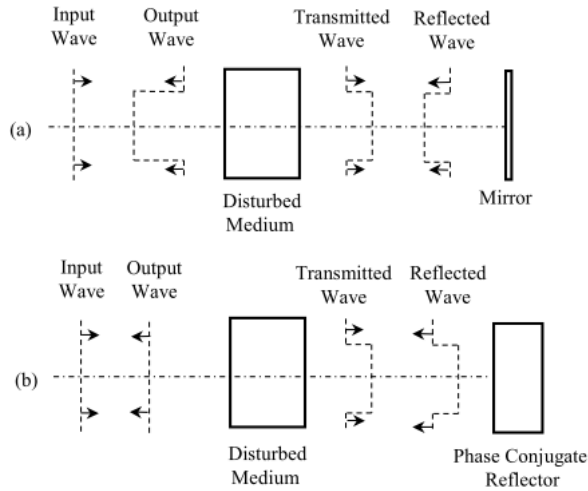


Figure 1.11: (a) A planar wavefront is distorted and then reflected on a conventional mirror. Distortion is accumulated as the reflection travels backwards. (b) In the case of a PCM the wavefront is maintained upon reflection and the distortion is reversed when the wave travels backwards. Figure from [49].

aligning the feedback wave into the laser cavity. It also means that our example works even if the wavefront is not planar⁴.

However, it only works if the disturbing medium is the same during the forward and backward propagation. Variations over time in the disturbing medium can be attributed to temperature changes inducing refractive index changes or motion of a non-homogeneous fluid in general, moving sample if it is live tissue for example. These phenomenon are generally quite slow relatively to the propagation of light forward and backward which usually occurs in less than a few nanoseconds. So it is safe to assume that in most cases the disturbing medium is the same during forward and backward propagation.

1.3.2 Experimental schemes

Backward four-wave mixing

Backward degenerate four-wave mixing is probably the most popular and most studied way of creating a PCM since it was proposed in 1977 [50]. It is achieved in

⁴ These properties mean that if one was looking at a phase-conjugate mirror, whatever the angle each eye would only see an image of its own pupil, assuming it would be possible to build such a mirror.

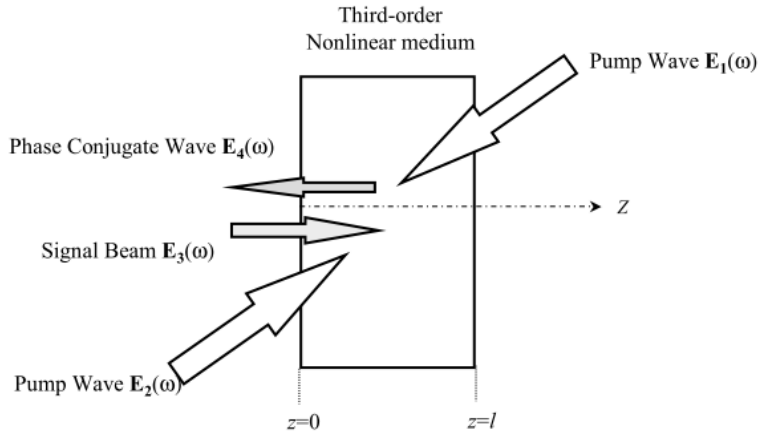


Figure 1.12: Schematic illustration of frequency-degenerate four-wave mixing. Two strong pump beams interact with a weak signal beam in a third-order nonlinear medium to create a fourth beam which is the phase-conjugate of the signal beam. If the pump beams are carefully aligned in the opposite direction, then the created beam is also in the opposite direction of the signal beam. All waves have the same frequency. Figure from [49].

a third-order non-linear medium thanks to two (strong) pump beams traveling in the opposite direction and one (weak) signal beam traveling in any direction. It can be shown that this configuration creates a refractive index grating inside the medium. Diffraction of the pumps and signal on the induced grating creates a fourth beam that is phase-conjugated with respect to the signal beam and which travels in the opposite direction, as illustrated in Fig. 1.12 [49]. Interestingly, such a configuration can yield a mirror reflectivity (the ratio between the power of the backward phase-conjugate wave and the power of the incident wave) greater than 100 % owing to the fact the power transferred to the phase-conjugate wave comes from the pump beams that can originate from an external source of high power compared to the signal beam.

Since the principle of this method is very general, any material can be used provided it has a strong enough third-order non-linearity – measured by its $\chi^{(3)}$ coefficient – at the desired wavelength. As such, a lot of different materials have been shown to be able to produce optical phase-conjugation⁵ [49]:

1. Absorbing liquid and solid materials, such as dye solutions [51], dye-doped matrices [52], impurity-doped glasses [53] and crystals [54], fullerenes-

⁵ The list of articles cited here is non-exhaustive and more examples can be found in the bibliographies of those references.

- related materials [55], and liquid crystals [56], where the refractive-index grating is induced by population change or opto-thermal effect.
2. Lasing media, such as CO₂ [57], Nd:YAG [58] and others, where the main mechanism of refractive-index change could be the periodic spatial modulation of population.
 3. Metal vapors, such as Na, K, Rb, Cs [59, 60].
 4. Photorefractive materials, such as LiNbO₃, BaTiO₃, SBN, SPS and much more [61], where the changes in the refractive index of the medium are photo-induced. These materials are among the most studied and we are going to use these for several reasons.

Backward stimulated scattering

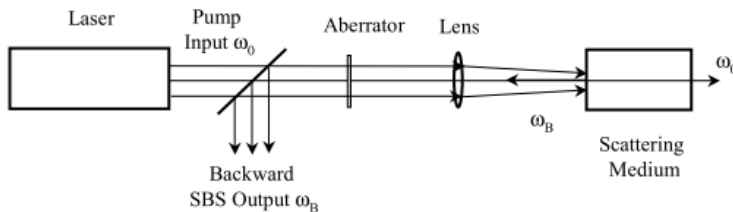


Figure 1.13: Experimental configuration for generating a phase-conjugated wave with a scattering medium. Figure from [49].

Probably the simplest setup of all, the backward stimulated scattering technique needs a focused laser beam input and a scattering medium (see Fig. 1.13). The theoretical explanation is based on the fact that the input wave is only quasi-collinear – especially with an aberrator – and the non-collinear parts of the wave act as signal beams that are phase-conjugated thanks to the incident wave and the main back-scattered component acting as pumps [49, 62]. As with other techniques, a refractive-index grating is formed in the scattering medium. But it produces a non-degenerate phase-conjugated wave which means that it would be more complicated to study for an optical feedback experiment.

First observed with stimulated Brillouin scattering in 1972 [63], it has also been reported to work with stimulated Raman scattering [64], and stimulated Rayleigh-wing scattering [65].

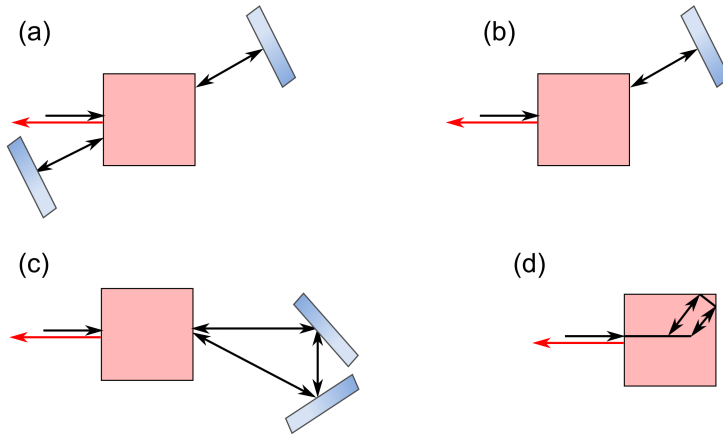


Figure 1.15: Four configurations for self-pumped optical phase-conjugation with a photorefractive crystal: (a) linear, (b) semi-linear, (c) ring cavity, and (d) CAT. The deviated beams are produced thanks to fanning in the photorefractive crystal, a phenomenon where diffusion is amplified in one direction of the crystal. CAT configuration requires the crystal to have polished faces to make use of total internal reflection.

self-pumped configuration where the reflectivity can theoretically reach 100 % [68–70]. Figure 1.15 presents examples of self-pumped configurations where thanks to multiple passes through the crystal, the same beam acts as the signal and as pumps. This makes the experiment easy to set up, with only one laser to align and most importantly, it produces a frequency-degenerate phase-conjugated signal. If we used external pumping, there would be a frequency detuning between the signal and the backward phase-conjugated wave, which would be an important parameter for optical feedback.

In practice, lower reflectivities have been reached, because of absorption losses in the medium, imperfect mirrors, Fresnel reflections. Examples in a ring cavity setup include 17 % reflectivity with BaTiO_3 in Ref. [71], 9 % with tellurium-doped $\text{Sn}_2\text{P}_2\text{S}_6$ in Ref. [72]. 50 % has been reached with KNbO_3 in a feedback loop configuration in Ref. [73] or 16 % in BaTiO_3 . Good results have been achieved using the CAT configuration and a BaTiO_3 crystal with 50 % in Refs. [32, 74].

In this thesis, we choose to make our PCM with four-wave mixing in a photorefractive medium for several reasons. Choosing a self-pumped configuration makes for easier alignment and simpler modeling since there is no detuning to account for. This leaves us with several choices for four-wave mixing medium.

Here, we choose photorefractive material since it has been used with good results in several previous experiments analyzing the behavior of semiconductor lasers with PCF [24, 32, 75–77]. Lasing medium and metal vapors have been used too but less frequently and not in self-pumped configurations [78, 79]. Finally, nonlinear optics is one of the strengths of our group and photorefractive materials were readily available for experimenting with.

In particular, we will use two different configurations in this thesis: the ring cavity (see Fig. 1.15-(c)) with a $\text{Sn}_2\text{P}_2\text{S}_6$ crystal doped with tellurium in Chapter 6 and the CAT configuration (see Fig. 1.15-(d)) with a rhodium-doped BaTiO_3 crystal in Chapter 7 since we wanted to reach higher values of the reflectivity.

For modeling and simulation in Part I, the method used to make the PCM does not have an influence on the model we use, as long as it is self-pumped, meaning that there is no frequency detuning.

1.4 SEMICONDUCTOR LASER WITH PHASE-CONJUGATE FEEDBACK

PCF into a semiconductor laser diode has already been performed in the past with studies dating back to 1986. At first, the motivations were to take advantage of the self-aligning property of the PCF and to get rid of the phase-dependence of COF [80, 81]. The first experimental study reported on enhancement of the spectral characteristics of the laser diode [80]. Theory reported on the analysis of the first Hopf bifurcation, the first ECM and its destabilization to quasiperiodicity and chaos, as well as confirming the analysis of linewidth enhancement [81, 82].

Studies continued to be published throughout the years, mostly exploring the rise and richness of chaotic dynamics, their spectral density as well as the stability of various solutions with rate equations models [83–88] – some including the detuning induced by non-frequency-degenerate PCMs. The first mapping of dynamics from a semiconductor laser with PCF was published in 1997 [89]. Only a few experimental studies were published [75, 78, 79].

Even though there were far less studies for PCF than for COF, the reports from the articles aforementioned already pointed to a well-understood route to chaos for a laser diode with PCF. The laser is in a stable Steady-State (SS) for really low values of the feedback rate, but quickly destabilizes through a first Hopf bifurcation, which has the effect of unlocking undamped relaxation oscillations. This oscillating dynamics then destabilizes multiple times when increasing the feedback strength through quasiperiodicity and gives birth to chaotic dynamics⁶ (coherence collapse), which is well illustrated in Fig. 1.16. The route is similar to

⁶ We will analyze this route to chaos theoretically in Section 2.3 and experimentally in Section 7.2.

the one for a laser diode with COF. Note that in the self-pumped configurations that we will use in the work presented here, we will not observe the locking illustrated in Fig. 1.16-(b), (c) because the phase-conjugated wave has the same optical frequency as the output beam of the laser.

An interesting and thorough experimental comparison of the two types of feedback with the same laser diode was published in 2001 [32], stressing the differences and similarities between the two feedback configurations. It confirmed that the feedback fraction needed to destabilize a laser diode is lower with PCF than with COF. However, the authors did not observe a route to chaos through undamped laser relaxation oscillations. This is most probably due to the fact that the authors used a highly damped laser diode.

The authors of Ref. [32] used the phenomenological classification introduced by Tkach and Chraplyvy in 1986 [90] which distinguishes five regimes of operation of a laser diode with COF: regimes I to III correspond to SS emission with properties specific to COF and do not really make sense for a laser with PCF⁷; regime IV where we reach coherence collapse and other forms of chaos after destabilization by excitation of relaxation oscillations or other mechanisms; regime V corresponds to a restabilization to a SS and increasing the feedback rate does not have any more influence on the laser diode dynamics. The experiment in Ref. [32] shows that the region of parameters exhibiting operation in regime IV is larger in the case of PCF than it is in the case of COF (see Fig. 1.17).

In the early 2000s, several studies focused on the analysis of bifurcations of the system, with tools such as continuation [91–93], analyzing among others the specific bifurcations of ECMs in the case of PCF. ECMs in PCF are oscillating solutions at harmonics of the EC frequency appearing between bubbles of chaos [87]. The study of ECMs will be more detailed in Chapters 2 and 3, along with the model we used which is the same as in Ref. [93].

Finally, more recent studies realized in our laboratory – before the work exposed in this thesis – expanded on the wealth of dynamics exhibited by a laser diode with PCF. They showed numerically how successive bifurcations to ECMs of higher orders should lead to a disappearance of chaos known as a chaos crisis. In the experiment, observation of stable ECMs – up to the fifth harmonic – were reported [24, 72]. Interesting chaotic dynamics were reported with regimes such as LFF [77] – previously numerically studied in Ref. [94] – and extreme events [76].

⁷ This is due to the fact that solutions known as ECMs are fundamentally different depending on the type of feedback considered. Chapters 2 and 3 will introduce and explain this difference in details.

However, more insight into the model would be needed to fully understand how these dynamics appear. Instead of using analytical tools and bifurcation analysis which were popular in the latest theoretical studies, we will use numerical simulations to understand the physics of the system. Also, it would be interesting to push the experiment further and see if we can reach the chaos crisis with high-order ECMs. Also, with better measurement tools now available – photodetectors with a large bandwidth, oscilloscopes with large sampling rates – we will be able to observe things that could have gone unnoticed in earlier experiments. Finally, chaos from a laser diode with PCF has never been characterized in terms of complexity or evaluated for possible applications. We therefore see that there is still work to be done for understanding PCF dynamics.

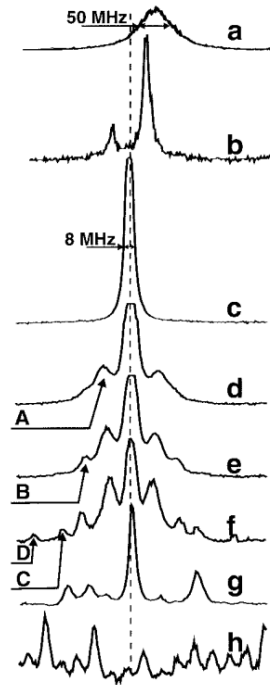


Figure 1.16: Optical spectra of a laser diode with PCF achieved in a rubidium vapor with a frequency-detuned pump. (a) Free-running laser, linewidth around 50 MHz. (b) Behavior attributed to four-wave mixing. (c) Locking of the laser diode to the pump frequency. (d) Undamped relaxation oscillations. Peak A is located 3.9 GHz from the central peak. (e) Destabilization through quasiperiodicity. Peak B is located 7.8 GHz from the central peak. (f) Quasiperiodicity increases. Peaks C and D are located 12 and 16 GHz from the central peak. (g) Broad spectra. (h) Coherence collapse. Figure from [79].

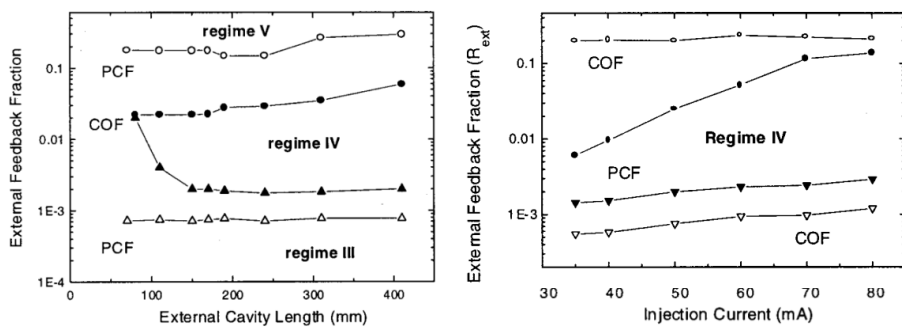


Figure 1.17: Mapping of dynamical regimes for the same laser diode with PCF and with COF when changing the feedback fraction (both sides), the EC length (left side), and the injection current (right side). Figure from [32].

1.5 CONCLUSION

1.5.1 *Motivations*

In this introduction, we have seen roughly how semiconductor lasers operate and we have explained their basic properties. Since their invention, laser diodes have always evolved and continue to do so to this day, with more research devoted to the design of lasers emitting at any desired wavelength, to the improvement of their properties, be it linewidth, stability, or energy consumption among others.

A lot of research has also been aimed towards applications of laser diodes. We have seen how such devices can be driven to exhibit non-linear dynamics, be they regular or chaotic oscillations of the output power. These types of dynamics are interesting from a purely scientific point of view since chaos represents a paradigm shift in our understanding of the behavior of complex systems. But they are also interesting from a practical point of view with several applications already demonstrated at realistic scales. Overall, the study of non-linear dynamics in lasers and their applications is still a strong field of research.

In particular, we are interested here in systems based on feedback which are interesting for their large dimensionality, potentially large chaotic bandwidths and thus for their use in a lot of applications using optical chaos. We especially focus on PCF here, and contrast it with COF. Many differences and similarities between the two kinds of feedback have already been shown but more can be done.

1.5.2 *Objectives*

In this context, we want to confirm that a simple mathematical model is enough to reproduce qualitatively all the recent experimental observations. This model only takes into account the phase-conjugate nature of the feedback and the time-delay, leaving aside gain saturation, possible multiple round-trips in the feedback loop, non-instantaneous phase-conjugation. Despite the simplicity we will show that the simulated model is capable of exhibiting periodic oscillations, quasi-periodicity, chaos in two distinctive regimes: LFF and extreme events.

Based on the expertise of the laboratory with this setup, we also want to continue to explore the experimental behavior. In particular, we will focus on reproducing any new feature that we could unveil thanks to our simulations, and

we will also begin to test if a chaotic signal from a laser diode with PCF can be suitable for applications using optical chaos.

1.5.3 *Outline*

Part I is dedicated to the theoretical part of our investigation, including modeling, the tools we use, and several investigations with numerical simulations in order to reproduce dynamics observed experimentally.

In Chapter 2, we will start from the standard equations modeling a semiconductor laser and derive the simple normalized model that we will use further in the thesis. We will describe the RK algorithm used to simulate time traces. Different tools stemming from signal analysis and non-linear dynamics will be introduced. They will be used through the rest of the work.

We will use our model and numerical simulations in Chapters 3-5 to show how we reproduce all kinds of dynamics – namely ECMs, LFF and extreme events. Interestingly, we will show that in chaotic dynamics, itinerancy happens along ruins of ECMs, as is the case for a laser with COF. Since the nature of ECMs is fundamentally different in the case of PCF, we expect to see very different frequency signatures in the chaotic signal.

In Part II are presented the results of our experimental investigations.

Based on our expectations acquired with simulated time traces, we will present the experiment in Chapter 6 where the whole setup along with measurement tools are presented. By operating in a long-cavity regime, we are able to show the peculiar frequency signature of PCF thanks to a new technique applied to laser dynamics analysis: Short-Time Fourier Transform (STFT). We also analyze the bandwidth of the signal when changing the reflectivity of the PCM and we compare with the COF configuration. We find that using PCF can lead to a larger bandwidth and thus could be suitable to applications. Interestingly, the bandwidth does not seem to saturate when the reflectivity increases, but this experiment does not allow for very large reflectivities.

To have the possibility to reach higher reflectivities, we propose in Chapter 7 to build a second experiment, using a CAT configuration: it will allow easier alignment of the PCM and provide higher reflectivities; we will also be able to obtain shorter cavities.

Finally, we conclude in Chapter 8 on our contributions to the field and we summarize the additional knowledge discovered thanks to this work. We also open the way to several ideas that could be pursued to extend this thesis work.

Part I

THEORY AND SIMULATION

MODEL AND SIMULATION OF A LASER DIODE WITH PHASE-CONJUGATE FEEDBACK

In this Chapter, we introduce the set of equations that we are going to use through the rest of Part I. We derive them from the rate equations of a semiconductor laser diode introduced in Chapter 1. These equations will be studied in the hope of reproducing the dynamics observed in Refs. [24, 72, 76, 77]. The model needs to include the optical feedback and its phase-conjugated nature, which are believed to be the sources responsible for dynamics observed experimentally.

However, we only wish to obtain a qualitative agreement, in order to understand the physics that lead to said dynamics. As such, we will not model complex behaviors that could have a minor influence on our system. Therefore we do not take into account the saturation of gain that can happen especially when working far from the laser threshold. Also, we suppose that only one round-trip in the External Cavity (EC) occurs, which is usually a right assumption in the case of low optical output power and low feedback rates.

Finally, for easier manipulation, we use a normalized form of the model and we will never bother to convert back to SI units since quantitative agreement is not our objective.

The need for a good theoretical model is crucial for the understanding of the physics of an optical system, since we can have access to the evolution of the electric field and its phase, as well as the dynamics of the carrier density. In an experiment, we can only measure the output power related to the squared modulus of the amplitude of the electric field. In some cases, phase evolution helps explaining how the dynamics appear [28] and having access to it via a model is important.

2.1 RATE EQUATION MODEL OF A SEMICONDUCTOR LASER WITH FEEDBACK

We have seen in Section 1.1 that a solitary semiconductor laser can be modeled with a set of two rate equations taking into account the dynamics of the complex electric field $\hat{\mathbf{E}}(t)$ and the carrier density $N(t)$. The polarization dynamics relaxes so fast that it can be adiabatically eliminated from the set of equations [12]. For the sake of simplicity, we consider that we work with a single-mode laser without nonlinear saturation of the gain, and we can use the following equations to model a semiconductor laser [6, 95]:

$$\frac{d\hat{\mathbf{E}}(t)}{dt} = \left[\frac{1 + \iota\alpha}{2} \left\{ G_N(N(t) - N_0) - \frac{1}{\tau_p} \right\} + \iota\omega \right] \hat{\mathbf{E}}(t), \quad (2.1)$$

$$\frac{dN(t)}{dt} = \frac{I}{q} - \frac{N(t)}{\tau_e} - G_N(N(t) - N_0)|\hat{\mathbf{E}}(t)|^2, \quad (2.2)$$

where N_0 is the carrier density at which the medium becomes transparent and α is the linewidth enhancement factor, also known as the Henry factor [7] or simply the alpha factor. Equation (2.1) models the evolution of the electric field $\hat{\mathbf{E}}(t)$, which is ruled by the stimulated emission of photons (with differential gain G_N) and the decaying rate of photons (τ_p) due to losses in the laser cavity. Equation (2.2) models the evolution of the carrier density $N(t)$, which is determined by the injection current I that adds carriers to the laser cavity, the spontaneous emission (at a rate τ_e) responsible for the decay of carriers, and the stimulated emission again with a negative contribution this time – because it consumes carriers.

We can also simplify the model by considering that the electric field is composed of a fast optical carrier with an angular frequency ω and a slowly evolving envelope, so that we can write:

$$\hat{\mathbf{E}}(t) = \mathbf{E}(t) \exp(\iota\omega t), \quad (2.3)$$

$$\frac{d\hat{\mathbf{E}}(t)}{dt} = \frac{d\mathbf{E}(t)}{dt} \exp(\iota\omega t) + \iota\omega \mathbf{E}(t) \exp(\iota\omega t). \quad (2.4)$$

By using Eqs. (2.3) and (2.4) in Eqs. (2.1) and (2.2), we obtain a simple model of a laser diode:

$$\frac{d\mathbf{E}(t)}{dt} = \frac{1}{2} \left[(1 + i\alpha) \left\{ G_N(N(t) - N_0) - \frac{1}{\tau_p} \right\} \right] \mathbf{E}(t), \quad (2.5)$$

$$\frac{dN(t)}{dt} = \frac{I}{q} - \frac{N(t)}{\tau_e} - G_N(N(t) - N_0)|\mathbf{E}(t)|^2. \quad (2.6)$$

We should note here that $\mathbf{E}(t)$ is still a complex variable accounting for the slowly varying envelope of the electric field.

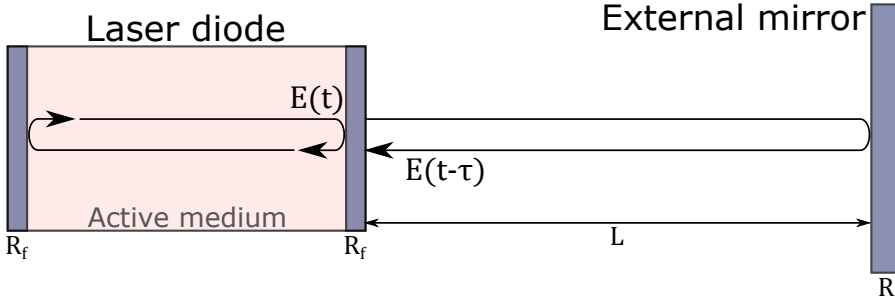


Figure 2.1: A semiconductor laser with COF: a laser cavity (left) composed of an active medium providing gain and two reflective facets, and a mirror (right) creating an EC of length L in the air.

Adding optical feedback to a semiconductor laser can be seen as simply adding a second cavity of length L to the already existing one, except that this additional cavity is composed of air, and not of an active medium (concept illustrated in Fig. 2.1). The round-trip in the EC delays the signal that is fed back into the laser cavity by a duration $\tau = \frac{2L}{c}$ typically varying between 0.1 to 10 ns for non-integrated cavities. Once again, for the sake of simplicity, we only consider a single round-trip in the EC, which is usually realistic for low values of the feedback rate. This means that optical feedback (at time t) can simply be modeled as an additional source for the electric field inside the laser cavity, but where the source is a delayed replica of the electric field (emitted at $t - \tau$) with a phase-shift taking into account the phase accumulated during the round-trip:

$$\kappa \mathbf{E}(t - \tau) \exp(-i\omega\tau). \quad (2.7)$$

Due to the power reflectivity R of the external mirror and the power reflectivity R_f of laser facets, only a fraction of the electric field is fed back into the laser

cavity: $\kappa = \frac{1-R_f}{\tau_{in}} \eta \sqrt{\frac{R}{R_f}}$, where η is the coupling efficiency of the feedback, and τ_{in} is the round-trip time in the laser cavity. This gives us the following model of a laser diode with optical feedback:

$$\frac{d\mathbf{E}(t)}{dt} = \frac{1}{2} \left[(1 + i\alpha) \left\{ G_N(N(t) - N_0) - \frac{1}{\tau_p} \right\} \right] \mathbf{E}(t) + \kappa \mathbf{E}(t - \tau) \exp(-i\omega\tau), \quad (2.8)$$

$$\frac{dN(t)}{dt} = \frac{I}{q} - \frac{N(t)}{\tau_e} - G_N(N(t) - N_0) |\mathbf{E}(t)|^2. \quad (2.9)$$

These equations were first introduced in 1980 [8] and are now famously known as the Lang-Kobayashi rate equations for a semiconductor laser with COF. They have been used in several theoretical studies [25, 28, 96, 97] and have been adapted to model other types of feedback or lasers such as Phase-Conjugate Feedback (PCF) or multimode lasers [81, 93, 98, 99].

2.2 NORMALIZED RATE EQUATIONS FOR A LASER DIODE WITH PCF

2.2.1 Normalization

Here, we are going to adapt Eqs. (2.8), (2.9) in order to model a semiconductor laser with PCF. For this, we must remind ourselves that a Phase-Conjugate Mirror (PCM) has the effect of reflecting the phase-conjugate of any wavefront that hits it, which means that the feedback term must contain the conjugate of the complex electric field and also that in the definition of the feedback rate κ , we can consider $\eta = 1$ because of the auto-aligning feature of the backward beam¹. Owing to the phase-conjugate nature of the feedback, any phase accumulated during the forward propagation of the laser beam will be compensated during the backward trip, thus there is no $\exp(-i\omega\tau)$ term for PCF. But to account for any phase-shift that can occur at the reflection on the PCM, we are going to use the variable Φ_{PCM} [81]. Finally, as we have seen in Section 1.3, we must account for the fact that some PCMs induce an angular frequency detuning $2\delta = 2(\omega - \omega_p)$ due to the angular frequency of a pump beam ω_p being offset from the angular frequency of the signal beam ω . We obtain the following model [95]:

$$\frac{d\mathbf{E}(t)}{dt} = \frac{1}{2} \left[(1 + i\alpha) \left\{ G_N(N(t) - N_0) - \frac{1}{\tau_p} \right\} \right] \mathbf{E}(t) + \kappa \mathbf{E}^*(t - \tau) \exp \left[-i2\delta \left(t - \frac{\tau}{2} \right) + i\Phi_{\text{PCM}} \right], \quad (2.10)$$

$$\frac{dN(t)}{dt} = \frac{I}{q} - \frac{N(t)}{\tau_e} - G_N(N(t) - N_0)|\mathbf{E}(t)|^2, \quad (2.11)$$

which is general enough to be used for simulating different experimental configurations. This model could be made even more complete by adding a filtering effect due to the penetration depth inside the medium used for creating the PCM, which has been done in other studies [99, 101].

However, since we use a PCM with self-pumped four-wave mixing in a photorefractive crystal in our experiments (see Chapters 6 and 7), there was no frequency detuning and thus we can take $2\delta = 0$ here. Also, we can assume that $\Phi_{\text{PCM}} = 0$ without any loss of generality [88].

¹ In an experiment, it is almost impossible to create a PCM with a perfect fidelity across the whole beam profile. The coupling efficiency thus cannot be exactly 1, but it can still attain large values and a PCM allows for a higher efficiency than a conventional mirror [100]. Since we do not aim for a quantitative model, we allow ourselves to use $\eta = 1$ in the model.

For easier use with mathematical tools, we are also going to normalize these equations, as was originally done by Erneux *et al.* [93] to obtain a formulation that was later adopted for several studies [35, 72, 101–103]. Details of the normalization can be found in Appendix A. It yields the following equations:

$$\frac{d\mathbf{Y}(t)}{dt} = (1 + i\alpha)\mathbf{Y}(t)Z(t) + \gamma\mathbf{Y}^*(t - \theta), \quad (2.12)$$

$$T \frac{dZ(t)}{dt} = P - Z(t) - (1 + 2Z(t))|\mathbf{Y}(t)|^2, \quad (2.13)$$

where the signification and typical values of all symbols can be found in Table 2.1. For the rest of the work presented here, these are the equations that will be used.

Symbol	Description	Typical value(s)
\mathbf{Y}	Complex normalized electric field	–
Z	Real normalized carrier density	–
t	Time in units of τ_p	–
τ_p	Photon lifetime in the laser cavity	1.4 ps
α	Linewidth enhancement factor	2 to 6
γ	Normalized feedback rate	0 to 0.05
θ	Delay in units of τ_p	10 to 3200
T	Ratio of carrier to photon lifetimes	1428
P	Pump parameter above threshold	0.0417

Table 2.1: Signification and typical values of notations used in the normalized equations (Eqs. (2.12), (2.13)) to model a semiconductor laser with PCF. Typical values mentioned either come from past studies [72, 84, 93, 102] for comparison or from new configurations we wanted to investigate [24, 35, 103].

2.2.2 Steady-state solutions

This set of equations, even though it models our system with several approximations, is still rather complex. Notably, it involves a nonlinear term in the equation for the electric field and introduces a time-delayed term, which gives an infinite dimension to the system. Overall, the system of equations cannot be solved an-

alytically. However it is possible to determine the Steady-State (SS) solutions of this system. We introduce the decomposition :

$$\mathbf{Y}(t) = Y(t) \exp(\imath\Phi(t)), \quad (2.14)$$

where Y is the real amplitude of \mathbf{Y} , and Φ is its phase. We substitute Eq. (2.14) into Eq. 2.12:

$$\begin{aligned} \frac{dY(t)}{dt} \exp(\imath\Phi(t)) + \imath \frac{d\Phi(t)}{dt} Y(t) \exp(\imath\Phi(t)) \\ = (1 + \imath\alpha)Y(t) \exp(\imath\Phi(t))Z(t) + \gamma Y(t - \theta) \exp(-\imath\Phi(t - \theta)). \end{aligned} \quad (2.15)$$

This simplifies easily by dividing by $\exp(\imath\Phi(t))$:

$$\begin{aligned} \frac{dY(t)}{dt} + \imath \frac{d\Phi(t)}{dt} Y(t) = (1 + \imath\alpha)Y(t)Z(t) \\ + \gamma Y(t - \theta) \exp[-\imath(\Phi(t - \theta) + \Phi(t))]. \end{aligned} \quad (2.16)$$

Using the relation $\exp(-\imath x) = \cos x - \imath \sin x$ we obtain:

$$\begin{aligned} \frac{dY(t)}{dt} + \imath \frac{d\Phi(t)}{dt} Y(t) = (1 + \imath\alpha)Y(t)Z(t) \\ + \gamma Y(t - \theta) \cos[(\Phi(t - \theta) + \Phi(t))] \\ - \imath \sin[(\Phi(t - \theta) + \Phi(t))]. \end{aligned} \quad (2.17)$$

Finally, we obtain the equations for the real amplitude $Y(t)$ and the real phase $\Phi(t)$ by separating real and imaginary parts of Eq. (2.17):

$$\frac{dY(t)}{dt} = Y(t)Z(t) + \gamma Y(t - \theta) \cos[(\Phi(t) + \Phi(t - \theta))], \quad (2.18)$$

$$\frac{d\Phi(t)}{dt} = \alpha Z(t) - \gamma \frac{Y(t - \theta)}{Y(t)} \sin[(\Phi(t) + \Phi(t - \theta))]. \quad (2.19)$$

A SS solution of this system implies $\frac{dY(t)}{dt} = \frac{d\Phi(t)}{dt} = \frac{dZ(t)}{dt} = 0$. This condition changes Eqs.(2.18), (2.19), and (2.13) into:

$$Z_0 = \frac{\gamma}{\alpha} \sin(2\Phi_0), \quad (2.20)$$

$$Z_0 = -\gamma \cos(2\Phi_0), \quad (2.21)$$

$$Y_0^2 = \frac{P - Z_0}{1 + 2Z_0}. \quad (2.22)$$

From these three equations we can find that there are two possible branches of solutions, depending on the value of 2Φ [93]:

$$2\Phi_0 = -\arctan(\alpha), Z_0 = -\frac{\gamma}{\sqrt{1+\alpha^2}}, \quad (2.23)$$

$$2\Phi_0 = \pi - \arctan(\alpha), Z_0 = \frac{\gamma}{\sqrt{1+\alpha^2}}, \quad (2.24)$$

$$\gamma_0^2 = \frac{P - Z_0}{1 + 2Z_0} > 0. \quad (2.25)$$

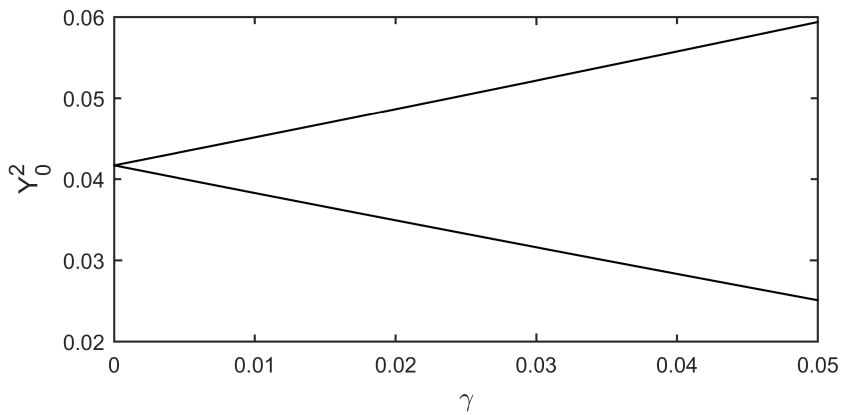


Figure 2.2: As we modeled it, we find that a laser diode with PCF can have only two SSs. We plot here the value γ_0^2 of the SSs versus the feedback rate γ .

These two possible branches of SSs are plotted in Fig. 2.2 and they are the only ones. But their stability cannot be evaluated analytically: authors of Ref. [93] have searched for the Hopf bifurcations that destabilize these SSs by introducing the growth rate of a small perturbation $\iota\sigma$ and $\epsilon = T^{-1}$ which gives the following transcendental equations:

$$\begin{aligned}
 0 = & \sigma \left\{ (1 + \alpha^2) Z_0^2 [\cos(2\sigma\theta) - 1] + \sigma^2 \right\} \\
 & + \epsilon \frac{1 + 2P}{1 + 2Z_0} \left[-(1 + \alpha^2) Z_0^2 \sin(2\sigma\theta) + 2\sigma Z_0 \right] \\
 & - 2\epsilon (P - Z_0) (1 + \alpha^2) Z_0 [\sin(\sigma\theta) - \sigma], \tag{2.26}
 \end{aligned}$$

$$\begin{aligned}
 0 = & \sigma \left[(1 + \alpha^2) Z_0^2 \sin(2\sigma\theta) - 2\sigma Z_0 \right] \\
 & + \epsilon \frac{1 + 2P}{1 + 2Z_0} \left\{ (1 + \alpha^2) Z_0^2 [\cos(2\sigma\theta) - 1] + \sigma^2 \right\} \\
 & + 2\epsilon (P - Z_0) (1 + \alpha^2) Z_0 [\cos(\sigma\theta) + 1]. \tag{2.27}
 \end{aligned}$$

In addition to being transcendental, these equations are hard to solve numerically. The authors proposed to take advantage of the large value of T to use asymptotic techniques [104, 105] and find approximations of the bifurcation points. Of the two branches that exist, they showed that the upper one quickly destabilizes through a Hopf bifurcation and that the lower one is always unstable [93].

Overall, they combined analytical tools with numerical tools and continuation [106] to study the SSs and three of the many oscillating solutions known as External-Cavity Modes (ECMs). These solutions are self-pulsating harmonics of the EC frequency that we define with their order n such that ECM_n has a frequency of oscillations equal to $f_n = \frac{n}{\tau_p} = n f_{\text{EC}}$. In that regard, they are fundamentally different from the ECMs of the laser with COF, a system for which they are SSs.

Asymptotic techniques are however limited. It has been shown in Ref. [102] that if continuation tools and asymptotic techniques give comparable results for the first Hopf bifurcations, it is not the case for the bifurcations occurring for large values of the feedback rate γ . We thus think it is useful to conduct a thorough analysis of the bifurcations and dynamics of the laser diode with PCF using numerical integration, which was used in Refs. [93, 102]. When possible we will compare our results with those given by continuation and asymptotic tools.

We are going to explore the transitions between several types of dynamics (oscillations, chaos) as well as characteristics of said dynamics. How we numerically integrate the set of equations of our model is described in the following section. We will also take a look at the dynamics that we can expect from this system when illustrating the tools we use to analyze time traces, and further studies of different types of dynamics will be presented in Chapters 3, 4, and 5.

2.3 NUMERICAL SIMULATION AND ANALYSIS TOOLBOX

Here, our theoretical work is not focused on the use of analytical tools, but rather on results of numerical simulation that aim at reproducing experimental results observed in Refs. [24, 72, 76, 77] for realistic values of the set of parameters. We wish to gain insight into the physics that drives the observed behaviors.

2.3.1 Runge-Kutta algorithm

Since Eqs. (2.12), (2.13) cannot be solved analytically, we have to use numerical integration methods to simulate the dynamics of the system. For easier use with programming tools and languages, we do not want to use complex numbers in the equations, so we need to derive either the amplitude and phase, or the real and imaginary electric-field equations from the complex electric-field equations. For some problems, phase dynamics can be quite important [28] so we choose to work with the amplitude and phase decomposition, which we already developed in the previous section and yielded the following set of equations modeling a laser diode with PCF:

$$\frac{dY(t)}{dt} = Y(t)Z(t) + \gamma Y(t - \theta) \cos [(\Phi(t) + \Phi(t - \theta))], \quad (2.28)$$

$$\frac{d\Phi(t)}{dt} = \alpha Z(t) - \gamma \frac{Y(t - \theta)}{Y(t)} \sin [(\Phi(t) + \Phi(t - \theta))], \quad (2.29)$$

$$T \frac{dZ(t)}{dt} = P - Z(t) - (1 + 2Z(t))Y(t)^2. \quad (2.30)$$

These equations are almost exactly the same as for a laser with COF, except that $\Phi(t) + \Phi(t - \theta)$ is replaced with $\Phi(t) - \Phi(t - \theta)$. And this slight change in the equations is responsible for the different physics of the ECMs as mentioned in Section 2.2 and for features of the dynamics that are specific to the laser with PCF as will be seen in the following chapters.

Having the equations written in the right form for our needs, we can use numerical integration to simulate the dynamics of our system. We choose here a 3/8-rule fourth-order Runge-Kutta (RK) method, which we detail in Appendix B, along with samples of code from the implementation in C and MATLAB.

This method of numerical integration has several advantages. It is an explicit method, which means that the next value at each iteration can be simply computed from the past approximated values, whereas an implicit method would require to solve an algebraic equation involving the next value at each iteration

of the algorithm. It gives a good estimation of the function we want to approximate: with a time-step h , the local truncation error is on the order of $O(h^5)$ and the accumulated error is on the order of $O(h^4)$. Finally, it is a fixed-step method, which means that if we take a value of h low enough, we do not need to adapt the length of the time-step at each iteration of the algorithm. All these points make for a robust approximating algorithm of the dynamics we want to simulate, while keeping the implementation quite easy (see samples of code in Appendix B) and not too costly in terms of computation time.

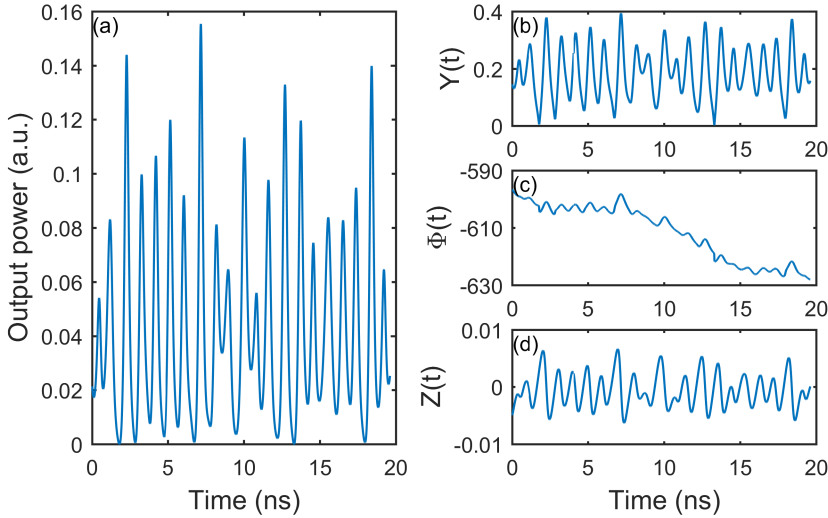


Figure 2.3: Numerical integration of Eqs. (2.28)-(2.30) yields time traces of (a) the output power of the laser equal to $|Y(t)|^2$ which is the typically measured in an experiment, (b) the normalized amplitude of the electric field $Y(t)$ and (c) its phase $\Phi(t)$, and (d) the normalized carrier density $Z(t)$.

This algorithm is used to generate (long) time traces of the three variables of the system: $Y(t)$, $\Phi(t)$ and $Z(t)$, snapshots of which are presented in Fig. 2.3 with an example of a chaotic time trace.

2.3.2 Bifurcation diagrams

To get a good overview of the dynamics that our system exhibits while changing a parameter without looking at all the individual time traces and to understand how they are linked together, one usually computes what we call a bifurcation diagram. For this, we take fixed values of all the parameters of our system, except

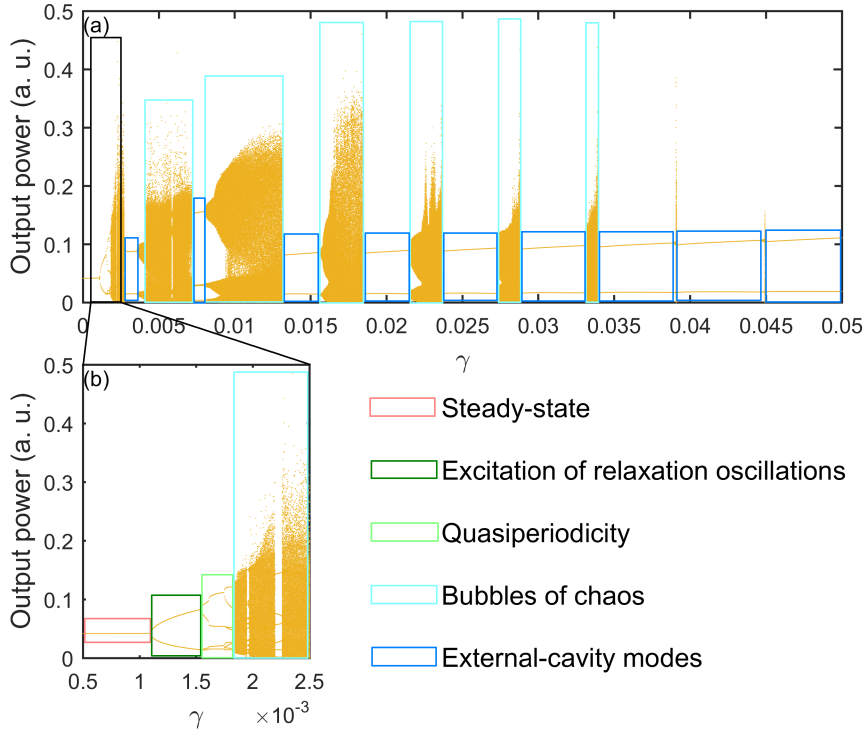


Figure 2.4: (a) Bifurcation diagram computed with increasing values of γ (from 0 to 0.05) for $\alpha = 3$ and $\theta = 476$ which corresponds to parameters used in Refs. [93, 102]. Different dynamical regimes can be observed. (b) Inset of the details of the transitions occurring for low values of feedback.

for the parameter for which we want to study the influence on the dynamics, e.g. the feedback rate γ .

Let us say we make γ vary from 0 to 0.05 in 1001 steps. Since we know that the system is sensitive to initial conditions, we are also going to simulate how the system would behave in a real experiment, meaning that the result of the first simulation (for $\gamma = 0$) will be used as the initial condition for the second simulation (for $\gamma = 0.00005$), and so on until we reach the last value of the feedback rate². For each of the simulated time traces, we extract all the local extrema of the optical power $|\mathbf{Y}(t)|^2 = Y^2(t)$ (as seen in Fig. 2.3-(a)), and plot them against

² This sensitivity to initial conditions means that a bifurcation diagram computed forward (from $\gamma = 0$ to $\gamma = 0.05$) can be different from one computed backward (from $\gamma = 0.05$ to $\gamma = 0$), exhibiting bistability of solutions or more complex situations. In the present demonstration, we only look at a forward bifurcation diagram.

the corresponding value of the feedback, which gives the bifurcation diagram in Fig. 2.4.

For really small values of the feedback rate (see Fig. 2.4-(b)), there is only one point in the diagram, meaning that we observe the stable SS mentioned earlier. It quickly becomes unstable and another dynamics appears through a Hopf bifurcation, with two points on the diagram: it means that we have reached an oscillating state, where the relaxation oscillations of the laser become undamped thanks to the feedback. This new state is quickly destabilized through quasiperiodicity, as can be observed in a laser with COF [107], and we enter a regime of chaos with a lot of different extrema appearing on the diagram. Finally, for larger values of the feedback rate, we observe a succession of ECMs, interspersed with shrinking windows of chaos. The fact that windows of chaos shrink as γ increases is related to a chaos crisis [87, 102].

As will be presented in Fig. 2.8 the ECMs observed here are indeed self-pulsating solutions at increasing harmonics of the EC frequency.

2.3.3 Signal analysis

We also use several tools borrowed from the field of signal analysis which prove to be very useful for understanding the physics behind non-linear dynamics.

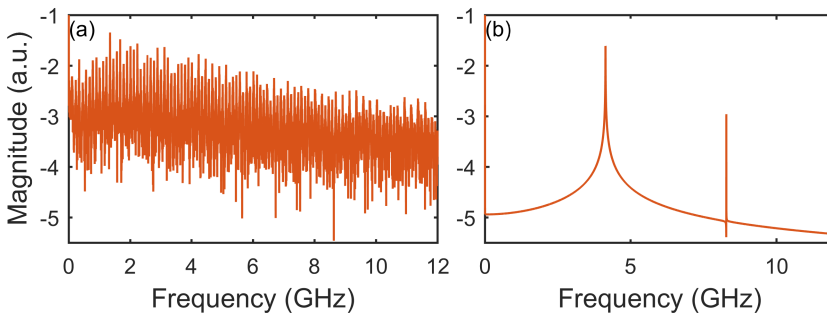


Figure 2.5: RF spectra can be used to gain more insight on the dynamics observed in a time trace. (a) RF spectrum of a chaotic time trace for a large delay, which translates into a short EC frequency and a lot of harmonics appearing. (b) RF spectrum of a time trace for a short cavity exhibiting the third harmonic of f_{EC} , which means that we observe an ECM of order 3.

Fast Fourier Transform (FFT) algorithms can be used on the optical power of the system $|Y(t)|^2$ to compute the RF spectrum of a time trace. As can be seen in Fig. 2.5-(a), the EC frequency and its multiples can often be found in chaotic

time traces from a laser with feedback. The peaks are large and high above the noise level, which suggests that we are in presence of chaos, and not simply noise. In Fig. 2.5-(b), we see the RF spectrum of an ECM, corresponding to only one multiple (the third) of the EC frequency and its harmonic. Here, the peak is sharp and the noise level is visible, which indicates that we observe a quasi-perfect sinusoid, representative of an ECM. In addition to computing RF spectra, FFT can also be used on $Y(t)$ to compute the optical spectrum of the laser from the electric field.

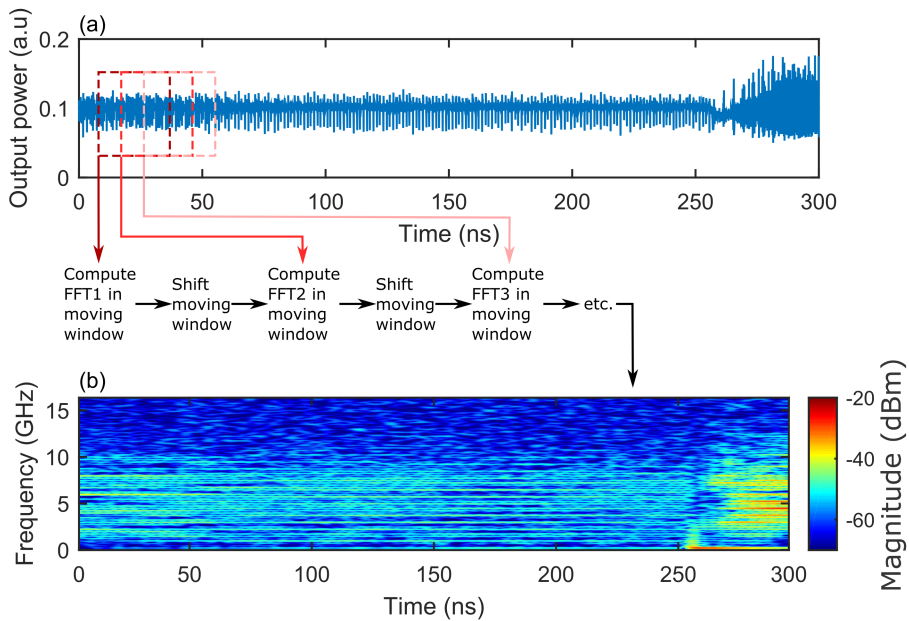


Figure 2.6: (a) Time trace we want to analyze with STFT. The first step consists in extracting the data in the moving window (dark red), computing the first FFT and storing it. The time window is then shifted further to the right by a fixed time increment. We repeat the process at the second position of the time window (red), the third position (light red), etc. (b) The spectrogram is obtained by positioning the successive FFTs next to each other with the magnitude of the spectrum represented by a color scale.

Adapted from the FFT algorithm is the STFT technique, which simply consists of doing a FFT on a short window of time (e.g. 10 ns) to get a RF spectrum, then shifting this window of a fraction of the time-window (e.g. 1 ns) to get a RF spectrogram of the time trace. This allows to observe the evolution of the frequency content versus time, which is useful in dynamics where brutal changes can appear. This technique is illustrated in Fig. 2.6 and is used in Chapter 6. The

time resolution is given by the time increment with which we shift the window and the frequency resolution is determined by the length of the window and the sampling rate with which the signal is acquired.

Autocorrelation techniques on the optical output power are also commonly used [108, 109]. They are another useful tool to analyze the presence of the time-delay in the time trace and are sometimes more useful to look at than the RF spectra, which gives a lot of information.

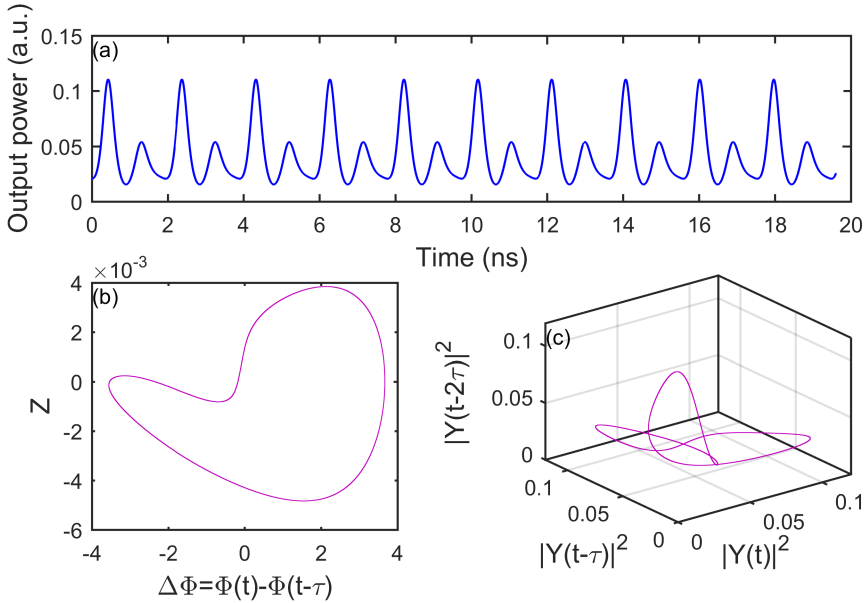


Figure 2.7: (a) Output power of the laser showing an oscillating state for $\gamma = 0.0017$. Different phase-spaces in which representation of trajectories is possible include (b) the plane $(Z, \Delta\Phi)$ where $\Delta\Phi = \Phi(t) - \Phi(t - \tau)$ which we will use in Chapter 4, (c) the 3D space comprised of the output power and delayed versions of the output power at $t - \tau$ and $t - 2\tau$.

To analyze the complex behavior of some systems, one can also use representation in a phase-space diagram. It consists of taking at least two representative variables of the system, and plotting one versus the other as time passes. This method can be used to identify chaotic attractors, or to recognize a periodic solution (which would give a limit-cycle in this representation). Examples on a quasiperiodic time trace in Fig. 2.7 show that several representations are possible, meaning that there is not a unique phase space and we can imagine several of them. Especially, the phase-space of time-delayed systems is infinite-dimensional. Representations in Figs. 2.7-(b) and (c) are projections of this phase-space in 2D

and 3D which can make their interpretation difficult when the trajectories are more complicated. The famous image of the Lorenz attractor – also known as the butterfly – as we have seen it in Section 1.2 (see Fig. 1.6) comes from its representation in a three-dimensional phase-space³. We use this tool in Chapter 4.

The techniques presented here that are applied to the optical output power can also be used on experimental time traces, since optical power is a measurable variable of the experiment. Techniques that require direct knowledge of the electric field or its phase are more difficult to implement since these physical values are typically not measurable. Although it is not commonly used, the carrier density can be measured from the bias voltage of the laser diode, provided that the injection current is close to the threshold [110]. This measurement can be useful to recreate the phase-space evolution of a laser with feedback. This result is recent (2015) and we did not implement this measurement in our experimental setups. It would be possible to make it by adding a bias tee to the electrical connection of the laser diode and use the RF port of the tee to measure the high-frequency fluctuations of the forward bias. But as we will see in Part II, we will always work far above the threshold so it is not guaranteed that the measurement of the high-frequency dynamics would be representative of the dynamics of the carrier density.

2.3.4 Summary

To illustrate the tools we use, we show the time traces, RF spectra and phase-space representations of the different dynamics represented in the bifurcation diagram of Fig. 2.4-(a).

After the initial SS is destabilized, we observe excitation of the relaxation oscillation frequency. At the bifurcation the output power exhibits an almost harmonic waveform but it becomes destabilized to a quasiperiodic state when increasing the feedback rate to e. g. $\gamma = 0.0016$ (see first row of Fig. 2.8). The RF spectrum has peaks at f_{RO} , $\frac{f_{RO}}{2}$ and corresponding harmonics. In the phase-space, this oscillating dynamics is represented by a distorted limit-cycle.

Increasing the feedback rate to larger values leads to a succession of chaotic bubbles for which the RF spectra are broad with some resonance at the harmonics of the EC frequency (see the second, third and sixth rows of Fig. 2.8). The trajectories in the phase-space are quite complicated and the system seems to never follow exactly the same path twice, which is characteristic of chaos. We

³ In the case of Lorenz equations, the system is 3D so finding a phase-space that represents adequately the trajectories of the system is easy.

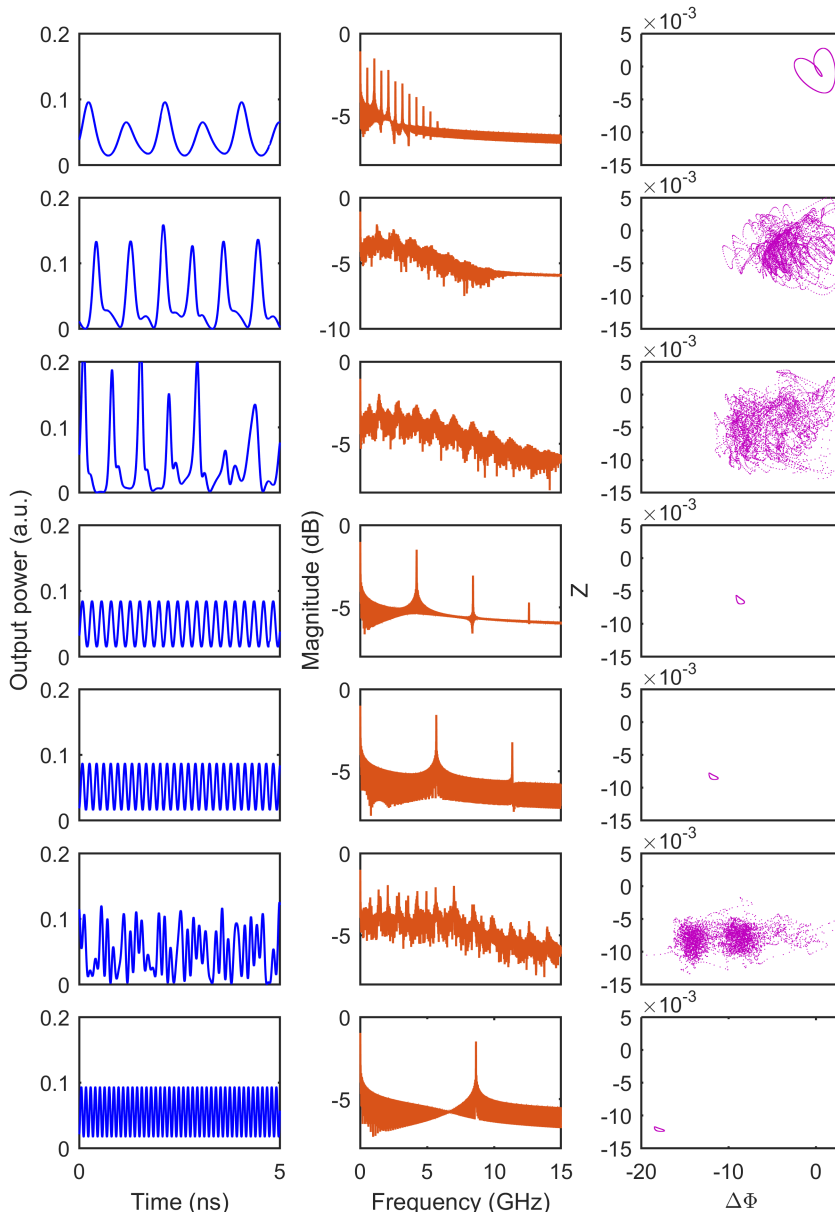


Figure 2.8: Time traces (left), RF spectra (middle), and phase-space (right) of several dynamics from the bifurcation diagram 2.4-(a) for values of the feedback rate γ 0.0016, 0.0066, 0.012, 0.015, 0.02, 0.023, 0.03 from top to bottom.

can note that there are basins of attractions in this space where the system goes more often. We will detail this behavior in Chapter 4.

Finally, we observe the stabilization of almost-perfect sinusoidal solutions – known as ECMs – as the bubbles of chaos shrink in size when increasing the feedback rate [87, 102]. Figure 2.8 shows three of these modes (fourth, fifth and seventh rows) with oscillation frequencies being close to increasing harmonics of the EC frequency which allows us to label them as (respectively) ECMs of orders 3, 4, and 6.

The dynamics illustrated in Fig. 2.8 do not represent all the bubbles of chaos and ECMs that appear in the bifurcation diagram of Fig. 2.4 but they give a good overview of what we will observe in the following chapters and how the different representations will allow us to explore different properties of the dynamics.

2.4 CONCLUSION

We have derived here in Eqs. (2.12) and (2.13) the model of a semiconductor laser with PCF. The advantage of this model, which has already been used in several articles [76, 93, 102], lies in its simplicity. Complex contributions from gain saturation or multiple round-trips in the EC cavity are neglected. We use a normalized version of the equation for easier manipulation since we only want to achieve qualitative reproduction of experimental results for realistic values of the parameters.

Numerical integration of the model will be carried out with a Runge-Kutta method (on phase and amplitude Eqs. (2.28)-(2.30) which offers a good compromise between ease of implementation, computing time and robustness. We will make use of several tools to analyze the dynamics generated and understand the physics behind them, which include bifurcation diagrams, FFT for RF spectra or phase-space projections.

The techniques presented here which are applied to the optical output power will also be used on experimental time traces, since optical power is a measurable physical value of the experiment. Techniques that require direct knowledge of the electric field, of its phase, or of the carrier density, are not considered in the present work. Only the model can help us in analyzing the phase and carrier dynamics.

Chapters 3, 4, and 5 will present all the theoretical results that we obtain with these model and tools.

SELF-DETERMINING HIGH-FREQUENCY SELF-PULSATIONS

In this chapter we focus on the emission of self-pulsating solutions from a laser diode with Phase-Conjugate Feedback (PCF). Chaotic dynamics will be studied in the following chapters. For some time, it has been considered a challenge to make a semiconductor laser oscillate at frequencies higher than its relaxation oscillation frequency. In a laser with Conventional Optical Feedback (COF), oscillations at a frequency inversely proportional to the External Cavity (EC) length can be obtained [25, 111–115]. Effort has been made on obtaining ultrashort cavities, which was achieved thanks to Distributed Feedback (DFB) lasers where the external cavity is integrated with the laser device [116] and oscillations at high frequency have been unlocked [117].

In Section 3.1 we show theoretically a way to achieve high-frequency oscillations without the need for a short EC cavity. A semiconductor laser with PCF is shown to exhibit oscillations at frequencies higher than the relaxation oscillation frequency, independently of the EC length, at large harmonics of the EC frequency. The driving parameter for the oscillation frequency is the feedback rate and the system locks on External-Cavity Modes (ECMs) [24, 93, 102] which have been introduced in Chapter 2. In Section 3.2 we study the model with bifurcation analysis and continuation. In Section 3.3 we compare the evolution of oscillating solutions frequencies in the case of COF. We conclude on this chapter in Section 3.4.

Part of the work presented in this chapter has been submitted for publication with the title “Self-determining high-frequency oscillation from an external-cavity laser diode”. Part of this work has been made in collaboration with master student Chi-Hak UY, post-doc Lionel WEICKER (CentraleSupélec, Metz) and Martin VIRTE (VUB, Brussels) under the supervision of Delphine WOLFERSBERGER, Marc SCIAMANNA, and myself.

3.1 EVOLUTION OF THE FREQUENCY OF AN EXTERNAL-CAVITY MODE

Symbol	Description	Typical value(s)
Y	Complex normalized electric field	–
Z	Real normalized carrier density	–
t	Time in units of τ_p	–
τ_p	Photon lifetime in the laser cavity	1.4 ps
α	Linewidth enhancement factor	3
γ	Normalized feedback rate	0 to 0.05
θ	Delay in units of τ_p	1 to 958
T	Ratio of carrier to photon lifetimes	1428
P	Pump parameter above threshold	0.0417

Table 3.1: Signification and values of notations used for the study of ECMs with the normalized equations (Eqs. (2.12), (2.13)) to model a semiconductor laser with PCF.

For the work presented in this chapter, we choose values of the parameters indicated in Table 3.1. This corresponds to a semiconductor laser working close to threshold. The values of the dimensionless delay θ considered in this study are in [1; 958] which corresponds to [0.0014; 1.34] ns in real time units. This range is centered around $\theta = 476$ which is the value used in several studies that considered a fixed time-delay [81, 93, 102]. The experiment that reported observation of the first orders of ECMs [24] had a time-delay around 1.4 ns and they only observed ECMs for short EC cavities [72]. So we decided to limit the studied range to a value close to that 1.4 ns time-delay. The values considered for the feedback rate are in the range of commonly used values in other studies [72, 102] and correspond to a maximum Phase-Conjugate Mirror (PCM) power reflectivity of about 4 %.

We explore the effects of both the delay θ and the feedback strength γ on the ECMs. To this end, our first step is to use our numerical integration algorithm to compute a bifurcation diagram of the output power versus the feedback rate for a given value of the time delay, as in Fig. 3.1. The typical behavior of a laser with PCF is observed, i.e. steady-state operation for a very low feedback rate, followed by a Hopf bifurcation leading to undamped oscillations at the relaxation frequency of the laser and followed by a complicated succession of bifurcations and a cascade of different dynamical regimes [87, 93]. For increasing

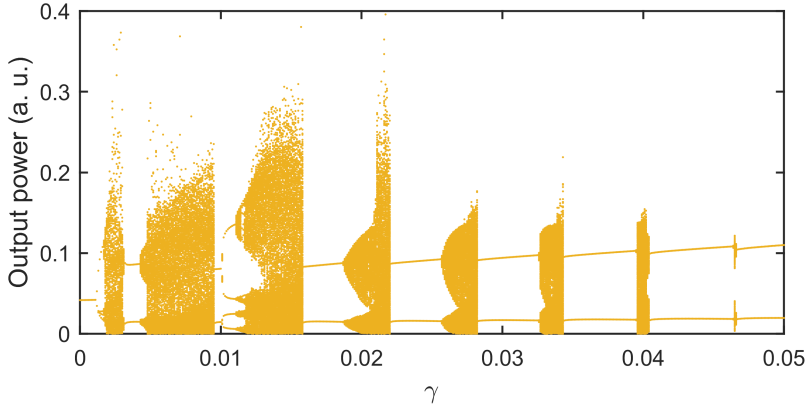


Figure 3.1: We compute consecutive time traces for $\theta = 400$ while increasing the feedback rate and report the extrema of the time traces on this bifurcation diagram, showing different types of dynamics, including oscillations and chaos.

values of γ , the system exhibits successive ECMs interspersed with shrinking regions of chaos. The transition from chaos to the next ECM occurs through a chaos crisis [102].

From this bifurcation diagram, we identify the oscillating solutions and by analyzing the associated time traces we measure their frequencies. We repeat the process for values of the θ in the aforementioned range and report the measured frequency of oscillations in Fig. 3.2, color-coded in the plane (θ, γ) . The white background corresponds to regions where there are either no dynamics (Steady-State (SS) solution), quasi-periodicity or chaotic evolution of the output power. Each band in the map corresponds to a unique ECM of order n (numerical labels), for which the oscillating frequency is given by $f_n = \frac{n}{\theta\tau_p}$.

We then explore the map by scanning it along different directions (see red arrows on Fig. 3.2). First, we look at the evolution of the oscillation frequency with a fixed time delay $\theta = \theta_1 = 400$. We observe in Fig. 3.3-(a) that the frequency of oscillations are close to harmonics of f_{EC} , as expected from the literature [24, 102] and as introduced in Chapter 2. Increasing the feedback rate leads to a strong increase in the frequency of oscillations, since the system visits a significant number of ECMs of higher order, which is illustrated with the time traces in Fig. 3.3-(b),(c).

When setting a fixed value of the feedback rate and increasing the time delay, we expect to observe a decrease in the oscillation frequency of the system. But interestingly, Fig. 3.4 illustrates that for two different values of the feedback rate

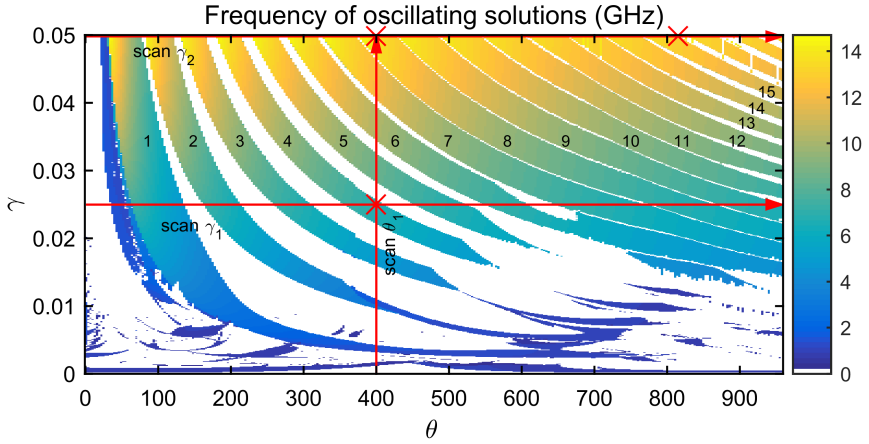


Figure 3.2: We compute bifurcation diagrams similar to Fig. 3.1 for different values of the time delay and report the frequency of oscillations on this map. The color bar on the right indicates the frequency of oscillation in gigahertz. The orders of ECMs are labeled on the bands of hyperbolic shape and the red arrows and crosses serve as indicators for Figs. 3.3 and 3.4.

($\gamma_1 = 0.025$ and $\gamma_2 = 0.05$), we observe the same behavior. Increasing the delay first leads to a slight decrease of the oscillation frequency, since we stay on the same ECM but f_{EC} decreases due to the increase in delay. The decrease is then followed by a slight increase of frequency because the system jumps to an ECM of higher order, and this pattern repeats itself. In the end, it seems that the oscillation frequency tends to a constant value when increasing the delay.

Contrary to intuition, the laser with PCF has a different behavior from other popular setups in that having a really short cavity does not necessarily yields the highest possible frequency of oscillation. Having a short cavity can slightly increase the frequency, but the most decisive parameter is the feedback rate. It means that faster oscillations are attainable in the system by simply increasing the reflectivity of the phase-conjugate mirror, rather than by decreasing the cavity length which may be hard to implement. In addition, it means that the frequency of oscillations is tunable to a precision of f_{EC} by adjusting only the feedback rate.

To summarize this result, we can say that the value of γ approximately sets a frequency of oscillation (f_γ) of the laser with PCF, and that the system will naturally find the order n of ECM that allows $f_n = n/\theta$ to be the closest possible to f_γ . In addition, f_γ is proportional to γ . To find a possible origin for this behavior, we take a closer look at the bifurcations of our system.

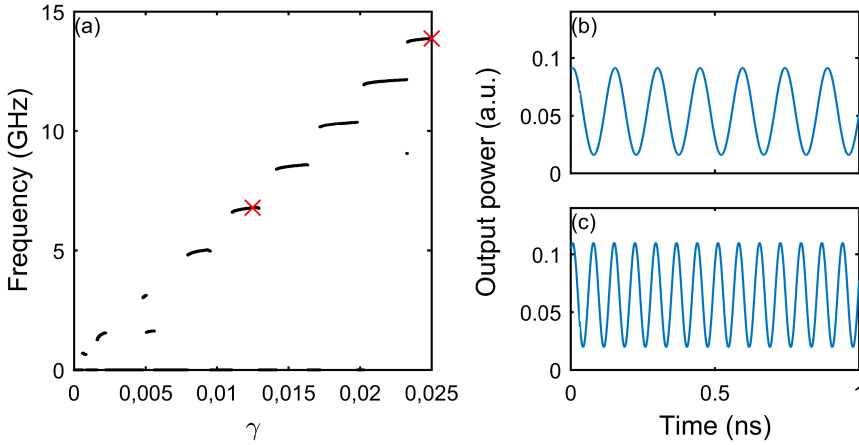


Figure 3.3: (a) We observe a significant increase in the oscillation frequency of ECMs when increasing the feedback rate for a fixed value $\theta = 400$. This is clearly seen in (b), (c) which present time traces for $\gamma = 0.025$, $\gamma = 0.05$ respectively and $\theta = 400$ in both cases. We also see that oscillations are almost perfect sinusoidal waveforms.

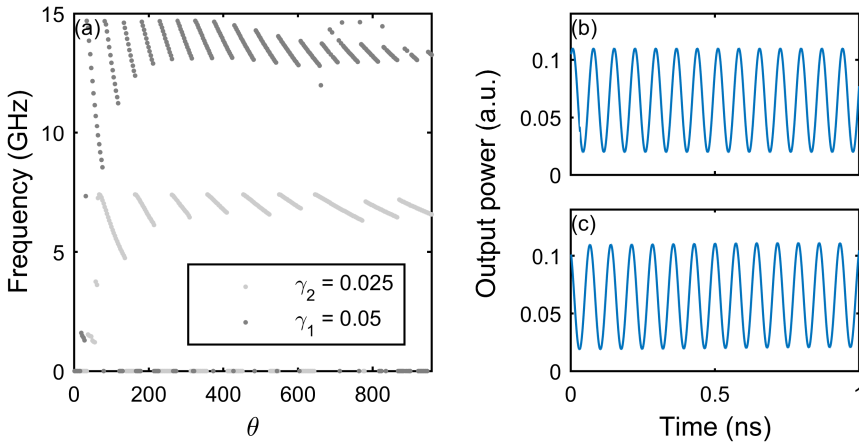


Figure 3.4: (a) Contrasting with Fig. 3.3, we don't observe a significant variation of the oscillation frequency of ECMs when changing the time delay for a fixed feedback rate. This is illustrated with time traces in (b), (c) for $\theta = 400$, $\theta = 815$ respectively, while $\gamma = 0.5$.

3.2 BIRTH OF AN EXTERNAL-CAVITY MODE

We investigate Eqs. (2.12) and (2.13) using a continuation method [106] with $\theta = 476$. Figure 3.5 shows the upper (red line) and lower (blue line) branches of SSs. Note that we only consider the interval of feedback strength $[0.018, 0.056]$, for clarity, but other bifurcations exist outside this interval. Also, in this range of feedback rates, both SS solutions are unstable. The Hopf bifurcations emerging from the SS branches are marked by circles. The black curves correspond to the maxima of the different ECMs and the thick purple lines correspond to the regions where they are stable. They are delimited by red squares and stars which are saddle-node and torus bifurcations, respectively. Green lines represent periodic solution branches that link the ECM to the SS branches by Hopf bifurcations. We observe that each branch of ECM is connected to two Hopf bifurcations. One from the upper SS and one from the lower SS.

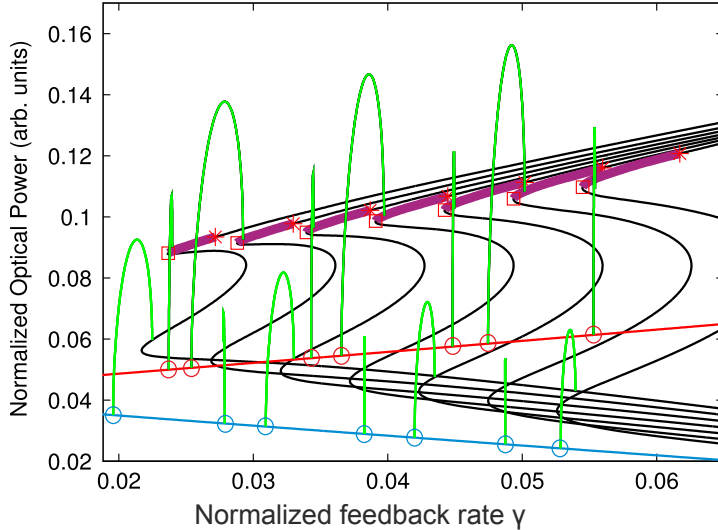


Figure 3.5: Bifurcation diagram obtained by continuation. Black lines are the maxima ECM branches, red and blue lines are the upper and lower steady state branches, respectively. Green lines corresponds to the periodic solution branches linking the ECM to the steady-states branches by Hopf bifurcation. Circles are Hopf bifurcations emerging from the steady states. Squares are saddle-node bifurcation and stars are torus bifurcations. The purple lines represent the areas where the ECM is stable. $\theta = 476$ and the other parameters are the same as in Fig. 3.1.

Continuation reveals that the ECMs appear through Hopf bifurcations, so we decide to specifically study the Hopf bifurcations and their frequencies in the parameter plan (θ, γ) with numerical methods. To this end, we consider the Hopf bifurcation conditions derived in Ref. [93] [Eqs. (B8) and (B9) reported in this document as Eqs. (2.26) and (2.27)] and use the Newton-Raphson method in order to find the different Hopf branches. We then follow each branch in the range of feedback rate and delay previously mentioned and obtain the same results obtained with continuation, which are displayed in Fig. 3.6-(a). In red, the Hopf bifurcation points emerging from the upper SS branch and in blue from the lower SS branch.

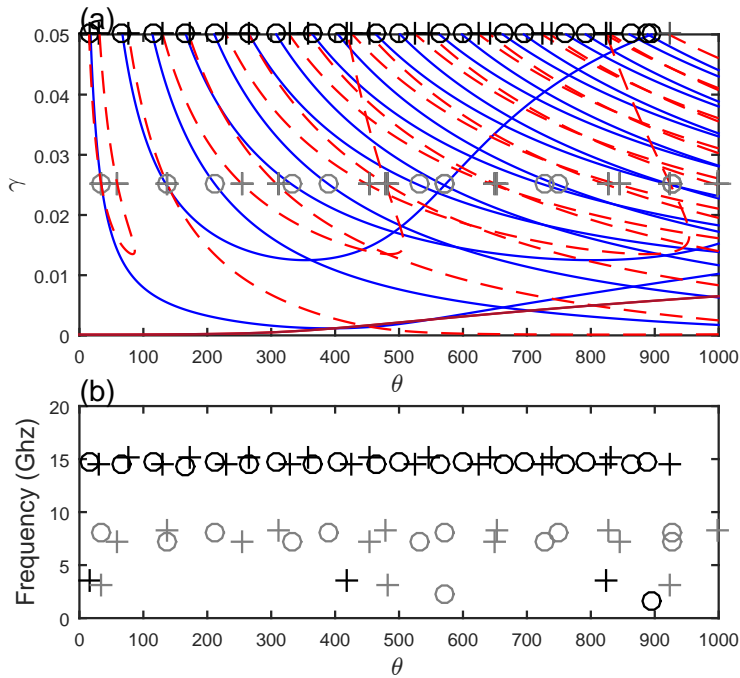


Figure 3.6: (a) Hopf bifurcation points emerging from the upper steady-state branch (dashed red) and from the lower steady-state branch (solid blue) in the (θ, γ) -plan. A perfect match has been obtained between the Newton-Raphson method and continuation techniques, thus only continuation results are shown. Values of the parameters are the same as in Fig. 3.1. (b) Hopf bifurcation frequency as function of θ . Crosses correspond to the Hopf bifurcation points that emerge from the upper steady state whereas circles correspond to the lower steady state. Grey and black colors correspond to $\gamma_1 = 0.025$ and $\gamma_2 = 0.05$, respectively. Other parameters are the same as in Fig. 3.2.

In comparison with Fig. 3.2, we first observe that the shape of the Hopf bifurcation branches follow the shape of the ECMs bands. Second, the total number of Hopf bifurcations emerging from the upper and lower steady states is approximately twice the number of ECMs which is consistent from our observation in Fig. 3.5.

Of particular interest is the frequency of the Hopf bifurcations. In Fig. 3.6-(b), we represent the Hopf bifurcation frequencies at two given values of γ (0.025 in blue and 0.05 in black). The circles correspond to the one emerging from the lower steady state whereas the crosses correspond to the upper steady state. As observed for the ECMs frequencies (See Fig. 3.4-(a)), the value of γ sets the frequency. For example, when $\gamma = 0.025$, the frequency of the Hopf bifurcations are around 7.5 Ghz whereas when $\gamma = 0.05$ the frequency is around 15 Ghz. These values are close to the ones found for the ECMs. Therefore, the ECM frequency expected at a given value of γ can be deduced only by the study of the Hopf frequency. Note that some of the Hopf bifurcation frequencies appear at low values. They appear when a branch of Hopf bifurcation in the (θ, γ) -plan folds back.

3.3 DIFFERENCE WITH CONVENTIONAL OPTICAL FEEDBACK

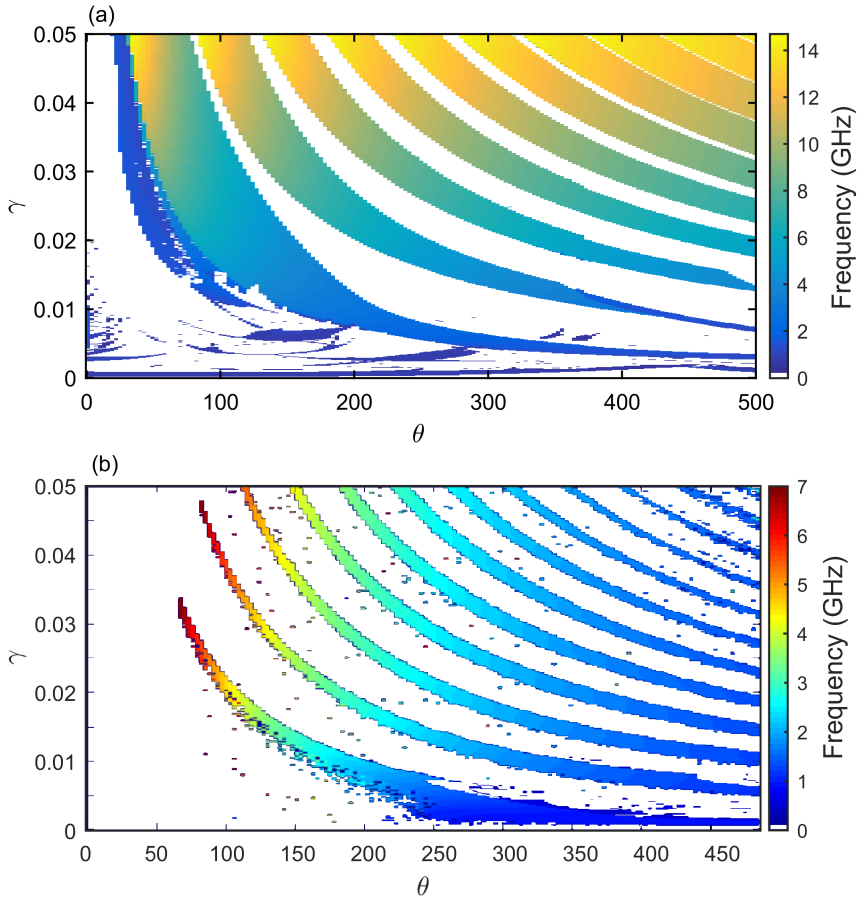


Figure 3.7: Similarly to Fig. 3.2 (recalled in (a) for a smaller range of time-delay values) we map the frequencies of oscillating solutions for a laser with COF in (b).

In this section we use the same model, but for COF – i. e. without the complex conjugate on the electric field variable – with the parameters of Table 3.1. Once again, we compute bifurcation diagrams for several values of the time-delay. We analyze time traces of the laser output power to detect oscillating solutions and their frequencies which are then plotted in the plane (θ, γ) in Fig. 3.7.

Overall, we observe less regions with oscillating solutions for the case of COF than we did for PCF. Figure 3.7 shows that the frequency of oscillating solutions in the case of COF behaves very differently than in the case of PCF studied in the previous sections of this chapter. The frequency of oscillations is mostly de-

pendent on the value of the time-delay θ , with the largest values attained for the small cavities. By contrast the value of the feedback rate γ does not have a strong influence on the frequency of oscillating solutions, therefore with frequencies scaling as $\frac{1}{\theta}$ where θ is the time delay.

This different behavior is due to the fact that in COF, there are no self-pulsating ECMs as with PCF. Rather, the ECMs are SS solutions and the oscillating solutions observed are either excitation of the relaxation oscillations or oscillations at the EC frequency [113].

This behavior was expected for the laser diode with COF but it is interesting to reproduce it here for comparison with the case of PCF to stress even more the fundamental difference between the nature of ECMs. ECMs are SS solutions for the laser with COF and self-pulsating solutions at self-determined harmonics of the EC frequency for a laser diode with PCF.

3.4 CONCLUSION

This first study of the ECMs from the laser with PCF confirms their difference in nature with the ECMs from the laser with COF. They are self-pulsating solutions at harmonics of the EC frequency whereas ECMs in the case of COF are all SSs, and they cannot be identified easily by looking at the time-trace only. The bifurcation diagram in Fig. 3.1, confirmed by continuation results in Fig. 3.5, indicates that there is only one stable SS in the case of PCF, and other solutions are either oscillating or chaotic.

From a scientific standpoint, this is a really interesting difference, considering the fact that the equations are almost the same and yet we have access to a lot of self-pulsating solutions at different frequencies in the case of PCF which we do not get with COF. Secondly, we found that the EC length does not have a strong influence on the frequency of an ECM. Rather, adjusting the feedback rate determines the frequency of oscillation and the system automatically selects the ECM order that allows it to oscillate at the ECM frequency being the closest to the self-determined frequency.

We expect these fundamental solutions to have a significant impact on the dynamics investigated in chapters 4 and 5. As the feedback rate increases, we can expect ECMs of higher frequencies to become excited which will lead to fast-evolving chaos.

We will investigate experimentally in Chapter 7 the behavior of high-order ECMs when changing the feedback rate.

LOW-FREQUENCY FLUCTUATIONS AND ITINERANCY ON EXTERNAL-CAVITY MODES

In this chapter, we simulate time traces of a laser diode with Phase-Conjugate Feedback (PCF). We choose a longer cavity than in the previous chapter to reflect the experimental observations of Low-Frequency Fluctuations (LFF) in Ref. [77]. This chaotic regime is interesting in that power dropouts happen at random time intervals that are not linked to any of the time constants of the system. Interestingly, for some values of the feedback rate, the power dropouts become more regular in the experiment. The aim of this chapter is to provide a theoretical explanation to the appearance of LFF in the case of a laser with PCF and how it relates to External-Cavity Modes (ECMs) that we have analyzed in Chapter 3, as well as investigate the resonance of power dropouts.

In Section 4.1 we introduce the LFF chaotic regime, which has been observed with both Conventional Optical Feedback (COF) [27, 29] and PCF [32, 77]. In the case of COF, a good theoretical explanation for the appearance of this dynamical regime has been developed [28], but we think that the theory in the case of PCF can be improved [94]. We propose to analyze the properties of LFF in Section 4.2. In Section 4.3 we evidence an itinerancy mechanism similar to the one for COF, but with motion on destabilized limit-cycles (the ruins of ECMs). Moreover, the fast pulsating dynamics that accompanies the onset of a power dropout gets faster when increasing the feedback rate. This unique feature of LFF in a laser diode with PCF is explained by the scaling of the ECM frequency with the feedback strength evidenced in Chapter 3. Finally, we investigate the appearance of coherence resonance where time intervals between power dropouts become more regular in Section 4.4, before concluding in Section 4.5.

Part of the work presented in this chapter has been published in Ref. [35].

4.1 A COMMON TYPE OF DYNAMICS IN LASER DIODES WITH OPTICAL FEEDBACK

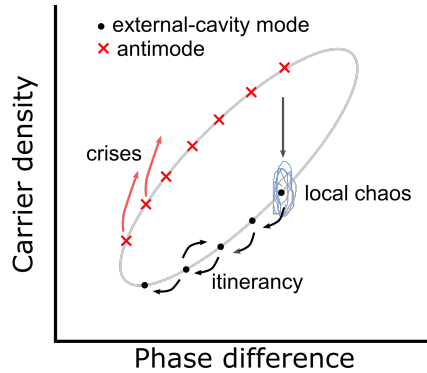


Figure 4.1: Schematic representation of the LFF phenomenon in a laser diode with COF. The trajectory is represented in a possible phase-space of the system composed of the phase difference $\Phi(t) - \Phi(t - \tau)$ and the carrier density, as mentioned in Section 2.3.

LFF refer to fluctuations of the output power – also called power dropouts – of a laser with optical feedback, which occur at much lower frequencies than the laser diode relaxation oscillation frequency or the External Cavity (EC) frequency [27]. In the case of COF, LFF have been identified as a deterministic high-dimensional chaos that result from chaotic itinerancy with a drift among the attractor ruins of destabilized fixed points [28, 29, 118] (the ECMs of the laser with COF). The system trajectory consists of two competing motions schematically represented in Fig. 4.1. One motion is a switching between the attractor ruins around each of the laser fixed points called *modes*, in direction to the mode with maximum output intensity. This motion is responsible for the fast pulsing dynamics that underlies the low-frequency power dropouts. The other motion is a repelling trajectory that is induced by the proximity of the many unstable fixed points called *antimodes* and that is responsible for a power dropout. The complete mechanism is illustrated in Fig. 4.1.

LFF have also been observed experimentally in a laser diode with PCF [32, 77] as pictured in Fig. 4.2. As the reflectivity of the PCM increases, we can observe the appearance of the power dropouts at random time intervals associated with increased energy in the low frequencies (below the EC frequency). However, we have seen in Chapter 2 that a laser diode with PCF admits only a single stable Steady-State (SS) that bifurcates to self-pulsating dynamics when increasing

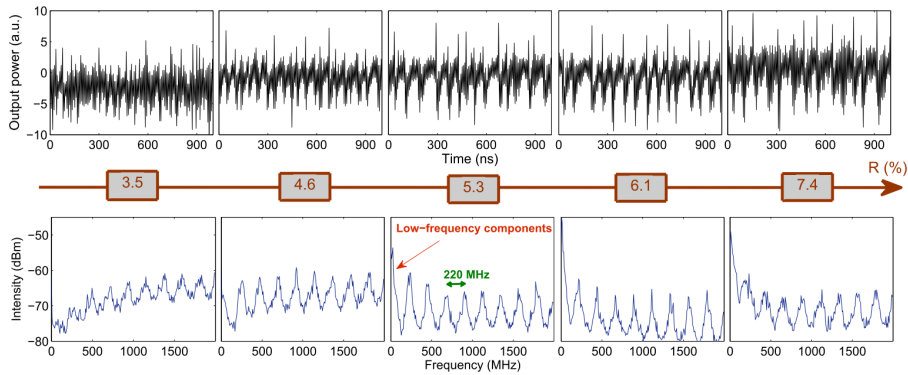


Figure 4.2: Experimental observation of LFF in a laser diode with PCF. Increasing the reflectivity R of the Phase-Conjugate Mirror (PCM) (boxed numbers) makes power dropouts appear, evidenced also by the increase of energy in the lower frequencies of the associated RF spectra. Figure from [72].

the feedback strength [81, 93, 102]. We have also seen that ECMs are different in nature – self-pulsing solutions instead of SSs – for a laser with PCF and the bifurcations leading to their existence and stabilization have been well-studied [81, 93, 102]. Therefore, we know that the mechanism for explaining the LFF regime cannot be exactly the same for the two different types of feedback. A previous theoretical analysis suggests that ECMs in the case of PCF play a similar role than the ECMs in the COF case, and therefore suggests a similar mechanism explaining LFF [94]. However a detailed description of how the global chaotic attractor originates from the bifurcations of the ECMs is still missing.

An interesting feature of the LFF regime as observed in Refs. [72, 77] is that for certain values of the reflectivity, the authors observe a coherence resonance where power dropouts become more regular. In the case of Fig. 4.2, this happens around $R = 6.1\%$ with the peaks of the RF spectra being sharper as a sign of resonance appearing at the time scale of the EC frequency. Resonance is a phenomenon observed in several physical systems where a defined event happens with more regularity under the influence of noise. Stochastic resonance for example is a phenomenon in which a nonlinear system shows an optimal response to a modulated input (largest signal to noise ratio) in the presence of an optimal amount of noise [119–122]. When the modulated input is replaced by an internal oscillation in the system dynamics, it is called coherence resonance [123–127]. This is characterized by a minimum in the standard deviation σ of the distribution of time intervals between consecutive events when changing the noise level. Instead of variance, it is common to use the normalized variance which is equal

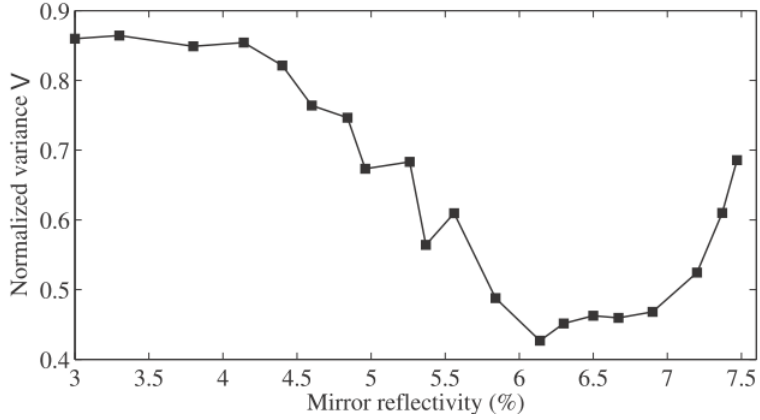


Figure 4.3: Normalized variance of the time intervals between power dropouts in the LFF regime of a laser diode with PCF as a function of the reflectivity of the PCM. The minimum of the normalized variances shows evidence of coherence resonance around $R = 6.1\%$. Figure from [72].

to the ratio of the variance to the mean μ : $V = \frac{\sqrt{\sigma^2}}{\mu}$ as illustrated in Fig. 4.3. It has been observed in deterministic chaotic systems [128–130] and in the case presented here, the authors of Refs. [72, 77] have named the observed phenomenon delay-induced deterministic coherence resonance because it is caused by a certain amount of time-delayed feedback, at the time-scale of the time-delay without addition of noise. We investigate theoretically this dynamics in Section 4.4.

Traces obtained here were simulated with the model presented in Eqs. (2.12), (2.13) numerically integrated with our Runge-Kutta (RK) algorithm, using the parameters in Table 4.1. For the most part of this chapter we use a really long delay $\theta = 3200$ which corresponds to a value $\tau = 4.48$ ns, which is close to the value used in the experimental observations of Ref. [72] we aim at reproducing.

Symbol	Description	Typical value(s)
Y	Complex normalized electric field	–
Z	Real normalized carrier density	–
t	Time in units of τ_p	–
τ_p	Photon lifetime in the laser cavity	1.4 ps
α	Linewidth enhancement factor	3
γ	Normalized feedback rate	0 to 0.05
θ	Delay in units of τ_p	3200
T	Ratio of carrier to photon lifetimes	1428
P	Pump parameter above threshold	0.0417

Table 4.1: Signification and values of notations used for the study of LFF with the normalized equations (Eqs. (2.12), (2.13)) to model a semiconductor laser with PCF.

4.2 PROPERTIES OF LFF IN A LASER DIODE WITH PCF

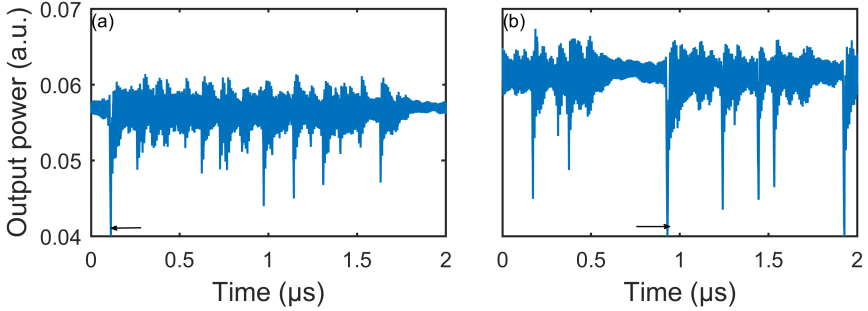


Figure 4.4: Simulated time traces low-pass filtered to show LFF for two different values of the feedback rate: (a) $\gamma = 0.03386$ and (b) $\gamma = 0.04460$.

Fig. 4.4 shows a typical time trace of chaotic LFF for two different values of the normalized feedback rate γ . The dynamics has been filtered with a moving average over 7 ns in order to better visualize the low-frequency power dropouts. Such dynamics looks qualitatively very similar to the one observed experimentally [32, 77], and at first sight resembles very much the LFF dynamics observed in a laser with COF. In particular the time between dropouts is a random variable whose mean value increases with the increase of the feedback rate γ [131].

A closer inspection of the LFF dynamics and its underlying bifurcation shows however unique features of LFF from a laser with PCF. Fig. 4.5-(a) is a bifurcation diagram of the output optical power ($|Y(t)|^2$) when increasing the feedback rate γ . As γ increases the laser diode undergoes a sequence of bifurcations to stable time-periodic dynamics in regions labeled A to J that correspond to the ECMs of the laser with PCF [93, 102]. As γ increases the mode order increases: for example the ECM in region D shows an order of $n = 40$, while in region E the order is $n = 42$. It is worth noting that some ECMs do not appear as being stable solutions, e.g. ECM_{41} is not observed as a stable solution numerically. In this configuration, the order of stable ECMs is quite high because the delay is large – which means that f_{EC} is small – and as we have seen in the previous Section, the frequency of oscillation of the laser with PCF is determined primarily by the value of γ .

The ECMs destabilize to chaotic dynamics that correspond to LFF in the tiny regions of chaos. By analogy to the case of COF, it is interesting to analyze the trajectory of the system close to the onset of LFF in the plane of the carrier inversion $Z(t)$ versus the phase difference $\Delta\Phi(t) = \Phi(t) - \Phi(t - \theta)$. Fig. 4.5-(b) shows

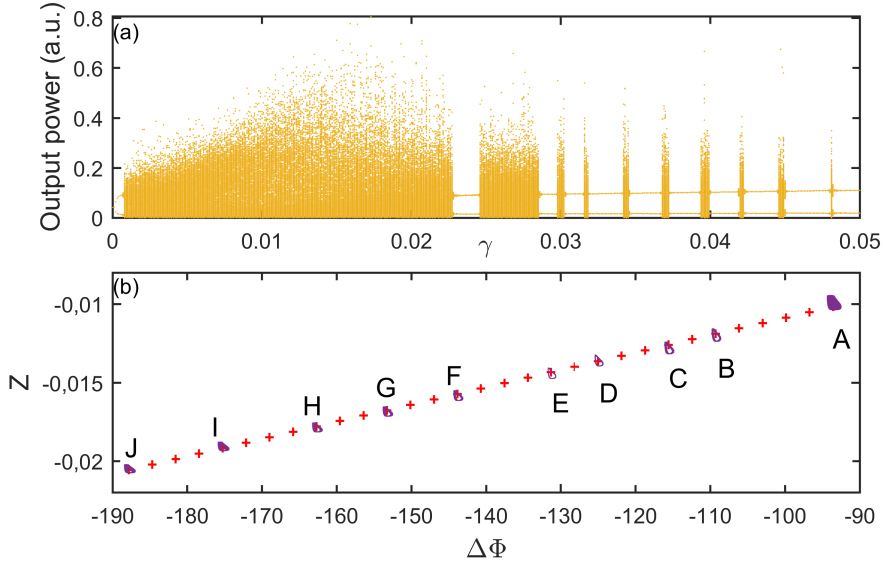


Figure 4.5: (a) Bifurcation diagram of the output power versus γ . When increasing the feedback rate γ the laser stabilizes on ECMs labeled from A to J. These ECMs are reported in the plane $(Z, \Delta\Phi)$ in (b) where they correspond to limit-cycle attractors. The red crosses show the mean values of the state variables corresponding to the ECMs. See Figure 4.6 for an inset of the area around ECMs E and F.

in black the limit cycle attractors corresponding to the stable ECMs in regions A to J, as we increase γ . Remarkably, the mean values of Z and $\Delta\Phi$ for the different stable ECMs lie on a straight line in that phase plane and the transition from one ECM of order n to an ECM of order $n + 1$ corresponds to a decrease of Z (and therefore an increase of the mean output power) and to a shift of the phase difference $\Delta\Phi$ equal to π (which is the phase-matching condition of constructive interference between outgoing and incoming fields). This feature is emphasized by the red crosses in Fig. 4.5-(b) that correspond to the mean values of the phase variables corresponding to all ECMs in the depicted region, even the ones that do not stabilize numerically – we have virtually positioned them in the phase-plane as well. Although the bifurcating solutions of the laser with PCF are limit-cycle attractors and not fixed points, we still observe – like with COF – that the increase of γ leads to directional motion in the phase-plane towards an ECM with higher output mean power [118].

4.3 ITINERANCY

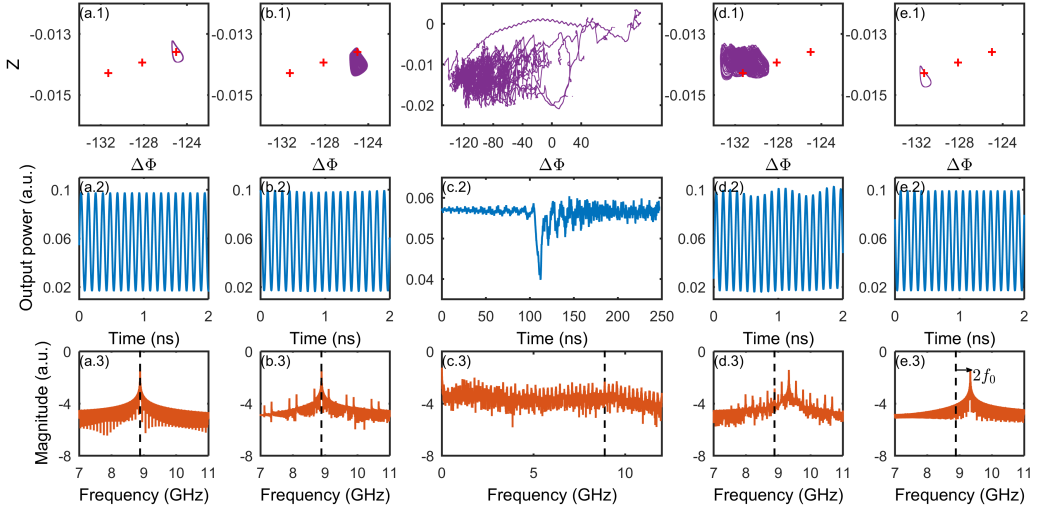


Figure 4.6: From left to right, (a) $\gamma = 0.03300$, (b) $\gamma = 0.03384$, (c) $\gamma = 0.03386$, (d) $\gamma = 0.03391$ and (e) $\gamma = 0.03500$. Top: system trajectory in the plane Z versus $\Delta\Phi$, middle: corresponding time-traces of $|Y|^2$, bottom: corresponding RF spectrum. The time-trace in (c.3) is filtered to show the dropout associated with the LFF regime.

Fig. 4.6 analyzes then the transition from ECM_{40} (D) to ECM_{42} (E) as the feedback rate γ increases and therefore as we cross a parameter range corresponding to LFF chaotic dynamics. The system trajectories in panels (a.1)-(e.1) are plotted in an enlarged part of the phase plane of Fig. 4.5-(b) in the area around modes D and E. The corresponding time-series and power spectra are shown in the panels (a.2)-(e.2) and (a.3)-(e.3) respectively. The sequence starts at $\gamma = 0.03300$ for which the laser diode shows a self-pulsating dynamics corresponding to a stable ECM in region D (panel a). As γ increases, this ECM undergoes a bifurcation to quasi-periodicity, with side peaks appearing around the main frequency and separated by the EC frequency; see Figs. 4.6 (b.1)-(b.3).

Further increasing the feedback rate destabilizes the ECM even more, and the system finally switches to a chaotic dynamics in panel (c). The trajectory in the phase-plane (c.1) is a global chaotic attractor visiting different destabilized ECMs and it resembles the chaotic itinerancy scenario evidenced for LFF from the case of COF [118]. The time-series in (c.2) corresponds to the trajectory (c.1) but low-pass filtered to better visualize the corresponding power dropout. When oscillat-

ing around the destabilized ECM in region D the trajectory is suddenly repelled to a larger value of Z and $\Delta\Phi$, hence creating a power dropout. The dropout is followed by a recovery process during which the system is successively attracted by the attractor ruins of ECMs around D and E, and then repelled in the phase-plane again, thus creating a succession of smaller dropouts that repeat every 2τ [panel (c.2)]. For a long enough time, the laser will finally stay around the attractors labeled D and E, before being subject to a new intense dropout.

For a larger value of γ the dynamics is again quasi-periodic and then bifurcates to a regular self-pulsating dynamics but around the ECM E, i.e. a mode of higher order and therefore of higher frequency as confirmed when comparing the power spectra (d.3) and (e.3).

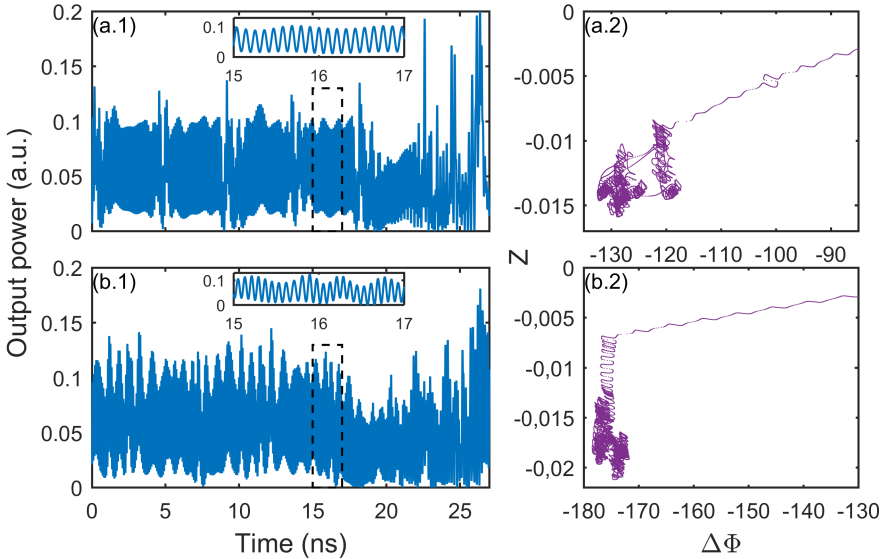


Figure 4.7: (a.1), (b.1): zoom on the fast pulsing dynamics accompanying the dropouts indicated with arrows in Figs. 4.4 (a), (b), respectively. (a.2), (b.2): corresponding trajectories in the phase plane.

A unique feature of the LFF from a laser diode with PCF is that the chaotic itinerancy occurs among destabilized limit-cycle dynamics and not destabilized fixed points. Although this is already clear from Fig. 4.6, the high-frequency signature is even more visible when comparing the fast pulsing dynamics underlying LFF for two increasing values of the feedback strength. Figure 4.7 shows the fast pulsing dynamics and the corresponding system trajectory in the phase-plane for a dropout event in Fig. 4.4. In both cases the dynamics is a chaotic

itinerancy followed by a power-dropout corresponding to a repulsing trajectory in phase-space. However since the involved ECMs in (b.2) are of higher mode index – transition from mode H to I in Fig. 4.5-(b) – than those involved in the dynamics of (a.2) – transition from mode D to E– the fast pulsing dynamics underlying LFF in the case (b.1) is of higher frequency than the one of case (a.1): the insets show pulsations with a dominant frequency of about 9 GHz for (a) and 12.5 GHz for (b).

Since this feature originates from the unique nature of ECMs from the laser with PCF, it is very unlikely that it could be observed in the case of COF – at least there has been no report of it to the best of our knowledge. Also, since it has not been observed experimentally from a laser with PCF, it will be one of the motivations for the experimental work presented in Chapter 6.

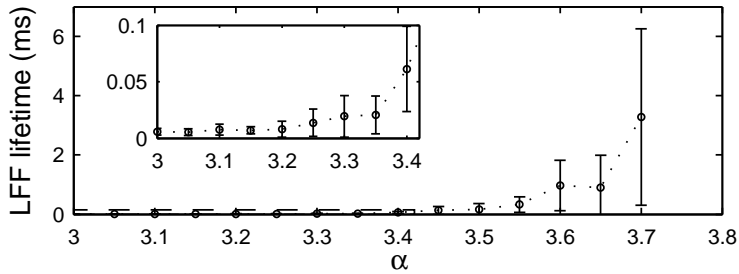


Figure 4.8: Evolution of the mean duration of the transient LFF as a function of α . The inset shows the evolution for the lowest values of α .

Finally, we analyze if LFF dynamics is maintained over a long time or is rather a transient state. By simulating over 14 ms we find that the LFF dynamics discussed above is not sustained for more than about 10-100 μ s and the dynamics then switches to a regular pulsation corresponding to an ECM. This result contrasts with the experimental observations of the same dynamics in a laser with PCF over several seconds and more [77]. As is also true for the case of COF [132, 133], we find that a small adjustment of α allows to significantly enlarge the duration of the LFF dynamics. In Fig. 4.8 we measure the lifetime of the chaotic dynamics as the time during which the signal is chaotic and not stabilized on an ECM (we consider that an ECM is stabilized when the power of the unfiltered time trace does not go above a threshold fixed at 0.12 for a duration of 1.4 μ s) over 21 simulations for different values of the feedback rate near $\gamma = 0.0415$. The LFF lifetime goes from about 10 μ s to 3 ms when α increases from $\alpha = 3$ to $\alpha = 3.7$. For $\alpha > 3.7$, we observe no extinction of the chaotic dynamics over the duration of the numerical simulation (14 ms).

We also test the influence of spontaneous emission noise by adding $\sqrt{R}\xi(t)$ as an additive term to Eq. 2.12, while ignoring the minor influence on the carrier density. With our parameters and similarly to the conclusions drawn from the COF case in [132], we find that the inclusion of spontaneous emission noise with R up to about 10^{-12} (which corresponds to $D = 10^{-4} \text{ ns}^{-1}$ in [132]) has little impact on the duration of the transient LFF. As suggested in [133] for COF, the impact of noise might be different when varying the laser parameters. This suggests that a large Henry factor is responsible for preventing the dynamics from vanishing. Also, it is possible that higher levels of noise or other sources of noise might contribute to the persistence of LFF dynamics and prevent the system from restabilizing on an ECM.

4.4 DETERMINISTIC COHERENCE RESONANCE

In this section, we investigate the coherence resonance presented in Section 4.1 and evidenced in Refs. [72, 77]. We first consider a shorter EC and use $\theta = 476$, the value used in Refs. [72, 84, 93, 102] and in Section 2.3.¹

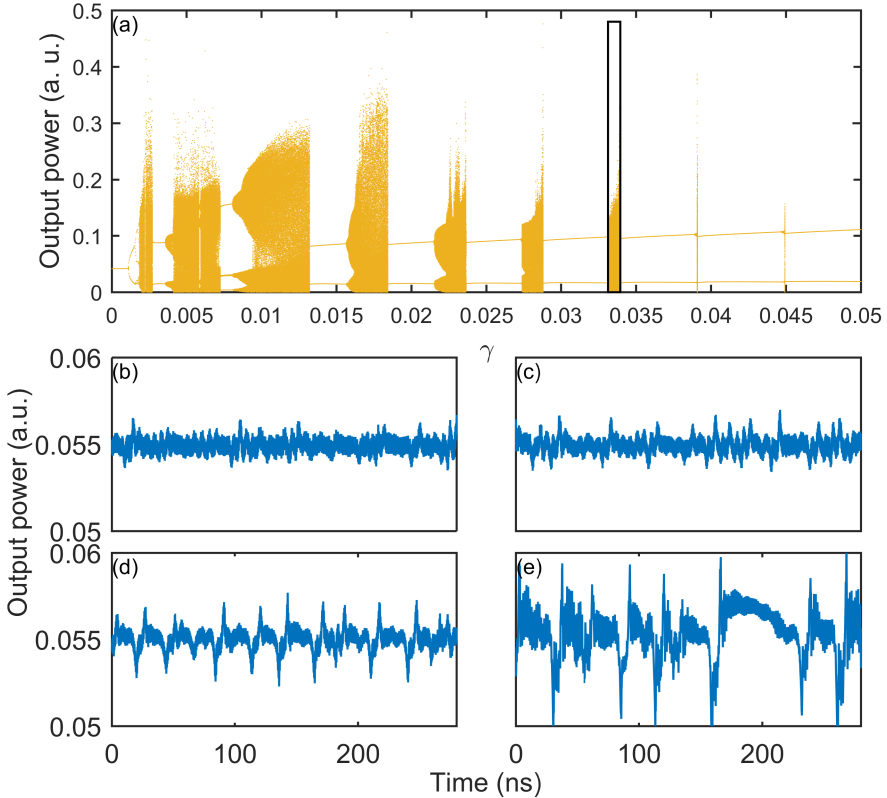


Figure 4.9: (a) Bifurcation diagram of the laser PCF for $\theta = 476$. In the last bubble of chaos (black box) appear LFF. Below are simulated time traces which have been low-pass filtered for increasing values of the feedback rate inside the bubble of chaos: (b) $\gamma = 0.0336$, (c) $\gamma = 0.0337$, (d) $\gamma = 0.0338$, and (e) $\gamma = 0.0339$.

Figure 4.9 shows the same bifurcation diagram as in Fig. 2.4-(a) since we work with the same set of parameters. Along with it are low-pass-filtered time traces for increasing values of the feedback rate inside the last bubble of chaos (in

¹ The work presented in this section has been made in collaboration with master students Armelle EVEN and Elodie MIRISOLA, under the supervision of Delphine WOLFERSBERGER, Marc SCIAMANNA, and myself.

the black box). It shows LFF appearing in this region of parameters, and as the value of γ increases inside the bubble of chaos, the dropouts appear more clearly, with more depth. Interestingly, the time intervals T_{LFF} between the dropouts also seem to be more regular for $\gamma = 0.0338$ (see Fig 4.9-(d)). As a result, we use the same tool as in Refs. [72, 77] to characterize this behavior: normalized variance $V = \frac{\sqrt{\sigma^2}}{\mu}$, where σ^2 is the variance of the distribution of T_{LFF} and μ is its mean.

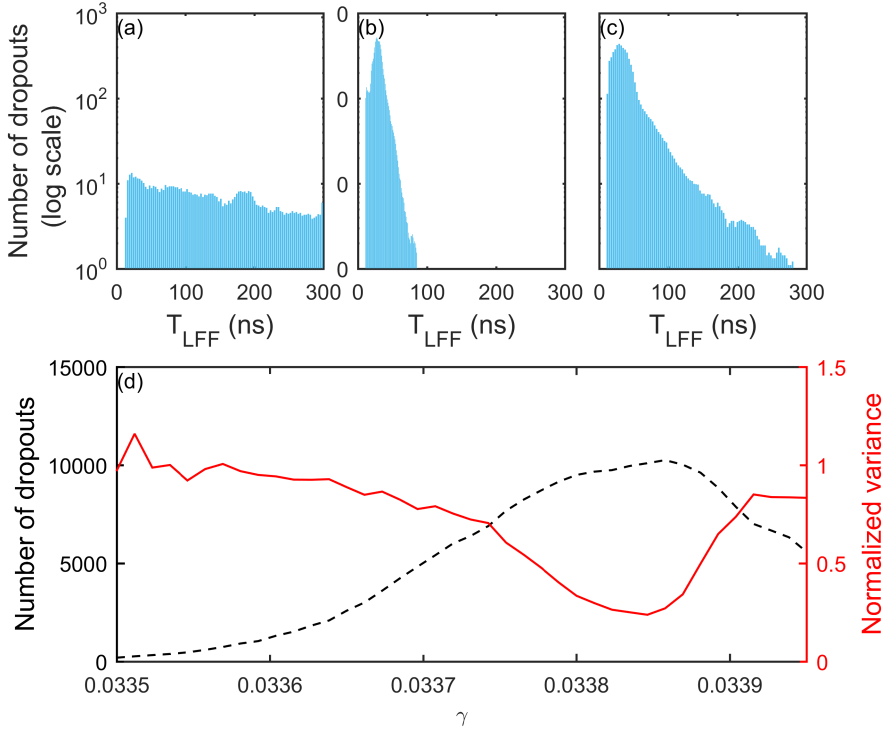


Figure 4.10: (a)-(c) Distributions of the time between consecutive power dropouts for $\gamma = 0.0336$, $\gamma = 0.0338$, and $\gamma = 0.03395$ respectively. (d) Evolution of the total number of dropouts and the normalized variance V of the time between dropouts inside the bubble of chaos highlighted in Fig. 4.9-(a). All measurements have been done on 280- μs -long simulations.

The results are presented in Fig. 4.10. Panels (a)-(c) show that as the feedback rate increases, the distribution of time between consecutive power dropouts changes drastically. In panel (a) the distribution extends well beyond 300 ns – larger values are not shown for clarity – and overall very few dropouts happen (see panel (d) for the total number of dropouts over a 280- μs -long duration). Increasing the feedback rate has three effects: 1/ it increases the number of

dropouts happening over a fixed duration, 2/ it decreases the mean value of T_{LFF} , 3/ it makes the normalized variance V decrease (as we can see in panel (d)). V reaches its minimum around $\gamma = 0.0339$, slightly off from the position where we detect the maximum number of dropouts. Finally, as the feedback rate continues to increase, the number of observed power dropouts decreases and the normalized variances increases, indicating that the system has left the region of coherence collapse. Overall, Fig. 4.10-(d) is very similar to Fig. 4.3 obtained with experimental measurements of LFF in a laser diode with PCF.

These simulations have been made without noise, reinforcing the notion of so-called delay-induced deterministic coherence resonance as the authors of Refs. [72, 77] have named it. It is surprising to see that in such a small bubble of chaos – i. e. for a small range of values of the feedback rate γ – we are able to observe the same behavior that was measured over several percents of the PCM power reflectivity value. It would be interesting to see how this resonance evolves when changing the EC length up to values comparable with the one used in the experiment for which the time delay was equal to 4.5 ns [72]. The system would probably maintain some of the properties exhibited here and we would see if the coherence resonance still appears over a tiny range of feedback rates or if this range expands. Still, it is interesting to see that the model is able to reproduce one of the characteristics of the dynamics, even though it is for a different set of parameters than the experimental one.

4.5 CONCLUSION

In this chapter, we have explained the appearance of LFF dynamics in a laser diode with PCF via an itinerancy mechanism on ECMs similar to the LFF in the case of COF. However, we have not been able to clearly identify the repelling mechanism responsible for the power dropouts. In the case of COF there are highly unstable *antimodes*. When the trajectory of the system comes too close to one of these, the instability is so strong that the system is completely repelled causing a power dropout. In the case of PCF, there are no known similar antimodes that would be responsible for this behavior but we suspect that unstable limit cycles may play a role similar to the one played by the unstable SSs corresponding to antimodes.

Additionally, we know from Chapter 3 that ECMs are fundamentally different for a laser diode with PCF. Since ECMs are self-pulsating solutions, each with their own frequency, we expect to observe their spectral signature in experimental RF spectra. We investigate the experiment in Chapter 6 and provide some evidence that the itinerancy is actually happening as predicted here.

A characteristic of the LFF observed in a laser diode with PCF in Refs. [72, 77] was the delay-induced deterministic coherence resonance appearing when varying the feedback rate. In other words, power dropouts become regular for some values of the feedback rate. We have been able to reproduce this behavior, albeit for a shorter EC length and over a small range of feedback rate. Still, we find it interesting that only a small bubble of chaos can contain a variety of dynamics rich enough to observe the delay-induced deterministic coherence resonance.

EXTREME EVENTS IN THE CHAOTIC DYNAMICS OF A LASER WITH PHASE-CONJUGATE FEEDBACK

By computing time traces of a laser diode with Phase-Conjugate Feedback (PCF) modeled by Eqs. (2.12) and (2.13), we have been able to analyze the properties of External-Cavity Modes (ECMs) as discussed in Chapter 3 and as observed experimentally in Ref. [24]. We have also been able to reproduce the emergence of Low-Frequency Fluctuations (LFF) as observed experimentally in Ref. [77]. There is one last type of dynamics we would like to reproduce with the same model which is what we call extreme events, inspired by rogue waves on the surface of the ocean and observed experimentally in a laser diode with PCF in Ref. [76].

In Section 5.1 we present the historical results that initiated the study of rogue waves in optical systems, along with the experimental observations in a laser diode with PCF and with the definition of an extreme event. In Section 5.2 we analyze the intensity distribution of events in simulated time traces, as well as distribution of the time between consecutive extreme events. Finally, we conclude on this chapter in Section 5.3.

Part of the work presented here has been published in Ref. [103]. It is the result of a project initiated with master students Armelle EVEN and Elodie MIRISOLA, which I supervised.

5.1 HISTORY AND DEFINITION OF A CRITERION

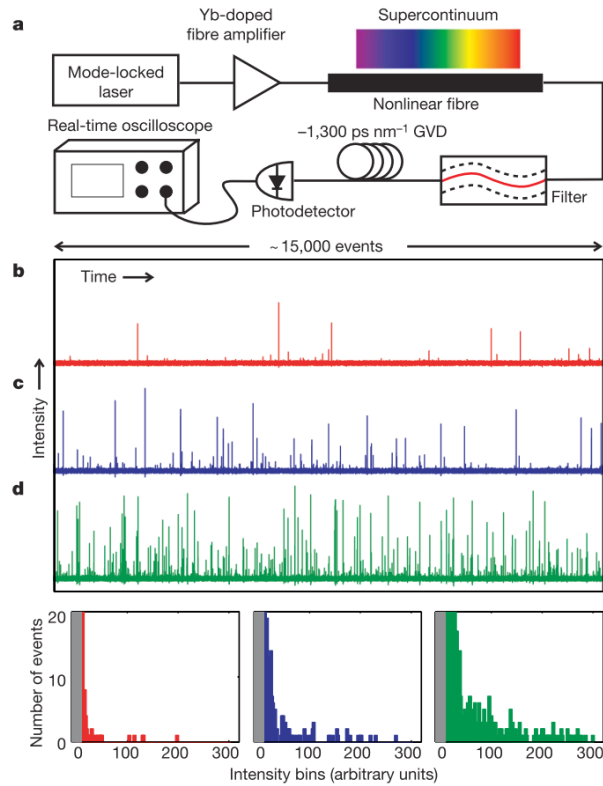


Figure 5.1: Experimental observation of optical rogue waves. (a) Schematic of experimental apparatus. (b)-(d) Single-shot time traces containing roughly 15000 pulses each and associated histograms (bottom of figure: left, b; middle, c; right, d) for increasing power levels. The vast majority of events are buried in the low-intensity range demarcated by the gray area. The rogue events reach intensities of at least 30-40 times the average value. Figure and legend from [134].

In this chapter, we focus on a specific dynamics of a laser diode with PCF, which consists of extremely high-intensity pulses that exhibit statistical properties similar to those observed in so-called rogue waves [76]. Rogue waves are inspired from oceanographic studies [135] and are rare and high-amplitude waves that appear randomly at the surface of an otherwise calm sea. They are not to be confused with tsunami for example, which are also rare and high-amplitude waves, but which have a clear origin of seismic nature. Rogue waves have been

observed in optics first in non-linear propagation of light launched in an optical fiber showing super-continuum [134].

Figure 5.1 shows the experimental setup used to evidence the apparition of rogue events: a high-power laser pulse is launched into a nonlinear fiber and it undergoes blue- and red-shift during propagation. Since it is difficult to record simultaneously the pulse packages at different wavelengths, the authors used a wavelength-to-time transformation technique to be able to acquire the time traces in Fig. 5.1 on which appear extreme events. By considering each pulse in the time trace as an event the authors plot the distribution of peak heights in the bottom of Fig. 5.1. The shape of these histograms differ from the results expected from a purely stochastic process which would give a Gaussian distribution. Deviation from a Gaussian distribution is one criterion that allows to define rogue events.

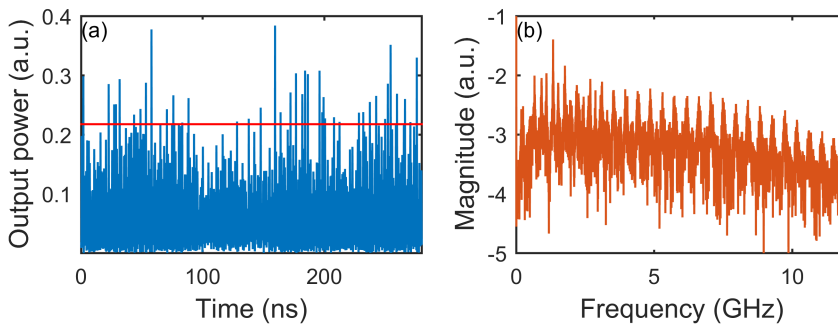


Figure 5.2: (a) Snapshot of a simulated time trace of a laser diode with PCF and (b) corresponding RF spectrum of a chaotic regime where pulses of high intensity appear randomly. The red line corresponds to the threshold $A = 2$ above which an event is considered extreme (see further down for details on this criterion).

The concept of optical rogue waves has then been generalized to include the study of extreme events in optics where a variation of a parameter leads to a deviation of the intensity statistics to the otherwise Gaussian distribution hence explaining the occurrence of rare and intense pulses. Even though rogue waves and extreme events are different in nature, they may share statistical properties owing to the fact that they both correspond to large deviations of the system state away from its nominal value [136]. Examples of rogue waves and extreme events include high-amplitude localized light peaks in the transverse plane of a spatially extended nonlinear optical cavity [137–139], and high-intensity pulses underlying chaotic dynamics in laser diodes with optical injection [140–142] or optical feedback [76, 143] as shown in Fig. 5.2.

Symbol	Description	Typical value(s)
Y	Complex normalized electric field	–
Z	Real normalized carrier density	–
t	Time in units of τ_p	–
τ_p	Photon lifetime in the laser cavity	1.4 ps
α	Linewidth enhancement factor	4
γ	Normalized feedback rate	0 to 0.05
θ	Delay in units of τ_p	1600
T	Ratio of carrier to photon lifetimes	1428
P	Pump parameter above threshold	0.0417

Table 5.1: Signification and values of notations used for the study of extreme events with the normalized equations (Eqs. (2.12), (2.13)) to model a semiconductor laser with PCF.

Our purpose is here to provide a theoretical framework to explain the emergence of these extreme events in a laser diode with PCF as observed experimentally in Ref. [76]. The authors of this study observed the appearance of extreme events in the output power of the laser diode, with an increasing number of them when increasing the feedback rate, associated with higher intensity of the extreme events. They also reported a peculiar statistical distribution of the time between consecutive extreme events and we will see how we can observe the same characteristic theoretically.

In order to reproduce the experimental results, we again use numerical integration with Eqs. (2.12) and (2.13), this time using parameters in Table 5.1. In this case, we use a normalized delay value $\theta = 1600$ which corresponds to $\tau = 2.24$ ns, i. e. the value of time-delay for which extreme events were observed experimentally in Ref. [76].

The study of extreme event requires also to define what we call an event and to identify a criterion that discriminates what is extreme in this population. Several definitions for extreme events can be found in the literature and appear as quite arbitrary. However, as will be discussed in the following, we have checked that our conclusions – and most importantly how the feedback strength in the PCF time-delayed system influences the occurrence and number of extreme events – are robust when applying the commonly suggested criteria for extreme events.

We first discuss the definition for extreme event applied in the corresponding PCF experiment [76], which is illustrated in Fig. 5.3. As in Ref. [76], we define

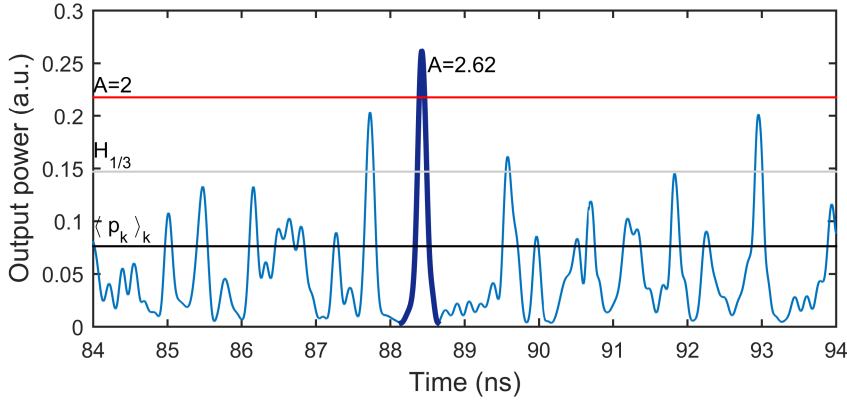


Figure 5.3: Illustration of the process used to compute the abnormality index A of an event (details in text). We analyze here the event stressed with the thick dark blue line. We find it has an abnormality index $A = 2.62 > 2$ so we consider it to be an extreme event.

an event as a local maximum of the filtered time trace of the optical output power of the laser diode. For each event k , we define the height of the peak p_k which is the optical output power of the local maximum. We then calculate Hf_k which is the difference between the peak height of the event k and the mean height of our population of events: $Hf_k = p_k - \langle p_k \rangle_k$. We also define the significant height $H_{1/3}$ as the average value among one third of the highest values of Hf_k . Finally, the abnormality index of event k is $A_k = \frac{Hf_k}{H_{1/3}}$. Any event that yields an abnormality index greater than 2 is then considered in the following as extreme. For example Fig. 5.3 illustrates an extreme event which has an abnormality index equal to 2.62. These definition and criterion are inspired from a proposal made to classify rogue waves in oceanographic studies [144] and have been used in several experimental and theoretical works reporting on extreme events in optics [139, 145–147].

Another definition of the significant height can be taken from a different proposal made in oceanography [135]: H_s defined as four times the standard deviation of the measured Hf_k . An event is called extreme if the corresponding abnormality index $A_k = \frac{Hf_k}{H_s} > 2$. This definition has been applied in the analysis of extreme events in the chaotic pulsing dynamics of a laser diode with optical injection [140, 141]. Although we will mainly use the traditional definition of the significant height $H_{1/3}$, in the following we shall discuss the robustness of our conclusions against the definition of an extreme event.

Figure 5.2 shows a chaotic pulsing dynamics where some pulses show an intensity much larger than the average intensity value. How many such extreme events occur can be quantified by considering the definition of the abnormality index relative to the third of the highest peaks. Pulses which have an abnormality factor greater than 2 are arbitrarily called extreme. This type of dynamics with the occurrence of rare but intense pulses resembles qualitatively the one observed recently in experiment [76]. We investigate in details these events in the next sections to see if they qualify as extreme events.

5.2 STATISTICAL CHARACTERIZATION OF EXTREME EVENTS

5.2.1 Counting and characterizing extreme events

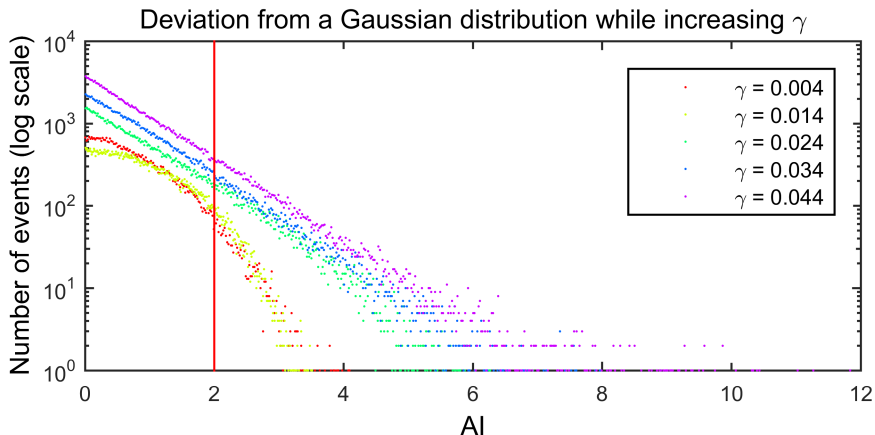


Figure 5.4: Evolution of the distribution of extreme events versus the abnormality index. Increasing the feedback rate leads to a greater deviation from a Gaussian distribution (from left to right), more extreme events, with a higher abnormality index. The red line corresponds to the threshold $A = 2$.

In this Section, all simulations are performed over a fixed duration of $56 \mu\text{s}$ and we observe how the number of extreme events evolves over this fixed duration when varying the feedback rate γ . The influence on the distribution of the number of events versus their abnormality index is clearly seen in Fig. 5.4. It is observed that the distribution deviates more and more from a Gaussian distribution when increasing γ . This tendency to deviate from a Gaussian distribution while increasing the driving parameter – here the feedback rate – is consistent with the experimental observations [76] and with other optical systems where extreme events or rogue waves appear when increasing e.g. the optical pump intensity [134, 137–139] or the optical injection strength [140].

Time traces of the optical output power present a strong pulsing behavior. In Fig. 5.5(a) where $\gamma = 0.004$, there are only few events above the threshold $A = 2$ and Fig. 5.4 tells us that the most extreme ones reach only $A = 4$. In Fig. 5.5(b) where $\gamma = 0.024$, there are more extreme events and they reach an high abnormality index, some of them going above $A = 6$ according to Fig. 5.4. The insets on the right in Fig. 5.5 show an interesting feature. For low feedback rates, extreme events appear isolated, which is the expected behavior of rogue waves. But

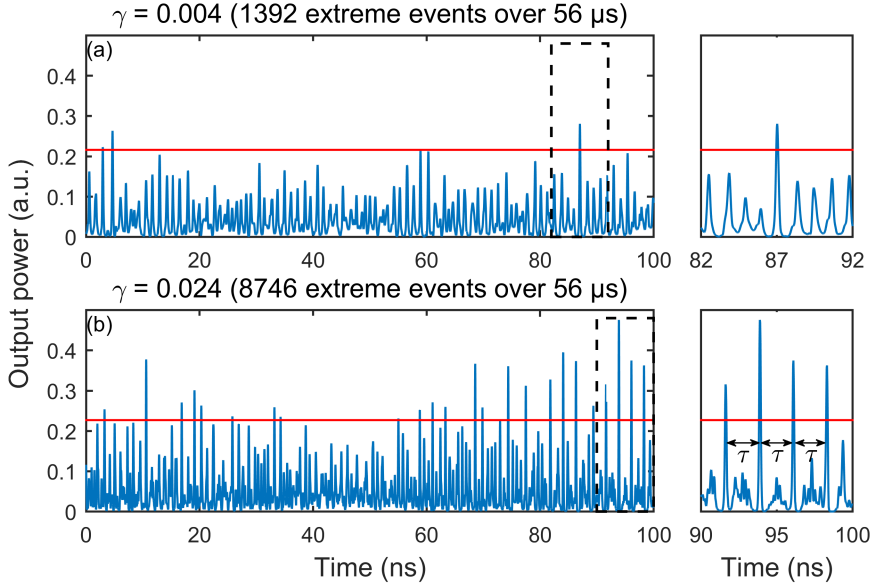


Figure 5.5: (a) and (b) illustrate the tendency of extreme events appearing more often for strong feedback values with snapshots of the time traces where the horizontal red line indicates the threshold over which an event is considered extreme. The insets on the right show the tendency for extreme events to appear in bunches with repetitions at the delay for some values of the feedback rate.

for higher values of the feedback rate, extreme events tend to appear in bunches of pulses that repeat at a period close to the time-delay value. The bifurcation study of the PCF laser system that we have previously explained [91, 93, 102, 148] tells us indeed that as the feedback rate increases, the laser experiences a cascade of bifurcations. The first one is a Hopf bifurcation close to the frequency of the laser relaxation oscillations. A further increase of the feedback strength leads to a cascade of Hopf bifurcations whose frequencies are close to harmonics of the External Cavity (EC) frequency; hence explaining the modulation of the laser intensity at the period of the time-delay. We will classify these events in two distinct categories: lone pulses will be labeled type I, and bunches of pulses will be labeled type II in agreement with the experimental observations of [76]. More specifically through an analysis of the time separating extreme events (which is detailed in Section 5.2.2), we shall consider in the following that any sequence of successive extreme events whose time separation is smaller than twice the time-delay value is called type II.

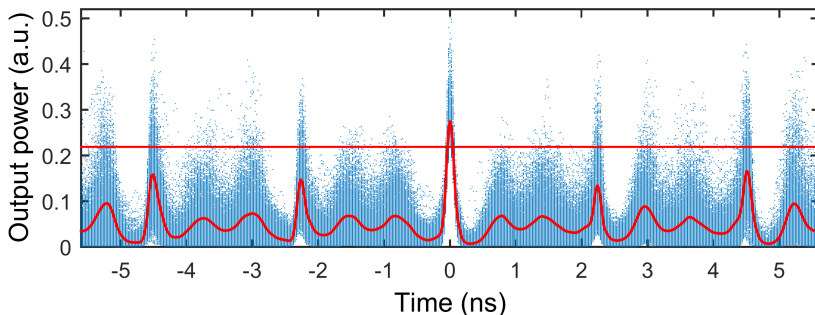


Figure 5.6: Analysis of the correlation between consecutive extreme events. Blue dots are 637 time traces centered around extreme events with the largest amplitude and plotted on a 11.2 ns time window for a feedback rate $\gamma = 0.025$. The red thick line is the averaged time trace of the 637 plotted time traces and the red horizontal line represents the $A = 2$ threshold.

Similarly to the corresponding experiment [76], we have also analyzed the correlation properties of successive extreme events in the laser time-series. For this purpose, in Fig. 5.6, we have superimposed 637 extreme events and centered them on a time window of 11.2 ns. In agreement with the experimental observation, successive extreme events are characterized by an extreme pulse of similar shape and duration, which is preceded and followed by pulses that are correlated and repeat at the period of the delay, with some of these pulses also being extreme events. The pulses that repeat at the period of the external-cavity therefore appear as precursors and replica of an extreme event. This property is highlighted by the red thick line showing the average time trace.

We can learn interesting facts by looking more carefully to the count of extreme events. Figure 5.7(a) confirms what we observed in Fig. 5.4: as the feedback rate increases, extreme events are more numerous in agreement with the experimental observations [76]. However Fig. 5.7(b) shows that extreme events never represent more than 4 % of the total number of events and this number saturates when further increasing the feedback rate, which is consistent with the fact that extreme events are supposed to be rare. This can be qualitatively explained by the bifurcations of the laser diode with PCF. Indeed it is known theoretically from Chapters 3 and 4 that as the feedback rate increases the PCF laser system oscillates around one or several ECMs with an increasing harmonic value of the EC frequency. Therefore the dynamics observed on the same time-interval shows a larger number of pulses and thus a larger number of events among which to count the extreme events. Both the number of events and the number

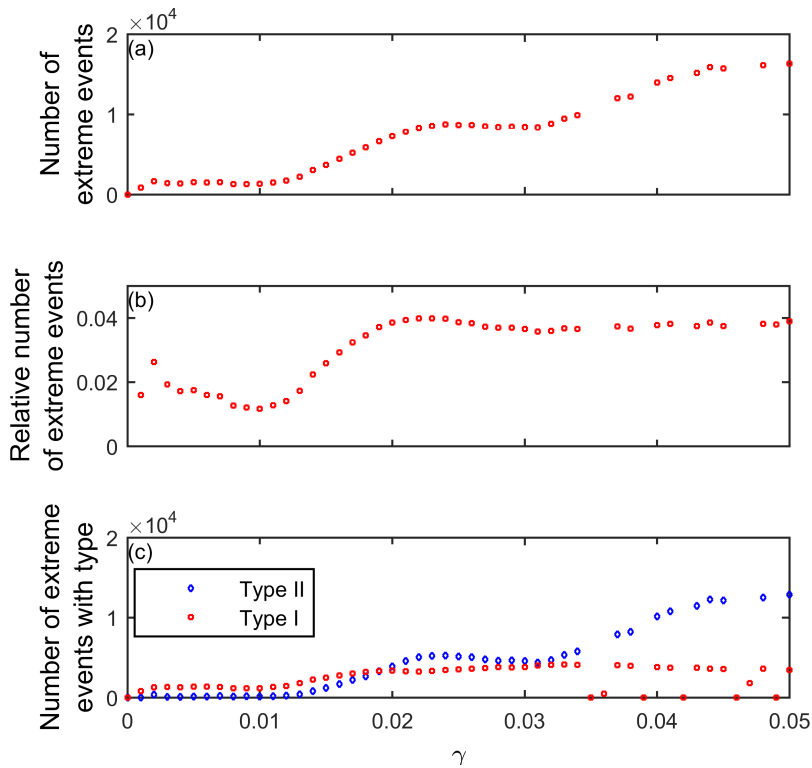


Figure 5.7: Evolution of the number of extreme events with the feedback rate: (a) absolute count over a fixed duration; (b) count relatively to the total number of maxima; (c) absolute count with distinction of types I and II (see text for details).

of extreme events increase with the increase of feedback rate and with approximately the same rate, such that the ratio of extreme events to total number of events remains roughly the same when increasing the feedback rate. In addition, Fig. 5.7(c) shows that although type I extreme events dominate for small values of the feedback rate, increasing the feedback rate leads to not only a larger proportion of type II extreme events (bunches of pulses) but even to a majority of type II extreme events for large values of γ .

This result agrees with the experimental observations of Ref. [76] where were reported an increasing number of extreme events and a larger proportion of type I extreme events when increasing the feedback rate. The crossing point around $\gamma = 0.02$ in Fig. 5.7(c) beyond which type II extreme events dominate over type I extreme events was not reached in the experimental study of Ref. [76], most

probably due to the limited feedback strength (related to the gain of the four-wave mixing in the photorefractive crystal).

As γ increases, we saw that more extreme events are detected over the same fixed duration. This implies that they are more frequent. In the following section, we will discuss how the time intervals between extreme events evolve when varying the feedback rate.

5.2.2 Time between extreme events

Experiments on a laser diode with optical feedback [76] but also on temporally-driven optical speckles [138, 149] suggest that the process generating extreme events behaves according to a Log-Poisson law described in Ref. [150]. To check this feature we define t_k as the time at which the extreme event k occurs, and we measure the logarithmic waiting time between two consecutive extreme events, as follows: $w_k = \ln(t_k) - \ln(t_{k-1}) = \ln(\frac{t_k}{t_{k-1}})$. If the logarithmic waiting times follows an exponential distribution – or a linear distribution when plotted in log-scale – then the appearance of extreme events follows a Log-Poisson law.

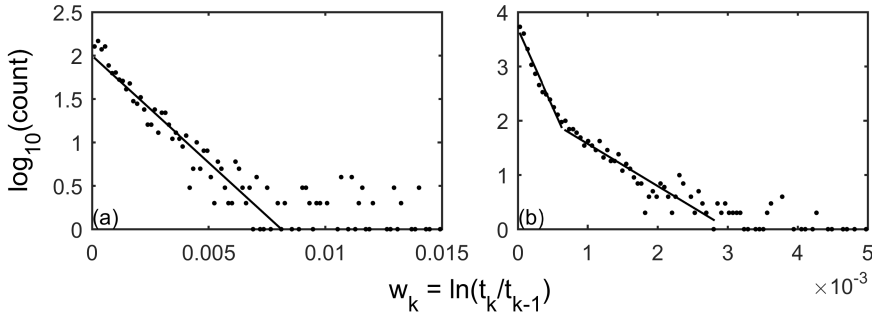


Figure 5.8: Logarithmic waiting times between consecutive extreme events plotted in log-scale. (a) $\gamma = 0.004$: distribution of the logarithmic waiting times is exponential – linear in log-scale – meaning that the generation of extreme events follows a Log-Poisson law. (b) $\gamma = 0.044$: the distribution of logarithmic waiting times splits into two linear portions in log-scale, suggesting two concurrent Log-Poisson processes at different time scales.

For low feedback rates [Fig. 5.8-(a)], we observe that the waiting times w_k are distributed exponentially, which is consistent with experimental observations [76, 138] and confirms that extreme events are generated according to a Log-Poisson law. However, as also observed in experiment [76], increasing the feedback rate leads to a deviation of the statistics of the waiting times w_k ; see

Fig. 5.8-(b). The best fitting unveils two different distributions depending on the time-separation between extreme events. The law for the longest waiting times represents the waiting times that would be normally observed, as in the case of a low feedback rate, while the distribution for the shortest waiting times accounts for repetitions of an extreme event at time intervals close to the time-delay. Indeed, increasing the feedback rate leads to a larger number of extreme events of type II for which not only a main pulse overshoots the threshold $A = 2$ but also do the smaller pulses that repeat at a time smaller or about the value of the time-delay. This yields an increasing proportion of counts of values of time-separation between extreme events smaller or close to the time-delay value, hence modifying the statistical distribution.

5.2.3 Bifurcation to extreme events

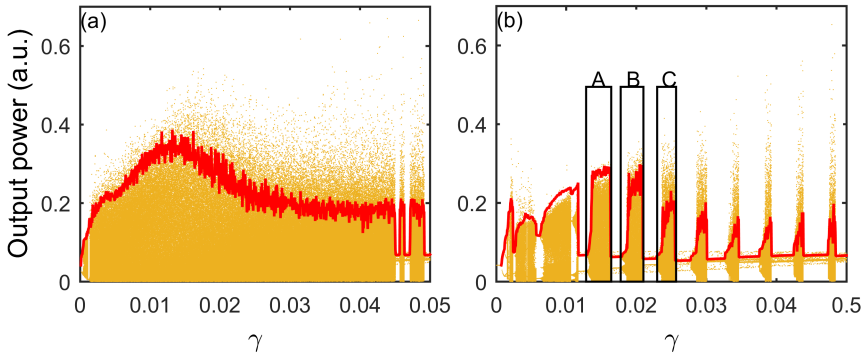


Figure 5.9: Bifurcation diagrams plotting extrema of the output power low-pass filtered at 4 GHz against the feedback rate γ for different EC lengths: (a) $\theta = 1600$, (b) $\theta = 476$. The red line is the $A = 2$ level. Extreme events seem to already appear for a short cavity. Labels A, B and C refer to three particular bubbles of chaos on which we focus in the text and in Fig. 5.10.

The rate-equation model reproduces qualitatively well the experimental observation of the role played by the feedback rate in modifying the number of extreme events, the type of extreme events (type I or type II) and the statistics of the time between extreme events. We will thus use it to bring new light into the sequence of bifurcations that yields extreme events.

Figure 5.9(a) shows the bifurcation diagram in the case of $\theta = 1600$ where local extrema of the filtered time traces are plotted versus the feedback rate γ . The bifurcations leading to chaotic dynamics in a PCF laser system have been analyzed

in depth by several groups, including with the use of so-called continuation methods for delay-differential equations [87, 91, 93, 102, 148]. Our purpose is here to identify the parameter range where extreme events are detected and to relate these regions of extreme pulses with the sequence of bifurcations leading to chaos. The evolution of the power for which $A = 2$ has also been plotted as the threshold above which we consider the intensity pulse as being extreme. This figure brings several new insights. First, it confirms that extreme events are observed in a large interval of feedback rate γ that corresponds to a region of parameters leading to chaotic dynamics, as also evidenced experimentally in Ref. [76]. This chaotic dynamics appears from a sequence of period-doubling and quasi-periodic bifurcations at small feedback rates and experiences a chaos crisis at larger values of the feedback rate, leading to ECMs [102]. Secondly, this figure confirms that as the feedback rate increases, the intensity pulses exceed more and more the threshold value for extreme events, hence increasing the number of counted extreme events when increasing γ .

To clarify the role played by the ECMs it is interesting to compare the bifurcation diagram with the one computed for a smaller value of θ , for example $\theta = 476$ in Fig. 5.9-(b). It corresponds to the situation analyzed theoretically in Ref. [102] and in other publications analyzing in depth the bifurcation scenarios of the PCF laser system [87, 93] as well as in Section 2.3. As γ increases, the first steady-state destabilizes to chaos and the laser experiences a cascade of bubbles of chaos that originate on self-pulsating dynamics and that terminate with chaos crisis leading to another ECM of higher frequency. The chaos crisis was analyzed in detail through continuation methods in Ref. [102] and the succession of ECM with increasing frequencies being harmonic of the EC frequency was evidenced in Chapter 3. This figure brings the same conclusions on first, the increasing number of extreme events when increasing γ , and secondly on the fact that extreme events appear in parameter ranges leading to chaos and close to the onset of a chaos crisis. The important role played by a chaos crisis in generating extreme events was also identified theoretically in a laser diode with optical injection [141].

Still, this figure brings an interesting new message into the mechanism that is responsible for an increasing number of extreme events when increasing the feedback rate. For this purpose we look more carefully into the pulsating dynamics in three different ranges of feedback strength corresponding to the three regions labeled A, B, and C in Fig. 5.9(b). Figure 5.10 compares the pulsating dynamics (with a zoom in the right panels) for increasing values of γ , respectively in regions A, B, C. Two ingredients contribute to increasing the number of extreme events from (a) to (c).

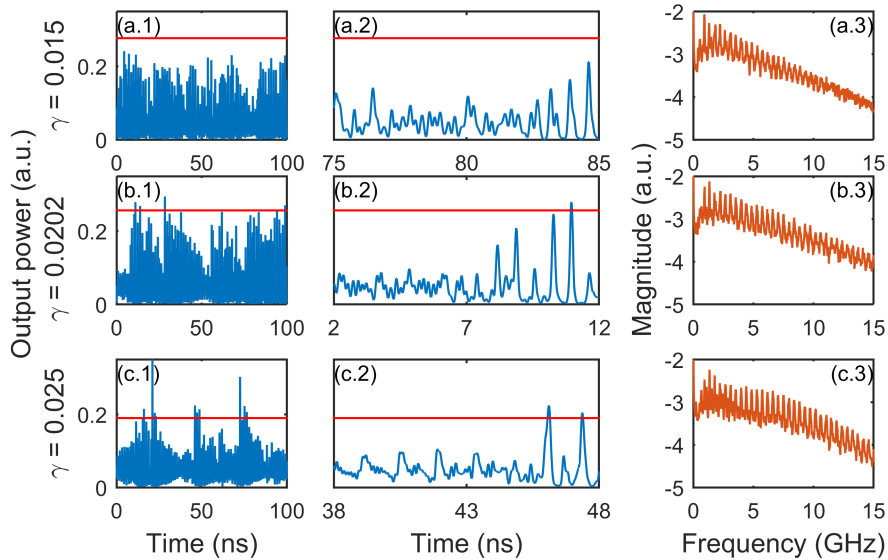


Figure 5.10: Snapshots of time traces in the case of $\theta = 476$ in three different bubbles of chaos labeled A, B and C in Fig. 5.9: (a) $\gamma = 0.015$, (b) $\gamma = 0.0202$ and (c) $\gamma = 0.025$. Left column are snapshots of 100 ns that show the evolution of the $A = 2$ level for similar waveforms. Middle column presents zooms on those time traces that show fast oscillations close to the mean power, with a frequency that increases with the feedback rate. This increase in frequency is responsible for lowering the $A = 2$ level, thus increasing the number of extreme events detected, which can be confirmed in the right column where power spectra of the output power are plotted, showing more higher-frequency content for high feedback rates.

First, as is known in any optical feedback configuration and also identified in PCF [35], increasing the feedback strength leads to an increased level of the average output power. Figure 5.10 furthermore shows that not only the averaged level of the power increases but also does the maximum power when increasing γ . Secondly, a specific feature of PCF is that when increasing γ the laser bifurcates to new ECMs with increasing (harmonic) frequencies [24, 102]. This is clear from panels (a.2)-(c.2). Although the time duration of a pulse that reaches the extreme event threshold remains similar, the dynamics pulsates faster in (c.2.) than in (b.2) or (a.2) for a smaller value of γ and this is mostly visible in the time interval that separates two extreme events. This is also clear in the corresponding spectra where we identify more higher-frequency content while increasing the feedback rate.

Indeed, as stated before, increasing γ means that the system has access to ECMs of higher frequencies. Because of the higher frequency in the dynamics of (c.2.), more pulses and therefore more events are counted in the same time-interval in (c.2.) than in (b.2) or (a.2) hence contributing to decreasing the average value of the pulse intensities among one third of the highest intensity pulses. To say this differently, this explains why the level $A = 2$ decreases with the increase of γ when comparing (a.1), (a.2)-(c.1), (c.2). The decreasing level of the threshold for defining an event as extreme and the larger value of the peak pulse intensity when increasing γ explain the increasing number of extreme events when increasing the feedback rate.

The conclusion drawn from Fig. 5.10 remains true when the criterion for an extreme event uses the definition of the significant height H_s instead of $H_{1/3}$. According to this new definition, the power values corresponding to the $A = 2$ change to 0.73, 0.60, 0.45 from (a) to (c), respectively. As mentioned before, increasing the feedback strength from (a) to (c) leads to a larger amount of events corresponding to pulsing intensities with higher frequencies. Since these high-frequency pulses typically have a small amplitude around the mean value of the output power, increasing the feedback strength leads to a decreasing value of the standard deviation of recorded events, hence to a decreasing value of the $A = 2$ level and to a larger amount of detected extreme events.

5.3 CONCLUSION

In summary, our numerical simulations are in good qualitative agreement with the three main conclusions of the experiment: when increasing the feedback rate 1) the deviation of the intensity statistics to the Gaussian statistics increases leading to a heavy-tailed or L-shaped statistics with a larger proportion of high-intensity pulses, as observed in general in rogue wave statistical studies [134], 2) the number of extreme events increases with an increasing proportion of so-called type II extreme events that consist of extreme intensity pulses repeating at a time smaller or of the order of the time-delay value, 3) the statistics of the time between extreme events deviates from a Log-Poissonian distribution due to the larger contribution of type II extreme events.

A good qualitative matching with all experimental observations is obtained although the rate equation model does not account for several features, as we have seen in Chapter 2. To our opinion this demonstrates the essential role played by the two basic ingredients of the system, the phase-conjugation and the time-delay, in explaining the emergence of extreme events and the corresponding statistics in our system.

CONCLUSIONS OF OUR THEORETICAL WORK

Overall, we have seen in this first part that by using a simple model of a laser with Phase-Conjugate Feedback (PCF) (see Eqs. 2.12 and 2.13) we are capable of qualitatively reproducing the different dynamics that had been reported experimentally: namely External-Cavity Modes (ECMs) which are oscillating solutions at harmonics of the External Cavity (EC) frequency, Low-Frequency Fluctuations (LFF) and the associated itinerancy among destabilized ECMs, and extreme events. Not only the general behavior is correct, with the correct dynamics appearing for ranges of parameters realistic in respect of the experimental configurations, but the model also catches the subtle characteristics of said dynamics: e. g. the difference between type-I and type-II extreme events is present. The only subtle characteristic that was not reproduced for a set of parameters corresponding exactly to the experiment is the coherence resonance in the LFF regime that has been shown to happen in a small bubble of chaos for a shorter cavity.

Since the model only includes the rate-equations of a laser diode with time-delayed feedback of phase-conjugate nature, this leads us to think that PCF is the main ingredient responsible for all the dynamics observed experimentally and that this model is suitable for reproducing the behavior of a laser diode with PCF.

There are several features that the model could include to maybe make it more accurate or to try to reach a more quantitative agreement. Among them, we can cite modeling of the gain saturation, which would probably limit the maximum abnormality index reached for extreme events. We could include the possibility of multiple round-trips in the EC, especially when we study the largest values of the feedback rate. The model would also be more general with the inclusion of frequency detuning between the laser and the phase-conjugated wave, which would lead to different regimes of operation whether the laser locks onto the feedback frequency or not. Finally, we could consider the finite penetration depth inside the photorefractive medium, which would have a filtering effect. But other studies have been made with this assumption and the conclusion seems to be that the filtering effect does not have a strong influence on the behavior of the system as long as the penetration depth is not too long, i. e. 1 cm or less, which is usually the case in the experiment that uses typically an 8-mm long photorefractive crystal [99, 101, 148].

In addition to reproducing the experimentally observed dynamics, we have discovered several things:

- We have confirmed the specific natures of ECMs in a laser diode with PCF. They are self-pulsating solutions at harmonics of the EC frequency and not Steady-State (SS) as in Conventional Optical Feedback (COF).
- ECMs behave surprisingly when changing parameters. Even though they are harmonics of the EC frequency, the actual value of the time-delay has little influence on the frequency of oscillations measured. Instead, the frequency increases with the feedback rate.
- The onset of high-frequency ECMs is responsible for the fast dynamics we observe – LFF and extreme events.
- In particular, an itinerancy among ruins of the ECM attractors happens before a dropout in the LFF regime.

These findings now motivate us to go back to the experiment in Part II to check whether these features unveiled theoretically can be observed in the real system.

For this, we explore a first experimental setup in Chapter 6 – the same as the one used in Refs. [24, 72, 76, 77] – to test the behavior of the system in the LFF regime and investigate the itinerancy. We also use this setup to begin the characterization of the optical chaos from a laser diode with PCF and find indications that it could perform better than a laser with COF for chaos-based applications.

In Chapter 7, we will explore a second original setup – similar to the one used in Ref. [32] – for which smaller cavities and larger feedback rates can be obtained. This setup allows us to observe high-order ECMs and to reproduce the whole succession of bifurcations that leads a laser diode with PCF from the SS, to chaotic dynamics, then to ECMs and finally back to a SS.

Part II

EXPERIMENT

ITINERANCY AMONG EXTERNAL-CAVITY MODES AND CHAOS BANDWIDTH OF A LASER DIODE WITH PHASE-CONJUGATE FEEDBACK

We have explored in Part I the richness of dynamics that a laser diode with Phase-Conjugate Feedback (PCF) can exhibit. Through simulation of a simple rate-equation model (see Eqs. 2.12 and 2.13), we have been able to reproduce the dynamics that had been previously observed experimentally [24, 32, 72, 75–77]. However, in the process, we have discovered new properties of dynamics of a laser diode with PCF that were not observed experimentally before.

Here, we investigate experimentally the itinerancy among destabilized External-Cavity Modes (ECMs) occurring in the Low-Frequency Fluctuations (LFF) regime, more specifically during the time intervals preceding power dropouts. This was unveiled theoretically in Chapter 3 and we explore it in this chapter with the same experiment that was used recently in Refs [24, 72, 76, 77] on which we base most of our work .

In Sections 6.1, 6.2, and 6.3 we present the different components used in the experiment, how they interact with each other and what measurement tools we can use to analyze the dynamics of the laser output. In Section 6.4 we observe experimentally LFF and we compute spectrograms of the time traces to provide evidence of the itinerancy among ECMs. In Section 6.5, knowing that the frequency of ECMs scales with the feedback rate (see Chapter 3), we investigate the possibility to take advantage of this property in order to generate chaos with a large chaotic bandwidth. In Section 6.6 we introduce a theoretical study in which we confirm the experimental results presented in this chapter, before concluding on this study in Section 6.7.

Throughout this chapter, we also make comparisons with the same laser but with Conventional Optical Feedback (COF) in order to provide more evidence of the differences between the two types of feedback. We make sure to have the same External Cavity (EC) length in both cases to guarantee a fair comparison.

Part of the work presented in this chapter has been published in Ref. [151]. Another part has been done in collaboration with Dr. Damien RONTANI and has been submitted for publication with the title “Enhanced complexity of optical chaos in a laser diode with phase-conjugate feedback”.

6.1 LASER DIODE

Nowadays, laser diodes based on semiconductor materials come in all sizes and geometries, for a wide range of wavelengths and different output powers. Here, we use a commercially available JDS UNIPHASE DL-SDL-5400. It is an edge-emitting laser which has an active layer based on quantum wells made of Al-GaAs in proportions such that the emitting wavelength is $\lambda = 852 \pm 4$ nm, which is in the near infrared domain. Typical applications of such a laser include printing, spectral analysis and optical data storage. This specific laser can emit up to 50 mW, but the one we will use in Chapter 7 can emit up to 150 mW.

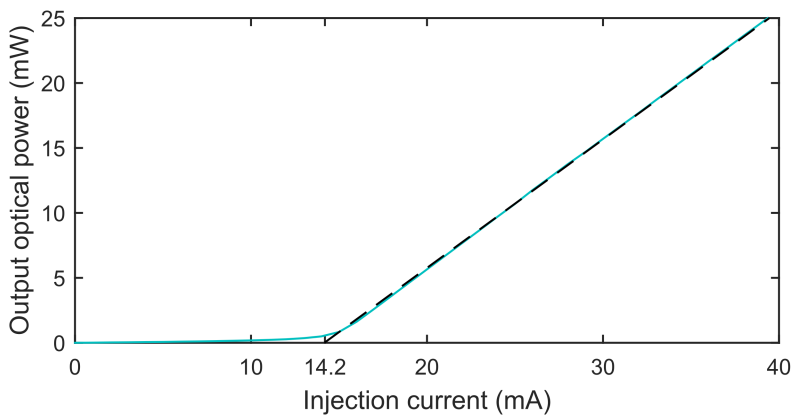


Figure 6.1: Characteristic plot of the optical power emitted by the solitary laser diode depending on the injection current. The dashed black line is a linear fit to the affine portion of the curve. We use it to determine the threshold of the laser where it crosses the horizontal axis: $J_{th} = 14.2$ mA.

The emitted power is varied by adjusting the injection current J of the diode and Fig. 6.1 shows the light-current characteristics of the solitary laser diode. The threshold current is measured as $J_{th} = 14.2$ mA and we will typically operate the laser diode between 25 to 35 mA, because close to the threshold, there is generally not enough power to activate the self-pumping nature of the four-wave mixing configuration in which we operate the Phase-Conjugate Mirror (PCM).

Through the range of injection currents used here, the solitary laser diode always emits in a Steady-State (SS), and in this Chapter, we will use a PCM to destabilize the laser diode and investigate some peculiar features of the dynamics that we unveiled in Chapter 4. Of interest here is the itinerancy among high-frequency ECMs in the LFF regime that our model predicted in Section 4.3.

However, we have not been able to verify if our laser is longitudinally monomode, as we have been assuming in our theoretical modeling in Part II. Indeed, for a semiconductor laser, the frequency interval $\Delta\nu$ between two longitudinal modes can be calculated with the formula

$$\Delta\nu = \frac{c}{2L_{\text{cav}}n_g}, \quad (6.1)$$

where L_{cav} is the length of the laser cavity and n_g is the group index of the active medium, in our case AlGaAs. We used a typical value of $L_{\text{cav}} = 300 \mu\text{m}$ and $n_g = 3.8$ which gives $\Delta\nu = 132 \text{ GHz}$. We can convert the frequency interval into a wavelength interval:

$$\Delta\lambda = \frac{c\Delta\nu}{\lambda^2}. \quad (6.2)$$

In our case, $\Delta\lambda = 0.3 \text{ nm}$. As we will see in Section 6.3.4, it is difficult to measure such a frequency interval with our equipment. The resolution of the optical spectrum analyzer is 0.1 nm and the free spectral range of our interferometer is only 10 GHz. We thus cannot conclude with absolute certainty on the monomode or multimode characteristic of our laser diode. Our measurements seem to indicate that the laser is longitudinally monomode for injection currents under 25 mA but we otherwise rely on the information provided by the data sheet which states that “the SDL-5400 series laser diodes operate in single longitudinal mode under some conditions.”

6.2 PHASE-CONJUGATE MIRROR

We have seen in Section 1.3 that there are multiple ways to experimentally realize a PCM. We decide here to make the mirror using the four-wave mixing process in a photorefractive crystal. For our experiment, we choose a SPS photorefractive crystal, placed in a self-pumped ring cavity setup. This section presents in more details the sample and the configuration it is used in, the motivations behind the choices made, and the characteristics of the mirror we obtain.

6.2.1 SPS crystal

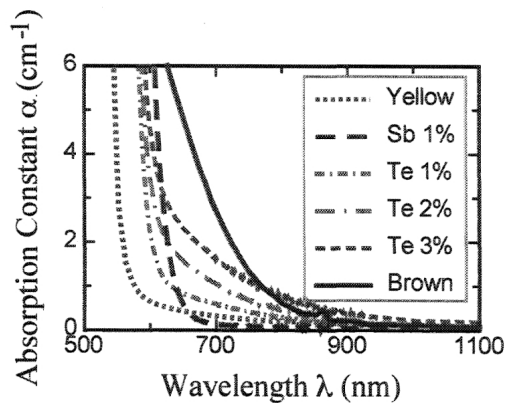


Figure 6.2: Absorption constant of SPS-based crystals with different compositions versus the wavelength. Figure from [152].

Among all the photorefractive crystals that exist, barium titanate (BaTiO_3) and SBN ($\text{Sr}_x\text{Ba}_{1-x}\text{Nb}_2\text{O}_6$) are probably the most commonly used, because they are transparent in the visible domain, they can be doped with several different chemical elements to enhance their properties at some particular wavelengths and they can be used for a lot of different experiments. A less-used, more-recent, but still interesting type of crystal, especially for us, is tin hypothiodiphosphate ($\text{Sn}_2\text{P}_2\text{S}_6$ simply referred to as SPS), which presents low absorption for wavelengths corresponding to red and into the infrared domain, as illustrated in Fig. 6.2. The crystal we use has been doped with 1 % of tellurium to enhance its photorefractive properties in the near-infrared [152], the wavelength of our laser diode. This crystal has been grown for us by A. Grabar from Uzghorod University who we thank here.

Another interesting feature of SPS crystals is their faster response time by comparison to BaTiO₃ or SBN. These crystals typically have a response time on the order of several seconds. Constructing a PCM with this kind of material can lead to build-up times of the mirror attaining several minutes before being completely stable [32]. SPS crystals are expected to respond a thousand times faster, on the order of milliseconds [153]. The original motivation for using this type of crystal was to check whether or not the build-up time of the PCM would have an influence on the laser dynamics when compared to experiments using a BaTiO₃ crystal. Furthermore, this type of crystal was available in our laboratory.

6.2.2 Self-pumped ring cavity setup

We have seen in Chapter 1 that several experimental configurations can be used with a photorefractive crystal to create a PCM[70]. Here, we put our tellurium-doped SPS crystal in a self-pumped ring cavity to perform the four-wave mixing necessary for creating the phase-conjugate of the output beam of the laser diode. This setup requires two conventional mirrors, but is quite easy to realize experimentally [69, 152]. The CAT configuration would probably have been the easiest to implement, but our SPS crystal does not have enough polished facets, required to make use of the total internal reflection. For comparison, in Chapter 7 we propose an experimental setup based on a barium titanate crystal with polished facets used in the CAT configuration.

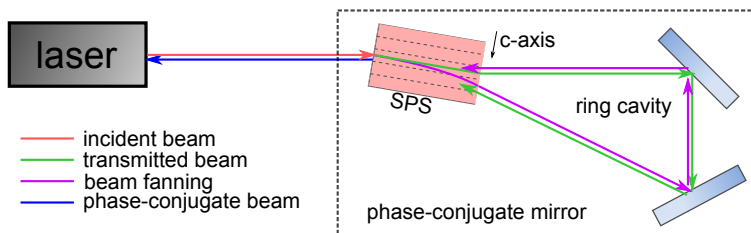


Figure 6.3: Ring-cavity configuration with the SPS crystal. The c-axis is perpendicular to the incident beam and in the plane of the laser polarization: this axis of spontaneous polarization deviates part of the incident beam to create what is called the beam fanning. Four-wave mixing inside the photorefractive SPS crystal creates a refractive-index grating in transmission (dashed gray lines inside the crystal), where the incident and fanning beams are the pumps, the transmitted beam is the signal and the phase-conjugate beam is created.

It is important for us to choose a *self-pumped* configuration because we want to study only the impact of phase-conjugation and not the impact of a wavelength detuning between the output beam of the laser and the beam reflected by the PCM. It is even more important because all our theoretical predictions have been made with a simple model for which we supposed that there was no detuning.

Figure 6.3 shows the ring-cavity experimental configuration with the SPS crystal. It also shows the direction of the c -axis, the spontaneous-polarization axis of the crystal. By having the c -axis parallel to the polarization axis of the laser, part of the beam power is spontaneously deviated in the direction of the c -axis: this effect is known as beam fanning. The dashed gray lines show the internal refractive-index grating that is created in transmission inside the crystal due to the four-wave mixing process¹. The diffraction on this grating yields the PCF field.

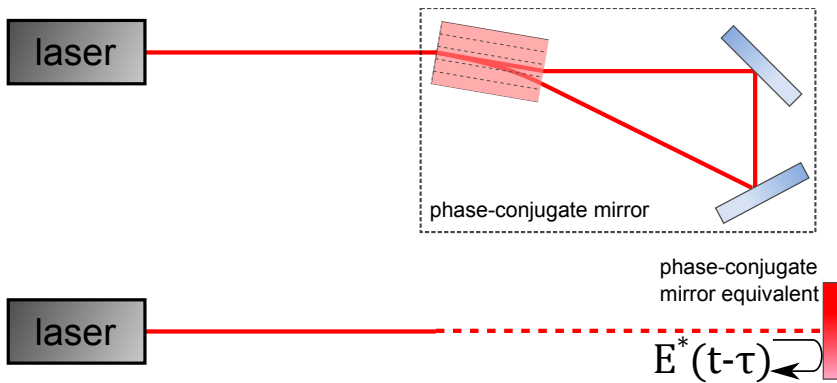


Figure 6.4: Due to the experimental configuration inducing a transmission grating in the photorefractive crystal, the EC length includes the path of light along the ring behind the SPS. The setup on top is thus equivalent in terms of EC length – and thus delay – to the setup on the bottom with a virtual PCM, would it be possible to have such a mirror available as a single component.

In this configuration, the effective length of the EC is equal to the sum of the round-trip length between the laser and the crystal plus the length of the ring behind the crystal. The equivalent setup with a virtual PCM is illustrated in Fig. 6.4. This configuration thus brings a problem to one who wants to study short EC lengths because one cannot get rid of the length introduced by the ring

¹ It is possible to create a reflection grating inside crystal, normal to the propagation axis, which is interesting because in this case the effective length of the cavity is only the round-trip between the laser and the crystal. This configuration allows for shorter delays. It has been reported previously [24, 73].

portion of the setup. In Chapter 7 we use the CAT configuration to obtain shorter EC lengths.

6.3 OPERATION AND MEASUREMENTS

6.3.1 Complete experimental setup

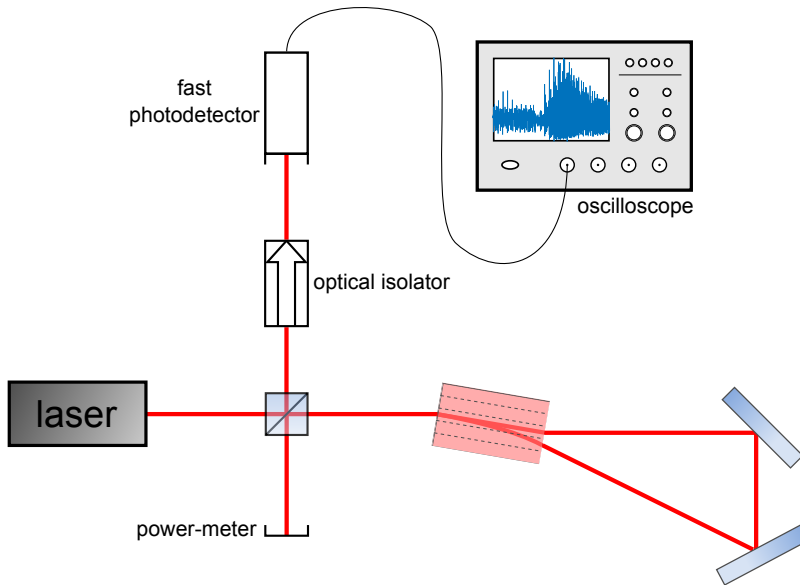


Figure 6.5: Complete experimental setup, with a beam-splitter inserted between the laser and the PCM to either pick up the output signal of the laser and send it through an optical isolator to a fast photodetector or to deviate part of the feedback beam to a power-meter in order to monitor the reflectivity of the PCM.

The complete experimental setup includes a beam splitter in-between the SPS crystal and the laser diode, as depicted in Fig. 6.5. It allows us to have two measurement arms. First, part of the light coming out of the laser is deviated towards an optical isolator, composed of two polarizers and a Faraday rotator. This prevents any reflection from what is placed behind the isolator to be fed back into the laser cavity. Thus we ensure that everything that we observe is due to the PCF and not any other kind of parasitic optical feedback. Figure 6.5 illustrates coupling to a fast photodetector and to an oscilloscope, but we will see in the following sections the different types of measurement available to us.

Secondly, the beam splitter also allows to deviate part of the phase-conjugate beam. This is useful to us because by placing a power-meter in this second arm, we can measure the mean power P_{PCM} coming from the PCM and thus, know-

ing the output power P_{out} of our laser, to estimate the feedback fraction R_{ext} at which we operate. The feedback fraction is defined as the ratio of power effectively going back into the cavity to the power emitted by the laser:

$$R_{\text{ext}} = \eta \frac{T_{\text{BS}} P_{\text{PCM}}}{R_{\text{BS}} P_{\text{out}}}, \quad (6.3)$$

where η is the coupling efficiency of the collimating optics, T_{BS} and R_{BS} are respectively the fractions of transmitted and reflected power from the beam splitter.

The authors of Ref. [100] estimated the value of the coupling efficiency in the case of PCF to be 0.7 ± 0.1 . This estimation is based on comparing power measurements of the laser with feedback to predictions obtained with equations from Refs. [154, 155]. These equations have been derived from an EC feedback model that takes into account multiple reflections for the case of COF. In one of the equations used to estimate the coupling efficiency the authors have to use an approximation of the value of the effective reflectivity of the external mirror which is only valid for small reflectivities and for an EC longer than the coherence length of the laser. As such, there is no guarantee that these equations are still valid when using PCF with large feedback fractions. In the work presented in this thesis, we constantly work with large values of the feedback fraction (up to about 10 %). So we prefer to not use this method due to its uncertainty and we consider $\eta = 1$ as predicted by the phase-conjugated nature of the feedback beam which is auto-aligned with the output beam of the laser. When discussing our conclusions we keep in mind that the coupling efficiency can be lower than unity.

In this Chapter, we adjust the total EC length to be 119 cm, which corresponds to a delay $\tau = 3.97$ ns or a EC frequency $f_{\text{EC}} = 252$ MHz. This delay corresponds to a cavity long enough to observe LFF with a large number of ECMs which will be useful to analyze itinerancy predicted in Section 4.3. It is close to the value used in a previous experiment observing LFF [72] and to the value used in Chapter 4. Further into the study, we will also make comparisons with an equivalent setup using COF instead of PCF. To this end, we also use the experimental setup shown in Fig. 6.6 where we put a conventional mirror in place of the virtual equivalent PCM previously described in Fig. 6.4. In the case of COF, we know that the coupling efficiency is probably not higher than 0.3 [100], so we will take this fact into account when discussing our conclusions.

Using this setup, we can make several types of measurements to gain insight in the dynamics of the system, which can be broken down into three categories:



Figure 6.6: For comparing the effect of PCF in the experiment relatively to the effect of COF, we use the same experimental setup with a conventional mirror (bottom) put in place of the equivalent virtual PCM. Placing the conventional mirror in this position takes into account the fact that the total EC length in the case of the PCM is composed of a round-trip plus the length of the ring. See Fig. 6.4.

- Acquiring time traces: it requires to convert the optical signal into an electrical signal and use an oscilloscope to follow the evolution of the output of a photodetector.
- Measurements in the Radio-Frequency (RF) domain: we use an RF spectrum analyzer in place of the oscilloscope.
- Visualization of the optical spectrum of the output.

We detail these types of measurements and the instruments we use in the following sections.

6.3.2 Measurements in the time domain

Contrary to the case of theory that we explored previously, it is not possible to measure the electric field $E(t)$ of the output beam of the laser diode. However, it is experimentally possible to measure the optical power proportional to $|E(t)|^2$. By using a fast photodetector, we are able to convert variations in the optical power into variations of the output voltage of the detector, which can then be acquired with an oscilloscope.

Since the dynamics we want to measure is typically really fast, we need to use photodetectors with a large bandwidth. In our case, it is a NEWFOCUS 1554-B with a 12-GHz-bandwidth which allows us to capture most of the dynamics we are interested in. To attain such a high electrical bandwidth, this kind of detectors need to have a really small sensing area, which means that they usually rely

on fiber – monomode for this model – input and that they have low sensitivity values. We thus need to couple light into a fiber before measuring, which implies that there are additional losses. Since we work with a high-power laser diode, this is not really an issue, even when taking into account the low sensitivity.

The output of the photodetector is then measured and acquired with a TEKTRONIX DPO 71604C which is a 16 GHz-bandwidth oscilloscope with a large sampling-rate of 100 GSa.s^{-1} . We make full use of these high-end specifications later in this chapter to compute spectrograms of our signals with quite good time and frequency resolutions.

The oscilloscope has a memory depth of up to 100 million points, which corresponds to time traces 1-ms-long at the fastest sampling rate. This duration is long compared to the time constants of the dynamics we are interested in and this means that one time trace is usually enough to make statistics on different properties of the signal.

6.3.3 *Measurements in the radio-frequency domain*

To acquire the RF spectrum associated with the observed dynamics, we have two solutions.

The first one simply consists in computing it from the time traces acquired, by using Fast Fourier Transform (FFT), as we did for simulated time traces previously. Given the specifications of our oscilloscope and the duration of the signals acquired, this method usually yields good results.

The other technique consists in connecting an RF spectrum analyzer in place of the oscilloscope – or to split the output of the photodetector to connect the two instruments at the same time. Here, we can use a ROHDE & SCHWARZ FSW43 which has a 43.5 GHz electrical bandwidth. The downside of using this instrument lies in the fact that it takes some time to scan and measure the whole bandwidth of the dynamics – up to hundreds of milliseconds for the finest resolutions. As such, it is not suitable for measuring transient dynamics, but it can be used in established regimes to offer a better resolution with a better dynamical range than when extracting the dynamics from the time trace.

6.3.4 *Measurements of the optical spectrum*

There are two different tools that we can use to measure the optical spectrum of the laser.

The first one is to use a confocal Fabry-Pérot interferometer, such as a THORLABS SA210-8B with the corresponding controller SA201-EC. It has a Free Spectral Range (FSR) of 10 GHz and a finesse of 150. This kind of measurement tool is useful to determine the shape of the envelope of the optical spectrum. It measures the optical frequency difference relatively to a reference but it does not give information on the absolute wavelength of the laser output. It can be used at the same time as the photodetector by simply adding a second beam splitter behind the optical isolator to deviate a small part of the power into the interferometer cavity.

The second tool available is an ANRITSU MS9740A which is an optical spectrum analyzer. This equipment has the advantage of giving the wavelength of emission with a good precision, but its resolution (0.1 nm or 41 GHz) is not fine enough to detect the details in the envelope of the optical spectrum. Also, it requires a fiber input so it cannot be used at the same time as the photodetector, unless we add a second fiber coupler.

Both tools are thus complimentary, the first one to know the details of the shape of the optical spectrum, and the second one to measure the wavelength of emission.

6.3.5 Clarification about the mirror dynamics

The dynamics responsible for the creation of the PCM are slow when compared to the dynamics of the laser diode – milliseconds compared to nanoseconds. So one could ask if the laser can be sensitive to PCF from a *slow* mirror. The reasoning would be that since the photorefractive material used to enable phase-conjugation – SPS in our case, barium titanate in others – has a slow response time when compared to the dynamics of the laser diode then it is not physically possible for the material to create a phase-conjugate wave at the nanosecond scale.

On the other hand, our view on the matter was that the timescale of the photorefractive material is only important during a transient duration, necessary for the refractive-index grating to build up in the crystal and thus create the PCM. Once the mirror is constructed, phase-conjugation is only produced by the propagation of signal and pump beams inside the grating and the timescale of the material is not important anymore.

In addition, self-pulsing ECMs theoretically shown to be exclusive to the laser with PCF and not possible in a laser with COF had already been reported [24, 72] with this same experimental setup. But we do not know if the PCM responds

instantaneously or if it creates a filtering effect. In order to address this question, we made a simultaneous measurement of the output of the laser and of the beam coming back from the SPS crystal. Instead of measuring the reflectivity with the power-meter, we put a second fiber coupler, which we connected to a second photodetector of the same model and we connected both detectors to our oscilloscope and acquired two time traces simultaneously.

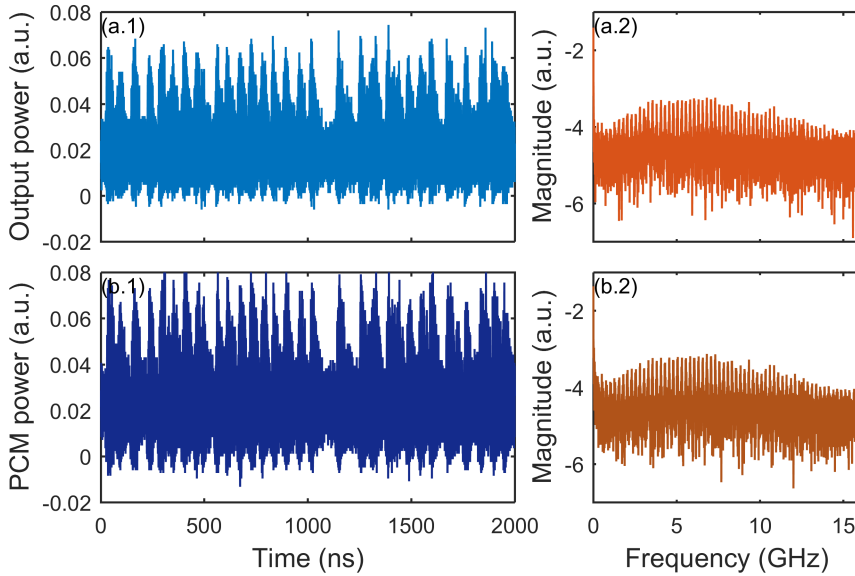


Figure 6.7: Simultaneous acquisitions of (a) the output signal of the laser diode and (b) the signal coming from the PCM. On the left are time traces and on the right the associated RF spectra.

The simultaneous acquisitions are presented in Fig. 6.7: they show that the time traces are almost identical. A small time-shift between the two traces can be seen but it is simply due to the fact that the two measurement arms do not have exactly the same length. When looking at the associated RF spectra in Fig. 6.7-(a.2), (b.2) we observe a very similar frequency content between the output signal of the laser and the signal reflected by the PCM. It shows clearly that the slow response time of the crystal does not have a filtering effect on the reflected signal.

6.4 LOW-FREQUENCY FLUCTUATIONS

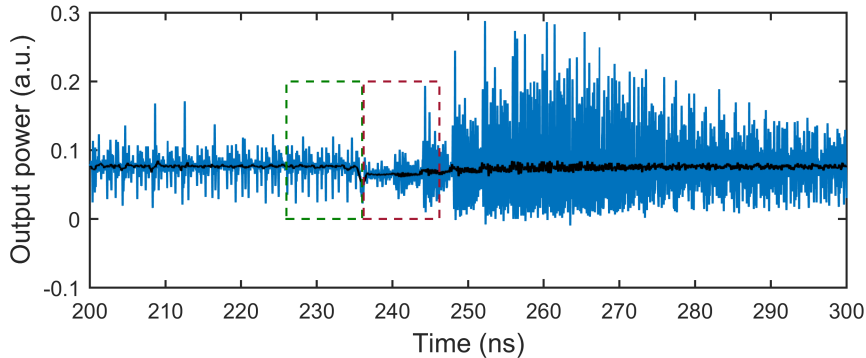
6.4.1 *Radio-frequency content of the signal*

Figure 6.8: Time trace acquired in the experimental conditions described in Section 6.3 where the laser emits in the LFF chaotic regime. The snapshot represented here focuses on a single dropout event. The black line shows the low-pass filtered signal that we use to identify the appearance of the dropout. Green and dark red dashed boxes represent 10 ns-long windows respectively before and after the dropout that are used to compute partial RF spectra in Fig. 6.9.

With the experimental parameters described in Section 6.3 the laser is destabilized into a well-known dynamical regime called LFF [27, 29, 77]. In this regime, the output power of the laser is chaotic and power dropouts occur randomly. This dynamics can be explained theoretically by an itinerancy among destabilized ECMs [28, 35], as we have seen in Section 4.3. A typical time trace is shown in Fig. 6.8 in blue. Superimposed in black is the low-pass filtered trace that allows us to identify the power dropouts.

The purpose of the following analysis is to gain insight into the frequency dynamics underlying LFF in the cases of both PCF and COF. To that end, we wish to discriminate the frequency content before a dropout and just after a dropout. Therefore, we developed a concatenation technique: for each dropout appearing in the time traces, we extract the 10 ns before the dropout (green dashed box in Fig. 6.8). We concatenate these 10-ns-long extracts together and compute the RF spectrum of the concatenated trace to obtain the green spectrum shown in Fig. 6.9. We use the same technique for the 10 ns of time trace following the dropout (dark red dashed box) and obtain the dark red spectra. The downside of this technique is that it introduces concatenating artifacts in the spectra at

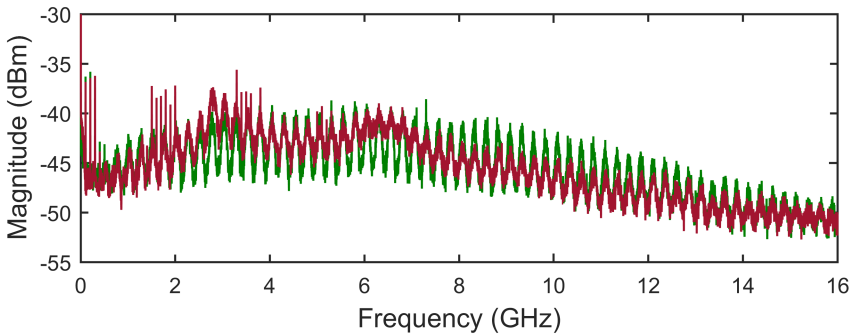


Figure 6.9: Using a concatenating technique (described in the text), we are able to clearly identify two different dynamics that take place in the LFF regime before a dropout (in green) and after a dropout (in dark red).

multiples of 0.1 ns^{-1} . But these artificial peaks are negligible because they are very narrow, usually no more than one point among the thousands of points the total spectrum is composed of.

We are then able to distinguish between the two different dynamics before and after a dropout. Before a dropout the dynamics is mainly dominated by resonances of destabilized high-frequency ECMs (dark red partial RF spectrum in Fig. 6.9), which we theoretically explained as an itinerancy among the ruins of ECMs of large order. We believe that these high-frequency oscillations in a chaotic regime can be useful for potential applications. We will develop that point further into this Chapter in Section 6.5.

After a dropout, the system enters a recovery (or refractory) phase where the laser returns to its average power value and during which no additional dropout can occur. During this phase, the green partial RF spectrum in Fig. 6.9 shows oscillations mainly at the natural relaxation oscillation frequency of the laser diode. This behavior is similar to the one observed for LFF in a semiconductor laser with COF [29].

6.4.2 Spectrogram – observing the itinerancy experimentally

In order to observe the itinerancy predicted in Chapter 4, it is interesting to get a closer look into the frequency dynamics on short time scales around a dropout. For that purpose we apply a STFT analysis on samples from the time traces. STFT consists of computing the RF spectrum on a small window of a signal (we use a 10 ns window, the same value that was used for the concatenation technique), then shifting this window to the next portion of the signal, and repeat the process

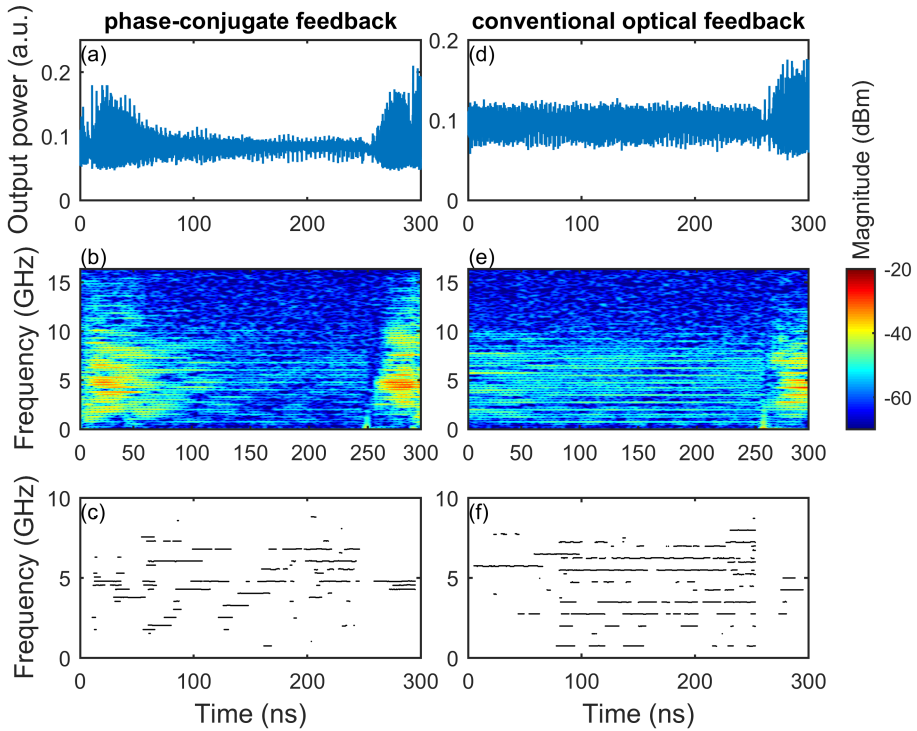


Figure 6.10: We compare the dynamics of PCF on the left and COF on the right. (a), (d) Time traces showing LFF. (b), (e) STFT of the previous time traces allow to follow the temporal evolution of the frequency content of the signals. (c), (f) We follow the highest frequency contributions in the panels of the bottom row, which show the peak with the highest magnitude and the peaks within 3 dB of this maximum.

to scan the entire time trace. Overlapping between consecutive windows (here taken as 95 %) and zero-padding are used to improve the time and frequency resolutions of the resulting spectrograms. Figure 6.10 only show snapshots of time traces but we observed a similar behavior over a lot of dropouts, for several values of experimental parameters (J and R_{ext}).

Figure 6.10 shows the evolution of the output power of the laser versus time, the associated spectrogram and the evolution of the dominant frequencies versus time in the PCF configuration. Dominant frequencies are those that share the frequency with the maximum power, within a 2 dB tolerance. Just after a dropout, i.e. for the first and last nanoseconds of the sample shown in Fig. 6.10-(a), the dynamics is dominated by frequency components around the relaxation oscillation frequency. However, before a dropout, the frequency content is always changing, with specific frequencies close to harmonics of f_{EC} starting or ending to resonate. Especially, panel Fig. 6.10-(c) indicates that there is a tendency for the system to build up higher and higher frequencies as time goes on, with erratic evolution. This erratic onset of harmonic frequencies of the EC frequency with a directional motion in favor of high frequencies is in good agreement with the theoretical predictions in Chapter 4 where in the LFF regime, the system is predicted to have a chaotic itinerancy among the ruins of self-pulsing ECMs, each with their own frequency being a multiple of f_{EC} .

In the case of COF, shown on the right side of Fig. 6.10, the behavior of the system after a dropout is similar to the PCF case, with frequencies around f_{RO} being dominant. However, before a dropout, we observe (Fig. 6.10-(e)) simultaneous resonance of frequency components close to multiples of f_{EC} , which is significantly different from the erratic behavior observed in the PCF case. LFF in a laser with COF have been described as a chaotic itinerancy with a drift [28, 29] which excites destabilized SSs. All of these destabilized modes have a similar frequency signature which is the result of non-linear frequency mixing between f_{RO} and sidebands at multiples of f_{EC} . Therefore when the system jumps from the ruin of a mode to the next one, the frequency spectrum does not vary much.

This analysis confirms our theory about the itinerancy among destabilized ECMs happening in the LFF regime, independently of the type of feedback considered, and stresses the fact that the nature of ECMs – self-pulsating in one case, SSs in the other – has a clear impact on the spectral signature of the dynamics, even though the time traces of the laser power in the LFF regime appear similar at first glance.

6.5 CHAOS BANDWIDTH AND PROPERTIES

Dynamical instabilities due to optical feedback have been known since the early laser developments in the 1970's[27]. Since then, numerous studies allowed for the development of applications using chaos [16] in semiconductor lasers with feedback, including random number generation[48] and encrypted communications[44, 156].

Random number generators need a fast entropy growth, and encryption must have a high data rate, meaning that these applications require high frequencies and large bandwidths to operate [20, 33]. The security of the encryption also relies on chaos complexity and the robustness of synchronization. Time-delayed feedback in a semiconductor laser generates chaos that has these properties. Non-linear frequency mixing leads to high harmonics of the EC frequency [20] and large bandwidths that can exceed the frequency of relaxation oscillations of the laser. Various techniques have been suggested to further enhance the chaos bandwidth [20, 36, 37] including optical injection or adapting the shape of the RF spectrum by using a fiber ring resonator. The time-delayed nature of the system also ensures a chaos of high dimension, with a large number of positive Lyapunov exponents[31].

COF has been used in numerous schemes designed for encrypted communications[16, 20, 36, 37, 44, 157]. In this Chapter, we focus on the properties of chaos from a laser with PCF, and how it compares to chaos from a laser with COF, which consists of feeding the phase-conjugate of the emitted beam back into the laser cavity. We will show that we can extract a chaotic signal with a wider bandwidth from the PCF configuration. In the range of feedback strengths that are achievable with the phase-conjugate mirror, we observe a chaos bandwidth enhanced by up to 27 %.

We focus here on one specific property of the signal, which we call the chaos bandwidth. The usual definition of the bandwidth at -3 dB for systems with a flat response and a cut-off frequency cannot be used for systems exhibiting chaos, since the shape of the RF spectrum is much more complicated, as shown in Fig. 6.11. In the field that studies applications of chaos, the bandwidth is often defined as the frequency that contains 80 % of the total power of the spectra, as commonly used in the literature[36, 37], even though other definitions have been proposed recently [38]. The concatenating artifacts mentioned earlier would influence our results here but as already stated, they are negligible because they represent only a few points. Even if they had an influence, they would lower the bandwidth since they are present at low frequencies. In addition, we also calculated the spectra of the 10 ns before each dropout individually and then

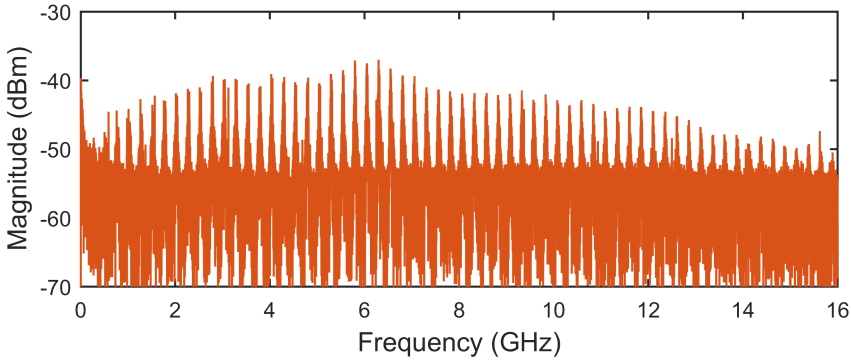


Figure 6.11: RF spectrum of the chaotic signal displayed in Fig. 6.8 shows excitation of harmonics of the EC frequency, and a shape that is not adapted to the classical definition of bandwidth at -3 dB.

averaged them to obtain the mean spectrum, repeating the same process for the 10 ns after each dropout. The resulting averaged spectra yielded conclusions similar to the ones obtained with the concatenation technique.

The concatenation technique is used to compute the spectra in Fig. 6.12. We observe that oscillations after the dropout are dominated by the relaxation-oscillation frequency f_{RO} [29], accompanied by some period-doubling with $\frac{f_{RO}}{2}$ resonating, especially in the case of PCF (Fig. 6.12 (a)-(d)). From the literature[95], we know that increasing the reflectivity can shift f_{RO} toward higher frequencies: f_{RO} goes from 4.5 to 6.5 GHz when increasing R_{ext} from 6.68 % to 9.65 % in the case of PCF, and from 7 to 8 GHz in the case of COF when increasing R_{ext} from 33.44 % to 77.39 %. We should note here that in our experiment, we optimized the COF alignment by maximizing the threshold reduction, assuring the maximum coupling efficiency achievable.

The RF spectra *after* dropouts are similar when comparing PCF with COF. However, the frequency content *before* dropouts is quite different. In the case of PCF, the spectrum extends up to higher frequencies than in the case of COF. Also, the high-frequency content increases with R_{ext} , whereas in the case of COF, the frequency content before dropouts remains relatively independent from R_{ext} .

To illustrate this conclusion, we compute the bandwidths of the spectra before dropouts and report them in Fig. 6.13 (a). We observe that over the course of a few percents of feedback-fraction increase, the bandwidth before dropouts increases drastically in the case of PCF, whereas in the case of COF, to observe the same bandwidth improvement, we have to increase R_{ext} from 20 to 80 % (comparing PCF with COF at $J = 30$ mA). In the range of feedback fractions

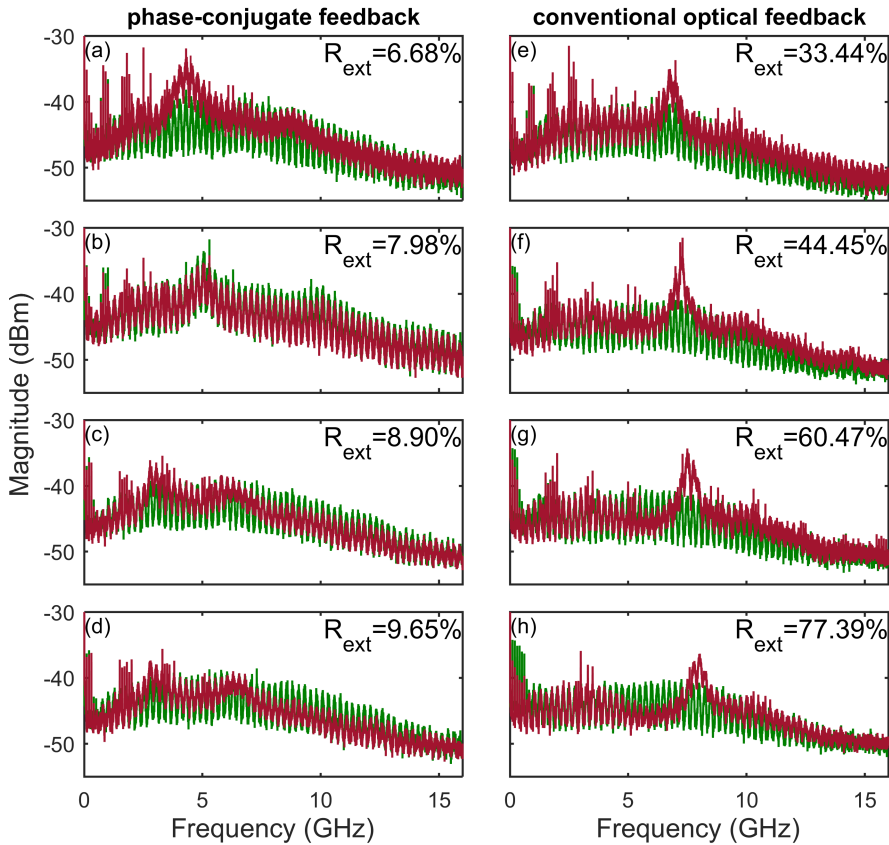


Figure 6.12: Comparison of RF spectra before (green) and after (dark red) dropouts from concatenated time traces between the PCF configuration on the left ((a)-(d)) and the case of COF on the right ((e)-(h)). Values of feedback fraction are indicated in the top right corner of each panel. Similarities and differences from the two types of feedback are commented in the text.

where comparison holds, i.e. being limited to about 14 % due to the limited non-linear interaction strength of the PCF configuration, the bandwidth enhancement ranges from 21 % for $R_{\text{ext}} = 5.9\%$ to 27 % for $R_{\text{ext}} = 12.1\%$.

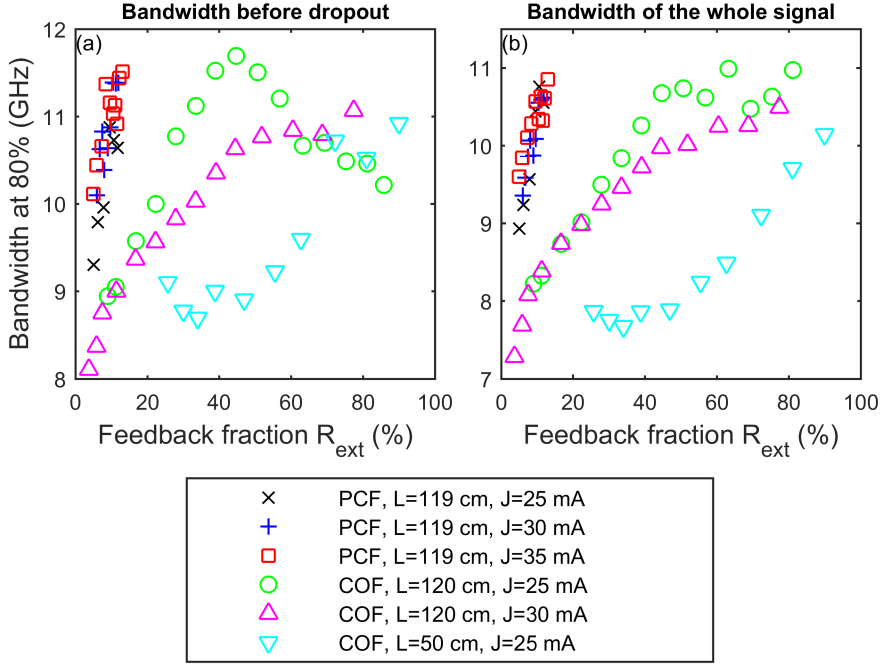


Figure 6.13: Chaotic bandwidth measured from the computed RF spectra (a) for the portion of signal before dropouts and (b) for the whole signal in different configurations: PCF, COF, different injection currents.

Interestingly, when comparing the evolution of bandwidth before dropouts (Fig. 6.13 (a)) and the evolution of bandwidth of the whole signal (Fig. 6.13 (b)) in the two different configurations, we see that they follow the same trends, with almost the same values. This suggests that the increase of the total bandwidth is driven by the frequency content before dropouts, which is consistent with what we observed in spectrograms in Section 6.4, where we demonstrated the itinerancy among high-frequency destabilized ECMs in the case of PCF. This itinerancy is shown here to drive the increase in the chaotic bandwidth of the signal.

For the sake of completeness, we also compare the bandwidth with the one achieved when COF occurs at the position of the crystal, i.e. with a shorter cavity. The results show that the bandwidth is much lower than in the case of the longer external cavity, i.e. the bandwidth increases with the time-delay. We could not test a shorter cavity in the case of PCF because of the way phase-conjugation is

made, we cannot get rid of the length of the cavity ring, and the crystal was already at the nearest possible position from the laser diode.

6.6 THEORETICAL INVESTIGATION OF CHAOS PROPERTIES

In Part I we did not investigate the chaos bandwidth nor the complexity properties of the chaos generated by a laser diode with PCF. After obtaining the experimental results presented in this chapter we initiated a theoretical study to see if simulated time traces reflect the same properties in terms of chaos bandwidth when compared to COF. Additionally, although the chaos from PCF reaches larger bandwidth, one could argue that this is achieved through excitation of several ECMs at higher frequencies. As a result, the chaotic time-trace might exhibit more regular self-pulsation corresponding to these ECMs. We test this hypothesis here with a theoretical study made in collaboration with Dr. Damien RONTANI and results have been submitted for publication [158].

We measured the chaos bandwidth and permutation entropy on time traces of the output power simulated with a non-normalized rate-equation model similar to the model introduced in Chapter 2 except it now includes gain saturation:

$$\frac{d\mathbf{E}(t)}{dt} = \frac{1 + \iota\alpha}{2} \left[g_N \frac{N(t) - N_0}{1 + \epsilon|\mathbf{E}|^2} - \frac{1}{\tau_p} \right] + \eta \mathbf{E}^*(t - \tau), \quad (6.4)$$

$$\frac{dN(t)}{dt} = J - \frac{N}{\tau_e} - g_N \frac{N(t) - N_0}{1 + \epsilon|\mathbf{E}|^2}, \quad (6.5)$$

where $\mathbf{E}(t)$ is the slowly-varying amplitude of the electric field and $N(t)$ is the population inversion. α is the Henry factor, g_N is the differential gain, ϵ is the saturation factor, τ is the time-delay of the feedback, J is the pumping current and τ_e is the carrier lifetime. Our purpose is to compare the properties of chaos generated from PCF with the ones of chaos from COF. An article published recently presented the analysis of the complexity of chaos in the COF case using permutation entropy [43]. For the sake of comparison, we choose here to work with the same model and parameters as in Ref. [43]: the time-delay is taken as $\tau = 1$ ns – although it is different from our experiment – and the pumping current is equal to 1.5 times its threshold value. The model for the case of COF is the same except that in the feedback term the complex electric field is not conjugated. Equations (6.4) and (6.5) are integrated with the same method described in Section 2.3.

With the parameter values used, the laser is quickly destabilized into a chaotic regime. As we have done for the experiment, we simulate time traces for increasing values of the feedback rate η and compute the RF spectra associated on which we measure the chaos bandwidth at 80 %. Figure 6.14-(a)-(c) show three RF spectra for increasing values of the feedback rate and we observe an in-

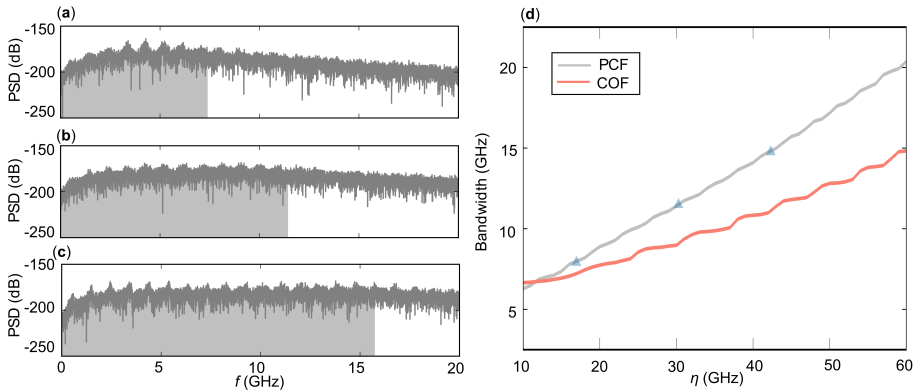


Figure 6.14: (a)-(c) Simulated RF spectra of chaotic dynamics of a laser diode with PCF for increasing values of the feedback rate – $\eta = 15, 30$, and 45 GHz respectively – show increase of the frequency content towards high frequencies. (d) Comparison of the bandwidth at 80 % for increasing values of the feedback rate for a laser diode with PCF and COF. Blue triangles indicate the values for which the RF spectra are shown on the left.

creasing amount of energy into high frequencies reminiscent of our experimental observations in Fig. 6.12.

Figure 6.14-(d) confirms the experimental observations of Fig. 6.13: the chaos bandwidth of a laser diode with PCF can go beyond the bandwidth of a laser with COF. The chaos-bandwidth rate of increase in the case of PCF is about twenty times larger than for COF. In this theoretical study, we find that only for really low values of the feedback rate – under $\eta = 10$ GHz – can the bandwidth be higher in the case of COF than it is for PCF.

Then, we investigate a measure of the chaos complexity called the permutation entropy to see if the increase of chaos bandwidth attributed to using PCF instead of COF can be associated with an increased complexity. Permutation entropy is a useful tool to characterize the chaos complexity of a system since it can be computed directly on time traces and provides good results even in the presence of a small amount of noise and it has been shown to give similar insight into the dynamics as Lyapunov exponents which are usually more complicated to obtain [159]. It is based on the analysis of fixed-length ordinal patterns inside the time traces and the apparition probability of each pattern.

Before giving the general definition of permutation entropy, let us take a simple example of a time series of length $l = 7$ s to explain how it works.

$$\{x_i\}_{i \in [1,l]} = \{5, 8, 4, 9, 7, 3, 1\}. \quad (6.6)$$

First, we consider patterns of length $D_e = 2$ called the embedding dimension, meaning that there are only $D_e! = 2$ possible ordinal patterns (noted π): 01 if $x_i < x_{i+1}$ and 10 when $x_i > x_{i+1}$. In our example, the first pattern 01 appears twice and the second pattern 10 appears four times. This gives us the probabilities $p(\pi)$ of apparition of each pattern, respectively $2/6$ and $4/6$, which allows to compute the permutation entropy of $\{x_i\}$:

$$H = - \sum p(\pi) \log(\pi) = -\frac{2}{6} \log\left(\frac{2}{6}\right) - \frac{4}{6} \log\left(\frac{4}{6}\right) \approx 0.918, \quad (6.7)$$

where we use the base-2 logarithm giving a result in bit. The same can be done for higher embedding dimensions, e.g. $D_e = 3$ for which possible ordinal patterns are 012, 021, 102, 120, 201, and 210. We typically use values of D_e between 4 and 7.

For a time series $\{x_i\}_{i \in [1,l]}$ of arbitrary length l , we define vectors:

$$X_i^{D_e, \tau_e} = (x_i, \dots, x_{i-(D_e-1)\tau_e}), \quad (6.8)$$

with $i = 1, \dots, (D_e - 1)\tau_e$. We add here the parameter τ_e called the time-delay embedding. It represents the time-delay between two consecutive values considered for a pattern and it is a multiple of the sampling period. In the case of time-delayed feedback systems, the permutation entropy is usually measured with a time-delay embedding close to the time-delay of the system [43, 160] to reproduce results given by another quantifier, the Kolmogorov-Sinai entropy [42]. To each of these $X_i^{D_e, \tau_e}$ vectors we attribute an ordinal pattern π of length D_e . We then compute the empirical probability of apparition of each pattern in the considered time series. This allows us to finally compute the permutation entropy H and its associated normalized value h :

$$H = - \sum p(\pi) \log(\pi), h = \frac{H}{H_{\max}}, \quad (6.9)$$

where $H_{\max} = \log(D_e!)$. Therefore $h = 1$ corresponds to the case of equiprobability for all the patterns.

In the case of a laser diode with PCF, Fig. 6.15 shows that over a large range of feedback rates, the permutation entropy is larger than in the case of COF. Only

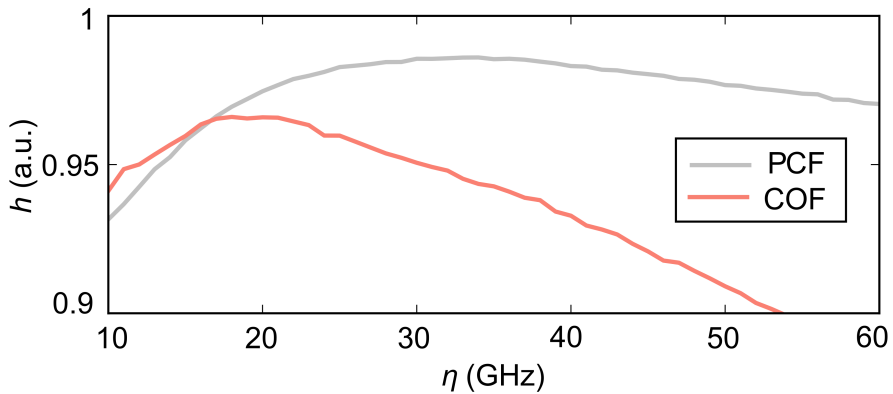


Figure 6.15: Permutation entropy of a laser with PCF and with COF measured as a function of the feedback rate η .

for the lowest feedback rates – below $\eta = 15$ GHz – is the permutation entropy higher in the case of COF. Interestingly, the crossing point of the two curves representing PCF and COF does not happen for the same value of the feedback rate when measuring the bandwidth and when computing the permutation entropy. This suggests that the permutation entropy is not directly correlated with the value of the chaos bandwidth at 80 %. But in the case of a laser diode with PCF, according to these simulations, we can obtain simultaneously a larger chaos bandwidth and a greater complexity than in a laser with COF.

Although it is only a preliminary study of the impact of phase-conjugation in a laser diode with optical feedback, this additional theoretical result confirms the results obtained experimentally. We have been able to reproduce the results of Ref. [43] and compare them to the same configuration but with PCF. Even though the time delay is different than in our experiment, we think that the properties of chaos exhibited in this section can be found for a large range of parameters of the system. In addition to RF spectra and permutation entropy, we have also analyzed the autocorrelation of the signal and the flatness of the spectra. We have found that overall, the laser with PCF shows a smaller autocorrelation at the time-delay which varies slowly with the increase of feedback rate. The RF spectra in the case of PCF have also been found to be more flat than for a laser with COF.

These first results encourage us to analyze the impact of PCF on chaos properties in more details in the future, i. e. with more indicators and a study of the influence of other parameters.

6.7 CONCLUSION

In summary, we have investigated chaotic behavior (LFF regime) of a semiconductor laser subjected to PCF and COF in a 120-cm-long cavity with moderate to strong feedback strength. We have confirmed the itinerancy among destabilized ECMs of the laser with PCF predicted in Chapter 4. In addition we have shown that the bandwidth of a system with optical feedback can be improved by using PCF instead of COF. We have attributed this bandwidth improvement mainly to the high-frequency dynamics that takes place before dropouts.

As evidenced here and besides its fundamental interest, the physics underlying PCF dynamics yields chaotic dynamics at higher frequencies than with COF. Still the present experiment does not aim at setting a new record on optical chaos bandwidth. Optical chaos extending up to 26.5 GHz bandwidth has for example been achieved by injecting the chaos light from a DFB laser with COF into a fiber ring resonator [36]. The bandwidth is however not related to the physics of the laser diode with feedback but to the filter frequency inserted into the ring resonator. It is known also that schemes using optical injection can further extend the chaos bandwidth up to 20 GHz [20] and even further (32.3 GHz) using dual wavelength injection scheme [37]. Injection schemes require however a careful matching of the coupled laser multiple parameters. These and similar bandwidth enhancement techniques [161, 162] can also be applied to further optimize the chaos bandwidth achieved here with PCF.

Additionally, we have shown here that the improvement of bandwidth lies in the self-pulsing nature of the ECMs in PCF. Since adjusting the EC length and more specifically the reflectivity has an impact on the frequencies of the ECMs [24, 93, 102], one can reasonably expect that obtaining a larger range of reflectivities could also improve the bandwidth of our system. Other configurations for the phase-conjugate mirror exist, e. g. using total internal reflection in the crystal [69], and could lead to higher values of the reflectivity. We will test this hypothesis in Chapter 7.

These results have been confirmed with a measurement of the chaos bandwidth in time traces simulated with a model very similar to the one introduced in Chapter 2. We have also introduced the permutation entropy used to characterize the complexity of the chaos emitted by the laser diode.

Finally, although the main focus here is on the fundamental properties of the dynamics of a laser with PCF, we believe this work motivates research in other directions. Since sequences of chaotic high-frequency pulses at harmonic frequencies appear in the recorded chaotic time-trace – due to onset of the destabilized ECMs of the PCF laser system – it would be interesting to check if this property

reflects itself into the spectrum of the Lyapunov exponents and the resulting entropy growth for random number generation[16, 48]. The theoretical study presented in Section 6.6 suggests that it might be the case since simulated time traces of a laser diode with PCF show an increase of bandwidth and complexity when compared to COF. Both theoretical and experimental cases should be analyzed with more details.

BIFURCATIONS TO HIGH-ORDER EXTERNAL-CAVITY MODES

With the ring-cavity setup studied in Chapter 6 we have observed Low-Frequency Fluctuations (LFF) and we have brought evidence of the itinerancy on destabilized External-Cavity Modes (ECMs) predicted in Chapter 4. We have also measured the bandwidth of the chaos emitted by a laser diode with Phase-Conjugate Feedback (PCF) and we have found that it can be up to 27 % larger than for Conventional Optical Feedback (COF).

However, we were limited in our experiment by the maximum reflectivity of our Phase-Conjugate Mirror (PCM) which did not allow to observe the chaos crisis [87, 102]. It was also difficult to study the case of a short cavity because the length of the ring has to be taken into account for the time-delay induced by the External Cavity (EC). We originally wanted to study short cavities because we thought that would be where we can observe the highest frequency of ECMs. But we learned in Chapter 3 that the feedback rate drives the frequency of the ECM oscillating solutions, regardless of the EC length.

In this Chapter, we propose to study a second PCM configuration, which is the CAT configuration we mentioned in Section 1.3. The facets of the crystal used in this chapter are polished and we use total internal reflection inside the photorefractive medium to enable the four-wave mixing process. This allows to obtain shorter ECs – which turns out to not be necessary for observing high-frequency ECMs – and more importantly larger reflectivity values.

In Section 7.1 we present the experimental setup, with the similarities and differences from the setup used in Chapter 6. In Section 7.2 we explore the range of dynamics that appear in a laser diode with PCF while increasing the feedback rate. We observe the excitation of relaxation oscillations, destabilized through quasiperiodicity to a chaotic regime. For large values of the feedback fraction we observe a chaos crisis and the appearance of high-order ECMs – up to ECM_{13} which means a frequency $f_{13} = 13f_{\text{EC}}$. We conclude on this chapter in Section 7.3.

7.1 EXPERIMENTAL SETUP

We propose now to study a second experimental setup, designed to obtain higher reflectivities, which was a limitation of the setup used in Chapter 6. We use a similar laser diode. The PCM is still made through self-pumped four-wave mixing in a photorefractive medium, but this time we use the CAT configuration introduced in Section 1.3 in a Rhodium-doped BaTiO₃ crystal. Incidentally, this setup also allows us to study shorter cavities.

7.1.1 Laser diode

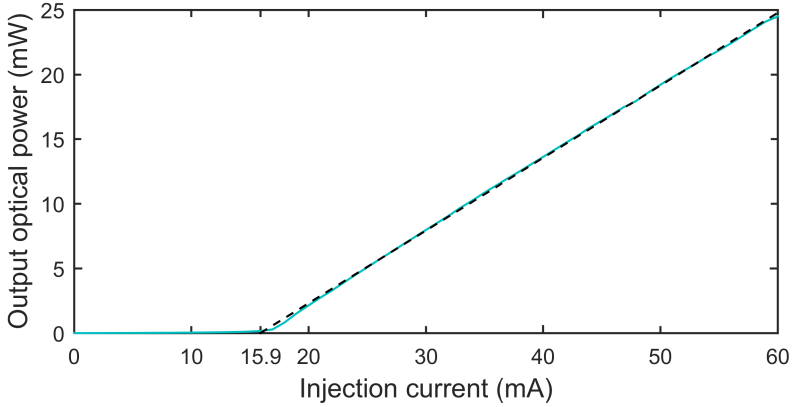


Figure 7.1: Light-current characteristic of the laser diode we use for the second experiment. We measured a threshold current $J_{th} = 15.9$ mA.

The laser diode we use here is a JDS UNIPHASE DL-SDL-5420, which has the same design as the laser diode used in Chapter 6, but this time its nominal power is 150 mW when biased at $J = 200$ mA. We can therefore expect to have similar dynamics but this time, we have more power available for the four-wave mixing process needed to achieve PCF. The light-current curve in Fig. 7.1 shows a threshold current $J_{th} = 15.9$ mA, which is similar to the value for the laser diode in the first experimental setup. According to the data sheet, the operating wavelength is $\lambda = 852 \pm 4$ nm.

In addition, we have also measured the frequency of relaxation oscillations as a function of the injection current in Fig. 7.2 by measuring the Radio-Frequency (RF) spectrum of the solitary laser at different injection currents, subtracting the frequency content due to the noise in the measurement line. This allows to detect

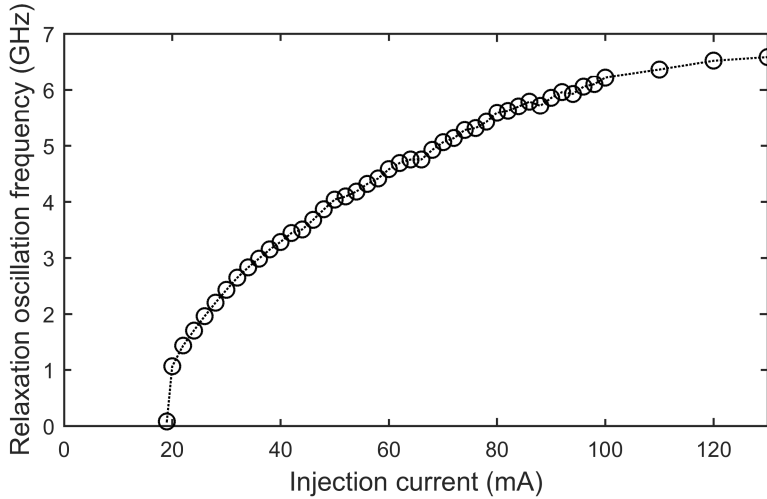


Figure 7.2: Evolution of the frequency of relaxation oscillations as a function of the injection current of the laser diode. The measurements were made with the NEWFOCUS 1554-B photodetector and the ROHDE&SCHWARZ FSW43 radiofrequency spectrum analyzer.

quite precisely the frequency of relaxation oscillations. It mostly follows a square root evolution of the injection current, as predicted by Eq. (1.3).

7.1.2 CAT configuration

The PCM of Chapter 6 is quite efficient, except that it is limited in reflectivity and we would like to operate at higher PCF strength. In addition, the major drawback of using the ring cavity setup is that it is not really practical to realign a crystal and two mirrors (for the ring cavity) every time one wants to change the EC length. That is why we propose here to use the CAT configuration, briefly mentioned in Fig. 1.15 and first introduced in 1982 [74, 163, 164]. Beam fanning inside the crystal and total internal reflection generate the two pump beams required for four-wave mixing. Figure 7.3 is a photograph from the original experiment showing the beams inside the crystal alongside a scheme of the principle of total internal reflection. This type of mirror has been successfully used for PCF experiments in Refs. [32, 75, 100].

Figure 7.3 shows that this setup is easier to use because there is only one element – the photorefractive crystal – to align for the PCM to work, instead of three different elements in the ring-cavity setup used in Chapter 6. Addi-

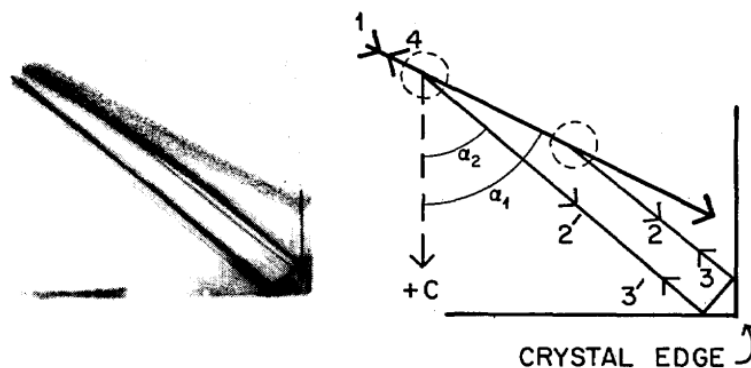


Figure 7.3: (a) Experimental photograph and (b) schematic representation of the beam trajectory inside the crystal in the CAT configuration. The incident beam (1) enters the crystal from top left. Beam 2 splits off due to fanning and is internally reflected twice near the crystal edge and becomes beam 3', which then intersects beam 1 slightly upstream. Beam 2' has also split off from beam 1 and travels around the loop in the opposite direction. Beams 1-3 generate beam 4 by four-wave mixing in the interaction region circled on the right, as do beams 1, 2', and 3' in the interaction region circled on the left. Beam 4 is the phase-conjugate replica of beam 1, and it leaves the crystal exactly back along the direction of the incident beam. Figure and legend from [163].

tionally, we have seen previously that we generally have to take into account the round-trip time inside the ring cavity as part of the total time-delay of the feedback. Since the physical space necessary to implement the ring cavity cannot be reduced infinitely, it is hard to study the short-cavity regime – unless the refractive-index grating is a reflection grating instead of a transmission one which has been observed only once with the ring-cavity setup [24] and is quite difficult to reproduce. Therefore, it is beneficial to use the CAT configuration since it allows obtaining a shorter EC without being constrained by the size and alignment of the ring cavity.

7.1.3 Barium titanate crystal

The original study of the CAT configuration in a photorefractive material used a non-doped BaTiO_3 crystal with an incident light from an argon-ion laser at 514.5 nm [163]. But this type of sample has a bad sensitivity to the wavelength we use. Previous PCF experiments used cerium-doped barium titanate with a red laser [75] or rhodium-doped barium titanate with a near-infrared laser [32, 100].

Through a project for which I supervised master students Cesare ALFIERI and Oulfa CHELLAI, we studied the possibility of making a PCM in the CAT configuration with BaTiO_3 . We used a barium titanate crystal doped with cobalt (10 ppm) and we were able to create an efficient PCM with an argon laser – 35 % power reflectivity with a reasonable response time on the order of ten seconds. Knowing how to do it with visible light, we decided to test the configuration with our infrared laser diode. Unfortunately, we were not able to achieve similar performance for the PCM in the near-infrared domain: the reflectivity was too low – 1 % at most – and the response time was really long – up to 15 minutes. This bad performance was due to the low doping concentration in the crystal. To perform adequately in the near infrared, we would need at least a 1000 ppm concentration of dopant in the barium titanate crystal [74].

After this project, we knew we needed a strong doping in the crystal for it to perform efficiently in the near infrared. After discussions with the German company FEE to see what crystal they could grow for us and we asked them to make a BaTiO_3 crystal doped with rhodium at 1000 ppm. This new crystal will allow us to obtain a greater reflectivity than we were able to do with the first BaTiO_3 crystal or with the SPS crystal in the ring-cavity setup. This will be useful for exploring the behavior of the system closer to the limit of dynamical instabilities (see Section 1.4).

7.1.4 *Experimental setup and phase-conjugation performance*

Besides the fact that we use a different PCM configuration and a slightly different laser diode, the setup is essentially the same as in Chapter 6: we will use the same equipment for measurements in the time-domain, in the RF domain, and optical measurements (details can be found in Section 6.3).

The first step when aligning this setup was to make sure that the lens used to collimate the laser beam was properly aligned, allowing the most efficient coupling of light emitted by the laser. As for the ring cavity setup, this is tricky because our laser is an edge-emitting device, meaning that the output beam is highly divergent in one direction, owing to the fact that the thin active region clad between higher-index regions acts as a slit and diffracts light. For this reason, we know that it is probably impossible to couple all the light, already limiting the maximum feedback fraction that we can obtain.

For maximizing the coupling efficiency, we put a conventional mirror after the coupling lens and align the lens and the mirror so that there is some light fed back into the laser cavity. Adding feedback to a laser brings more light in the

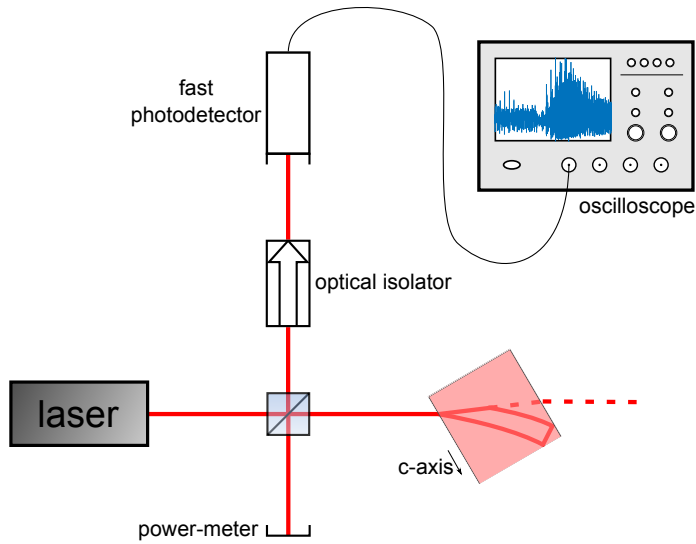


Figure 7.4: We use a similar setup as in Chapter 6, but this time with a barium titanate crystal doped with cobalt in a CAT configuration. We use the same measurements tools as presented in Section 6.3.

laser cavity. This reduces the losses inside the lasing medium. The gain can therefore be used to produce more light, which actually reduces the lasing threshold of the device. This can actually be used as a tool to measure the amount of light going back into the laser cavity: the more the threshold is reduced, the higher is the feedback fraction.

We use this effect here, not to measure quantitatively the feedback fraction, but to align our lens and mirror to maximize the threshold reduction, i. e. to lower the threshold as much as possible. This way, we determine the conditions when we have optimized the lens alignment so that most of the power emitted by the laser is actually coupled back in the laser, and the beam is well collimated so that even a conventional mirror can produce an effective feedback. Figure 7.5 shows that we have reduced the threshold to $J_{th}^{COF} = 12.1 \text{ mA}$ with a conventional mirror in front of the coupling lens. This amounts to 24 % reduction of the injection current threshold of the laser¹.

After the initial alignment of the coupling lens, we put the barium titanate crystal in place and began testing of the optimal configuration. We determined

¹ We have been able to reduce the threshold even further – about 30 % reduction – but the direction of propagation of the beam after the coupling lens was not parallel enough with respect to the table and it was causing problems to align properly the optical isolator and fiber coupler.

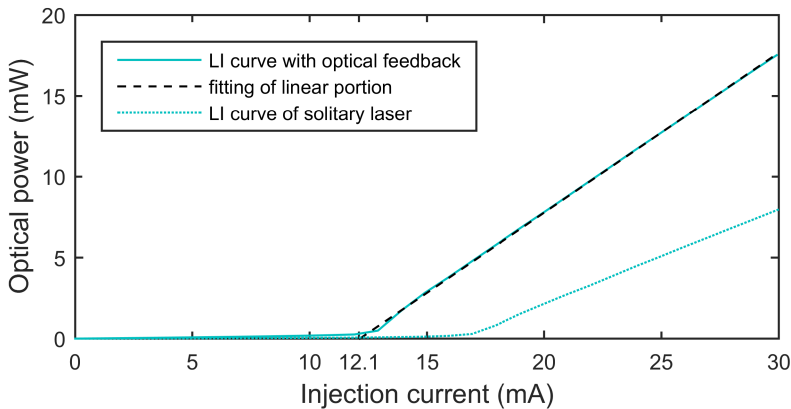


Figure 7.5: Adding conventional feedback to the laser causes a reduction of the lasing threshold – 24 % in this case – measured on LI curves of the laser. We use this technique to optimize the alignment of the coupling lens placed in front of the laser to focus the output beam.

that an incident angle of the laser beam on the crystal in the range of $70\text{-}80^\circ$ produced the best reflectivity results. With such a high angle of incidence, the beam inside the crystal is already close to the critical angle and fanning in the photorefractive medium bends the beam slightly more so that the angle of incidence on the opposite facet is just above the critical angle, thus allowing for total internal reflection needed for the CAT configuration (see again the scheme in Fig. 7.3-(b)).

In Figure 7.6, we present the maximum reflectivity we were able to obtain with an incident angle around 75° for several values of the injection current of the laser. Below $J = 20$ mA the laser does not emit enough power and the four-wave mixing process cannot be initiated, therefore we did not detect any backward phase-conjugated wave. At $J = 20$ mA the crystal begins to act as a PCM but the reflectivity R is not high enough for unlocking the dynamics we wish to analyze, i. e. how the laser with PCF behaves for large feedback fractions. Starting with $J = 35$ mA the PCM reflectivity reaches levels above 20 % which is probably high enough to drive the laser up to regime V. Between $J = 35$ mA and $J = 65$ mA it is relatively easy to obtain values of R between 20 % and 30 %, so we will usually bias the laser diode in this range of injection currents. Above $J = 65$ mA good values for the PCM reflectivity can still be achieved – 10 % and more – but the PCM is more difficult to stabilize, hence the huge variations of reflectivity with large injection currents. This could be due to a saturation of the photorefractive process in the crystal or more complex mechanisms such as

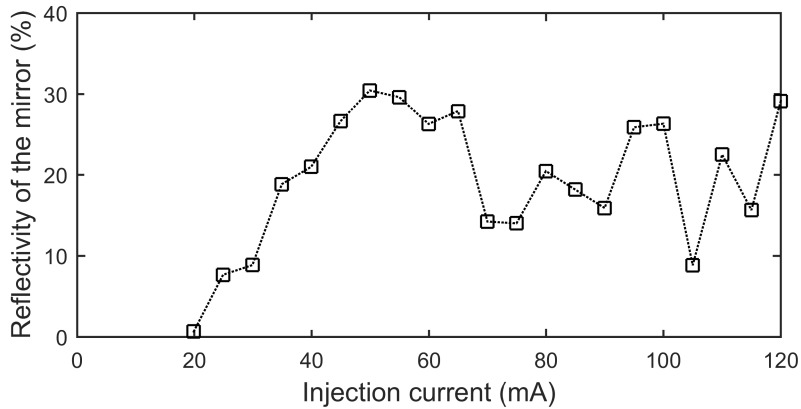


Figure 7.6: With an incident angle of 75° of the laser beam on the photorefractive crystal, we have been able to obtain the maximum stable reflectivity reported on this plot, depending on the injection current of the laser.

competition between gratings in the crystal or the competition between different interacting regions in the crystal which can potentially lead to chaotic behavior of the PCM [165, 166].

It should also be noted that we were able to obtain peak reflectivities slightly higher than the values reported in Fig 7.6 – up to 40 % – but we were never able to stabilize the mirror with such a high reflectivity. Finally, after taking into account the power lost with the beam splitter – $T_{BS} = 79\%$ of power transmitted, $R_{BS} = 18\%$ of power reflected – the feedback fraction F , i.e. the ratio of the amount of power that is fed back into the laser cavity to the amount of power emitted by the laser, is $F = T^2R$. As an example, $R = 30\%$ corresponds to a feedback fraction $F = 18.7\%$, considering that the coupling efficiency of the feedback beam is $\eta = 1$.

Finally, to easily control the amount of feedback, instead of adjusting the gain of the four-wave mixing by changing the position or tilt of the crystal – which would probably give erratic control – we insert a variable attenuator between the beam splitter and the crystal, allowing for precise control of the feedback fraction.

7.2 BIFURCATIONS FROM STEADY-STATE OPERATION TO REGIME V

In this Section, we drive the laser with a constant injection current of 40 mA, and the total EC length – i. e. for the whole round-trip – is fixed at 48 cm. This corresponds to a frequency of relaxation oscillations $f_{RO} = 3.3$ GHz and a time-delay $\tau = 1.6$ ns or $f_{EC} = 616$ MHz. We should note here that we measured the frequency of relaxation oscillations at 3.3 GHz but the RF spectrum of the solitary laser diode at that current is really broad, so that in reality it would be better to describe the relaxation oscillations as a range of frequencies between 2.6 and 4.2 GHz as we can see in Fig. 7.7. We should keep that in mind when looking for the presence of relaxation oscillations in the RF spectra of the laser diode with PCF.

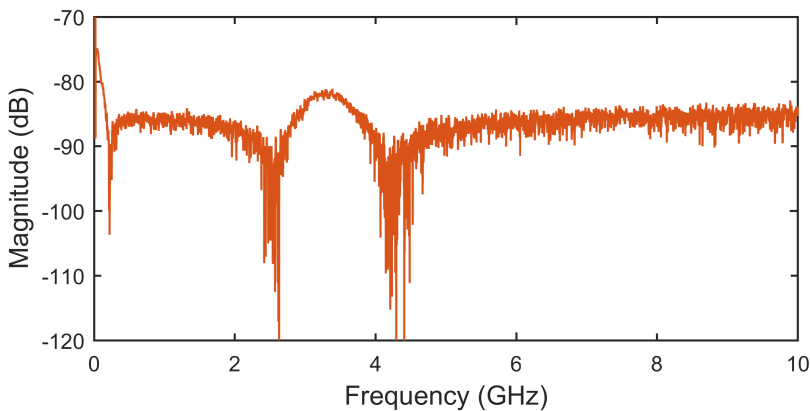


Figure 7.7: Measurement of the RF spectrum of the solitary laser without the noise due to measurement apparatus with an injection current $J = 40$ mA. The relaxation oscillations manifest themselves over a large range of frequencies between 2.6 and 4.2 GHz, with a maximum at $f_{RO} = 3.3$ GHz.

With the variable attenuator, we change the feedback fraction and we observe the dynamics of the system mainly in the time domain, with the photodetector NEWFOCUS 1554-B connected to our oscilloscope TEKTRONIX DPO 71604C. The corresponding RF spectra are computed off-line.

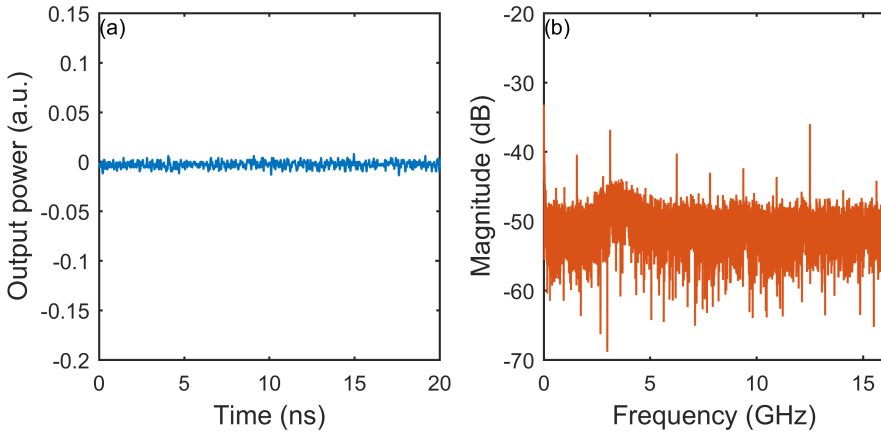


Figure 7.8: (a) Time trace and (b) corresponding RF spectrum of the laser with PCF with no feedback. We can see the laser relaxation oscillations being excited even without feedback.

7.2.1 Evolution of dynamics with mirror reflectivity

No feedback

Without the presence of feedback, the laser is in a Steady-State (SS) as seen in Fig. 7.8-(a). Note that the output power is equal to zero because we have cut the DC for these measurements. Though the time trace seems to show only noise, the RF spectrum in Fig. 7.8-(b) reveals the presence of relaxation oscillations. These are most probably excited by the noise naturally present in the laser diode.

There are unfortunately some sharp peaks appearing on the RF spectrum, which are manifestations of the working frequency of the Analog to Digital Converters (ADCs) and its harmonics. However, for most of our measurement they are not really a problem because the signal we are interested in is powerful enough so that those peaks are drowned in the rest of the frequency content. Moreover, we know their position and they have a sharper linewidth than any frequency component we shall measure so it is easy to know if what we see is due to the frequency of ADCs or is a feature of the dynamics.

Destabilization through quasiperiodicity

For a really low value of the feedback fraction ($F = 0.027\%$), the laser is already destabilized from its initial SS (see Fig. 7.9-(a)). The addition of feedback excites the laser at frequencies 2.92 and 3.42 GHz, which are both well within the range

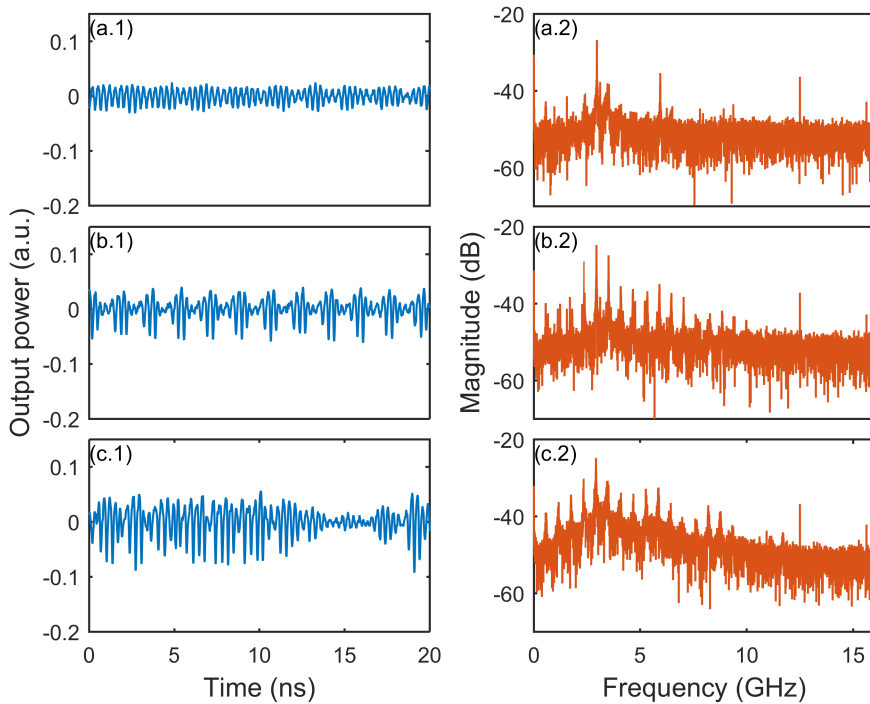


Figure 7.9: Time traces (left side) and corresponding RF spectra (right side) for different values of the feedback fraction. (a) $F = 0.027\%$, (b) $F = 0.031\%$, (c) $F = 0.044\%$. We observe a route to chaos through quasiperiodicity.

of frequencies we defined as the relaxation oscillation frequency in the previous section. As we have seen in Chapter 2, the laser diode with weak PCF undergoes first an undamping of the relaxation oscillations pulsations before entering into a sequence of bifurcations to chaos and ECMs.

Figure 7.9-(b.1), (b.2) show a clearly quasiperiodic time trace. The associated RF spectrum tells us that more and more harmonics of the EC frequency are being excited as we increase the feedback fraction, mixed with the frequency of relaxation oscillations around which the peaks are the strongest.

Finally, in Fig. 7.9-(c.1), (c.2) we can see that the system is already transitioning to chaos with a lot of excited harmonics of the EC frequency and most importantly the base line of the spectrum is gaining some power. This is indicative of frequency content present over a large range of frequencies with significant energy suggesting chaotic behavior. This represents the boundary between quasiperiodicity and fully-developed chaos.

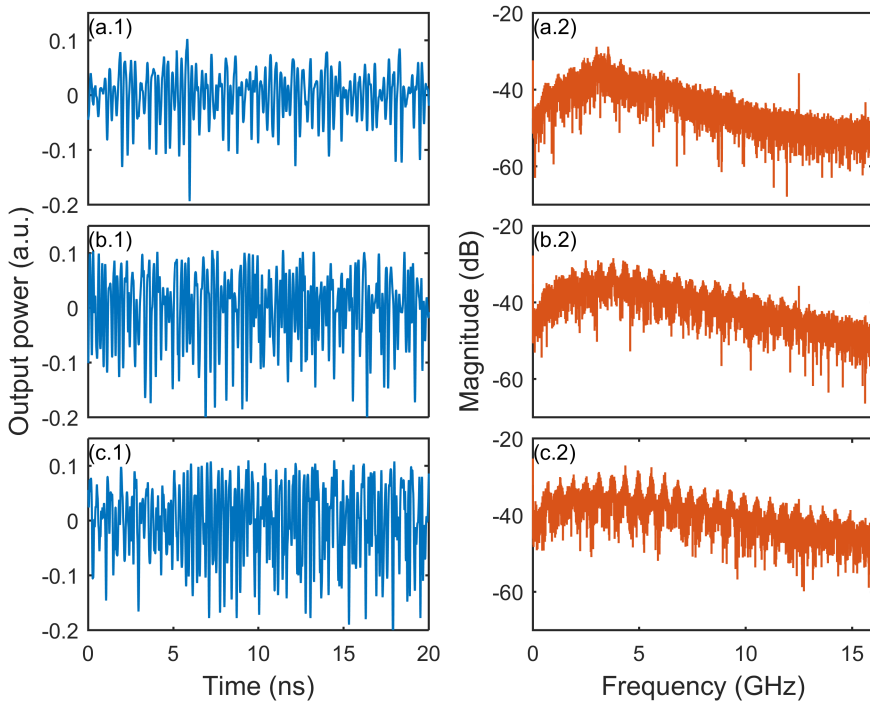
Chaos

Figure 7.10: Time traces (left side) and corresponding RF spectra (right side) for different values of the feedback fraction. (a) $F = 0.101\%$, (b) $F = 0.502\%$, (c) $F = 1.42\%$. Fully-developed chaos gets more energy for high frequencies as the feedback fraction increases.

For values of the feedback fraction over 0.044% , the system is completely chaotic. As we increase the feedback fraction we observe an evolution consistent with the picture depicted with the first experiment in Chapter 6. Figures 7.10-(a.1), (a.2) show a chaotic time trace and its associated RF spectrum where all the peaks observed in the quasiperiodic regime have fully merged into a continuous spectrum with a strong bump around the frequency of relaxation oscillations.

Figures 7.10-(b.1)-(c.2) show the evolution when we increase the feedback fraction up to $F = 1.42\%$. We can see on the time traces that the chaotic oscillations have a larger amplitude. This is consistent with the RF spectra where there is more and more energy, especially in the high frequencies. For frequencies over 5 GHz peaks corresponding to the excitation of high-order ECMs are also more and more present. In Chapter 6, we showed that this increase in energy at high

frequencies led to a bandwidth increase of the optical chaos emitted by the system [151]. Even though the time-delay is really different in this case – 1.6 ns here and 4 ns in Chapter 6 – we observe a similar evolution of behavior in the two experiments.

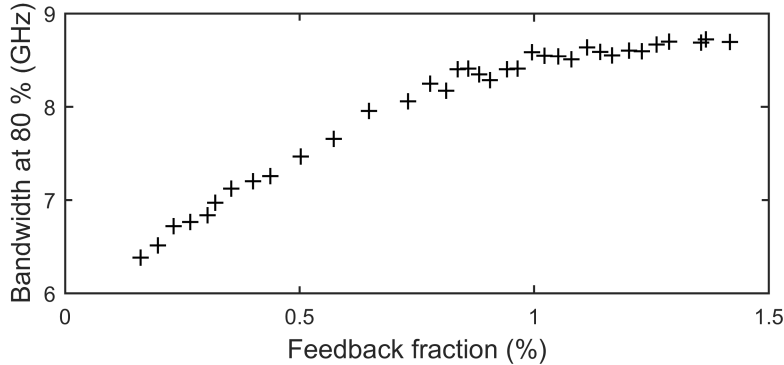


Figure 7.11: Evolution of the chaos bandwidth at 80 % when varying the feedback fraction. We observe a quasi-monotonous increase of the bandwidth, as in Chapter 6, but the values reached are lower and it seems to reach saturation here.

Figure 7.11 presents our measurements of the bandwidth at 80 % in the range of feedback fractions for which the signal is chaotic – between $F = 0.1\%$ and $F = 1.42\%$. The trend is the same as the one observed in Chapter 6: the bandwidth increases with the feedback fraction, though saturation is reached slightly below 9 GHz. In the case of the ring-cavity setup, the largest bandwidth obtained was around 11 GHz and we did not reach saturation. We might observe here the influence of the time delay on the properties of chaos, where decreasing the EC length seems to make the chaos bandwidth decrease too. It would be interesting to make an in-depth experimental analysis of the influence of the EC length, since it is easier to do now with the CAT configuration than it was for the ring cavity in terms of alignment. Additionally, the measurements should be made with a photodetector of larger electrical bandwidth to make sure that the detection fully captures the dynamics created by the laser with PCF. Using a faster photodetector requires to have more power in the detection branch of the setup, which requires further adjustment. So far, our measurements with a faster photodetector have not yield satisfying results due to a low level of optical power.

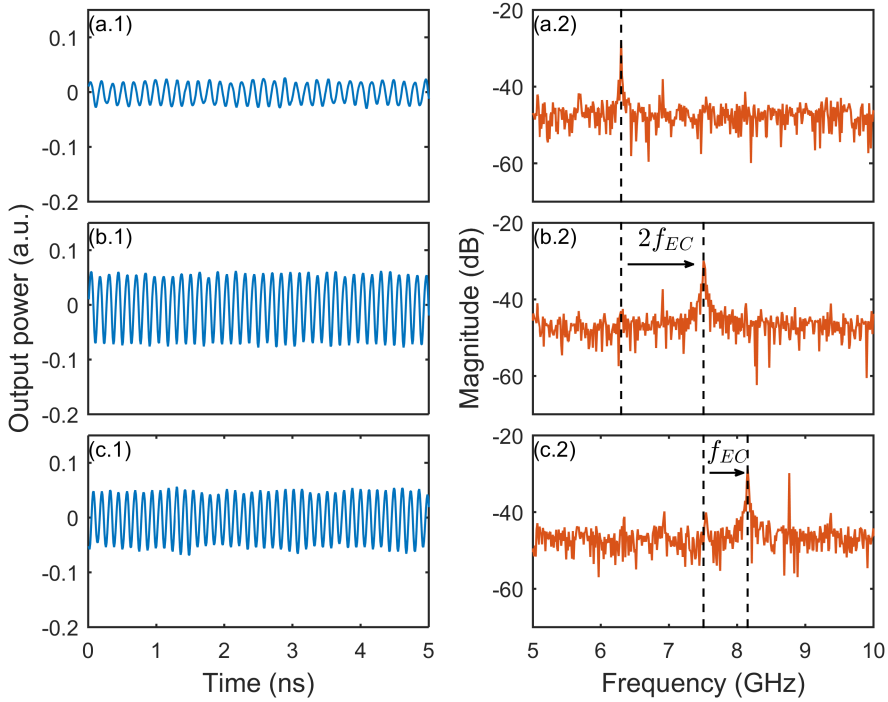


Figure 7.12: Time traces (left side) and corresponding RF spectra (right side) for different values of the feedback fraction. (a) $F = 4.08\%$, (b) $F = 5.77\%$, (c) $F = 6.21\%$. We observe here ECMs of high order for the first time. Note that we changed the axes compared to Figs. 7.8-7.10 so that we see more clearly what happens.

7.2.2 High-order external-cavity modes

By increasing the feedback fraction even further, we observe the predicted chaos crisis [102]. There is no longer chaos and we report here the observation of three different ECMs illustrated in Fig. 7.12-(a.1)-(c.2). The time traces show almost perfect sinusoidal waveforms, which is confirmed by the corresponding RF spectra – only on Fig. 7.12-(c.2) can we observe a second peak near the position of the next ECM which is indicative of some quasiperiodicity or the transition between the two ECMs.

Figures 7.12-(a.1),(a.2) show an ECM solution at a frequency $f = 6.299$ GHz which gives $\frac{f}{f_{EC}} = 10.24 \approx 10$ meaning that this is ECM₁₀ at a feedback fraction $F = 4.08\%$. Next at $F = 5.77\%$ we have a jump of two orders to ECM₁₂ with a

frequency $f = 7.507$ GHz (see Figs. 7.12-(b.1),(b.2)). Finally, we observe a jump to ECM_{13} at a frequency $f = 8.154$ GHz for $F = 6.21$ % in Figs. 7.12-(c.1),(c.2). This is a strong improvement from our previous experimental setup where the limited reflectivity did not allow us to observe these high-order ECMs – ECMs of order up to 5 had been reported [24, 72].

7.2.3 Regime V

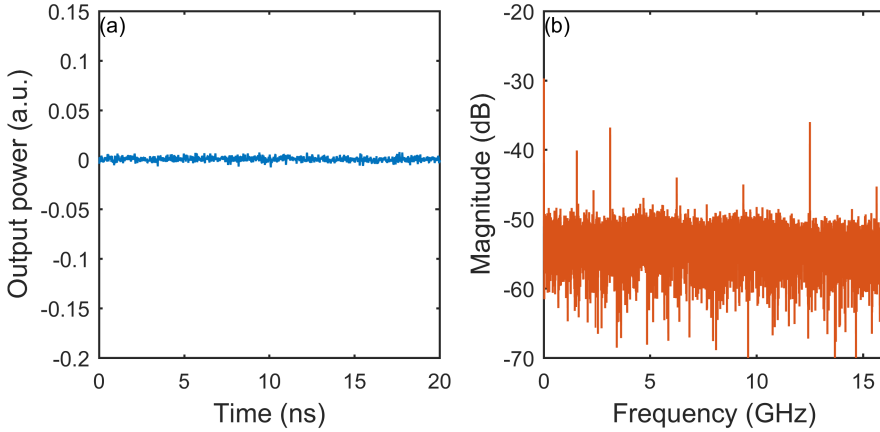


Figure 7.13: (a) Time trace and (b) corresponding RF spectra for feedback fraction $F = 9.62$ %. The laser stabilizes on a SS for large feedback fractions, which is called regime V.

For larger values of the feedback fraction, we do not observe any dynamics, the feedback is too strong and the laser restabilizes on a SS, which is what we called the regime V (see Fig. 7.13). Increasing the feedback fraction further – we were able to reach $F = 25$ % with this setup – does not have any impact on the dynamics and the laser stays in this SS. This behavior is not predicted by the theory we developed in Part I, where we only predicted a succession of ECMs of higher and higher order after the chaos crisis. This is not so surprising when considering that the Lang-Kobayashi model [8] for a laser with COF – from which Eqs. (2.12) and (2.13) are adapted – does not predict the apparition of this regime V. However, what can be surprising here is the fact that a laser diode with PCF can restabilize on a SS, when all the other solutions of the system – the ECMs – are self-pulsating solutions except for the initial SS that is quickly destabilized to chaos. This surprising finding will require further classification, however beyond the purpose of this thesis.

The possibility to observe these high-order ECMs is a crucial achievement of this thesis. It was a long-time goal of our group to show that they were experimentally observable. Lower orders had been observed before in the same experiment as the one described in Chapter 6: ECMs of orders up to 5 had been observed with an EC frequency of 680 MHz. Here, with a similar EC frequency $f_{\text{EC}} = 616$ MHz, we observe orders up to 13, but we lack the observation of the low-order ones. Another study that mapped the frequency of dynamics in a laser with PCF did not report on the observation of high-order ECMs even though they went up to regime V [32] and reported some intriguing behavior at the transition from regime IV to V. They suggested that this might be due to bifurcations on high-frequency solutions. They only clearly observed the first ECM during the route to chaos but not the quasiperiodicity following self-pulsation at the frequency of relaxation oscillations.

We attribute this success to the fact that we use a design optimized to allow us to explore the largest values of the feedback fraction – up to regime V – and also to the fact that we now have better tools for measurement that allow us to observe oscillations at frequencies up to 16 GHz in our case.

7.2.4 *Instability of the mirror*

Figure 7.12 shows ECMs of orders 10, 12, and 13 with increasing values of the feedback fraction, respectively 4.08, 5.77, and 6.21 %, but the order 11 is missing. If we had made a measurement at $F \approx 5$ %, we would probably have been able to catch it. This brings us to one actual problem with this experimental setup: the instability of the PCM.

Up to feedback fractions where the system is chaotic – around $F = 2$ % – the mirror behaves nicely. The response time is quite slow due to fact that we use a BaTiO_3 crystal for which time constants are of the order of the second. It is thus easy to precisely tune the feedback fraction to the desired value and to make all the needed measurements.

However, the situation changes for $F > 2$ % when the reflectivity of the mirror starts to drastically and erratically increase over a few seconds resulting in a feedback fraction increase of more than 10 %. After this quick evolution, the feedback fraction stabilizes again around 15 % and begins to slowly decrease, until the four-wave mixing process inside the crystal completely stops and the mirror is destroyed, thus falling back to a feedback fraction of 0 %. Then the mirror builds up again and the cycle is repeated, sometimes almost periodically. Figure. 7.14 illustrates this behavior.

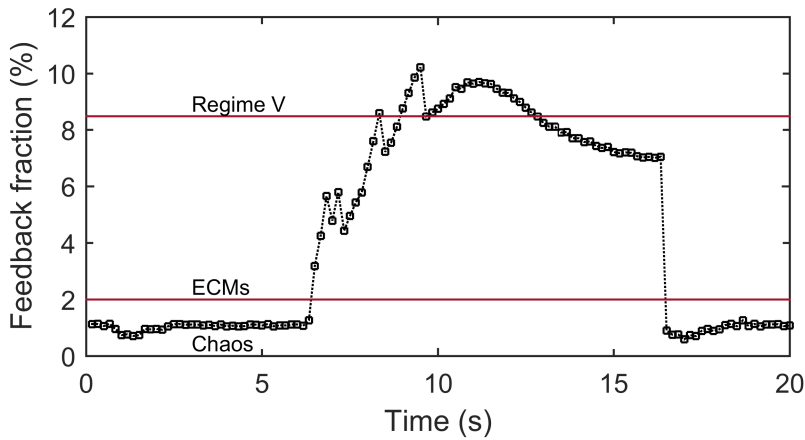


Figure 7.14: Evolution of the feedback fraction versus time when we try to reach $F > 2\%$. The mirror behaves erratically for a time until the feedback fraction stabilizes to a level above 8%, then it starts to slowly decrease and finally drops off suddenly.

During the rapid increase of the feedback fraction, we can observe the high-order ECMs reported in the previous sections, sometimes mixed with quasiperiodicity – due to the fact that the system jumps from one ECM to another. By precisely timing a measurement of the feedback fraction and an acquisition on the oscilloscope we have been able to observe the measurements of Fig. 7.12 but it is impossible to finely tune the feedback fraction in this case. That is why we have not been able to obtain a measurement of ECM_{11} .

We have no clear understanding of the reasons for this behavior but a possible explanation would be the presence of chaos in self-pumped photorefractive materials which has been reported previously [167] with similar waveforms [166]. Other explanations would include a modification of the intensity profile of the laser at the transition from chaos to ECMs which would result in a change of the refractive-index grating inside the crystal which would make it unstable.

7.3 CONCLUSION

In this chapter, we have designed a second experiment which makes use of the CAT configuration and a rhodium-doped BaTiO₃ photorefractive crystal which has a good sensitivity to the near-infrared wavelength of the laser diode – a similar but more powerful version of the diode used in Chapter 6. The CAT configuration is based on total internal reflection inside the crystal, meaning that there is no more need for an additional ring cavity. This means that it is easier to investigate configurations with a smaller EC cavity length and therefore a smaller time-delay. By choosing a material highly sensitive to the 852 nm wavelength, we can also build a PCM with a greater reflectivity than obtained with the first experiment. This allows us to explore the full range of dynamics that our laser can exhibit.

We have observed the relaxation oscillation frequency of our laser being stimulated even when solitary. We have experimentally reported on the cascade of dynamics when increasing the feedback: excitation of relaxation oscillations, destabilization through quasiperiodicity, chaos and its expansion towards excitation of high frequencies, and finally observation of high-order ECMs. This evolution matches predictions from the theory (see Ref. [102], Chapter 2) and the experimental observations of Chapter 6.

ECMs of frequencies up to 8 GHz (ECM₁₃) have never been reported experimentally and offer a good confirmation of the prediction of a chaos crisis for large values of the feedback rate. This finding possibly opens the way to applications where optical oscillators of high-frequency are needed [114], a role that is usually filled by lasers with an integrated Distributed Feedback (DFB) cavity.

However, we also report on a technical difficulty of the experimental setup that makes the PCM unstable for the larger values of the feedback fraction. We have no clear reason as to why this happens. Leads include: an effect of temperature since our crystal is not cooled, additional non-linear effects inside the photorefractive crystal, changes in the spatial profile of the laser beam under strong feedback, chaotic or oscillating behavior of the PCM [166, 167]. Adding an optical isolator in front of the laser diode and see if this behavior can be reproduced would allow to identify the source of the problem. If the same observations are made, then we would know this is due to a physical effect inside the photorefractive crystal. If the same behavior is not observed, then this is due to a change in the laser-beam properties due to optical feedback.

Part III

CONCLUSION

CONTRIBUTIONS AND PERSPECTIVES

8.1 SUMMARY OF THE RESULTS

The work of this thesis is part of an ongoing field of research studying the impact of optical feedback on laser diode dynamics and more specifically Phase-Conjugate Feedback (PCF). We have seen in Chapter 1 that only a few studies have been published about PCF, in contrast to similar works related to Conventional Optical Feedback (COF). Feedback from a Phase-Conjugate Mirror (PCM) has an interesting feature in that it generates External-Cavity Modes (ECMs) which are self-pulsating solutions at harmonics of the frequency of the External Cavity (EC). This feature, specific to PCF is the first motivation for us to analyze this system.

The second motivation came from recent experimental results which showed that a laser with PCF can exhibit a whole range of chaotic dynamics. But there was a lack of theoretical understanding of the physics of the system. Our second motivation was therefore to analyze with more depth the theory to reproduce and to explain the experimental observations.

In this context, we decided to take a look at a simple rate-equation model taking only into account a time-delayed contribution to the electric field which is phase-conjugated with respect to the output of the laser. This model was primarily investigated through numerical simulations. Here are a summary of the theoretical results:

- with the help of analytical calculations and continuation, we first showed that ECMs of a laser diode with PCF can be stable for a large range of feedback rates, allowing to obtain self-pulsating solutions at frequencies up to several gigahertz and higher, potentially corresponding to more than ten times the EC frequency.
- these ECMs show peculiar self-pulsation properties: the system self-determines its frequency of oscillation depending on the value of the feedback rate and independently from the value of the EC. This leads to oscillating solutions for which the frequency is equal to more than ten times the EC frequency. It is a counterintuitive result for a laser diode with an EC in which oscillating solutions usually happen at the EC frequency.

- the model reproduces the Low-Frequency Fluctuations (LFF) regime where dropouts of power occur at random time intervals. We showed that a dropout was associated with a repulsive trajectory in the phase space of the system, and that the recovery process involved itinerancy among the ruins of destabilized ECMs attractors. Knowing that each ECM is a self-pulsating solution with a different frequency that scales with the feedback rate, we can analyze the time traces of the output power and therefore visualize the evolution of the frequency content over time during the itinerancy or when changing the feedback rate.
- the model also reproduces a chaotic regime where extreme events appear. We show that the statistics of the height of the events follows a deviation from a Gaussian law, typical from rogue waves or extreme events. Subtle features of the dynamics are well reproduced, such as the separation into two types of events: the ones repeating at the time-delay and the ones happening at random time intervals.

To us, all these results put together show that a simple model is enough to reproduce qualitatively the experimental observations. Additionally, this also shows that PCF alone can account for the reported observations, and therefore that said observations were indeed the result of PCF and do not come from other sources such as noise, nor other nonlinear phenomena in the photorefractive crystal.

With this new theoretical knowledge in mind, we went back to the experiment to see especially how we could take advantage of the high-frequency dynamics coming from high-order ECMs, and if we could indeed observe the aforementioned itinerancy. For this, we relied on the same setup that was used for the recent experimental observations and we also designed a second experiment to test the behavior of the system at larger feedback rates. Here are the main experimental results:

- we actually observed the itinerancy among ruins of ECMs in a LFF regime by using a large-sampling-rate oscilloscope and a technique called Short-Time Fourier Transform (STFT) which allows us to compute spectrograms with fairly good frequency and time resolutions. We showed that ECMs exhibit their different spectral signature as time goes on before a dropout. We also contrasted this result with a study of COF where there is clearly no observation of similar spectral signatures, owing to the Steady-State (SS) nature of ECMs in the case of COF.

- we showed, again by contrasting with COF, that a laser with PCF could perform better in terms of chaos bandwidth. Up to 27 % increase of the chaos bandwidth has been recorded for PCF in comparison with COF for the same laser and feedback parameters. This opens the way for using PCF in chaos-based applications that require a large bandwidth such as chaos-encrypted communications and random number generation.
- this experimental measurement was followed by a short theoretical study which confirmed the trends we observed. The bandwidth measured on simulated time traces was larger for PCF than COF and associated with a higher complexity, measured by the permutation entropy.
- we have observed a signal coming back from the PCM and compared it to the output of the signal, showing that the high-frequency features of the signal are present in the reflected beam. This clarifies definitively that the time constant of the photorefractive material has no filtering effect on the laser dynamics.
- we were able to reproduce entirely the succession of bifurcations the system undergoes when increasing the feedback rate. We report on the experimental observation of the predicted chaos crisis that happens for large values of the feedback rate as well as ECMs of order up to 13, corresponding to an oscillation frequency of about 8 GHz for an EC frequency of 616 MHz. This is a great achievement when considering that ECMs have been observed only once in experiment and their observation was limited to low-order ECMs (nearby ECM_2 and ECM_3).

When compiling these experimental results, we believe that we have brought significant new light into the understanding of the dynamics of a laser diode with PCF, their richness, and their differences when compared to a laser diode with COF. By going back and forth between experiment and theory, we have proven that the model used is qualitatively accurate, without taking into account complex phenomena (e. g. influence of the process responsible for phase-conjugation, multiple round-trips in the EC). Finally, we have showed that chaos from a laser diode with PCF exhibits interesting features that might be advantageous to applications using optical chaos as a physical source of entropy. The peculiar nature of ECMs of the laser diode with PCF could make it a source for tunable microwave oscillations.

8.2 PERSPECTIVES

Looking at the work presented in this thesis, in particular the main achievements that we have summarized, we suggest perspectives for further studies that we deem interesting.

8.2.1 *Chaos properties*

Work could be done in further analyzing the complexity and the properties of optical chaos from a laser with PCF. By measuring the chaos bandwidth and having a look at the permutation entropy of the system, we have only analyzed part of the complexity issues. For example, it would be helpful to test, at least numerically, how a random number generator behaves when simply replacing COF with PCF. There would probably be some parameters to tune but it would give a good overview of whether this alternative type of feedback could effectively yield interesting or better results.

On the same subject, experimental analysis of the chaos complexity would be interesting. Since permutation entropy has been shown to characterize the complexity of chaotic time traces faithfully, even in the presence of noise, it is reasonable to think that we could measure it on experimental time traces. Additionally, we now have a setup capable of attaining large reflectivity values of the PCM thanks to the CAT configuration. By recording the output of the laser diode with photodetectors of larger bandwidth, we could see if even the chaos bandwidth could be increased even further, as suggested by our theoretical predictions.

Having this second setup with the CAT configuration allows to change the ECs length easily. It would be interesting to see how our conclusions hold up when working with a short EC. How would the chaos bandwidth evolve when changing the time-delay? Are ECMs more or less stable experimentally in the case of a short EC?

8.2.2 *Understanding the physics*

In our theoretical investigations of the chaotic dynamics of the laser diode with PCF, we have focused on LFF and extreme events, which have been observed for two different sets of parameters. Experimental observations prior to this thesis work have also focused on LFF and extreme events for different configurations.

It would be interesting to study the link and transition between these two types of dynamics.

We have experimentally observed the signal coming back from the PCM and we noticed no filtering effect due to the response time of the photorefractive crystal or the penetration depth inside it. But theoretical studies on models including the effect of the penetration depth inside the phase-conjugating medium suggest that a large interaction length in the crystal could have a filtering effect on the dynamics. With our relatively short crystals we have not evidenced this effect. Studying longer crystals would allow to conclude on the accuracy of these models.

8.2.3 *Other perspectives*

Other ways of making the PCM could be explored. In particular, the digital optical phase-conjugation method presented in Section 1.3.2 could give interesting results. It uses a camera to record the phase profile of the incident beam and computes the image to input into an Spatial Light Modulator (SLM) so that it produces the phase-conjugate wave of the incident beam upon reflection. We have experimentally observed that the response time of the photorefractive material had no influence on the dynamics of the phase-conjugated signal. Even if the refresh rate of the SLM is slow when compared to the time scale of laser dynamics, it would be interesting to test if, as for a relatively slow photorefractive crystal, digital optical phase-conjugation could be used to make a PCM. Provided that it works, this would remove the need of a four-wave mixing process, which requires a pumping beam of high intensity and is sometimes difficult to control, as we have observed in Section 7.2.4.

Part IV

APPENDICES

NORMALIZATION OF THE MODEL

Considering Eqs. (2.10) and (2.11) and the simplifications mentioned in Section 2.2, the equations are now:

$$\frac{d\mathbf{E}(t)}{dt} = \frac{1}{2} \left[(1 + \iota\alpha) \left(G_N(N(t) - N_0) - \frac{1}{\tau_p} \right) \right] \mathbf{E}(t) + \kappa \mathbf{E}^*(t - \tau), \quad (\text{A.1})$$

$$\frac{dN(t)}{dt} = \frac{I}{q} - \frac{N(t)}{\tau_e} - G_N(N(t) - N_0)|\mathbf{E}(t)|^2. \quad (\text{A.2})$$

Now, as has been done before by Erneux *et al.* [93], we introduce new variables:

$$s \equiv \frac{t}{\tau_p},$$

$$\mathbf{Y}(t) \equiv \sqrt{\frac{\tau_e G_N}{2}} \mathbf{E}(t) \text{ and}$$

$$Z(t) \equiv \frac{G_N \tau_p}{2} (N(t) - N_{\text{sol}}) \iff G_N(N(t) - N_0) = \frac{2Z(t) + 1}{\tau_p},$$

where $N_{\text{sol}} = N_0 + \frac{1}{G_N \tau_p} = \frac{\tau_e I_{\text{sol}}}{q}$ is the carrier density at threshold for the solitary laser and I_{sol} the corresponding injection current. Equation (A.1) becomes:

$$\begin{aligned} \frac{d\mathbf{Y}(s)}{ds} &= \frac{1}{2} \left[(1 + \iota\alpha) \left(\tau_p \frac{2Z(s) + 1}{\tau_p} - 1 \right) \right] \mathbf{Y}(s) + \kappa \tau_p \mathbf{Y} \left(s - \frac{\tau}{\tau_p} \right) \\ &= (1 + \iota\alpha) Z(s) \mathbf{Y}(s) + \kappa \tau_p \mathbf{Y} \left(s - \frac{\tau}{\tau_p} \right), \end{aligned} \quad (\text{A.3})$$

and Eq. (A.2) becomes:

$$\begin{aligned} \frac{2}{G_N \tau_p} \frac{dZ(s)}{ds} &= \frac{\tau_p I}{q} - \frac{\tau_p}{\tau_e} \left(\frac{2Z(s)}{G_N \tau_p} + N_{\text{sol}} \right) - (2Z(s) + 1) \frac{2}{G_N \tau_e} |\mathbf{Y}(s)|^2 \\ \iff \frac{\tau_e}{\tau_p} \frac{dZ(s)}{ds} &= \frac{G_N \tau_p \tau_e I}{2q} - Z - \frac{G_N \tau_p \tau_e I_{\text{sol}}}{2q} - (2Z(s) + 1) |\mathbf{Y}(s)|^2 \\ \iff \frac{\tau_e}{\tau_p} \frac{dZ(s)}{ds} &= \frac{G_N \tau_p \tau_e}{2q} (I - I_{\text{sol}}) - Z - (2Z(s) + 1) |\mathbf{Y}(s)|^2 \end{aligned} \quad (\text{A.4})$$

Finally, we introduce new parameters:

$$\gamma = \kappa\tau_p, \theta = \frac{\tau}{\tau_p}, \Gamma = \frac{\tau_e}{\tau_p} \text{ and } P = \frac{G_N\tau_p\tau_e}{2q}(I - I_{sol}),$$

and we redefine the normalized time as t (instead of s) to obtain the normalized equations modeling a semiconductor laser with Phase-Conjugate Feedback (PCF):

$$\frac{d\mathbf{Y}(t)}{dt} = (1 + i\alpha)\mathbf{Y}(t)Z(t) + \gamma\mathbf{Y}^*(t - \theta), \quad (\text{A.5})$$

$$\Gamma \frac{dZ(t)}{dt} = P - Z(t) - (1 + 2Z(t))|\mathbf{Y}(t)|^2, \quad (\text{A.6})$$

which are the same as Eqs. (2.12) and (2.13) in the main text.

NUMERICAL INTEGRATION OF THE MODEL

We describe here the general concept of numerical integration of a set of ordinary differential equations with a Runge-Kutta (RK) method.

Let us take an ordinary differential equation

$$\frac{dy}{dt} = f(t, y), \quad (\text{B.1})$$

and an initial value

$$y(t_0) = y_0. \quad (\text{B.2})$$

$y(t)$ is an unknown vectorial function of t (time, for example) that we want to approximate, $f(y, t)$, t_0 and y_0 are known. We choose a fixed-size step h and we can compute approximations y_n of $y(t)$ at every step $n = 1, 2, 3, \dots$ by using the formula for the s^{th} order:

$$y_{n+1} = y_n + \sum_{i=1}^s b_i k_i, \quad (\text{B.3})$$

$$k_i = f \left(t_n + c_i h, y_n + \sum_{j=1}^{i-1} a_{ij} k_j \right), \quad (\text{B.4})$$

$$t_{n+1} = t_n + h, \quad (\text{B.5})$$

where values of coefficients a , b and c are given by the general Butcher tableau:

c_1	a_{11}	a_{12}	\dots	a_{1s}
c_2	a_{21}	a_{22}	\dots	a_{2s}
\vdots	\vdots	\vdots	\ddots	\vdots
c_s	a_{s1}	a_{s2}	\dots	a_{ss}
	b_1	b_2	\dots	b_s

In our case here, we choose the 3/8-rule fourth order ($s = 4$) RK algorithm, for which the Butcher tableau is:

0	0	0	0	0
1/3	1/3	0	0	0
2/3	-1/3	1	0	0
1	1	-1	1	0
	1/8	3/8	3/8	1/8

As presented here, the method can be applied to approximate the solution of a set of ordinary differential equations. However, it is easy to adapt it to a set of ordinary time-delayed differential equations: one simply needs to provide a vector of initial values corresponding to the past of the system over a duration equal to the time-delay of the system.

In terms of implementation, the RK algorithm in itself is done in C to speed up the computing. We choose to use MATLAB for interfacing the inputs and outputs of the function and to plot the results we are interested in. The code we use to apply this algorithm to our model (Eqs. (2.28), (2.29), (2.30)) is presented below.

```

1 #include "mex.h"
  #include "math.h"
  #include "stdlib.h"

5 //Matlab I/O
  double *params_laser, *params_temp, *PAST, *RESULTS, *X, *Xd, *dX, *K;
  //Parameters
  double alpha, T, P, theta, gamma, h, horizon;
  int steps, delay;
10 //RK coefficients and parameters
  double a[4] =
  {
    0.0,          1.0/3.0,          2.0/3.0,          1.0};
  double b[4][4] = {
  {
    0.0,          0.0,          0.0,          0.0},
```

```

15 {      1.0/3.0,      0.0,      0.0,      0.0},
{      -1.0/3.0,      1.0,      0.0,      0.0},
{      1.0,      -1.0,      1.0,      0.0}};
double c[4] =
{      1.0/8.0,      3.0/8.0,      3.0/8.0,      1.0/8.0};
20 int DIM = 3, S = 4;

//Equations of the system
void eval(double *dX, double *X, double *Xd) {
    dX[0] = X[0]*X[2] + gamma*Xd[0]*cos(X[1]+Xd[1]);
25    dX[1] = alpha*X[2] - gamma*(Xd[0]/X[0])*sin(X[1]+Xd[1]);
    dX[2] = (1.0/T)*(P - X[2] - (1.0+2.0*X[2])*X[0]*X[0]);
}

//Runge-Kutta
30 void simu() {
    int i, j, s, n;
    X = (double *)malloc(DIM *sizeof(double)); //input of eval
    Xd = (double *)malloc(DIM *sizeof(double)); //delayed input of eval
    dX = (double *)malloc(DIM *sizeof(double)); //output of eval
35    K = (double *)malloc(S*DIM *sizeof(double)); //increment values

    //RESULTS initialized with PAST
    for (i=0; i<delay+1; i++){
        for (n=0; n<DIM; n++){
40            RESULTS[n+DIM*i] = PAST[n+DIM*i];
        }
    }

    //K initialized to zero
    for (s=0; s<S; s++){
45        for (n=0; n<DIM; n++){
            K[n+DIM*s] = 0;
        }
    }

    //RK algorithm for specified horizon (steps)
50    for (i=delay; i<steps+delay+1; i++){
        //Computing all increments K for all the variables of the system
        for (s=0; s<S; s++){
            for (n=0; n<DIM; n++){
                X[n] = RESULTS[n+DIM*i];
55                Xd[n] = RESULTS[n+DIM*(i-delay)]*(1-a[s]) + RESULTS[n+DIM*(i
                    -delay+1)]*a[s];
            }
            for (j=0; j<s; j++){

```

```

        for (n=0; n<DIM; n++)
            X[n] += h*b[s][j]*K[n+DIM*j];
60     }
        eval(dX, X, Xd);
        for (n=0; n<DIM; n++)
            K[n+DIM*s] = dX[n];
    }
65     //Evaluating next approximate value of the variables based on K
    for (n=0; n<DIM; n++){
        RESULTS[n+DIM*(i+1)] = RESULTS[n+DIM*i];
        for (s=0; s<S; s++)
            RESULTS[n+DIM*(i+1)] += h*c[s]*K[n+DIM*s];
70     }
    }
    free(dX);
    free(X);
    free(Xd);
75     free(K);
}

//Adapt Matlab and C I/O
void mexFunction(int nlhs, mxArray *plhs[], int nrhs, const mxArray * prhs
80     []) {
    //Check number of inputs and outputs
    if (nlhs != 1)
        mexErrMsgTxt("Wrong number of outputs!");
    if (nrhs !=3)
        mexErrMsgTxt("Wrong number of inputs!");
85     //Get inputs
    params_laser = mxGetPr(prhs[0]);
    params_temp = mxGetPr(prhs[1]);
    PAST = mxGetPr(prhs[2]);
    //Parameters
90     alpha = params_laser[0];
    T = params_laser[1];
    P = params_laser[2];
    theta = params_laser[3];
    gamma = params_laser[4];
95     h = params_temp[0];
    horizon = params_temp[1];
    steps = floor(horizon/h);
    delay = floor(theta/h);
    //Prepare OUTPUT matrix
100    plhs[0] = mxCreateDoubleMatrix(DIM*(steps+delay+1), 1, mxREAL);

```

```

RESULTS = mxGetPr(plhs[0]);
//MAIN
simu();
}

```

And below is the MATLAB function used to adapt inputs and outputs to call the function written in C. Results are presented in a matrix with three columns, storing values of Y , Φ and Z with each row corresponding to an iteration of the RK algorithm.

```

1 function OUTPUT = sim_laser_PCF(params_laser, params_temp, INPUT)
%SIM_LASER_PCF interfaces with fast_sim_laser_PCF in C which simulates the
%temporal evolution of a laser diode subject to PCF modeled with LK
%equations, using RK4 method.
5 %
%Inputs params_laser and params_temp are used to provide parameters for the
%simulation and are necessary:
% #params_laser is a vector formatted as follows:
% [alpha, T, P, theta, gamma]
10 % *alpha: linewidth enhancement factor
% *T: electron to photon lifetime ratio
% *P: normalized pump current above threshold, (I-I_th)/I_th
% *theta: normalized value of the delay of the external cavity
% *gamma: normalized value of feedback rate
15 % #params_temp is a vector formatted as follows:
% [h, horizon]
% *h: normalized time step for numerical integration with RK4 method
% *horizon: normalized duration of simulation
%
20 %Input INPUT is optional and used to provide the past temporal evolution of
%the system. If no value is provided, past is considered to be constant and
%equal to zero.
% INPUT is a matrix with three columns, corresponding to iterations of E,
% phi and N.
25 %
%Output consists of matrix OUTPUT which stores values computed by the
%RK4 algorithm.
% OUTPUT is a matrix with three columns, corresponding to iterations of E,
% phi and N.
30 %
%%%%%%%%%%%%%%%%%%%%%%%%%%%%%%%%%%%%%%%%%%%%%%%%%%%%%%%%%%%%%%%%%%%%%%%%
%%%% Read the input parameters
%%%%%%%%%%%%%%%%%%%%%%%%%%%%%%%%%%%%%%%%%%%%%%%%%%%%%%%%%%%%%%%%%%%%%%%%

```

NUMERICAL INTEGRATION OF THE MODEL

```

35 theta = params_laser(4);
   h = params_temp(1);
   horizon = params_temp(2);

   %%%%%%%%%%%%%%%%%%%%%%%%%%%%%%%%%%%%%%%%%%%%%%%%%%%%%%%%%%%%%%%%%%%%%%%%%
40 %%% Prepare indices values and storage
   %%%%%%%%%%%%%%%%%%%%%%%%%%%%%%%%%%%%%%%%%%%%%%%%%%%%%%%%%%%%%%%%%%%%%%%%%

   %Dimensions variables
   delay = floor(theta/h); %number of indices corresponding to the delay
45 steps = floor(horizon/h); %number of lines of the OUTPUT matrix

   %Preparation of the past values of variables
   %If no INPUT is provided
   %PAST is set to a value near zero
50 %If the past provided in INPUT is shorter than the delay
   %PAST is created from INPUT completed with values near zero
   %If the past provided in INPUT is long enough
   %PAST is extracted from INPUT, keeping only the values needed
   if (nargin<3) || isempty(INPUT)
55     PAST = zeros(delay+1, 3) + 1e-5;
   elseif length(INPUT) < delay+2
       PAST = vertcat(zeros(delay+1-size(INPUT,1),3) + 1e-5, INPUT);
   else
       PAST = INPUT(end-delay:end,:);
60 end

   PAST = reshape(PAST.',(delay+1)*3,1);

   %%%%%%%%%%%%%%%%%%%%%%%%%%%%%%%%%%%%%%%%%%%%%%%%%%%%%%%%%%%%%%%%%%%%%%%%%
65 %%% Call fast function in C
   %%%%%%%%%%%%%%%%%%%%%%%%%%%%%%%%%%%%%%%%%%%%%%%%%%%%%%%%%%%%%%%%%%%%%%%%%

   RESULTS = fast_sim_laser_PCF(params_laser,params_temp,PAST);

70 %%%%%%%%%%%%%%%%%%%%%%%%%%%%%%%%%%%%%%%%%%%%%%%%%%%%%%%%%%%%%%%%%%%%%%%%%
   %%% Return OUTPUT
   %%%%%%%%%%%%%%%%%%%%%%%%%%%%%%%%%%%%%%%%%%%%%%%%%%%%%%%%%%%%%%%%%%%%%%%%%

   %Only return the initial value and new simulated output
75 RESULTS = RESULTS(3*(delay+1)-2:end);
   OUTPUT = reshape(RESULTS,3,steps+1).';
   end

```

FRENCH SUMMARY – RÉSUMÉ EN FRANÇAIS

Ce manuscrit relatant mon travail en vue de l'obtention du diplôme de doctorat a été rédigé en langue anglaise, simplement car la majorité de la communauté est anglophone. La plupart du travail réalisé avant moi se trouve en anglais et les publications relatives au travail décrit ici n'ont été publiées qu'en anglais. Cela garantit que le manuscrit puisse être lu par la majorité du public intéressé, à commencer par les membres du jury de thèse qui ne sont pas tous francophones.

Le but de cette annexe est d'offrir en quelques pages un résumé en français du travail décrit dans la partie principale du manuscrit. Nous introduisons en section [C.1](#) les concepts forts qui ont mené à se poser les questions auxquelles nous avons répondu durant les trois années de travail. Nous détaillerons particulièrement les résultats théoriques en section [C.2](#), puis les résultats expérimentaux visant à valider la théorie en section [C.3](#). Enfin, nous concluons sur l'impact de ce travail en section [C.4](#).

C.1 INTRODUCTION

C.1.1 *Diode laser*

Depuis leur invention en 1960, les lasers ont connu un succès fulgurant en termes d'applications, ainsi qu'une grande diversification. De nombreuses technologies ont été développées pour fabriquer des lasers, utilisant du gaz, un cristal solide, un matériau semiconducteur, avec pompage optique ou électrique. Cela a permis de fabriquer des lasers à de nombreuses longueurs d'onde avec différents niveaux de puissance. Toutes ces technologies partagent cependant le même principe de fonctionnement : l'amplification de lumière par émission stimulée de radiation (d'où vient l'acronyme en anglais Light Amplification by Stimulated Emission of Radiation (LASER)). Les applications des lasers incluent la visée, le guidage, la découpe, la chirurgie, la mesure de différentes grandeurs, les télécommunications et bien d'autres.

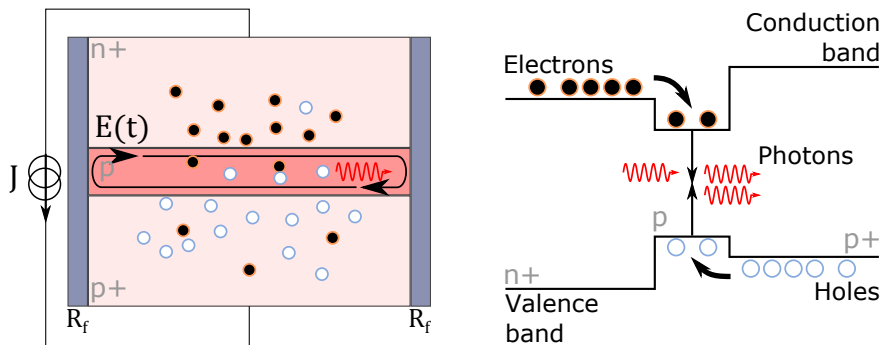


Figure C.1: À gauche, schéma de principe de la double hétérostructure permettant l'émission laser dans une diode. À droite, représentation du bandgap à l'intérieur du matériau, agencé de manière à créer un puits d'énergie dans la région centrale afin de concentrer l'émission stimulée dans une fine couche.

Ce qui nous intéresse ici est d'étudier le comportement dynamique d'une diode laser, composée de matériaux semiconducteurs. La configuration la plus répandue pour fabriquer une diode laser est la double hétérostructure, représentée en figure C.1. En choisissant des dopants et des concentrations de dopage différents selon la couche, il est possible de créer une structure de bande similaire à ce qui est représenté dans la partie droite de la figure. Le puits d'énergie dans la couche centrale capture les porteurs de charge injectés électriquement, qui se recombinent en émettant un photon d'énergie correspondant au bandgap

entre la bande de conduction et la bande de valence dans cette couche. Une fois que quelques photons sont présents dans la cavité, l'émission stimulée peut démarrer et créer de nombreux photons identiques en terme de direction, phase et énergie, ce qui donne la cohérence propre aux faisceaux laser.

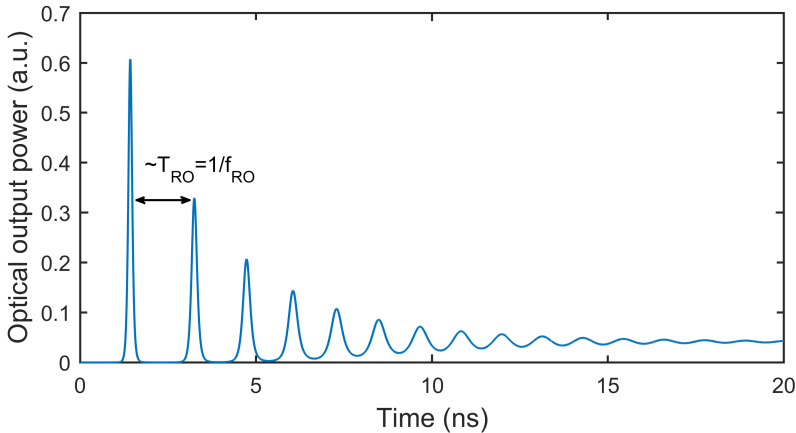


Figure C.2: La réponse du laser à une consigne en intensité fixe donne une émission de pics successifs à une fréquence nommée fréquence des oscillations de relaxation. Après quelques cycles d'oscillation, l'équilibre entre photons et charges est atteint et le système émet de manière continue.

En terme de dynamique, il est intéressant d'observer l'évolution de la puissance en sortie du laser lors de l'allumage du composant en figure C.2. Durant les premiers instants, il n'y a pas d'émission de photons car il faut du temps pour que la population de charges dans le composant soit suffisamment élevée pour permettre l'émission stimulée. Une fois ce seuil atteint, l'émission stimulée démarre et consomme tous les porteurs, créant un premier pic, puis le cycle se répète en s'atténuant à chaque fois, jusqu'à atteindre l'équilibre entre les populations de porteurs de charge et les photons. Le laser émet alors une puissance continue. Ces simples oscillations de relaxation ne présentent pas de grand intérêt en terme de richesse dynamique, surtout du point de vue de l'étude des dynamiques non-linéaires, que nous allons désormais aborder.

c.1.2 Dynamique non-linéaire – Chaos

En 1963, Lorenz découvre la notion de chaos en faisant des simulations numériques sur le système d'équations suivant, basé sur les équations de Navier-Stokes :

$$\frac{dx}{dt} = \sigma(x - y), \quad (\text{C.1})$$

$$\frac{dy}{dt} = \rho x - xz - y, \quad (\text{C.2})$$

$$\frac{dz}{dt} = xy - \beta z. \quad (\text{C.3})$$

Ce système de dimension 3 peut être le siège de dynamiques chaotiques. Le chaos peut-être défini par les trois propriétés suivantes :

- Déterminisme : le comportement chaotique du système est intrinsèque à son mécanisme de fonctionnement. Une simulation est capable de reproduire les dynamiques observées sans ajout de bruit ou perturbation extérieure.
- Sensibilité aux conditions initiales : deux conditions initiales très proches donneront lieu à un comportement similaire dans les premiers instants, mais les trajectoires finissent par diverger de manière exponentielle.
- Attracteur étrange : représenter la trajectoire du système dans un espace des phases approprié donne lieu à la création d'un objet de dimension non entière, appelé attracteur étrange et dont l'étude fait le lien avec les fractales.

Et ce comportement ne peut être observé que dans des systèmes de dimension supérieur ou égale à 3. Dans les systèmes de dimension inférieur, le théorème de Poincaré-Bendixon prouve que la dynamique à long terme d'un système est soit un point fixe (solution stationnaire) ou un cycle limite (solution oscillante).

c.1.3 *Chaos dans une diode laser*

Une diode laser peut-être modélisée avec un système d'équations de dimension 2 seulement et ne peut donc pas être le siège de dynamiques chaotiques si elle est seule. En revanche, il existe plusieurs méthodes qui permettent de déstabiliser une diode laser afin de débloquent des dynamiques non linéaires. La méthode qui nous intéresse ici est appelée rétroaction optique et consiste à simplement placer un miroir devant le laser afin de renvoyer une partie de la lumière dans la cavité laser avec un retard proportionnel à la distance L entre le miroir et le composant (illustration en figure C.3). Dans la configuration étudiée dans cette thèse, nous utilisons un miroir à conjugaison de phase.

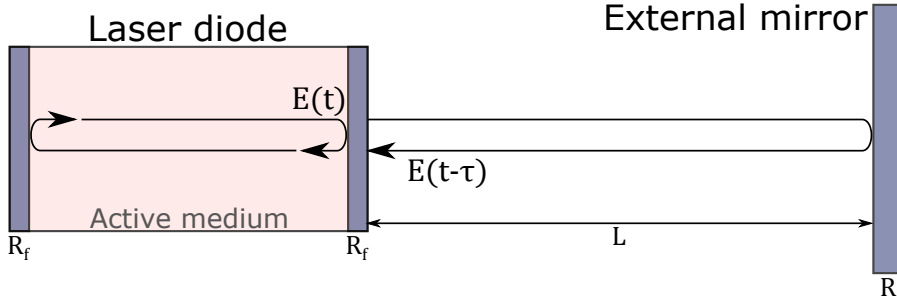


Figure C.3: En ajoutant un miroir à une distance L du laser, on renvoie une partie de la lumière dans le laser avec un délai $\tau = \frac{2L}{c}$.

Cela crée un système dont la dimension est théoriquement infinie. Cela est visible dans les équations que nous utilisons pour modéliser ce système :

$$\frac{d\mathbf{Y}(t)}{dt} = (1 + \imath\alpha)\mathbf{Y}(t)Z(t) + \gamma\mathbf{Y}^*(t - \theta), \quad (\text{C.4})$$

$$T \frac{dZ(t)}{dt} = P - Z(t) - (1 + 2Z(t))|\mathbf{Y}(t)|^2, \quad (\text{C.5})$$

où Y est la valeur complexe normalisée du champ électrique, Z est la valeur normalisée de la densité de porteurs de charges. α est le facteur de Henry, γ est le taux de rétroaction, mesurant la quantité de lumière retournant dans le laser, θ est la valeur normalisée du retard, T est le ratio du temps de vie des charges sur le temps de vie des photons, et P est le courant d'injection au-delà du seuil. Ici, on voit que le terme modélisant la rétroaction inclue le conjugué de l'onde réfléchie, puisque nous utilisons un miroir à conjugaison de phase.

Même si à première vue ce système semble être de dimension 2, la dimension infinie vient de la dépendance dans Eq. (C.4) de la valeur retardée du champ électrique. Cela peut se comprendre car si l'on imagine résoudre ce système d'équations différentielles, alors la condition initiale n'est plus seulement un vecteur de 2 coordonnées mais un segment contenant l'évolution passée du système pendant une durée τ avant le temps $t = 0$. Et un segment comprend une infinité de points.

En ajoutant simplement cette rétroaction optique à conjugaison de phase, nous avons donc désormais accès à une multitude de dynamiques intéressantes, qui n'étaient pas présentes avec la diode laser seule. Le diagramme de bifurcation en figure C.4 permet de s'en convaincre puisque l'on voit pour un taux de rétroac-

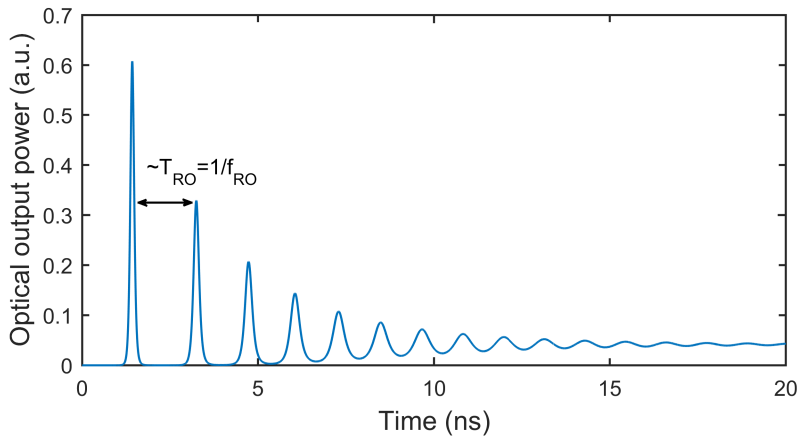


Figure C.4: Un diagramme de bifurcations permet de se rendre compte de l'ensemble des dynamiques émises par une diode laser avec rétroaction à conjugaison de phase.

tion très faible le seul état stationnaire d'un laser avec conjugaison de phase. En augmentant le taux de rétroaction, on voit l'excitation des oscillations de relaxation, puis leur déstabilisation par quasipériodicité jusqu'à atteindre le chaos. Enfin, on observe une alternance de fenêtres chaotiques et de solutions oscillantes à des fréquences multiples de la fréquence de cavité externe. Ces solutions sont appelées modes de cavité externe, et leur observation est limitée aux premiers ordres dans une expérience récente. Nous verrons qu'il est possible d'observer des ordres plus élevés. Également, nous verrons les dynamiques qui peuvent être reproduites par notre modèle en section C.2. Enfin, nous retournerons à l'expérience dans la section C.3 avant de conclure en section C.4.

C.2 RÉSULTATS THÉORIQUES

C.2.1 Modes de cavité externe

Comme nous venons de le présenter, une diode laser avec rétroaction optique à conjugaison de phase peut produire des modes de cavité externe qui sont des solutions oscillantes à des fréquences proches des multiples de la fréquence de cavité externe. Ces solutions sont spécifiques au type de rétroaction étudié et nous nous intéressons dans un premier temps à l'évolution de ces fréquences vis à vis des paramètres γ et θ .

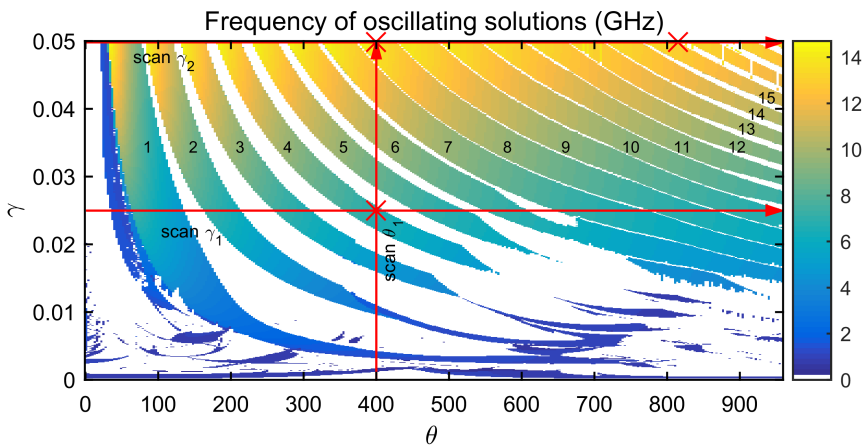


Figure C.5: Carte représentant la fréquence des solutions oscillantes d'un laser avec rétroaction optique à conjugaison de phase. Le fond blanc correspond à des solutions stationnaires ou chaotiques.

Pour cela, nous faisons de nombreuses simulations pour des valeurs de θ comprises entre 0 et 0.05 et des valeurs de délai comprises entre 1 et 1000 (entre 0.0014 et 1.4 ns en temps réel). Nous identifions les traces où la puissance de sortie du laser est oscillante, nous mesurons cette fréquence et la reportons sur la carte reproduite en figure C.5.

Nous observons un comportement intéressant ici :

1. à délai fixé, augmenter le taux de rétroaction fait croître la fréquence de manière linéaire.
2. à taux de rétroaction fixé, changer la valeur du délai a une influence minimale sur la fréquence d'oscillation, qui reste quasiment la même.

Ainsi, pour obtenir des solutions oscillantes à hautes fréquences, il suffit d'avoir un fort taux de rétroaction, quelle que soit la valeur du délai. Cela est contre-intuitif car dans le cas d'une rétroaction classique, on aurait des solutions à la fréquence de cavité externe (et non aux multiples), et il est donc nécessaire d'avoir une longueur de cavité externe très courte pour atteindre les mêmes valeurs de fréquence.

c.2.2 Fluctuations à basses fréquences

Un des régimes chaotiques auquel nous nous intéressons est appelé fluctuations à basses fréquences durant lequel des chutes de puissance se produisent aléatoirement dans l'évolution du signal. Cette dynamique n'est pas propre à la rétroaction optique à conjugaison de phase, mais son mécanisme n'a pas été déterminé dans ce cas. C'est pourquoi nous nous y intéressons ici, dans le cas d'un délai $\theta = 3200$, soit 4.5 ns en temps réel.

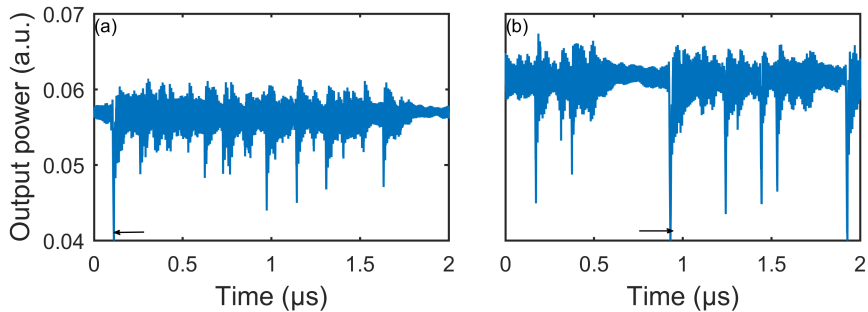


Figure C.6: Traces simulées pour des valeurs de taux de rétroaction : (a) $\gamma = 0.03386$ et (b) $\gamma = 0.04460$.

La simulation reproduit correctement ce type de comportement, comme en témoignent les traces représentées en figure C.6. Désormais, nous nous intéressons au mécanisme responsable de ce comportement. Pour cela, nous décidons de représenter l'évolution du système au sein d'un espace de phase, composé sur l'axe horizontal de la différence de phase du faisceau sortant ($\Delta\Phi = \Phi(t) - \Phi(t - \tau)$) et sur l'axe vertical de la densité de porteurs de charges Z .

On voit sur la figure C.7 que lorsque l'on augmente le taux de rétroaction, on passe d'un mode de cavité externe, par un régime chaotique avec des fluctuations à basses fréquences, à un mode de cavité externe de fréquence plus élevée. Dans l'espace de phase, nous observons le cycle limite se déstabiliser d'abord, avant d'exploser dans le régime chaotique. La trajectoire de la trace chaotique

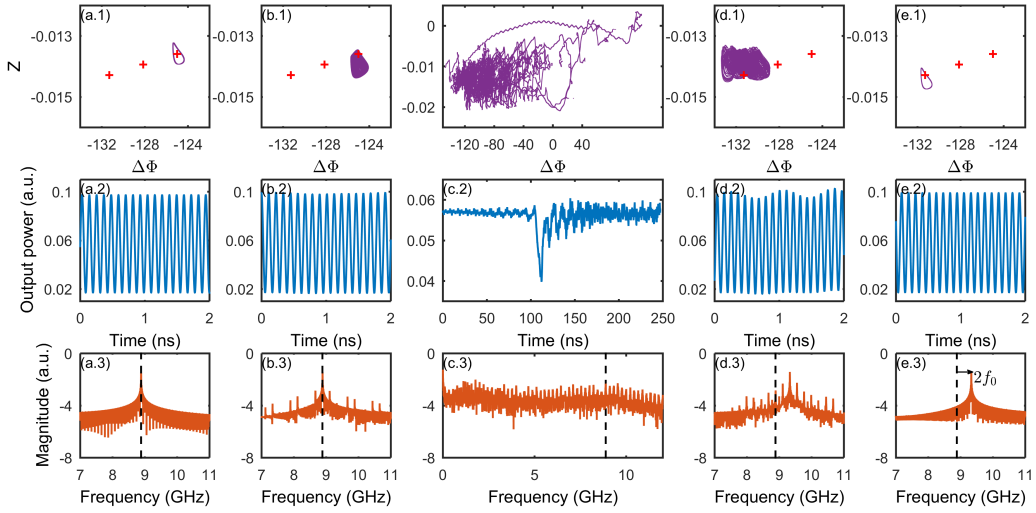


Figure C.7: De gauche à droite, (a) $\gamma = 0.03300$, (b) $\gamma = 0.03384$, (c) $\gamma = 0.03386$, (d) $\gamma = 0.03391$ et (e) $\gamma = 0.03500$. Haut: trajectoire dans l'espace de phase, milieu: traces temporelles correspondantes de $|Y|^2$, bas: spectres radiofréquences correspondants.

passé en fait par les endroits où se trouvent les modes de cavité externe d'ordres inférieurs. On observe ainsi une itinérance sur les modes de cavité externe, similaire au cas de la rétroaction conventionnelle. La grosse différence étant que, comme chaque mode de cavité externe a sa propre signature spectrale, alors cette itinérance sera observable dans un spectrogramme de la trace temporelle, ce que nous verrons expérimentalement en section C.3.

Ce résultat montre que les fluctuations à basses fréquences sont un phénomène commun à différents types de rétroactions, que les mécanismes impliqués peuvent être similaires, mais que la manière de les observer peut-être différente, ici à cause de la nature différente des modes de cavité externe.

C.2.3 Événements extrêmes

L'étude des événements extrêmes est inspirée des vagues scélérates à la surface de l'océan. Ce type de vague est caractérisé par une amplitude grande par rapport à l'amplitude moyenne des autres vagues, ainsi que par leur apparition soudaine, difficilement prédictible, et rare. Les vagues scélérates apparaissent donc de manière aléatoire dans le temps et l'espace. Les événements extrêmes sont leur équivalent dans un système où l'on ne s'intéresse qu'à l'évolution tem-

porielle d'une grandeur physique, ici la puissance optique émise par le laser. Il y a donc deux critères majeurs permettant d'identifier la présence d'événements extrêmes au sein d'une trace temporelle :

- des événements intenses et rares se produisent, modifiant la distribution des intensités mesurées et provoquant une déviation par rapport à une distribution gaussienne.
- la durée entre ces événements est aléatoire et obéit, par exemple à un processus de Poisson, ou un processus similaire.

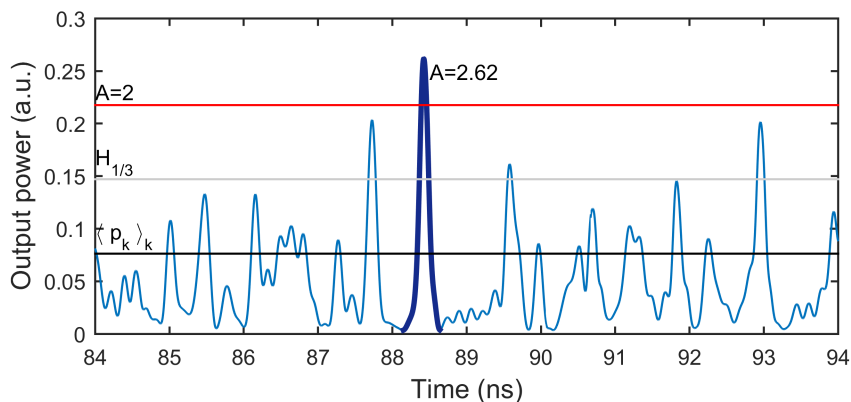


Figure C.8: Illustration d'un événement extrême et de la méthode utilisée pour calculer l'indice d'anormalité A permettant de déterminer si l'événement est extrême ou non.

Dans le cas, de l'étude présentée ici, un événement est un pic dans la trace temporelle, et nous choisissons d'utiliser l'indice d'anormalité A comme critère caractérisant l'aspect extrême ou non d'un événement. À partir d'une population p_k d'événements, l'indice d'anormalité se calcule comme suit (voir figure C.8 illustrant le procédé avec un exemple) :

1. Calcul de la moyenne de cette population $\langle p_k \rangle_k$. Cela correspondrait au niveau moyen de notre mer d'événements.
2. La hauteur d'un pic est ensuite définie comme sa hauteur relative par rapport au niveau moyen $H_k = p_k - \langle p_k \rangle_k$.
3. On définit $H_{1/3}$ comme étant la moyenne du tiers des hauteurs les plus grandes.

4. L'indice d'anormalité est alors défini par $A_k = \frac{H_k}{H_{1/3}}$.

Si l'indice d'anormalité d'un événement est supérieur à 2, alors celui-ci est considéré comme extrême.

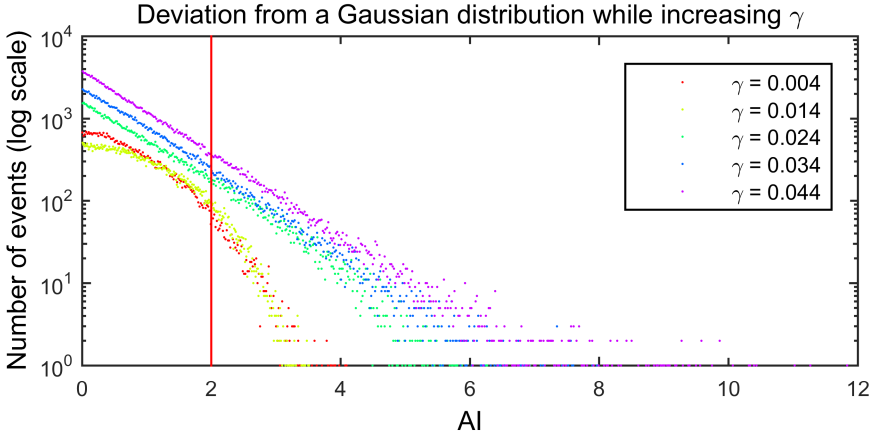


Figure C.9: Évolution de la distribution des intensités des événements en augmentant le taux de rétroaction γ . La ligne rouge indique le seuil à partir duquel un événement est considéré comme étant extrême. Evolution of the distribution of extreme events versus the abnormality index. Increasing the feedback rate leads to a greater deviation from a Gaussian distribution (from left to right), more extreme events, with a higher abnormality index. The red line corresponds to the threshold $A = 2$.

Afin de se placer proche des conditions expérimentales, nous utilisons une valeur de délai $\theta = 1600$ correspondant à un retard de 2.25 ns en temps réel. Dans ces conditions, le modèle reproduit effectivement des événements extrêmes, comme l'illustre la figure C.9. On observe bien la déviation depuis une distribution gaussienne pour les valeurs de γ les plus faibles, vers une distribution très déformée et des pics atteignant des indices d'anormalité supérieurs à 8, largement au-dessus du seuil $A = 2$. Ainsi, le taux de rétroaction favorise l'apparition d'événements extrêmes, ainsi que leur intensité, comme observée expérimentalement dans des études antérieures.

Ensuite, nous nous intéressons temps d'attente entre deux événements successifs, en échelle logarithmique, soit $w_k = \ln\left(\frac{t_k}{t_{k-1}}\right)$. La figure C.10-(a) montre que le temps logarithmique entre événements successifs suit une loi de Poisson pour les faibles taux de rétroaction, on dit alors que le temps entre événements extrêmes successifs suit une loi de log-Poisson. Le panneau (b) de la figure montre que pour un taux de rétroaction élevé, cette distribution se casse en deux dis-

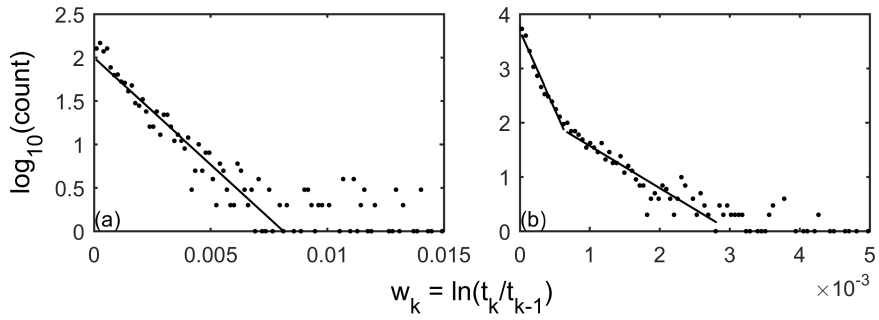


Figure C.10: Distribution du temps d'attente logarithmique entre deux événements successifs pour (a) $\gamma = 0.004$, (b) $\gamma = 0.044$.

tributions de log-Poisson, avec de nombreux événements étant séparés par des durées courtes. Cela s'explique par le fait que pour de larges taux de rétroaction, la dynamique du laser est dominée par de nombreuses répétitions de pics à la valeur du retard, ce qui implique qu'un événement extrême est généralement suivi de plusieurs répliques. Pour de faibles taux de rétroaction, la dynamique est constituée uniquement d'événements extrêmes solitaires. Cela correspond encore une fois aux observations expérimentales antérieures.

C.3 RÉSULTATS EXPÉRIMENTAUX

Afin de valider certains aspects explorés théoriquement, nous avons utilisé deux montages expérimentaux légèrement différents. Le premier est un montage hérité de l'étudiant présent avant moi et travaillant sur le même sujet, qui sert à explorer les dynamiques chaotiques, et notamment l'itinérance dans le régime des fluctuations à basses fréquences. Le second utilise un miroir légèrement différent et est utilisé pour explorer les bifurcations menant à l'observation de modes de cavité externe à des ordres élevés.

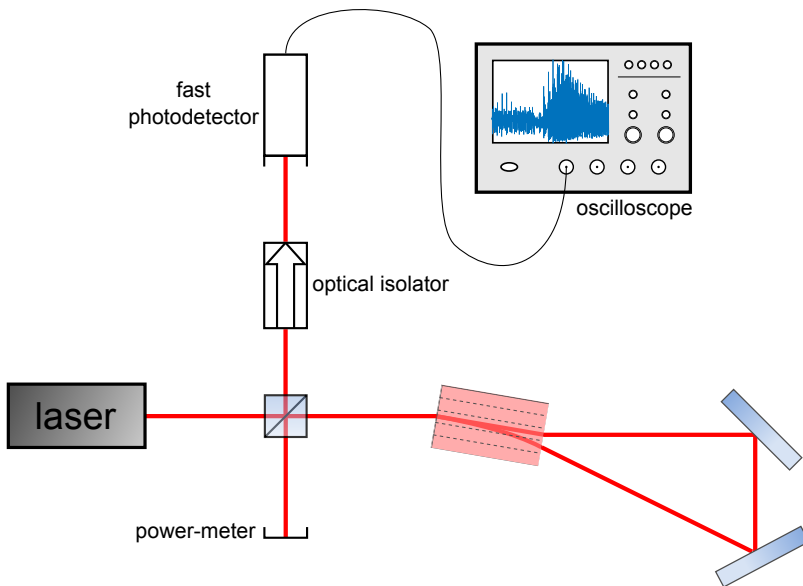
C.3.1 *Itinérance*

Figure C.11: Montage expérimental utilisant un cristal SPS en configuration 'anneau' pour réaliser le mélange à quatre ondes générant le conjugué de l'onde émise par le laser. Grâce à une photodiode rapide et un oscilloscope à larges bande passante et taux d'échantillonnage, nous pouvons mesurer avec une bonne fidélité les dynamiques de notre laser.

Le premier montage expérimental est présenté en figure C.11. La diode laser utilisée émet à 850 nm et le délai associé est égal à 4 ns. La fraction de puissance retournant dans le laser est réglable entre 0 et 14 %. Cette limitation est due au gain limité du mélange à quatre ondes servant à générer l'onde conjuguée.

Dans cette configuration, le laser émet dans un régime de fluctuations à basses fréquences. Afin d'observer l'itinérance, nous calculons des spectrogrammes du signal grâce à une méthode de transformée de Fourier à court terme et fenêtre glissante.

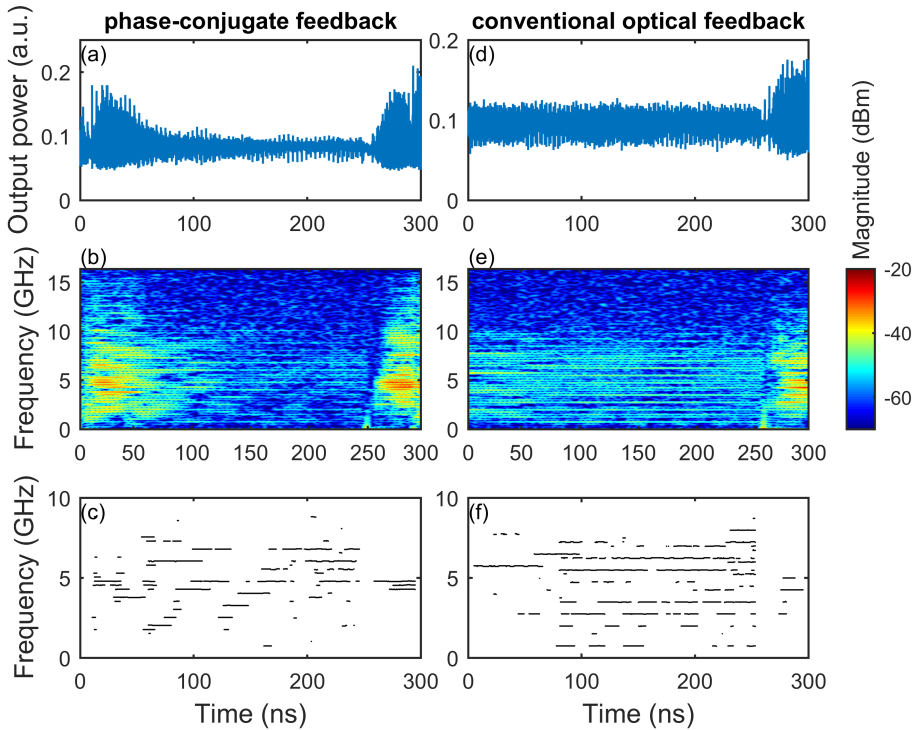


Figure C.12: Dynamiques d'un laser avec rétroaction à conjugaison de phase à gauche et rétroaction classique à droite. (a), (d) Traces temporelles. (b), (e) Spectrogrammes correspondants. (c), (f) Modes dominants, i.e. le pic ayant l'intensité la plus forte et les pics d'intensité comparable (tolérance de 3 dB).

Cela nous permet de suivre l'évolution temporelle du contenu fréquentiel du signal, grâce notamment aux spectrogrammes en figure C.12, mais aussi grâce à l'évolution des modes dominants. Nous appelons modes dominants le pic de magnitude le plus élevé dans le spectre radiofréquence, ainsi que les pics ayant la même magnitude, ou une magnitude jusqu'à 3 dB plus faible. Ainsi, nous observons dans le cas de la rétroaction optique à conjugaison de phase un contenu fréquentiel évoluant sans cesse, de manière cyclique, avec une tendance à aller vers les fréquences les plus élevés. Nous interprétons cela comme la signature de l'itinérance sur les modes de cavité externe déstabilisés, ayant chacun leur

signature fréquentielle propre. Dans le cas de la rétroaction classique, le contenu fréquentiel ne change que très peu avec le temps, car l'itinérance a aussi lieu sur les modes de cavité externe déstabilisés, mais ceux-ci n'ont pas de signature propre.

Ce premier résultat est déjà satisfaisant vis à vis de nos prédictions théoriques. Cependant, nous décidons de nous intéresser à la bande passante du signal chaotique dans le cas de notre rétroaction particulière. La bande passante chaotique est définie comme la fréquence en-dessous de laquelle 80 % de la puissance du signal est comprise.

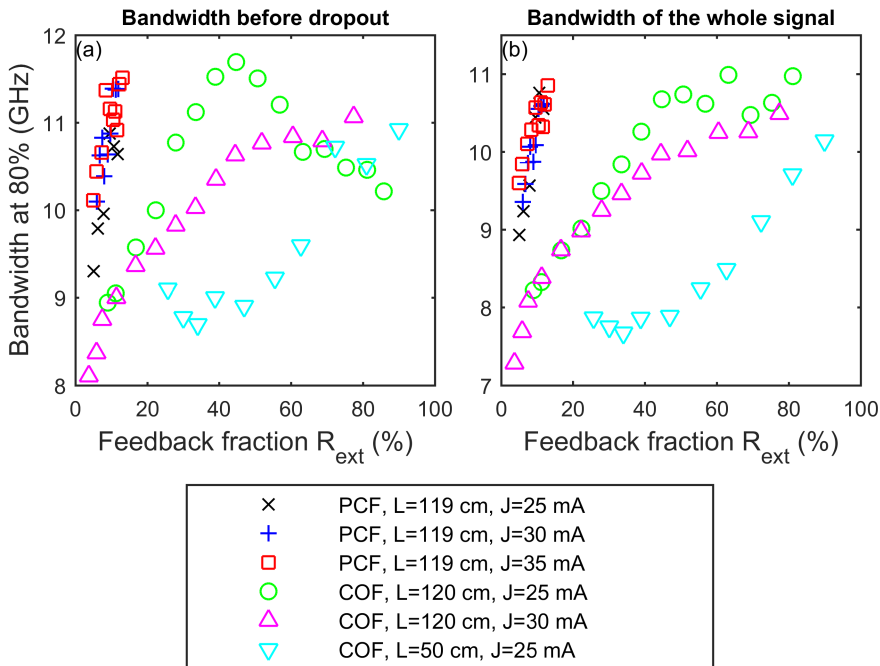


Figure C.13: Bande passante chaotique mesurée (a) pour la portion de signal comprise juste avant une chute de puissance et (b) pour le signal entier dans deux configurations différentes : rétroaction à conjugaison de phase (PCF) et rétroaction classique (COF) et pour des courants d'injection différents.

La figure C.13-(b) montre que la bande passante évolue bien rapidement lorsque l'on augmente le taux de rétroaction dans le cas de la rétroaction à conjugaison de phase. D'autant plus, la bande passante sature dans le cas de la rétroaction classique, alors qu'elle n'atteint pas encore cette saturation dans le cas de la rétroaction à conjugaison de phase. Malheureusement, nous n'avons pas pu vérifier cette tendance plus loin, due aux réflectivités limitées atteignables avec cette

expérience. Pour des fractions de rétroaction comparables, la rétroaction à conjugaison de phase donne des résultats jusqu'à 27 % plus grands. Le panneau (a) montre l'évolution de la bande passante mesurée sur une portion du signal comprise juste avant les chutes de puissances et montre une évolution similaire au panneau (b). Cela suggère que l'augmentation de la bande passante est bien due à l'itinérance sur des modes de cavité externe à hautes fréquences.

C.3.2 Bifurcations

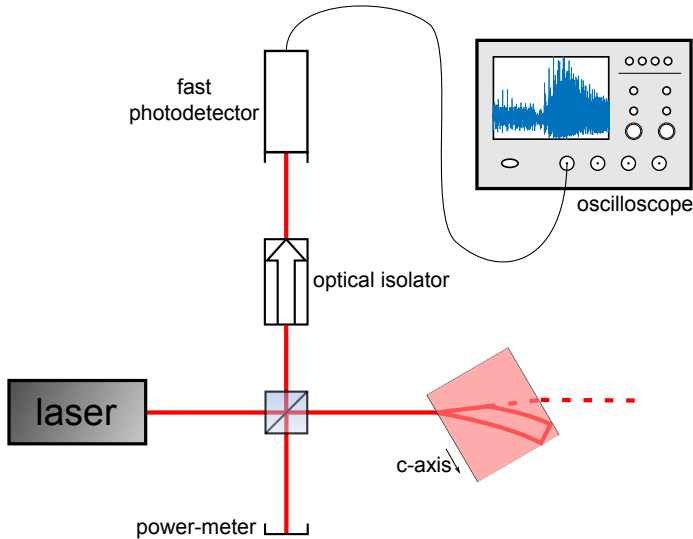


Figure C.14: Le second montage utilise une diode similaire, mais une technique différente pour générer le miroir à conjugaison de phase, puisque le cristal photoréfractif est en configuration de réflexion totale interne.

Avec ce second montage, nous avons pu obtenir des fractions de rétroaction plus élevées et grâce à un réglage plus fin, nous avons ainsi retracé toute la succession de bifurcations subies par un laser soumis à rétroaction à conjugaison de phase pour un délai égal à 1.6 ns. Pour les taux de rétroaction faibles, nous observons l'état stationnaire, puis l'excitation des oscillations de relaxation et sa déstabilisation par quasipériodicité vers des dynamiques chaotiques. Nous n'analysons pas plus ici les dynamiques chaotiques car cela a été fait dans la section précédente.

Pour des taux de rétroaction plus forts, nous observons alors la transition vers des modes de cavité externe d'ordres élevés. La figure C.15 montre la stabilisation de modes de cavités externes à des fréquences égales à 6,3, 7,5 et 8,1 GHz, soient des ordres 10, 12 et 13. Cela constitue un résultat majeur de ce travail car la restabilisation de modes de cavités externe pour de grands taux de rétroaction était un résultat anticipé par la théorie depuis plusieurs années.

Enfin, pour des taux de rétroaction encore plus élevés, nous avons observé la restabilisation d'un état stationnaire. Ceci est inattendu car le seul état stationnaire d'un laser avec rétroaction optique à conjugaison de phase est sensé être

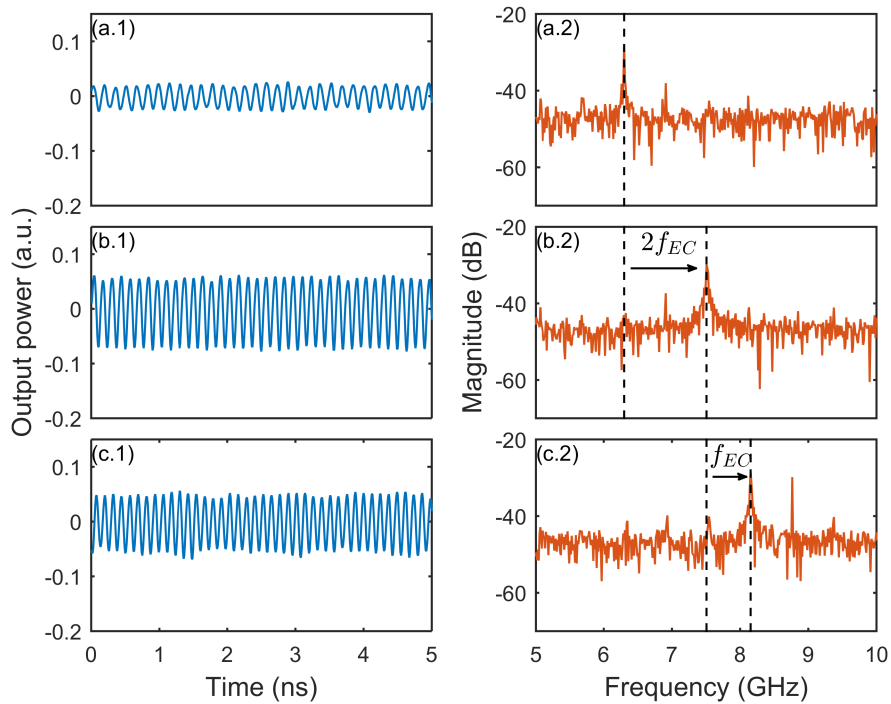


Figure C.15: Traces temporelles (gauche) et spectres radiofréquence correspondants (droite) pour différentes valeurs de la fraction de rétroaction. (a) $F = 4.08\%$, (b) $F = 5.77\%$, (c) $F = 6.21\%$.

celui qui est stable pour des taux de rétroaction proches de 0. Ce résultat pourrait être expliqué par un effet filtrant du miroir, dû à la longueur de pénétration à l'intérieur du milieu photoréfractif. Cette supposition est en train d'être explorée actuellement.

C.4 CONCLUSION

Pour résumer, le travail réalisé durant ces trois dernières années et présenté dans cette thèse nous a permis de réaliser plusieurs avancées dans la connaissance des dynamiques de laser soumis à rétroaction. Nous avons en effet pu :

- reproduire les observations expérimentales de publications antérieures à notre travail en utilisant un modèle simple, prouvant ainsi que les observations effectuées étaient en effet dues à la nature de la rétroaction.
- découvrir de nouvelles propriétés du signal non identifiées précédemment dans l'expérience.
- montrer que ces nouvelles propriétés étaient bien présentes dans l'expérience, en mesurant les dynamiques chaotiques avec des outils plus performants.
- explorer la richesse dynamique d'une diode laser avec rétroaction à conjugaison de phase, ainsi que la succession de bifurcations liant les différents régimes. Nous avons également découvert un résultat inattendu qui est la restabilisation d'un état stationnaire pour un fort taux de rétroaction.

Ce travail laisse la porte ouverte à de nombreuses perspectives. En effet, il serait utile d'explorer certains aspects nouveaux, ou inexplorés par manque de temps, notamment :

- analyser plus en détail les propriétés du chaos optique émis grâce à ce type de rétroaction, et notamment l'influence du retard.
- tester les signaux chaotiques à large bande passante dans des cas d'applications à des communications cryptées par chaos ou à de la génération de nombres aléatoires.
- analyser expérimentalement l'évolution de la fréquences des modes de cavité externe. Ceci est rendu réalisable aisément grâce au second montage expérimental.
- étudier le lien entre les différentes dynamiques : fluctuations à basses fréquences et événements extrêmes notamment.
- étudier l'influence du type de cristal et de la longueur du cristal, afin de voir si la restabilisation est liée à ce phénomène.
- dans le même temps, reproduire les résultats expérimentaux avec un modèle prenant en compte cet effet de filtrage.

- trouver d'autres moyens de réaliser le miroir à conjugaison de phase, notamment pour le rendre encore plus pratique à aligner ou pour le rendre plus stable et faciliter le réglage fin du taux de rétroaction.

BIBLIOGRAPHY

- [1] A. Einstein. "Strahlungs-emission und absorption nach der quantentheorie." *Deutsche Physikalische Gesellschaft* 18 (1916).
- [2] A. Einstein. "Zur quantentheorie der strahlung." *Physikalische Zeitschrift* 18 (1917).
- [3] T. H. Maiman. "Stimulated Optical Radiation in Ruby." *Nature* 187.4736 (1960), pp. 493–494. DOI: [10.1038/187493a0](https://doi.org/10.1038/187493a0).
- [4] A. Yariv. *Optical electronics*. Oxford University Press, USA, 1990.
- [5] R. Hall, G. Fenner, J. Kingsley, T. Soltys, and R. Carlson. "Coherent Light Emission From GaAs Junctions." *Physical Review Letters* 9.9 (1962), pp. 366–368. DOI: [10.1103/physrevlett.9.366](https://doi.org/10.1103/physrevlett.9.366).
- [6] A. Uchida. *Optical Communication with Chaotic Lasers*. Wiley VCH Verlag GmbH, 2012. 640 pp.
- [7] C. Henry. "Theory of the linewidth of semiconductor lasers." *Quantum Electronics, IEEE Journal of* 18.2 (1982), pp. 259–264. DOI: [10.1109/jqe.1982.1071522](https://doi.org/10.1109/jqe.1982.1071522).
- [8] R. Lang and K. Kobayashi. "External optical feedback effects on semiconductor injection laser properties." *Quantum Electronics, IEEE Journal of* 16.3 (1980), pp. 347–355. DOI: [10.1109/JQE.1980.1070479](https://doi.org/10.1109/JQE.1980.1070479).
- [9] M. Henkel. "Sur la solution de Sundman du probleme des trois corps." *Philosophia Scientiae* 5 (2002), pp. 161–184.
- [10] E. N. Lorenz. "Deterministic Nonperiodic Flow." *Atmospheric Sciences, Journal of the* 20.2 (1963), pp. 130–141. DOI: [10.1175/1520-0469\(1963\)020<0130:dnf>2.0.co;2](https://doi.org/10.1175/1520-0469(1963)020<0130:dnf>2.0.co;2).
- [11] B. B. Mandelbrot. *Fractals – Form, Chance and Dimension*. Freeman, 1977.
- [12] P. Mandel. *Theoretical Problems in Cavity Nonlinear Optics*. Cambridge University Press (CUP), 1997. DOI: [10.1017/cbo9780511529337](https://doi.org/10.1017/cbo9780511529337).
- [13] F. T. Arecchi, G. L. Lippi, G. P. Puccioni, and J. R. Tredicce. "Deterministic chaos in laser with injected signal." *Optics Communications* 51.5 (1984), pp. 308–314. DOI: [10.1016/0030-4018\(84\)90016-6](https://doi.org/10.1016/0030-4018(84)90016-6).

Bibliography

- [14] H. Haken. "Analogy between higher instabilities in fluids and lasers." *Physics Letters A* 53.1 (1975), pp. 77–78. DOI: [10.1016/0375-9601\(75\)90353-9](https://doi.org/10.1016/0375-9601(75)90353-9).
- [15] M. Virte, K. Panajotov, H. Thienpont, and M. Sciamanna. "Deterministic polarization chaos from a laser diode." *Nature Photonics* 7.1 (2013), pp. 60–65. DOI: [10.1038/nphoton.2012.286](https://doi.org/10.1038/nphoton.2012.286).
- [16] M. Sciamanna and K. A. Shore. "Physics and applications of laser diode chaos." *Nature Photonics* 9.3 (2015), pp. 151–162. DOI: [10.1038/nphoton.2014.326](https://doi.org/10.1038/nphoton.2014.326).
- [17] J. R. Tredicce, F. T. Arecchi, G. L. Lippi, and G. P. Puccioni. "Instabilities in lasers with an injected signal." *Journal of the Optical Society of America B* 2.1 (1985), pp. 173–183. DOI: [10.1364/JOSAB.2.000173](https://doi.org/10.1364/JOSAB.2.000173).
- [18] J. Sacher, D. Baums, P. Panknin, W. Elsässer, and E. O. Göbel. "Intensity instabilities of semiconductor lasers under current modulation, external light injection, and delayed feedback." *Physical Review A* 45.3 (1992), p. 1893. DOI: [10.1103/PhysRevA.45.1893](https://doi.org/10.1103/PhysRevA.45.1893).
- [19] G. H. M. v. Tartwijk and D. Lenstra. "Semiconductor lasers with optical injection and feedback." *Quantum Semiclassical Optics* 7.2 (1995), pp. 87–143. DOI: [10.1088/1355-5111/7/2/003](https://doi.org/10.1088/1355-5111/7/2/003).
- [20] A. Uchida, T. Heil, Y. Liu, P. Davis, and T. Aida. "High-frequency broadband signal generation using a semiconductor laser with a chaotic optical injection." *Quantum Electronics, IEEE Journal of* 39.11 (2003), pp. 1462–1467. DOI: [10.1109/JQE.2003.818281](https://doi.org/10.1109/JQE.2003.818281).
- [21] C.-H. Lee, T.-H. Yoon, and S.-Y. Shin. "Period doubling and chaos in a directly modulated laser diode." *Applied Physics Letters* 46.1 (1985), pp. 95–97. DOI: [10.1063/1.95810](https://doi.org/10.1063/1.95810).
- [22] H.-F. Liu and W. F. Ngai. "Nonlinear dynamics of a directly modulated 1.55 μm InGaAsP distributed feedback semiconductor laser." *Quantum Electronics, IEEE Journal of* 29.6 (1993), pp. 1668–1675. DOI: [10.1109/3.234419](https://doi.org/10.1109/3.234419).
- [23] T. Erneux, A. Gavrielides, and M. Sciamanna. "Stable microwave oscillations due to external-cavity-mode beating in laser diodes subject to optical feedback." *Physical Review A* 66.3 (2002), p. 033809. DOI: [10.1103/PhysRevA.66.033809](https://doi.org/10.1103/PhysRevA.66.033809).

- [24] A. Karsaklian Dal Bosco, D. Wolfersberger, and M. Sciamanna. "Superharmonic self-pulsations from a time-delayed phase-conjugate optical system." *Applied Physics Letters* 105.8 (2014), p. 081101. DOI: [10.1063/1.4894119](https://doi.org/10.1063/1.4894119).
- [25] T. Heil, I. Fischer, W. Elsässer, and A. Gavrielides. "Dynamics of Semiconductor Lasers Subject to Delayed Optical Feedback: The Short Cavity Regime." *Physical Review Letters* 87.24 (2001), p. 243901. DOI: [10.1103/physrevlett.87.243901](https://doi.org/10.1103/physrevlett.87.243901).
- [26] A. Tabaka, K. Panajotov, I. Veretennicoff, and M. Sciamanna. "Bifurcation study of regular pulse packages in laser diodes subject to optical feedback." *Physical Review E* 70.3 (2004), p. 036211. DOI: [10.1103/physreve.70.036211](https://doi.org/10.1103/physreve.70.036211).
- [27] C. Risch and C. Voumard. "Self-pulsation in the output intensity and spectrum of GaAs-AlGaAs cw diode lasers coupled to a frequency-selective external optical cavity." *Journal of Applied Physics* 48.5 (1977), p. 2083. DOI: [10.1063/1.323922](https://doi.org/10.1063/1.323922).
- [28] T. Sano. "Antimode dynamics and chaotic itinerancy in the coherence collapse of semiconductor lasers with optical feedback." *Physical Review A* 50.3 (1994), pp. 2719–2726. DOI: [10.1103/physreva.50.2719](https://doi.org/10.1103/physreva.50.2719).
- [29] I. Fischer, G. H. M. Van Tartwijk, A. Levine, W. Elsässer, E. Göbel, and D. Lenstra. "Fast pulsing and chaotic itinerancy with a drift in the coherence collapse of semiconductor lasers." *Physical Review Letters* 76.2 (1996), pp. 220–223. DOI: [10.1103/PhysRevLett.76.220](https://doi.org/10.1103/PhysRevLett.76.220).
- [30] D. Lenstra, B. Verbeek, and A. Den Boef. "Coherence collapse in single-mode semiconductor lasers due to optical feedback." *Quantum Electronics, IEEE Journal of* 21.6 (1985), pp. 674–679. DOI: [10.1109/jqe.1985.1072725](https://doi.org/10.1109/jqe.1985.1072725).
- [31] R. Vicente, J. Dauden, P. Colet, and R. Toral. "Analysis and characterization of the hyperchaos generated by a semiconductor laser subject to a delayed feedback loop." *Quantum Electronics, IEEE Journal of* 41.4 (2005), pp. 541–548. DOI: [10.1109/jqe.2005.843606](https://doi.org/10.1109/jqe.2005.843606).
- [32] J. Lawrence and D. Kane. "Contrasting conventional optical and phase-conjugate feedback in laser diodes." *Physical Review A* 63.3 (2001), p. 033805. DOI: [10.1103/physreva.63.033805](https://doi.org/10.1103/physreva.63.033805).

Bibliography

- [33] K. Hirano, K. Amano, A. Uchida, S. Naito, M. Inoue, S. Yoshimori, K. Yoshimura, and P. Davis. "Characteristics of fast physical random bit generation using chaotic semiconductor lasers." *Quantum Electronics, IEEE Journal of* 45.11 (2009), pp. 1367–1379. DOI: [10.1109/JQE.2009.2031310](https://doi.org/10.1109/JQE.2009.2031310).
- [34] J. Saucedo Solorio, D. Sukow, D. Hicks, and A. Gavrielides. "Bifurcations in a semiconductor laser subject to delayed incoherent feedback." *Optics Communications* 214.1-6 (2002), pp. 327–334. DOI: [10.1016/s0030-4018\(02\)02184-3](https://doi.org/10.1016/s0030-4018(02)02184-3).
- [35] É. Mercier, D. Wolfersberger, and M. Sciamanna. "Bifurcation to chaotic low-frequency fluctuations in a laser diode with phase-conjugate feedback." *Optics Letters* 39.13 (2014), p. 4021. DOI: [10.1364/ol.39.004021](https://doi.org/10.1364/ol.39.004021).
- [36] A. Wang, Y. Wang, Y. Yang, M. Zhang, H. Xu, and B. Wang. "Generation of flat-spectrum wideband chaos by fiber ring resonator." *Applied Physics Letters* 102.3 (2013), p. 031112. DOI: [10.1063/1.4789366](https://doi.org/10.1063/1.4789366).
- [37] M. Zhang, T. Liu, P. Li, A. Wang, J. Zhang, and Y. Wang. "Generation of broadband chaotic laser using dual-wavelength optically injected Fabry–Pérot laser diode with optical feedback." *IEEE Photonics Technology Letters* 23.24 (2011), pp. 1872–1874. DOI: [10.1109/LPT.2011.2170560](https://doi.org/10.1109/LPT.2011.2170560).
- [38] F.-Y. Lin, Y.-K. Chao, and T.-C. Wu. "Effective bandwidths of broadband chaotic signals." *Quantum Electronics, IEEE Journal of* 48.8 (2012), pp. 1010–1014. DOI: [10.1109/JQE.2012.2198195](https://doi.org/10.1109/JQE.2012.2198195).
- [39] A. Wolf, J. B. Swift, H. L. Swinney, and J. A. Vastano. "Determining Lyapunov exponents from a time series." *Physica D: Nonlinear Phenomena* 16.3 (1985), pp. 285–317. DOI: [10.1016/0167-2789\(85\)90011-9](https://doi.org/10.1016/0167-2789(85)90011-9).
- [40] P. Frederickson, J. L. Kaplan, E. D. Yorke, and J. A. Yorke. "The liapunov dimension of strange attractors." *Journal of Differential Equations* 49.2 (1983), pp. 185–207. DOI: [10.1016/0022-0396\(83\)90011-6](https://doi.org/10.1016/0022-0396(83)90011-6).
- [41] K. Ikeda and K. Matsumoto. "High-dimensional chaotic behavior in systems with time-delayed feedback." *Physica D: Nonlinear Phenomena* 29.1 (1987), pp. 223–235. DOI: [10.1016/0167-2789\(87\)90058-3](https://doi.org/10.1016/0167-2789(87)90058-3).
- [42] H. Kantz and T. Schreiber. *Nonlinear time series analysis*. Vol. 7. Cambridge university press, 2004.
- [43] L. Zunino, O. Rosso, and M. C. Soriano. "Characterizing the hyperchaotic dynamics of a semiconductor laser subject to optical feedback via permutation entropy." *Selected Topics in Quantum Electronics, IEEE Journal of* 17.5 (2011), pp. 1250–1257. DOI: [10.1109/JSTQE.2011.2145359](https://doi.org/10.1109/JSTQE.2011.2145359).

- [44] A. Argyris, D. Syvridis, L. Larger, V. Annovazzi-Lodi, P. Colet, I. Fischer, J. García-Ojalvo, C. R. Mirasso, L. Pesquera, and K. A. Shore. "Chaos-based communications at high bit rates using commercial fibre-optic links." *Nature* 438.7066 (2005), pp. 343–346. DOI: [10.1038/nature04275](https://doi.org/10.1038/nature04275).
- [45] L. M. Pecora and T. L. Carroll. "Synchronization in chaotic systems." *Physical Review Letters* 64.8 (1990), pp. 821–824. DOI: [10.1103/physrevlett.64.821](https://doi.org/10.1103/physrevlett.64.821).
- [46] H. G. Winful and L. Rahman. "Synchronized chaos and spatiotemporal chaos in arrays of coupled lasers." *Physical Review Letters* 65.13 (1990), pp. 1575–1578. DOI: [10.1103/physrevlett.65.1575](https://doi.org/10.1103/physrevlett.65.1575).
- [47] P. Colet and R. Roy. "Digital communication with synchronized chaotic lasers." *Optics letters* 19.24 (1994), pp. 2056–2058. DOI: [10.1364/OL.19.002056](https://doi.org/10.1364/OL.19.002056).
- [48] A. Uchida et al. "Fast physical random bit generation with chaotic semiconductor lasers." *Nature Photonics* 2.12 (2008), pp. 728–732. DOI: [10.1038/nphoton.2008.227](https://doi.org/10.1038/nphoton.2008.227).
- [49] G He. "Optical phase conjugation: principles, techniques, and applications." *Progress in Quantum Electronics* 26.3 (2002), pp. 131–191. DOI: [10.1016/s0079-6727\(02\)00004-6](https://doi.org/10.1016/s0079-6727(02)00004-6).
- [50] R. W. Hellwarth. "Generation of time-reversed wave fronts by nonlinear refraction." *Journal of the Optical Society of America* 67.1 (1977), pp. 1–3. DOI: [10.1364/josa.67.000001](https://doi.org/10.1364/josa.67.000001).
- [51] A. Costela and I. Garcia-Moreno. "Degenerate four-wave mixing in phenylbenzimidazole proton-transfer laser dyes." *Chemical Physics Letters* 249.5-6 (1996), pp. 373–380. DOI: [10.1016/0009-2614\(95\)01401-2](https://doi.org/10.1016/0009-2614(95)01401-2).
- [52] R. K. Mohan and C. Subramanian. "Transient phase conjugation in dyedoped polymer saturable absorbers." *Optics Communications* 144.4-6 (1997), pp. 322–330. DOI: [10.1016/s0030-4018\(97\)00413-6](https://doi.org/10.1016/s0030-4018(97)00413-6).
- [53] P. Nandakumar, C. Vijayan, and Y. V. G. S. Murti. "Quantum size effects on the third order optical nonlinearity of CdS quantum dots in Nafion." *Optics Communications* 185.4-6 (2000), pp. 457–465. DOI: [10.1016/s0030-4018\(00\)01009-9](https://doi.org/10.1016/s0030-4018(00)01009-9).
- [54] Y. Zhao, C. Wu, P. Shah, M. K. Kim, and L. R. Dawson. "Optical phase conjugation in InGaAs/GaAs multiple quantum wells at 1.06 μm wavelength." *Applied Physics Letters* 63.3 (1993), p. 281. DOI: [10.1063/1.110078](https://doi.org/10.1063/1.110078).

Bibliography

- [55] A. Costela, I. Garcia-Moreno, and J. L. Saiz. "Thermally Induced Optical Phase Conjugation in Solutions of C_{60} in a Variety of Organic Solvents." *The Journal of Physical Chemistry B* 101.25 (1997), pp. 4897–4903. DOI: [10.1021/jp970285a](https://doi.org/10.1021/jp970285a).
- [56] I. C. Khoo and Y. Liang. "Stimulated orientational and thermal scatterings and self-starting optical phase conjugation with nematic liquid crystals." *Physical Review E* 62.5 (2000), pp. 6722–6733. DOI: [10.1103/physreve.62.6722](https://doi.org/10.1103/physreve.62.6722).
- [57] R. A. Fisher and B. J. Feldman. "On-resonant phase-conjugate reflection and amplification at $10.6 \mu\text{m}$ in inverted CO_2 ." *Optics Letters* 4.5 (1979), p. 140. DOI: [10.1364/ol.4.000140](https://doi.org/10.1364/ol.4.000140).
- [58] G. J. Crofts, R. P. M. Green, and M. J. Damzen. "Investigation of multipass geometries for efficient degenerate four-wave mixing in Nd:YAG." *Optics Letters* 17.13 (1992), p. 920. DOI: [10.1364/ol.17.000920](https://doi.org/10.1364/ol.17.000920).
- [59] M. Y. Lanzerotti, R. W. Schirmer, A. L. Gaeta, and G. S. Agarwal. "Measurements of quantum noise in optical phase conjugation via four-wave mixing in an atomic vapor." *Physical Review A* 60.6 (1999), pp. 4980–4985. DOI: [10.1103/physreva.60.4980](https://doi.org/10.1103/physreva.60.4980).
- [60] G. C. Cardoso and J. W. R. Tabosa. "Four-wave mixing in dressed cold cesium atoms." *Optics Communications* 185.4–6 (2000), pp. 353–358. DOI: [10.1016/s0030-4018\(00\)01033-6](https://doi.org/10.1016/s0030-4018(00)01033-6).
- [61] P. Günter and J.-P. Huignard. *Photorefractive Materials and Their Applications 1*. Springer New York, Apr. 9, 2006.
- [62] G. S. He, D. Liu, and S. H. Liu. "A new physical explanation of producing phase-conjugate wave process in backward stimulated scattering." *Bulletin of the American Physical Society* 30 (1985), p. 1800.
- [63] B. Y. Zel'Dovich. "Wave-front inversion in induced light scattering." *JETP Letters* 15 (1972), pp. 109–113.
- [64] B. Y. Zel'Dovich, N. A. Mel'nikov, N. F. Pilipetskii, and V. V. Ragul'Skii. "Observation of wave-front inversion in stimulated Raman scattering of light." *ZhETF Pisma Redaktsiiu* 25 (1977), p. 41.
- [65] A. D. Kudriavtseva, A. I. Sokolovskaia, J. Gazengel, N. P. Xuan, and G. Rivoire. "Reconstruction of the laser wave-front by stimulated scatterings in the pico-second range." *Optics Communications* 26.3 (1978), pp. 446–448. DOI: [10.1016/0030-4018\(78\)90243-2](https://doi.org/10.1016/0030-4018(78)90243-2).

- [66] M. Cui and C. Yang. "Implementation of a digital optical phase conjugation system and its application to study the robustness of turbidity suppression by phase conjugation." *Optics Express* 18.4 (2010), p. 3444. DOI: [10.1364/oe.18.003444](https://doi.org/10.1364/oe.18.003444).
- [67] T. R. Hillman, T. Yamauchi, W. Choi, R. R. Dasari, M. S. Feld, Y. Park, and Z. Yaqoob. "Digital optical phase conjugation for delivering two-dimensional images through turbid media." *Scientific Reports* 3 (2013), p. 1909. DOI: [10.1038/srep01909](https://doi.org/10.1038/srep01909).
- [68] M. Cronin-Golomb, B. Fischer, J. O. White, and A. Yariv. "Passive (self-pumped) phase conjugate mirror: Theoretical and experimental investigation." *Applied Physics Letters* 41.8 (1982), pp. 689–691. DOI: [10.1063/1.93652](https://doi.org/10.1063/1.93652).
- [69] M. Cronin-Golomb, B. Fischer, J. O. White, and A. Yariv. "Passive phase conjugate mirror based on self-induced oscillation in an optical ring cavity." *Applied Physics Letters* 42.11 (1983), pp. 919–921. DOI: [10.1063/1.93800](https://doi.org/10.1063/1.93800).
- [70] M. Cronin-Golomb, B. Fischer, J. O. White, and A. Yariv. "Theory and applications of four-wave mixing in photorefractive media." *Quantum Electronics, IEEE Journal of* 20.1 (1984), pp. 12–30. DOI: [10.1109/JQE.1984.1072267](https://doi.org/10.1109/JQE.1984.1072267).
- [71] M. Cronin-Golomb and A. Yariv. "Self-induced frequency scanning and distributed Bragg reflection in semiconductor lasers with phase-conjugate feedback." *Optics letters* 11.7 (1986), pp. 455–457. DOI: [10.1364/OL.11.000455](https://doi.org/10.1364/OL.11.000455).
- [72] A. Karsaklian Dal Bosco. "Chaos and high-frequency self-pulsations in a laser diode with phase-conjugate feedback." PhD thesis. Supélec, 2013.
- [73] V. A. D'yakov, S. A. Korol'kov, A. A. Zozulya, A. V. Mamaev, and V. V. Shkunov. "Reflection-grating photorefractive self-pumped ring mirror." *Optics Letters* 16.20 (1991), p. 1614. DOI: [10.1364/ol.16.001614](https://doi.org/10.1364/ol.16.001614).
- [74] D. Rytz, M. S. Keirstead, T. M. Baer, R. R. Stephens, and B. A. Wechsler. "Efficient self-pumped phase conjugation at near-infrared wavelengths using cobalt-doped BaTiO₃." *Optics Letters* 15.22 (1990), pp. 1279–1281. DOI: [10.1364/OL.15.001279](https://doi.org/10.1364/OL.15.001279).
- [75] A. Murakami and J. Ohtsubo. "Dynamics of Semiconductor Lasers with Optical Feedback from Photorefractive Phase Conjugate Mirror." *Optical Review* 6.4 (1999), pp. 359–364. DOI: [10.1007/s10043-999-0359-y](https://doi.org/10.1007/s10043-999-0359-y).

Bibliography

- [76] A. Karsaklian Dal Bosco, D. Wolfersberger, and M. Sciamanna. "Extreme events in time-delayed nonlinear optics." *Optics Letters* 38.5 (2013), p. 703. DOI: [10.1364/ol.38.000703](https://doi.org/10.1364/ol.38.000703).
- [77] A. Karsaklian Dal Bosco, D. Wolfersberger, and M. Sciamanna. "Delay-induced deterministic resonance of chaotic dynamics." *Europhysics Letters* 101.2 (2013), p. 24001. DOI: [10.1209/0295-5075/101/24001](https://doi.org/10.1209/0295-5075/101/24001).
- [78] P. Kürz and T. Mukai. "Frequency stabilization of a semiconductor laser by external phase-conjugate feedback." *Optics Letters* 21.17 (1996), p. 1369. DOI: [10.1364/ol.21.001369](https://doi.org/10.1364/ol.21.001369).
- [79] O. K. Andersen, A. P. A. Fischer, I. C. Lane, E. Louvergnaux, S. Stolte, and D. Lenstra. "Experimental stability diagram of a diode laser subject to weak phase-conjugate feedback from a rubidium vapor cell." *Quantum Electronics, IEEE Journal of* 35.4 (1999), pp. 577–582. DOI: [10.1109/3.753662](https://doi.org/10.1109/3.753662).
- [80] K. Vahala, K. Kyuma, A. Yariv, S.-K. Kwong, M. Cronin-Golomb, and K. Y. Lau. "Narrow linewidth, single frequency semiconductor laser with a phase conjugate external cavity mirror." *Applied physics letters* 49.23 (1986), pp. 1563–1565. DOI: [10.1063/1.97280](https://doi.org/10.1063/1.97280).
- [81] G. P. Agrawal and J. T. Klaus. "Effect of phase-conjugate feedback on semiconductor laser dynamics." *Optics Letters* 16.17 (1991), p. 1325. DOI: [10.1364/ol.16.001325](https://doi.org/10.1364/ol.16.001325).
- [82] G. Agrawal and G. Gray. "Effect of phase-conjugate feedback on the noise characteristics of semiconductor lasers." *Physical Review A* 46.9 (1992), pp. 5890–5898. DOI: [10.1103/physreva.46.5890](https://doi.org/10.1103/physreva.46.5890).
- [83] G. H. M. Van Tartwijk, H. J. C. Van der Linden, and D. Lenstra. "Theory of a diode laser with phase-conjugate feedback." *Optics Letters* 17.22 (1992), pp. 1590–1592. DOI: [10.1364/OL.17.001590](https://doi.org/10.1364/OL.17.001590).
- [84] G. R. Gray, D. Huang, and G. P. Agrawal. "Chaotic dynamics of semiconductor lasers with phase-conjugate feedback." *Physical Review A* 49.3 (1994), p. 2096. DOI: [10.1103/PhysRevA.49.2096](https://doi.org/10.1103/PhysRevA.49.2096).
- [85] L. N. Langley and K. A. Shore. "Intensity noise and linewidth characteristics of laser diodes with phase conjugate optical feedback." *IEE Proceedings-Optoelectronics* 141.2 (1994), pp. 103–108. DOI: [10.1049/ip-opt:19949917](https://doi.org/10.1049/ip-opt:19949917).
- [86] G. R. Gray, D. H. DeTienne, and G. P. Agrawal. "Mode locking in semiconductor lasers by phase-conjugate optical feedback." *Optics Letters* 20.11 (1995), p. 1295. DOI: [10.1364/ol.20.001295](https://doi.org/10.1364/ol.20.001295).

- [87] B. Krauskopf, G. R. Gray, and D. Lenstra. "Semiconductor laser with phase-conjugate feedback: Dynamics and bifurcations." *Physical Review E* 58.6 (1998), p. 7190. DOI: [10.1103/PhysRevE.58.7190](https://doi.org/10.1103/PhysRevE.58.7190).
- [88] A. Murakami and J. Ohtsubo. "Dynamics and linear stability analysis in semiconductor lasers with phase-conjugate feedback." *Quantum Electronics, IEEE Journal of* 34.10 (1998), pp. 1979–1986. DOI: [10.1109/3.720236](https://doi.org/10.1109/3.720236).
- [89] A. Murakami, J. Ohtsubo, and Y. Liu. "Stability analysis of semiconductor laser with phase-conjugate feedback." *Quantum Electronics, IEEE Journal of* 33.10 (1997), pp. 1825–1831. DOI: [10.1109/3.631288](https://doi.org/10.1109/3.631288).
- [90] R. Tkach and A. Chraplyvy. "Regimes of feedback effects in 1.5- μm distributed feedback lasers." *Journal of Lightwave Technology* 4.11 (1986), pp. 1655–1661. DOI: [10.1109/jlt.1986.1074666](https://doi.org/10.1109/jlt.1986.1074666).
- [91] K. Green and B. Krauskopf. "Global bifurcations and bistability at the locking boundaries of a semiconductor laser with phase-conjugate feedback." *Physical Review E* 66.1 (2002), p. 016220. DOI: [10.1103/physreve.66.016220](https://doi.org/10.1103/physreve.66.016220).
- [92] K. Green and B. Krauskopf. "Bifurcation analysis of frequency locking in a semiconductor laser with phase-conjugate feedback." *International Journal of Bifurcation and Chaos* 13.09 (2003), pp. 2589–2601. DOI: [10.1142/S0218127403008107](https://doi.org/10.1142/S0218127403008107).
- [93] T. Erneux, A. Gavrielides, K. Green, and B. Krauskopf. "External cavity modes of semiconductor lasers with phase-conjugate feedback." *Physical Review E* 68.6 (2003), p. 066205. DOI: [10.1103/PhysRevE.68.066205](https://doi.org/10.1103/PhysRevE.68.066205).
- [94] D. O'Brien, G. Huyet, and J. McInerney. "Low-frequency fluctuations in a semiconductor laser with phase conjugate feedback." *Physical Review A* 64.2 (2001), pp. 466–472. DOI: [10.1103/PhysRevA.64.025802](https://doi.org/10.1103/PhysRevA.64.025802).
- [95] J. Ohtsubo. *Semiconductor Lasers*. Springer Berlin Heidelberg, 2013. DOI: [10.1007/978-3-642-30147-6](https://doi.org/10.1007/978-3-642-30147-6).
- [96] J. Mork, B. Tromborg, and P. L. Christiansen. "Bistability and low-frequency fluctuations in semiconductor lasers with optical feedback: a theoretical analysis." *Quantum Electronics, IEEE Journal of* 24.2 (1988), pp. 123–133. DOI: [10.1109/3.105](https://doi.org/10.1109/3.105).
- [97] M. Sciamanna, P. Mégret, and M. Blondel. "Hopf bifurcation cascade in small-alpha laser diodes subject to optical feedback." *Physical Review E* 69.4 (2004), p. 046209. DOI: [10.1103/physreve.69.046209](https://doi.org/10.1103/physreve.69.046209).

Bibliography

- [98] A. T. Ryan, G. P. Agrawal, G. R. Gray, and E. C. Gage. "Optical-feedback-induced chaos and its control in multimode semiconductor lasers." *Quantum Electronics, IEEE Journal of* 30.3 (1994), pp. 668–679. DOI: [10.1109/3.286153](https://doi.org/10.1109/3.286153).
- [99] D. H. DeTienne, G. R. Gray, G. P. Agrawal, and D. Lenstra. "Semiconductor laser dynamics for feedback from a finite-penetration-depth phase-conjugate mirror." *Quantum Electronics, IEEE Journal of* 33.5 (1997), pp. 838–844. DOI: [10.1109/3.572159](https://doi.org/10.1109/3.572159).
- [100] J. Lawrence and D. Kane. "Determination of external cavity coupling-coefficient for diode laser with phase-conjugate feedback." *Electronics Letters* 36.6 (2000), pp. 535–537. DOI: [10.1049/el:20000402](https://doi.org/10.1049/el:20000402).
- [101] L. Weicker, T. Erneux, D. Wolfersberger, and M. Sciamanna. "Laser diode nonlinear dynamics from a filtered phase-conjugate optical feedback." *Physical Review E* 92.2 (2015), p. 022906. DOI: [10.1103/physreve.92.022906](https://doi.org/10.1103/physreve.92.022906).
- [102] M. Virte, A. Karsaklian Dal Bosco, D. Wolfersberger, and M. Sciamanna. "Chaos crisis and bistability of self-pulsing dynamics in a laser diode with phase-conjugate feedback." *Physical Review A* 84.4 (2011), p. 043836. DOI: [10.1103/PhysRevA.84.043836](https://doi.org/10.1103/PhysRevA.84.043836).
- [103] É. Mercier, A. Even, E. Mirisola, D. Wolfersberger, and M. Sciamanna. "Numerical study of extreme events in a laser diode with phase-conjugate optical feedback." *Physical Review E* 91.4 (2015), p. 042914. DOI: [10.1103/physreve.91.042914](https://doi.org/10.1103/physreve.91.042914).
- [104] C. M. Bender and S. A. Orszag. *Advanced Mathematical Methods for Scientists and Engineers I*. Springer Science & Business Media, 1999. DOI: [10.1007/978-1-4757-3069-2](https://doi.org/10.1007/978-1-4757-3069-2).
- [105] J. Kevorkian and J. D. Cole. *Perturbation Methods in Applied Mathematics*. Springer New York, 1981. DOI: [10.1007/978-1-4757-4213-8](https://doi.org/10.1007/978-1-4757-4213-8).
- [106] K. Engelborghs, T. Luzyanina, and G. Samaey. *DDE-BIFTOOL v. 2.00: a Matlab package for bifurcation analysis of delay differential equations*. Tech. rep. TW-330. Department of Computer Science, K. U. Leuven, Belgium, 2001.
- [107] J. Mork, B. Tromborg, and J. Mark. "Chaos in semiconductor lasers with optical feedback: theory and experiment." *Quantum Electronics, IEEE Journal of* 28.1 (1992), pp. 93–108. DOI: [10.1109/3.119502](https://doi.org/10.1109/3.119502).

- [108] D. Rontani, A. Locquet, M. Sciamanna, and D. S. Citrin. "Loss of time-delay signature in the chaotic output of a semiconductor laser with optical feedback." *Optics Letters* 32.20 (2007), pp. 2960–2962. DOI: [10.1364/OL.32.002960](https://doi.org/10.1364/OL.32.002960).
- [109] D. Rontani, A. Locquet, M. Sciamanna, D. S. Citrin, and S. Ortin. "Time-delay identification in a chaotic semiconductor laser with optical feedback: a dynamical point of view." *Quantum Electronics, IEEE Journal of* 45.7 (2009), pp. 879–891. DOI: [10.1109/JQE.2009.2013116](https://doi.org/10.1109/JQE.2009.2013116).
- [110] D. Brunner, M. C. Soriano, X. Porte, and I. Fischer. "Experimental Phase-Space Tomography of Semiconductor Laser Dynamics." *Physical Review Letters* 115.5 (2015), p. 053901. DOI: [10.1103/physrevlett.115.053901](https://doi.org/10.1103/physrevlett.115.053901).
- [111] R. F. Broom. "Self modulation at gigahertz frequencies of a diode laser coupled to an external cavity." *Electronic Letters* 5.23 (1969), p. 571. DOI: [10.1049/el:19690430](https://doi.org/10.1049/el:19690430).
- [112] K. Ikeda, K. Kondo, and O. Akimoto. "Successive higher-harmonic bifurcations in systems with delayed feedback." *Physical Review Letters* 49.20 (1982), p. 1467. DOI: [10.1103/PhysRevLett.49.1467](https://doi.org/10.1103/PhysRevLett.49.1467).
- [113] A. A. Tager and K. Petermann. "High-frequency oscillations and self-mode locking in short external-cavity laser diodes." *Quantum Electronics, IEEE Journal of* 30.7 (1994), pp. 1553–1561. DOI: [10.1109/3.299487](https://doi.org/10.1109/3.299487).
- [114] E. A. Avrutin, E. L. Portnoi, and J. H. Marsh. "Monolithic and multi-GigaHertz mode-locked semiconductor lasers: Constructions, experiments, models and applications." *IEE Proceedings Optoelectronics* 147.4 (2000), pp. 251–278. DOI: [10.1049/ip-opt:20000282](https://doi.org/10.1049/ip-opt:20000282).
- [115] O. Ushakov, S. Bauer, O. Brox, H.-J. Wünsche, and F. Henneberger. "Self-Organization in Semiconductor Lasers with Ultrashort Optical Feedback." *Physical Review Letters* 92.4 (2004), p. 043902. DOI: [10.1103/physrevlett.92.043902](https://doi.org/10.1103/physrevlett.92.043902).
- [116] O. Brox, S. Bauer, M. Radziunas, M. Wolfrum, J. Sieber, J. Kreissl, B. Sartorius, and H.-J. Wünsche. "High-frequency pulsations in DFB lasers with amplified feedback." *Quantum Electronics, IEEE Journal of* 39.11 (2003), pp. 1381–1387. DOI: [10.1109/JQE.2003.818313](https://doi.org/10.1109/JQE.2003.818313).
- [117] B. Pan, L. Yu, D. Lu, L. Zhang, and L. Zhao. "Simulation and experimental characterization of a dual-mode two-section amplified feedback laser with mode separation over 100 GHz." *Chinese Optics Letters* 12.11 (2014), p. 110605.

Bibliography

- [118] G. H. M. Van Tartwijk, A. M. Levine, and D. Lenstra. "Sisyphus effect in semiconductor lasers with optical feedback." *Selected Topics in Quantum Electronics, IEEE Journal of* 1.2 (1995), pp. 466–472. DOI: [10.1109/2944.401230](https://doi.org/10.1109/2944.401230).
- [119] B. McNamara, K. Wiesenfeld, and R. Roy. "Observation of Stochastic Resonance in a Ring Laser." *Physical Review Letters* 60.25 (1988), pp. 2626–2629. DOI: [10.1103/physrevlett.60.2626](https://doi.org/10.1103/physrevlett.60.2626).
- [120] L. Gammaitoni, P. Hänggi, P. Jung, and F. Marchesoni. "Stochastic resonance." *Reviews of Modern Physics* 70.1 (1998), pp. 223–287. DOI: [10.1103/revmodphys.70.223](https://doi.org/10.1103/revmodphys.70.223).
- [121] G. Giacomelli, F. Marin, and I. Rabbiosi. "Stochastic and Bona Fide Resonance: An Experimental Investigation." *Physical Review Letters* 82.4 (1999), pp. 675–678. DOI: [10.1103/physrevlett.82.675](https://doi.org/10.1103/physrevlett.82.675).
- [122] J. M. Buldú, J. García-Ojalvo, C. R. Mirasso, and M. C. Torrent. "Stochastic entrainment of optical power dropouts." *Physical Review E* 66.2 (2002), p. 021106. DOI: [10.1103/physreve.66.021106](https://doi.org/10.1103/physreve.66.021106).
- [123] A. S. Pikovsky and J. Kurths. "Coherence resonance in a noise-driven excitable system." *Physical Review Letters* 78.5 (1997), p. 775. DOI: [10.1103/PhysRevLett.78.775](https://doi.org/10.1103/PhysRevLett.78.775).
- [124] D. E. Postnov, S. K. Han, T. G. Yim, and O. V. Sosnovtseva. "Experimental observation of coherence resonance in cascaded excitable systems." *Physical Review E* 59.4 (1999), R3791–R3794. DOI: [10.1103/physreve.59.r3791](https://doi.org/10.1103/physreve.59.r3791).
- [125] G. Giacomelli, M. Giudici, S. Balle, and J. R. Tredicce. "Experimental Evidence of Coherence Resonance in an Optical System." *Physical Review Letters* 84.15 (2000), pp. 3298–3301. DOI: [10.1103/physrevlett.84.3298](https://doi.org/10.1103/physrevlett.84.3298).
- [126] M. Arizaleta Arteaga, M. Valencia, M. Sciamanna, H. Thienpont, M. López-Amo, and K. Panajotov. "Experimental Evidence of Coherence Resonance in a Time-Delayed Bistable System." *Physical Review Letters* 99.2 (2007), p. 023903. DOI: [10.1103/physrevlett.99.023903](https://doi.org/10.1103/physrevlett.99.023903).
- [127] A. Gavrielides, T. Newell, V. Kovanis, R. Harrison, N. Swanston, D. Yu, and W. Lu. "Synchronous Sisyphus effect in diode lasers subject to optical feedback." *Physical Review A* 60.2 (1999), pp. 1577–1581. DOI: [10.1103/physreva.60.1577](https://doi.org/10.1103/physreva.60.1577).

- [128] Y. Hong and K. A. Shore. "Influence of optical feedback time-delay on power-drops in vertical-cavity surface-emitting lasers." *Quantum Electronics, IEEE Journal of* 41.8 (2005), pp. 1054–1057. DOI: [10.1109/jqe.2005.850698](https://doi.org/10.1109/jqe.2005.850698).
- [129] J. M. Buldú, J. García-Ojalvo, and M. C. Torrent. "Delay-induced resonances in an optical system with feedback." *Physical Review E* 69.4 (2004), p. 046207. DOI: [10.1103/physreve.69.046207](https://doi.org/10.1103/physreve.69.046207).
- [130] J. F. Martinez Avila, H. L. D. de S. Cavalcante, and J. R. R. Leite. "Experimental Deterministic Coherence Resonance." *Physical Review Letters* 93.14 (2004), p. 144101. DOI: [10.1103/physrevlett.93.144101](https://doi.org/10.1103/physrevlett.93.144101).
- [131] A. Hohl, H. J. C. van der Linden, and R. Roy. "Determinism and stochasticity of power-dropout events in semiconductor lasers with optical feedback." *Optics Letters* 20.23 (1995), p. 2396. DOI: [10.1364/ol.20.002396](https://doi.org/10.1364/ol.20.002396).
- [132] J. Zamora-Munt, C. Masoller, and J. García-Ojalvo. "Transient low-frequency fluctuations in semiconductor lasers with optical feedback." *Physical Review A* 81 (3 2010), p. 033820. DOI: [10.1103/PhysRevA.81.033820](https://doi.org/10.1103/PhysRevA.81.033820).
- [133] A. Torcini, S. Barland, G. Giacomelli, and F. Marin. "Low-frequency fluctuations in vertical cavity lasers: Experiments versus Lang-Kobayashi dynamics." *Physical Review A* 74.6 (2006), p. 063801. DOI: [10.1103/PhysRevA.74.063801](https://doi.org/10.1103/PhysRevA.74.063801).
- [134] D. R. Solli, C. Ropers, P. Koonath, and B. Jalali. "Optical rogue waves." *Nature* 450.7172 (2007), pp. 1054–1057. DOI: [10.1038/nature06402](https://doi.org/10.1038/nature06402).
- [135] K. Dysthe, H. E. Krogstad, and P. Müller. "Oceanic Rogue Waves." *Annual Review of Fluid Mechanics* 40.1 (2008), pp. 287–310. DOI: [10.1146/annurev.fluid.40.111406.102203](https://doi.org/10.1146/annurev.fluid.40.111406.102203).
- [136] H. L. D. de S. Cavalcante, M. Oria, D. Sornette, E. Ott, and D. J. Gauthier. "Predictability and Suppression of Extreme Events in a Chaotic System." *Physical Review Letters* 111.19 (2013), p. 198701. DOI: [10.1103/physrevlett.111.198701](https://doi.org/10.1103/physrevlett.111.198701).
- [137] A. Montana, U. Bortolozzo, S. Residori, and F. Arecchi. "Non-Gaussian Statistics and Extreme Waves in a Nonlinear Optical Cavity." *Physical Review Letters* 103.17 (2009), p. 173901. DOI: [10.1103/physrevlett.103.173901](https://doi.org/10.1103/physrevlett.103.173901).
- [138] S. Residori, U. Bortolozzo, A. Montana, F. Lenzini, and F. T. Arecchi. "Rogue waves in spatially extended optical systems." *Fluctuation and Noise Letters* 11.01 (2012), p. 1240014. DOI: [10.1142/S0219477512400147](https://doi.org/10.1142/S0219477512400147).

Bibliography

- [139] N. Marsal, V. Caullet, D. Wolfersberger, and M. Sciamanna. "Spatial rogue waves in a photorefractive pattern-forming system." *Optics Letters* 39.12 (2014), p. 3690. DOI: [10.1364/ol.39.003690](https://doi.org/10.1364/ol.39.003690).
- [140] C. Bonatto, M. Feyereisen, S. Barland, M. Giudici, C. Masoller, J. R. R. Leite, and J. R. Tredicce. "Deterministic optical rogue waves." *Physical Review Letters* 107.5 (2011), p. 053901. DOI: [10.1103/PhysRevLett.107.053901](https://doi.org/10.1103/PhysRevLett.107.053901).
- [141] J. Zamora-Munt, B. Garbin, S. Barland, M. Giudici, J. R. R. Leite, C. Masoller, and J. R. Tredicce. "Rogue waves in optically injected lasers: Origin, predictability, and suppression." *Physical Review A* 87.3 (2013), p. 035802. DOI: [10.1103/PhysRevA.87.035802](https://doi.org/10.1103/PhysRevA.87.035802).
- [142] J. Ahuja, D. B. Nalawade, J. Zamora-Munt, R. Vilaseca, and C. Masoller. "Rogue waves in injected semiconductor lasers with current modulation: role of the modulation phase." *Optics Express* 22.23 (2014), p. 28377. DOI: [10.1364/oe.22.028377](https://doi.org/10.1364/oe.22.028377).
- [143] J. A. Reinoso, J. Zamora-Munt, and C. Masoller. "Extreme intensity pulses in a semiconductor laser with a short external cavity." *Physical Review E* 87.6 (2013), p. 062913. DOI: [10.1103/PhysRevE.87.062913](https://doi.org/10.1103/PhysRevE.87.062913).
- [144] C. Kharif, E. Pelinovsky, and A. Slunyaev. *Rogue Waves in the Ocean*. Springer Science + Business Media, 2009. DOI: [10.1007/978-3-540-88419-4_1](https://doi.org/10.1007/978-3-540-88419-4_1).
- [145] C. Lecaplain, P. Grelu, J. M. Soto-Crespo, and N. Akhmediev. "Dissipative Rogue Waves Generated by Chaotic Pulse Bunching in a Mode-Locked Laser." *Physical Review Letters* 108.23 (2012), p. 233901. DOI: [10.1103/physrevlett.108.233901](https://doi.org/10.1103/physrevlett.108.233901).
- [146] A. Zaviyalov, O. Egorov, R. Iliev, and F. Lederer. "Rogue waves in mode-locked fiber lasers." *Physical Review A* 85.1 (2012), p. 013828. DOI: [10.1103/physreva.85.013828](https://doi.org/10.1103/physreva.85.013828).
- [147] J. M. Dudley, F. Dias, M. Erkintalo, and G. Genty. "Instabilities, breathers and rogue waves in optics." *Nature Photonics* 8.10 (2014), pp. 755–764. DOI: [10.1038/nphoton.2014.220](https://doi.org/10.1038/nphoton.2014.220).
- [148] K. Green and B. Krauskopf. "Bifurcation analysis of a semiconductor laser subject to non-instantaneous phase-conjugate feedback." *Optics communications* 231.1 (2004), pp. 383–393. DOI: [10.1016/j.optcom.2003.12.026](https://doi.org/10.1016/j.optcom.2003.12.026).

- [149] F. T. Arecchi, U. Bortolozzo, A. Montina, and S. Residori. "Granularity and Inhomogeneity Are the Joint Generators of Optical Rogue Waves." *Physical Review Letters* 106.153901 (2011), p. 4. DOI: [10.1103/physrevlett.106.153901](https://doi.org/10.1103/physrevlett.106.153901).
- [150] P. Sibani. "Extremal noise events, intermittency, and Log-Poisson statistics in non-equilibrium aging of complex systems." In: *SPIE Third International Symposium on Fluctuations and Noise*. International Society for Optics and Photonics. 2005, pp. 271–282. DOI: [10.1117/12.600964](https://doi.org/10.1117/12.600964).
- [151] É. Mercier, D. Wolfersberger, and M. Sciamanna. "High-frequency chaotic dynamics enabled by optical phase-conjugation." *Scientific Reports* 6 (2016), p. 18988. DOI: [10.1038/srep18988](https://doi.org/10.1038/srep18988).
- [152] T. Bach, M. Jazbinsek, G. Montemezzani, P. Günter, A. Grabar, I. Stoika, and Y. M. Vysochanskii. "Enhanced near-infrared photorefractive properties of Te-doped Sn₂P₂S₆." In: *Holography 2005: International Conference on Holography, Optical Recording, and Processing of Information*. Vol. 6252. International Society for Optics and Photonics. SPIE, 2006, p. 625208. DOI: [10.1117/12.676508](https://doi.org/10.1117/12.676508).
- [153] M. Jazbinšek, G. Montemezzani, P. Günter, A. A. Grabar, I. M. Stoika, and Y. M. Vysochanskii. "Fast near-infrared self-pumped phase conjugation with photorefractive Sn₂P₂S₆." *Journal of the Optical Society of America B* 20.6 (2003), pp. 1241–1246. DOI: [10.1364/JOSAB.20.001241](https://doi.org/10.1364/JOSAB.20.001241).
- [154] A. Olsson and C. Tang. "Coherent optical interference effects in external-cavity semiconductor lasers." *Quantum Electronics, IEEE Journal of* 17.8 (1981), pp. 1320–1323. DOI: [10.1109/jqe.1981.1071272](https://doi.org/10.1109/jqe.1981.1071272).
- [155] J. Osmundsen and N. Gade. "Influence of optical feedback on laser frequency spectrum and threshold conditions." *Quantum Electronics, IEEE Journal of* 19.3 (1983), pp. 465–469. DOI: [10.1109/jqe.1983.1071857](https://doi.org/10.1109/jqe.1983.1071857).
- [156] G. D. Vanwiggeren and R. Roy. "Communication with chaotic lasers." *Science* 279.5354 (1998), pp. 1198–1200. DOI: [10.1126/science.279.5354.1198](https://doi.org/10.1126/science.279.5354.1198).
- [157] R. Vicente, C. R. Mirasso, and I. Fischer. "Simultaneous bidirectional message transmission in a chaos-based communication scheme." *Optics Letters* 32.4 (2007), pp. 403–405. DOI: [10.1364/OL.32.000403](https://doi.org/10.1364/OL.32.000403).
- [158] D. Rontani, É. Mercier, D. Wolfersberger, and M. Sciamanna. "Enhanced complexity of optical chaos in a laser diode with phase-conjugate feedback." *Submitted for publication* (2016).

Bibliography

- [159] C. Bandt and B. Pompe. "Permutation Entropy: A Natural Complexity Measure for Time Series." *Physical Review Letters* 88.17 (2002), p. 174102. DOI: [10.1103/physrevlett.88.174102](https://doi.org/10.1103/physrevlett.88.174102).
- [160] J. P. Toomey and D. M. Kane. "Mapping the dynamic complexity of a semiconductor laser with optical feedback using permutation entropy." *Optics Express* 22.2 (2014), p. 1713. DOI: [10.1364/oe.22.001713](https://doi.org/10.1364/oe.22.001713).
- [161] P. Perez and A. Valle. "Enhancement of chaotic signal bandwidth in VCSELs induced by polarized optical injection." *Quantum Electronics, IEEE Journal of* 51.6 (2015), p. 2400207. DOI: [10.1109/JQE.2015.2429122](https://doi.org/10.1109/JQE.2015.2429122).
- [162] Y. Hong, P. S. Spencer, and K. A. Shore. "Wideband chaos with time-delay concealment in vertical-cavity surface-emitting lasers with optical feedback and injection." *Quantum Electronics, IEEE Journal of* 50.4 (2014), pp. 236–242. DOI: [10.1109/JQE.2014.2304745](https://doi.org/10.1109/JQE.2014.2304745).
- [163] J. Feinberg. "Self-pumped, continuous-wave phase conjugator using internal reflection." *Optics Letters* 7.10 (1982), pp. 486–488. DOI: [10.1364/OL.7.000486](https://doi.org/10.1364/OL.7.000486).
- [164] A. A. Zozulya, G. Montemezzani, and D. Z. Anderson. "Analysis of total-internal-reflection phase-conjugate mirror." *Physical Review A* 52.5 (1995), p. 4167. DOI: [10.1103/PhysRevA.52.4167](https://doi.org/10.1103/PhysRevA.52.4167).
- [165] M. Belić, D. Timotijević, and R. W. Boyd. "Wave mixing in photorefractive crystals with saturable couplings: stable solutions and instabilities." *Optics Communications* 96.4-6 (1993), pp. 283–288. DOI: [10.1016/0030-4018\(93\)90276-b](https://doi.org/10.1016/0030-4018(93)90276-b).
- [166] M. Goetz. "Conception et réalisation d'un banc automatisé de caractérisation du comportement temporel des miroirs auto-pompés à conjugaison de phase photoréfractive : cartographie d'échantillons et modélisation physique." PhD thesis. Supélec, 1994.
- [167] P. Günter, E. Voit, M. Z. Zha, and J. Albers. "Self-pulsation and optical chaos in self-pumped photorefractive BaTiO₃." *Optics communications* 55.3 (1985), pp. 210–214. DOI: [10.1016/0030-4018\(85\)90049-5](https://doi.org/10.1016/0030-4018(85)90049-5).

COLOPHON

This document was typeset using the typographical look-and-feel `classicthesis` developed by André Miede. The style was inspired by Robert Bringhurst's seminal book on typography "*The Elements of Typographic Style*". `classicthesis` is available for both \LaTeX and \LyX :

<https://bitbucket.org/amiede/classicthesis/>

Happy users of `classicthesis` usually send a real postcard to the author, a collection of postcards received so far is featured here:

<http://postcards.miede.de/>

Final Version as of October 27, 2016 (`classicthesis` 4.2).